

# INVESTIGATING THE RECOGNITION AND INTERACTIONS OF NON-POLAR $\alpha$ HELICES IN BIOLOGY

A THESIS SUBMITTED TO THE UNIVERSITY OF MANCHESTER  
FOR THE DEGREE OF DOCTOR OF PHILOSOPHY  
IN THE FACULTY OF SCIENCE AND ENGINEERING

2019

**James A. Baker**

School of Chemistry

# Contents

<b>Abstract</b>	<b>15</b>
<b>Lay Abstract</b>	<b>16</b>
<b>Declaration</b>	<b>17</b>
<b>Copyright Statement</b>	<b>18</b>
<b>Acknowledgements</b>	<b>19</b>
<b>1 Introduction</b>	<b>20</b>
1.1 Transmembrane proteins . . . . .	20
1.1.1 A brief history of the discovery and exploration of the transmembrane proteins . . . . .	20
1.1.2 Transmembrane proteins in disease . . . . .	22
1.1.3 The transmembrane protein problem . . . . .	23
1.1.4 The transmembrane protein revolution . . . . .	24
1.1.5 The role of bioinformatics in transmembrane biology . . . . .	26
1.2 Biological membranes . . . . .	28
1.2.1 Membrane lipids . . . . .	28
1.2.2 Membrane potential . . . . .	30
1.3 $\alpha$ helices in the membrane; structure and function . . . . .	31
1.3.1 Transmembrane helix sequence composition . . . . .	31
1.3.2 The hydrophobicity of transmembrane segments . . . . .	35
1.3.3 Sequence complexity . . . . .	38
1.4 Biogenesis of transmembrane proteins . . . . .	40
1.4.1 An overview of translocation . . . . .	40

1.4.2	Signal peptides . . . . .	44
1.4.3	$\beta$ sheets in the membrane . . . . .	45
1.5	The aims of this thesis . . . . .	48
<b>2</b>	<b>The “negative-outside” rule</b>	<b>50</b>
2.1	Summary . . . . .	50
2.1.1	Background . . . . .	50
2.1.2	Results . . . . .	50
2.1.3	Conclusions . . . . .	51
2.2	Introduction . . . . .	51
2.3	Results . . . . .	56
2.3.1	Acidic residues within and nearby transmembrane helix segments are rare . . . . .	56
2.3.2	Amino acid residue distribution analysis reveals a “negative-not-inside/negative-outside” signal in single-pass transmembrane helix segments . . . . .	60
2.3.3	Amino acid residue distribution analysis reveals a general negative-charge bias signal in outside flank of multi-pass transmembrane helix segments — the negative outside enrichment rule . . . . .	64
2.3.4	Further significant sequence differences between single-pass and multi-pass helices: distribution of tryptophan, tyrosine, proline and cysteine . . . . .	69
2.3.5	Hydrophobicity and leucine distribution in transmembrane helices in single- and multi-pass proteins . . . . .	71
2.3.6	A negative-outside (or negative-non-inside) signal is present across many membrane types . . . . .	73
2.3.7	Amino acid compositional skews in relation to transmembrane helix complexity and anchorage function . . . . .	76
2.4	Discussion . . . . .	82
2.5	Methods . . . . .	90
2.5.1	Datasets . . . . .	90

2.5.2	On the determination of flanking regions for transmembrane helices and the transmembrane helix alignment . . . . .	97
2.5.3	Separating simple and complex single-pass helices . . . . .	99
2.5.4	Distribution normalisation . . . . .	100
2.5.5	Hydrophobicity calculations . . . . .	101
2.5.6	Normalised net charge calculations . . . . .	101
2.5.7	Statistics . . . . .	102
<b>3</b>	<b>Collation and analysis of tail-anchored protein transmembrane helices reveals subcellular variation in flanking charged residue distribution and the transmembrane helix core hydrophobicity</b>	<b>104</b>
3.1	Abstract . . . . .	104
3.2	Introduction . . . . .	105
3.3	Methods . . . . .	110
3.3.1	Building a list of tail-anchors . . . . .	110
3.3.2	Calculating hydrophobicity . . . . .	115
3.3.3	Calculating sequence information entropy . . . . .	116
3.3.4	Statistics . . . . .	116
3.3.5	Modelling cytochrome b5 and PTP1b . . . . .	117
3.3.6	Availability of materials . . . . .	118
3.4	Results and discussion . . . . .	118
3.4.1	A comparison of up-to-date tail-anchored protein datasets . . . . .	118
3.4.2	It is difficult to observe any hydrophobic variation of tail-anchored protein transmembrane helices from different species . . . . .	121
3.4.3	There are biochemical differences between tail-anchored transmembrane helices from different organelles . . . . .	123
3.4.4	More annotation is required to identify chaperone interaction factors of the transmembrane helix. . . . .	131
3.4.5	Spontaneous insertion may be achieved by polar strips in the transmembrane helix of tail-anchored proteins . . . . .	133
3.5	Summary . . . . .	135

<b>4 Sequence analysis of polarity in transmembrane helices suggests that translocation of marginally hydrophobic helices could be facilitated by neighbouring typically hydrophobic helices</b>	<b>139</b>
4.1 Abstract . . . . .	139
4.2 Introduction . . . . .	140
4.2.1 The ribosome-translocon complex in the biogenesis of membrane proteins . . . . .	141
4.2.2 Cooperative transmembrane helix insertion by the translocon-ribosome complex . . . . .	143
4.2.3 Aims . . . . .	145
4.3 Methods . . . . .	145
4.3.1 Datasets . . . . .	145
4.3.2 Gene ontology . . . . .	147
4.3.3 Complexity and hydrophobic estimation . . . . .	147
4.3.4 Statistics . . . . .	148
4.3.5 Availability of materials . . . . .	148
4.4 Results and discussion . . . . .	149
4.4.1 Large contrasts in transmembrane helix hydrophobicity occur in channels and receptors . . . . .	149
4.4.2 GPCRs contain conserved relatively polar TMH7, which follows the typically hydrophobic TMH6 . . . . .	150
4.4.3 6TMH ion channels contain polar-hydrophobic transmembrane helix pairs/groups indicative of conserved cooperative insertion .	155
4.4.4 The prevalence of the high hydrophobic discrepancy of transmembrane helices amongst other common ‘transporter’ transmembrane protein classes . . . . .	159
4.5 Summary . . . . .	161
<b>5 Conclusions and outlook</b>	<b>164</b>

# List of Tables

2.1	Acidic residues are rarer in transmembrane helices of single-pass proteins than in transmembrane helices of multi-pass proteins. . . . .	57
2.2	Statistical significances for negative charge distribution skew on either side of the membrane in single-pass transmembrane helices. . . . .	63
2.3	Statistical significances for negative charge distribution skew on either side of the membrane in multi-pass transmembrane helices. . . . .	67
2.4	Leucines at the inner and outer leaflets of the membrane in transmembrane helices. . . . .	74
2.5	Simple transmembrane helices are less similar than complex transmembrane helices to transmembrane helices from multi-pass proteins in Uni-Human. . . . .	79
2.6	Simple transmembrane helices are less similar than complex transmembrane helices to transmembrane helices from multi-pass proteins in Ex-pAll. . . . .	80
2.7	The experimental evidences of TOPDB. . . . .	92
2.8	Records with INTRAMEM and TRANSMEM flanking region overlap. .	99
3.1	Hydrophobicity statistical comparisons between mouse and human, yeast, and plants in the SwissProt Filtered Dataset. . . . .	121
3.2	Hydrophobicity statistical comparisons between mouse and human, yeast, and plants in the UniProt Curated Dataset. . . . .	123
3.3	Statistical comparisons between TMH sequences from organelles in the UniProt Curated Dataset. . . . .	123
3.4	Statistical comparisons between transmembrane helix sequences from organelles in the SwissProt Filtered Dataset. . . . .	129

4.1 Dataset sizes of common transmembrane protein families of transporters and channels. . . . .	146
--	-----

# List of Figures

1.1	A selection of figures demonstrating important discoveries of membrane proteins and their environment. . . . .	21
1.2	The structure of SecYE in a nanodisc at near atomic resolution. . . . .	25
1.3	A comparison of a single structure held by commonly used structural transmembrane protein databases. . . . .	28
1.4	A cartoon showing the general components of the membrane and a typical transmembrane helix. . . . .	32
1.5	A cartoon of the topological clustering of positively-charged residues near transmembrane helices in relation to subcellular location. . . . .	33
1.6	The hydropathic index of rabbit cytochrome b5. . . . .	37
1.7	The hydrophobic-complexity continuum distinguishes between transmembrane helix anchors and those with function beyond anchoring. . .	39
1.8	A simplified schematic of the co-translational Sec pathway and the post-translational pathway. . . . .	41
1.9	The pore, the plug, and the lateral gate of the translocon. . . . .	42
1.10	The key components of a signal peptide. . . . .	45
1.11	Cartoons showing the structural differences of the outer membrane $\beta$ -barrel proteins, transmembrane $\alpha$ -helix channels, and transmembrane $\alpha$ -helix signal transducers in the membrane. . . . .	46
1.12	A cartoon of the biogenesis of $\beta$ barrel membrane proteins in mitochondria and Gram-negative bacteria. . . . .	47
2.1	Negatively-charged amino acids are amongst the rarest residues in transmembrane helices and $\pm 5$ flanking residues. . . . .	58

2.2	Relative percentage normalisation reveals a negative-outside bias in transmembrane helices from single-pass protein datasets. . . . .	61
2.3	Negative-outside bias is very subtle in transmembrane helices from multi-pass proteins. . . . .	65
2.4	The net charge across multi-pass and single-pass transmembrane helices shows a stronger positive inside charge in single-pass transmembrane helices than multi-pass transmembrane helices. . . . .	66
2.5	Relative percentage heat-maps from predictive and experimental datasets corroborate residue distribution differences between transmembrane helices from single-pass and multi-pass proteins. . . . .	70
2.6	There is a difference in the hydrophobic profiles of transmembrane helices from single-pass and multi-pass proteins. . . . .	72
2.7	There is a difference in the hydrophobic profiles of transmembrane helices from single-pass and multi-pass proteins. . . . .	73
2.8	Comparing charged amino acid distributions in transmembrane helices of multi-pass and single-pass proteins across different species and organelles. . . . .	75
2.9	Comparing the amino acid relative percentage distributions of simple and complex transmembrane helices from single-pass proteins and transmembrane helices from multi-pass proteins. . . . .	77
2.10	Residue distributions of transmembrane anchors. A view showing additional residue distribution features that transmembrane helices with an anchorage function display. . . . .	89
2.11	The lengths of flanks and transmembrane helices in multi-pass and single-pass proteins in the UniHuman and ExpAll dataset. . . . .	98
2.12	Relative percentage heatmaps from the predictive datasets calculated by fractions of the absolute maximum and by the relative percentage of a given amino acid type. . . . .	102
3.1	An overview of the biogenesis of tail-anchored proteins. . . . .	107
3.2	The sources, methods, and filters applied to the sequences in the tail-anchored protein datasets. . . . .	111

3.3	A Venn diagram showing tail-anchored protein UniProt ids present in each of the datasets as well as those present in multiple datasets. . . . .	119
3.4	Average values of species datasets from UniProt manually curated set and SwissProt automatically filtered dataset. . . . .	122
3.5	Average sequence-based biochemical values of organelle datasets from UniProt manually curated set and SwissProt automatically filtered dataset. . . . .	124
3.6	The normalised skews of each amino acids from tail-anchored proteins grouped by localisation from the SwissProt automatically filtered dataset. . . . .	126
3.7	The normalised skews of each amino acids from tail-anchored proteins grouped by localisation from the SwissProt automatically filtered dataset. . . . .	128
3.8	The profile of transmembrane helix and flanks hydrophobicity from tail-anchored protein groups stratified by chaperone interactors. . . . .	133
3.9	Structural biochemical analysis of a homology model of cytochrome b5. . . . .	135
3.10	Structural biochemical analysis of a homology model of PTP1b. . . . .	136
3.11	A cartoon of a potential method the cytochrome b5 and PTP1b transmembrane helix could integrate spontaneously into the membrane. . . . .	137
4.1	A cartoon showing the generally accepted schematic of sequential multipass transmembrane helix insertion into the membranes. . . . .	140
4.2	A cartoon of the ribosome in association with the translocon during insertion. . . . .	142
4.3	Pie charts of a non-redundant list of transmembrane proteins compared to a list of transmembrane proteins containing the most hydrophobically different transmembrane helix pairs. . . . .	149
4.4	The hydrophobicity and complexity of GPCR transmembrane helices. . . . .	151
4.5	The hydrophobic difference observed between TMH6 and TMH7 in GPCRs is not due to the choice of hydrophobic scale. . . . .	153
4.6	The hydrophobicity of transmembrane helices in GPCR subfamilies. . . . .	154
4.7	The hydrophobicity of transmembrane helices in ion channels. . . . .	157
4.8	The hydrophobic difference observed between TMH4 and the neighbouring transmembrane helices in 6TMH ion channels is not due to the choice of hydrophobic scale. . . . .	159

4.9 Sequence entropy is unsuitable for assessing function in TMH4 of ion channels. . . . .	160
4.10 High polarity discrepancy between sequentially adjacent transmembrane helices is not present in all transmembrane protein transporter families. . . . .	161
4.11 A cartoon of potential cooperative transmembrane helix insertion methods. . . . .	162

# Acronyms

**AP** Arrest Peptide. 141–144, 163, 165

**EM** Electron Microscopy. 21, 22, 25–27, 43, 163, 165

**EMC** ER Membrane protein Complex. 23, 43, 44, 107, 109, 162, 165

**ER** Endoplasmic Reticulum. 30–32, 37, 40, 43, 54, 86, 87, 106–110, 112–114, 123–126, 128–131, 140, 144, 155

**GPCR** G protein-coupled receptor. 28, 46, 145–147, 149–155, 162, 163, 165

**K-S** Kolmogorov-Smirnov. 78–81, 103, 116

**K-W** Kruskal-Wallis. 63, 67, 78–81, 102, 103, 116

**MD** Molecular Dynamics. 27, 29, 35, 165

**MOM** Mitochondrial Outer Membrane. 46–48, 109, 130, 131, 135, 136

**PDB** Protein Data Bank. 22, 28, 32, 55

**PM** Plasma Membrane. 40, 43, 86, 87, 112, 114, 123–125, 127, 129, 130

**POPC** Palmitoyloleylphosphatidylcholine. 38, 73

**RNA** Ribonucleic Acid. 41, 140–142

**SNARE** Soluble N-ethylmaleimide-sensitive factor attachment protein receptor. 105, 109, 164

**SP** Signal Peptide. 24, 26, 43–45, 47, 48, 112, 113, 131

**SR** Signal Recognition Particle Receptor. 41, 43, 44, 106, 140, 141

**SRP** Signal Recognition Particle. 41, 43, 44, 106–108, 115, 140, 141

**TA** Tail Anchor. 27, 37, 40, 43, 49, 105–110, 113–115, 118–125, 127, 129–133, 135–137, 164, 165

**TM** Transmembrane. 21, 26, 28, 34, 39, 41, 52–55, 69, 71, 78, 85, 98, 109

**TMH** Transmembrane Helix. 20, 23–46, 48, 49, 51–78, 81–91, 93, 94, 96–103, 105–110, 112–114, 116–118, 120–138, 140–145, 147–158, 160–166

**TMP** Transmembrane Protein. 20–27, 29, 31, 35, 40, 42–45, 48, 49, 51, 53, 55, 58, 59, 68, 71, 73, 82–87, 108, 121, 131, 140–143, 149, 150, 155, 162–166

**TMS** Transmembrane Segment. 24, 32, 101, 117, 143

**TOM** Translocase of the Outer Membrane. 47, 48, 109

# The University of Manchester

James A. Baker

Doctor of Philosophy

Investigating the Recognition and Interactions of Non-Polar  $\alpha$  Helices in  
Biology

January 24, 2019

# Abstract

Non-polar helices feature prominently in structural biology. Transmembrane  $\alpha$  helix containing proteins make up around a third of all proteins, represent around 40% of drug targets, and contain some of the most critical proteins required for life as we know it. Yet they are fundamentally difficult to study experimentally. This is in part due to the very features that make them so biologically influential; their non-polar transmembrane helical regions.

By leveraging large data-sets of transmembrane proteins, this thesis is focused on characterising features of transmembrane  $\alpha$  helices en masse, particularly regarding their topology, membrane–protein interactions, and intramembrane protein interactions.

In this study, we present statistical evidence demonstrating the ‘negative-outside’ rule in opposition to the ‘positive-inside’ rule. We also identify stabilising amino acid distributions in anchoring transmembrane helices compared to transmembrane helices with function beyond anchoring.

Tail-anchored proteins are a group of post-translationally inserting proteins. In this thesis we show adaptations of hydrophobicity and residue distributions through the transmembrane helices of tail-anchored proteins to different membrane environments within the cell (the mitochondria, endoplasmic reticulum, the Golgi, and the plasma membrane). However, we could not detect a hydrophobic difference between global populations of tail-anchored proteins in different species (mammals, plants, and fungi). A handful of these proteins are capable of integrating into the membrane without the need for membrane integration proteins. Structural modelling of transmembrane helices from PTP1b and cytochrome b5 reveals a 3D amphipathic arrangement of residues. This structural feature may play a role in their spontaneous membrane insertion.

Finally, we find a conserved pattern of typically hydrophobic transmembrane helices neighbouring marginally hydrophobic helices in some families of transmembrane proteins. This feature corresponds to transmembrane helices that have the potential to cooperate in order to integrate the more polar, but functionally important, transmembrane helix of the pair into the membrane.

# Lay Abstract

The survival of each of our cells relies on a cellular barrier (called the membrane) to separate themselves from the surrounding environment. The membrane works by being chemically very different from both the outside environment and the inside of the cell, which in both cases is mostly water. The membrane is fatty so repels water.

Proteins are the molecular machinery that forms much of the cell structure and shape as well as carrying out many of the cell's routine tasks. Around a third of our genome codes for membrane-embedded proteins. But because these membrane-proteins are adapted for a life in the water-repelling cell membrane, they are very hard to study in laboratories which often rely on methods that hold proteins in water-based solutions.

In this thesis, we focus particularly on the parts of the protein that are embedded in the water repelling membrane. We computationally analysed the biochemical make-up of thousands of proteins from openly available biological databases.

This thesis demonstrates three features of membrane proteins:

- the radically different evolutionary story that membrane-bound regions have compared to other proteins; the sacrifices they make for their stability in order to maintain their function, and their optimisation through evolutionary timescales to adapt to the membrane as best they can.
- a distinct sub-group of membrane-proteins that have a radically different membrane-insertion mechanism (tail-anchored proteins) have adaptations in their membrane regions depending on where they are located in the cell.
- some types of membrane proteins may use several membrane elements to ensure the least stable, but functionally important, elements are correctly inserted into the membrane.

These results will go on to inform more specific studies about membrane proteins. These findings will provide insight into the causes of some genetic diseases as well as drug targets in the case of pathogenic infections and cancers.

# **Declaration**

No portion of the work referred to in the thesis has been submitted in support of an application for another degree or qualification of this or any other university or other institute of learning.

# Copyright Statement

- i. The author of this thesis (including any appendices and/or schedules to this thesis) owns certain copyright or related rights in it (the “Copyright”) and s/he has given The University of Manchester certain rights to use such Copyright, including for administrative purposes.
- ii. Copies of this thesis, either in full or in extracts and whether in hard or electronic copy, may be made **only** in accordance with the Copyright, Designs and Patents Act 1988 (as amended) and regulations issued under it or, where appropriate, in accordance with licensing agreements which the University has from time to time. This page must form part of any such copies made.
- iii. The ownership of certain Copyright, patents, designs, trade marks and other intellectual property (the “Intellectual Property”) and any reproductions of copyright works in the thesis, for example graphs and tables (“Reproductions”), which may be described in this thesis, may not be owned by the author and may be owned by third parties. Such Intellectual Property and Reproductions cannot and must not be made available for use without the prior written permission of the owner(s) of the relevant Intellectual Property and/or Reproductions.
- iv. Further information on the conditions under which disclosure, publication and commercialisation of this thesis, the Copyright and any Intellectual Property and/or Reproductions described in it may take place is available in the University IP Policy (see <http://documents.manchester.ac.uk/DocuInfo.aspx?DocID=487>), in any relevant Thesis restriction declarations deposited in the University Library, The University Library’s regulations (see <http://www.manchester.ac.uk/library/aboutus/regulations>) and in The University’s Policy on Presentation of Theses.

# Acknowledgements

I would like to thank all members of both the Eisenhaber research group, as well as the Curtis and Warwicker research group for their interesting and engaging discussions throughout my PhD. In particular, I would like to acknowledge the patience, direction, and exceptional supervision from Dr Jim Warwicker of the University of Manchester along with Dr Frank Eisenhaber and Dr Birgit Eisenhaber from the Singapore Bioinformatics Institute. I also express my gratitude towards Dr Wing Cheong Wong and Dr Max Hebditch for working with me on many fiddly problems. I would also like to thank my advisor, Professor Stephen High, for his stimulating discussions and guidance throughout the project.

I also thank the University of Manchester and the ARAP programme at the A\*STAR for funding the project.

I thank my parents Janet and Martin, my brother Tim, and my partner Emily for their unwavering support of me in undertaking a PhD based for two years on the other side of the planet. Being so far from my family and loved ones was certainly the most challenging part of this process.

# Chapter 1

## Introduction

Membrane biology is a huge and varied field that is ultimately the study of the interface between compartments of the cell. The Transmembrane Protein (TMP) group include some of the most critical to life proteins as well as a large number of drug targets. However, the experimental inaccessibility of the Transmembrane Helix (TMH) has hampered the progress of study compared to their globular structural analogues. Despite progress over the last decade, the understanding of the relationship between the sequence and function of a TMH is incomplete.

In this chapter we will place the TMH problem in context, discuss some of the tools and methods that allow us to analyse the TMHs, describe the important biological aspects of the TMH, and discuss other membrane spanning protein segments.

### 1.1 Transmembrane proteins

#### 1.1.1 A brief history of the discovery and exploration of the transmembrane proteins

Due to the ability to segregate biochemical environments, the cellular barrier and resultant compartmentalisation has been described as one of the fundamental pillars of life as we know it [1, 2].

The significance of the cellular barrier was first noted in 1665 with the dawn of the microscope, when Robert Hooke described the cell wall of the cork plant (Figure 1.1A), with the clear distinction of the barrier giving rise to the term “cell” [3, 4].

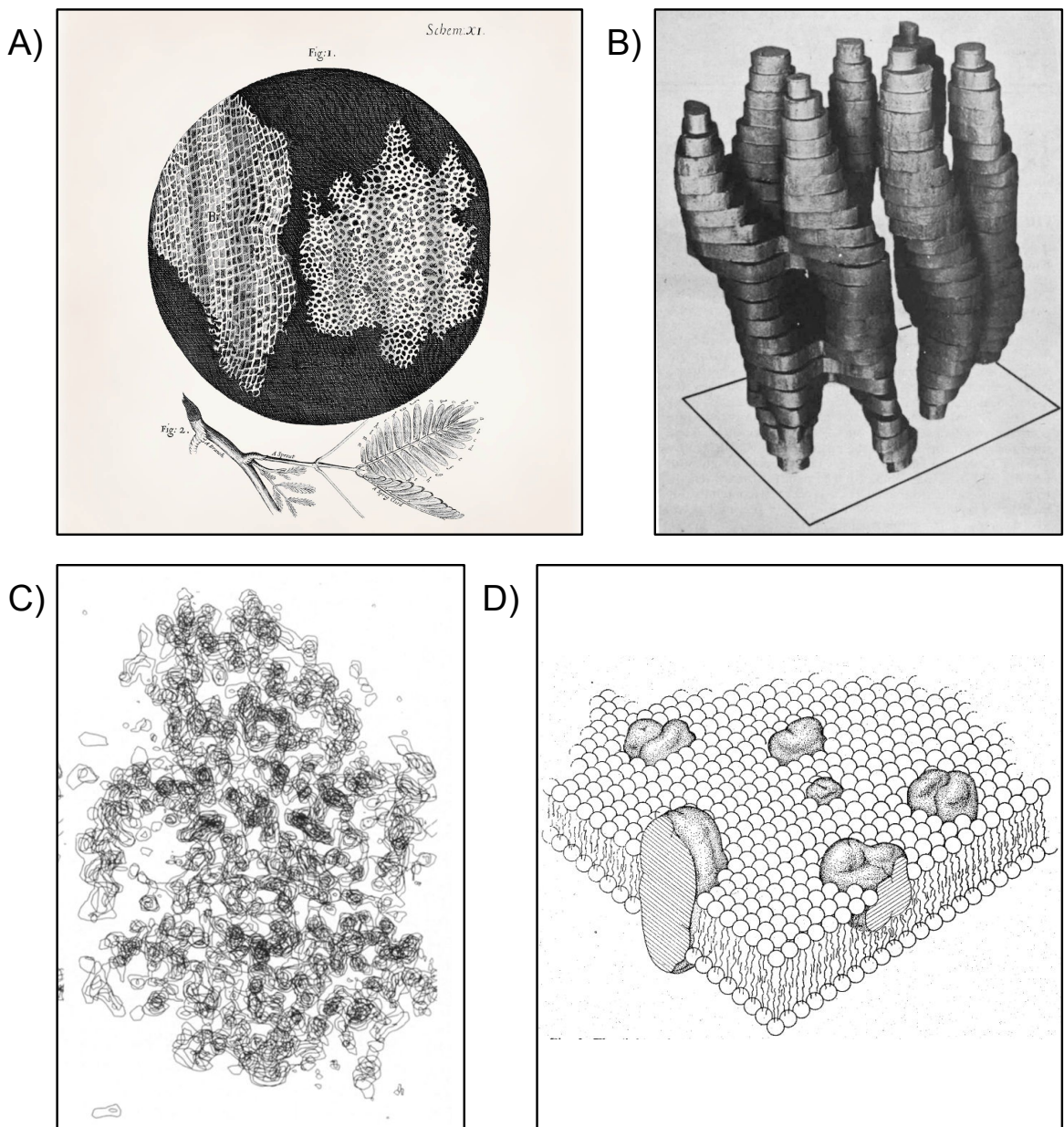


**Figure 1.1: A selection of figures demonstrating important discoveries of membrane proteins and their environment.** A) (Above/“Fig 1”) A diagram of the cork plant as viewed through an optical microscope drawn by Hooke circa 1665. Note the observable cellular barrier between what we now know to be the plant cells. (Below/“Fig 2”) The cork plant used in the microscope observations. From Hooke, republished in 1961 [4]. B) The first near-atomic resolution ( $7\text{\AA}$  resolution map) structure of a TMP acquired by Electron Microscopy (EM). This is a model of the 7Transmembrane (TM) bacteriorhodopsin single protein from the purple membrane viewed roughly parallel to the plane of the membrane. From Henderson & Unwin, 1975 [5]. C) The electron density map of the first crystal structure of a TMP [6]. The image shows 11 layers with contours representing  $1.2\text{\AA}$  between layers at  $3\text{\AA}$  resolution. As in B, this structure is from phototrophic purple bacteria. The chromophores are made up of cytochrome (can be seen at the top of the image) and the H-subunit (which can be seen at the bottom). From Deisenhofer *et al.*, 1984. D) The first drawing in which the fluid mosaic model was presented in the bilayer. From Singer & Nicolson, 1972 [7]

Throughout the early 20th century several theories were explored regarding the

composition of the membrane. In 1925, by scrutinising the concentration of chromocytes in the blood, and the surface area of the cells in blood from a variety of mammals Gorter and Grendel concluded that: “chromocytes are covered by a layer of fatty substances that is two molecules thick” [8]. This established the awareness of the lipid bilayer. Later, the popular Danielli and Davson model correctly identified a phospholipid bilayer, however also incorrectly suggested a lipoid space existed within the phospholipid bilayer [9]. Eventually, as these ideas were explored, the fluid mosaic model was established in 1972 (Figure 1.1D) [7]; the membrane has a fluid behaviour, due to the gel-like nature of its composition, which allows proteins to move throughout the membrane bilayer.

In order to fully understand the relationship between TMPs and the membrane, molecular details would be needed. By the 1970s, reasonably detailed structures of membrane-spanning segments of TMPs were available by EM [5] (Figure 1.1B). However, the real goal was to have the atomic resolution available. The advent of x-ray crystallography through the first half of the 20th century showed that it was possible to solve atomically resolved structures of small organic molecules [10, 11] and larger proteins such as a steroid [12], penicillin [13], and vitamin B12 [14]. Dorothy Hodgekin was awarded the Nobel prize for chemistry in 1964 for the elucidation of these complex structures [15]. Seven years after the creation of the Protein Data Bank (PDB) [16], the first TMP was successfully solved by x-ray crystallography in 1984 [6] (Figure 1.1C). Because of this discovery Johann Deisenhofer, Robert Huber, and Hartmut Michel won the Nobel prize in chemistry in 1988 for solving with atomistic resolution the 3D structure of a photosynthetic reaction centre [17]. In the following decades, x-ray crystallography of TMPs, despite the challenges therein, remained the predominant method of elucidating the structures of TMPs [18]. Currently, we are in a revolution of TMP structural acquisition, which will be discussed further in section 1.1.4.

### 1.1.2 Transmembrane proteins in disease

Membrane-bound proteins underpin almost every biological process directly, or indirectly, from photosynthesis to respiration. Integral TMPs are encoded by between a third to a half of the genes in the human genome [19–21] and account for 40% of drug

targets [22] which reflects their biological and physiological importance. TMPs allow biochemical pathways that traverse the various biological membranes used in life, either by transporting molecules or transducing signals across the bilayer. Misfolding of these proteins during the complex process of translocation is common in both normal and diseased cells [23]. The mechanisms of folding are actively studied even recently revealing new systems of translocation, such as the role of the ER Membrane protein Complex (EMC) in both co-translational [24] and post-translational [25] TMP integration. Mutations tend to cluster in the TMH regions of the genes [26], which can cause the misfolding. Glycine to arginine mutations occur statistically more frequently in TMHs compared to their globular  $\alpha$ -helix counterparts [27]. This can result in a range of diseases including but not limited to: cystic fibrosis caused by mutations in the cystic fibrosis conductance regulator [28], Charcot-Marie–Tooth disease caused by mutations in the PMP22 gene [29] and the connexin 32 gene [30], diabetes insipidus caused by mutations in the aquaporin 2 water channel [31], retinitis pigmentosa caused by a point mutation in rhodopsin [32], and Niemann-Pick disease for which there are over 200 disease-causing mutations identified [33–36].

### 1.1.3 The transmembrane protein problem

Studying TMPs in a laboratory typically presents several challenges not so often faced when investigating their globular counterparts which are pointed out in a review by Seddon *et al.*, 2004 [37]. TMPs are typically difficult to obtain in a useful quantity. They do not exist in high enough quantities naturally, and overexpression often results in aggregation in the cytoplasm due to the hydrophobic nature of the TMHs. Also, the complexity of their native environments limits structural studies. Even relatively simple lipid bilayers cannot be probed by conventional structural techniques, so study in the native state by traditional structural methods is difficult and involves suspending the protein in detergent or lipid environments, leading to difficulties in sample preparations. Their insolubility in aqueous solutions also leads to the requirement of specialised synthetic *in vitro* systems which have been difficult to introduce purified proteins into [37].

In addition to the practical difficulties in studying TMPs, it has become clear that they have a rich structural diversity. Throughout the 1990s the concept of a TMH

was simple and fairly assured: they were greasy peptides of around 30Å in length, often bundled together and oriented perpendicularly to the membrane [38]. By 2007, crystallography had elucidated 368 TMP structures from 148 unique proteins [18]. Whilst this accumulation of structures was growing exponentially, at the same time, there were in excess of 50,000 protein structures in the PDB. What became clear when examining the newly available large number of TMPs was that although the classic TMH structures were broadly prevalent, these structures contained a plethora of unusual TMHs [38]. Transmembrane Segment (TMS)s are capable of partial spanning of the membrane, spanning using oblique angles, and even lying flat on the membrane surface [38, 39]. The classical model was incomplete. Even recently, there is a contingency in the TMP biology field that despite progress over the last decade there is still a lack of information regarding the relationship between TMH sequences and function, TMH structure, intra-membrane TMP assembly, and the behaviour of TMHs in the lipid bilayer; the native biological environment of TMHs [1].

Furthermore, the insertion and formation of the unusually orientated TMHs and of the more traditional TMHs have been shown to be underpinned by complex thermodynamic equilibrium and electrostatic interactions [40–42]. As well as being a biophysically convoluted system, TMHs are biologically functional beyond anchoring in many cases. TMSs have been identified as regulators of protein quality control and trafficking mechanisms, shifting the idea away from TMHs exclusively functioning as anchors [43], and crucially this function beyond anchoring can be revealed by sensitive analysis of the sequence information alone [44, 45].

There is also an issue of silent homology extension from  $\alpha$ -helices [46]. TMHs often share sequence composition similarities due to membrane requirements and restraints, not necessarily due to common ancestry which underpins homology-based domain libraries like Pfam [47] and SMART [48]. It was found that between 2.1% and 13.6% of Pfam hits for Signal Peptide (SP)s or TMSs are positive hits that were misreported as homologous among distantly related proteins in Pfam [46].

#### 1.1.4 The transmembrane protein revolution

Over the last decade or so, several significant steps have been made toward overcoming the challenges in solving the structures of TMPs. Firstly, improvements in expression

and purification occurred thanks to cleavable green fluorescent protein (allowing protein tracking during purification) [49, 50] and antibody tagging for purification [51] at the colony level [52] greatly increased the throughput of TMP expression and purification.

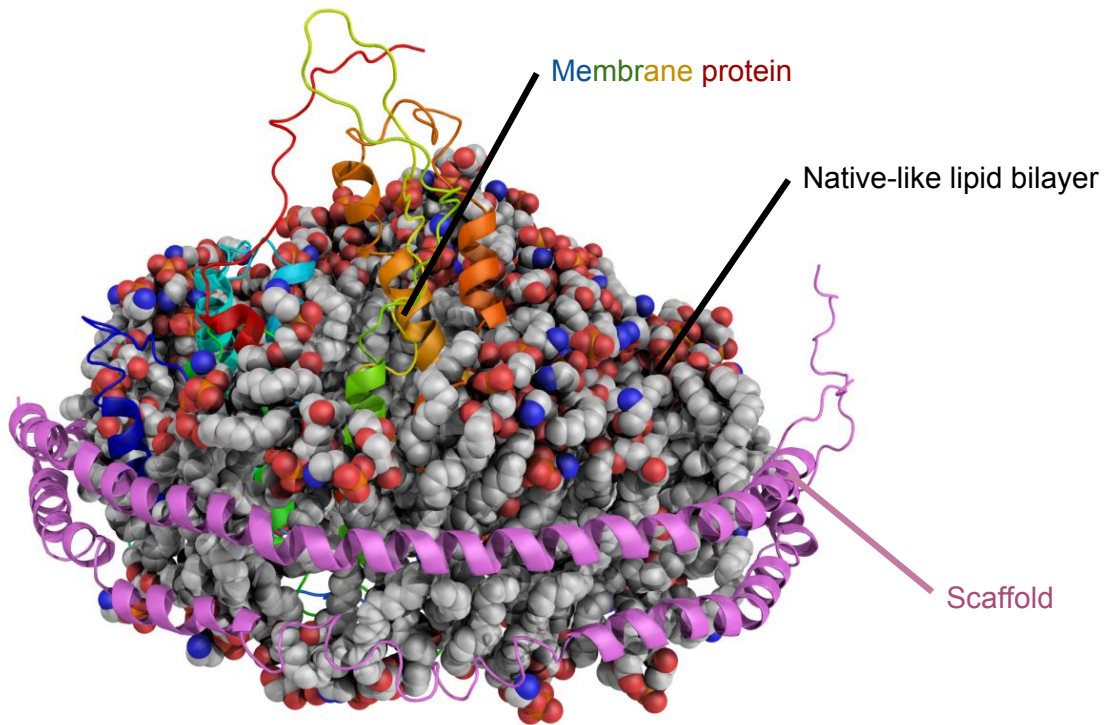


**Figure 1.2: The structure of SecYE in a nanodisc at near atomic resolution.** A single particle cryo-EM structure of SecYE in complex with the ribosome (not shown) with the TMHs held in a reconstituted nanodisc (PDB code 4v6m [53]). The resolution is 7.1 Å. The protein structure is depicted by a rainbow coloured cartoon in the centre of the assembly. The lipids are modelled as spherical atoms coloured by atom (carbon and hydrogen are white, oxygen is red and nitrogen is blue). The peptide scaffold is shown in pink.

The folding of the TMP often depends on the lipid environment. Finding conditions that encourage protein stability was shown to improve crystallisation [18, 54]. The technology behind nanodiscs was originally published in 2002 [55]. The method was originally shown to be a viable method for obtaining native condition TMP crystals for cytochrome P450 [56]. The structure of the nanodisc is formed from two scaffold peptide helices wrapped around a group of self-associating phospholipids for which the composition can now be tuned [57] (Figure 1.2A). Nanodiscs have been routinely used to much more easily obtain crystal structures in native-like condition. Nanodiscs overcome some of the major challenges caused by the hydrophobic helices and a more faithful representation of the biological membranes than alternative model membranes

like liposomes which allows investigation into TMP-lipid interactions [58].

Still, the challenge remained of getting crystals of sufficient quality for x-ray diffraction. Although many TMPs readily formed low-resolution 2D crystals for cryo-EM [59, 60], and genome sequencing resulted in an exponential increase in structures derived from x-ray crystallography [61], the dependency on crystallising TMPs has always resulted in a hindrance.

In a full circle from the EM studies of the fluid mosaic model in the 1970s [7], once more EM techniques were applied to TMPs albeit now in single molecule systems. This method escapes the need for TMP crystals [59]. The resolution and dynamics of structures have been captured in unprecedented detail in EM systems in recent years thanks, in part, to the development of direct electron detectors which are radiation hardened CMOS sensors that have deposed as the highest quality EM method plate cameras and CCD detectors [62]. The elucidation of the sub 3Å structures utilising this method [63, 64] have exceeded the near atomistic resolutions that were called a revolution in TMP biology not a year earlier [65].

### 1.1.5 The role of bioinformatics in transmembrane biology

Due to the experimental difficulties of working with TMPs, often it is only possible to experiment on the TMPs *in silico*, or at least common tasks that would involve expensive time-consuming processes become relatively cheap and non-time-intensive.

Traditionally, the role of bioinformatics has been to predict TM regions of a protein. There are countless methods that can perform this. Many rely on statistical patterns to identify TMHs such as the neural network approach of MEMSAT3 [66] and the Hidden Markov models used in TMHMM [67], HMMTOP [68], S-TMHMM [69], OCTOPUS [70], Phobius [71]. Unsatisfied with a statistical approach, Scampi seq [72] uses a first principles method following the Kyte & Doolittle suggestion 26 years previously that a biophysical scale can predict TMHs [73] and applies a score based on the von Heijne biological scale [74] (scales described in section 1.3.2). Predicting the presence of a typical TMH based on a protein sequence is currently a fairly trivial task and typically relies on a consensus of several prediction programs, such as the automated TRANSMEM annotation used by UniProt [75]. Yet several challenges remain in separating SPs from TMHs [76] and correctly predicting the topology of a

TMP. Generally, topology prediction algorithms score, using various scoring methods, the likelihood of all possible combinations of TMH topologies within the TMP, and pick the highest scoring viable conformation.

Due to the under-representation of TMPs among protein structures, understanding the biochemical role TMHs play within the membrane from sequence alone is often desirable. As more data is becoming available, bioinformatic methods that use multiple biochemical traits are being developed. Sequence information entropy in conjunction with hydrophobicity can predict the presence of a functional role of the TMH beyond anchoring [44, 45]. Machine learning approaches have allowed prediction of which residues could be involved in pore lining from sequence alone [77]. Protein trafficking signals from a combination of hydrophobicity and charged residues may be involved in the localisation of TMHs belonging to post-translational Tail Anchor (TA) proteins [78].

Despite the advances in the availability of TMP structures over the last decade, most are obtained from membrane free environments via x-ray diffraction of crystals, single-molecule cryo-EM, and NMR techniques [59, 79]. The relationship between the membrane and TMPs is underpinned by complex thermodynamic and electrostatic equilibrium [40]. Although sometimes there are bound lipids and detergents included in the crystal lattice, or the TMPs are integrated into a micelle or bicelle environment this is often insufficient to account for the complex lipodynamics of the membrane-TMH interactions [79, 80].

There have been several approaches used to attempt to find a more biologically relevant structure contextualised in the membrane (Figure 1.3). OPM [83] and PDBTM [84] use simplified models of the membrane's hydrophobic environment to orientate the TMP into position. MemProtMD [79] uses explicit lipids, a phosphatidylcholine bilayer, in a flexible Molecular Dynamics (MD) simulation along with TMPs accessed from the PDB [82]. These approaches allow us to enhance our understanding of the TMP structures in the context of the membrane environment.

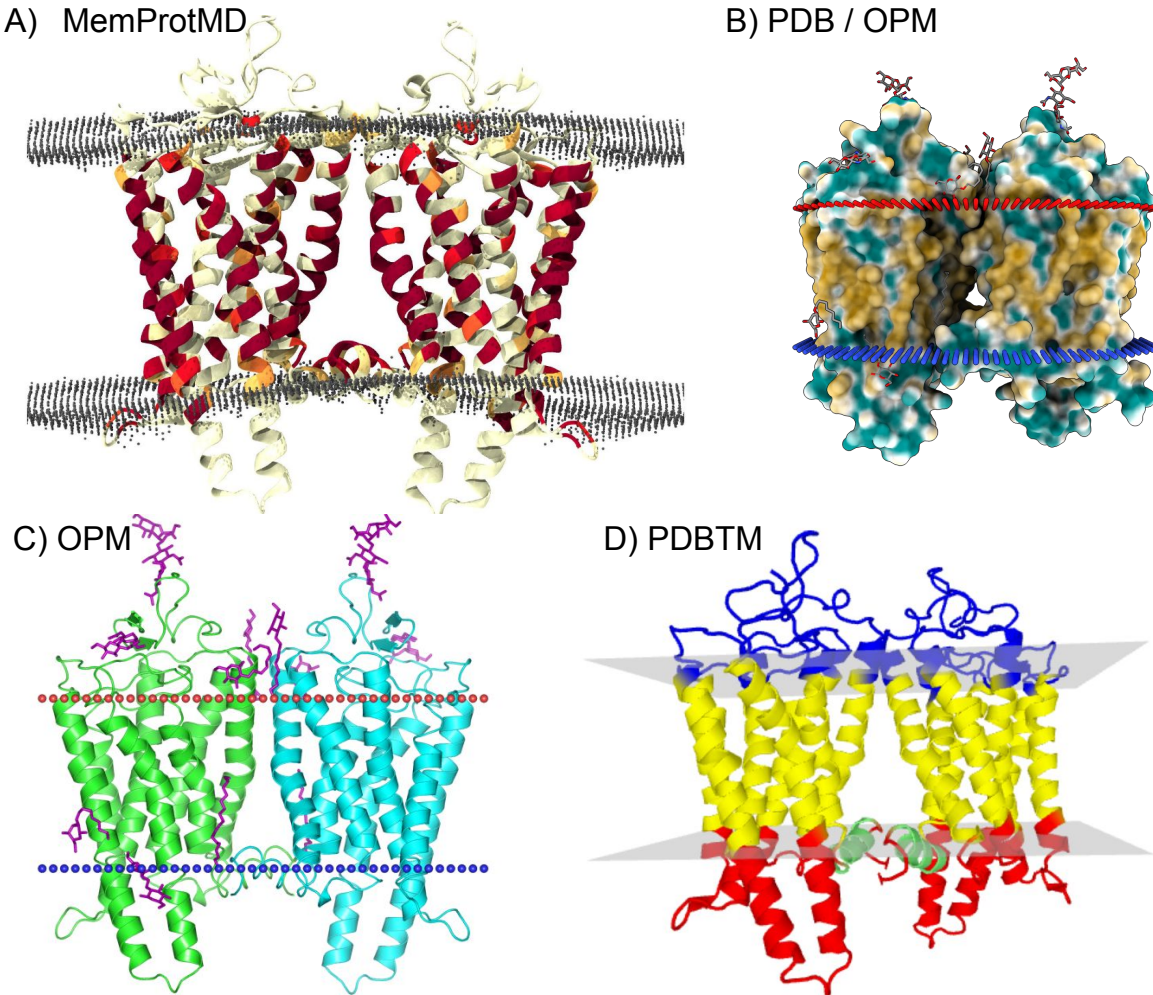


**Figure 1.3: A comparison of the raw outputs from commonly used structural transmembrane protein databases.** The example used here is a ligand-free G protein-coupled receptor (GPCR) rhodopsin (PDB 3cap) [81]. A) The structure held by MemProtMD [79]. A cartoon of the structure coloured according to hydrophobicity. Red indicates hydrophobic residues and the cream colour represents hydrophilic residues. Note the flexing and distortion of the membrane. B) The RCSB PDB [82] showing the hydrophobic patches on the surface (yellow is hydrophobic, cyan is hydrophilic) of the membrane proteins using OPM for topological orientation [83]. The blue lines indicate the cytoplasmic side whilst the red indicates the extracellular side. C) The cartoon structure of 3cap from OPM [83] coloured by the protein chain. Again, the blue lines indicate the cytoplasmic side whilst the red indicates the extracellular side. D) The PDBTM [84] record coloured by the TM regions predicted by TMDET [85] in yellow, intramembrane regions in green. In this case, the non-membrane components are coloured according to side 1 and side 2 rather than a topological prediction.

## 1.2 Biological membranes

### 1.2.1 Membrane lipids

It is critical to understand that the lipid bilayer and the transmembrane  $\alpha$  helices are inextricably linked. Often TMHs reflect the membrane environments they exist in, for

example, the hydrophobicity, asymmetry, and thickness of the membrane lipids are reflected when looking at large numbers of TMPs [86].

The lipid membranes influence the local structure, dynamics, and activity of proteins in the membrane in non-trivial ways [87, 88], as well as protein folding via repositioning of TMHs [89]. For example, cross-linking a  $\beta$  secretase, BACE, with lipid rafts revealed that protein activity is modulated by lipids [90]. Furthermore, bilayer deformations induced by rhomboid protease, a polypeptide cleavage protein, allow substrate access to the active site [91].

The lipids that make up these membranes are very diverse. Not only do different cells have different membrane compositions but so do different subcellular compartments which again is reflected in the TMH composition of TMPs [86, 92].

Individual lipid molecules consist of a polar head group and a hydrophobic region and so are described as being amphiphilic molecules. This factor, along with geometric constraints of the membrane lipids causes them to not only be insoluble molecules but also that they readily self-associate into complex ordered structures that have been demonstrated *in silico* with coarse grain MD simulations [93]. This self-association is entropically driven by water molecules. There is a rich variety of lipid molecules that make up the biological membranes. Furthermore, the bilayer maximises van der Waals interactions between the closely-packed hydrocarbon chains, which contributes to the stability of the bilayer. This can be seen even in relatively early MD simulations [94].

The majority of lipids in higher organism membranes are phospholipids, sphingolipids, and sterols. The hydrophobicity of a membrane lipid can be caused by several features; (i) aliphatic chains such as in the most abundant membrane lipids, glycerophospholipids and the sphingolipids, (ii) aromatic groups, or (iii) polycyclic structures such as the sterols most abundantly of which in mammals is cholesterol [95, 96]. Phospholipids are composed of a glycerol molecule. Bonded to the glycerol molecule are two hydrophobic fatty acid tail groups and a negatively-charged polar phosphate group. The polar phosphate group is modified with an alcohol group. Often these are represented as a polar head group with two fatty chains extending into the membrane, and a bilayer is formed from two sheets of these molecules with the polar headgroups facing outwards towards either side of the membrane and the fatty side chains filling the interior of the membrane space (Figure 1.1D).

It has been known for almost 4 decades that biological bi-layer membranes are asymmetric [7, 97]. For example, in the outer membranes of Gram-negative bacteria, the outer membrane leaflet contains lipopolysaccharide, whilst the inner is a mixture of approximately 25 phospholipid types [92]. Adding to the membrane asymmetry composition story, a thorough analysis of residue composition in yeast and human TMH regions revealed intra-membrane leaflet composition asymmetry in the Endoplasmic Reticulum (ER), but not the Golgi [86]. Furthermore, protein-lipid interactions have been shown to be determinants of membrane curvature [88], and undertake complex orientations and conformations to allow for hydrophobic mismatch [98].

### 1.2.2 Membrane potential

Simply put, membrane potential is the voltage across a membrane. If the membrane is permeable to a certain type of ion, then the ion will experience an electrical pulling force during the diffusion process that pulls toward the “preferred” biological location. This clearly depends on a chemical component involving both the charge and ion concentration gradient. There are various ways of estimating the membrane potential.

The Nernst equation can be derived directly from the simplified thermodynamic principles (i) the Boltzmann distribution, and (ii) a field charge interaction energy [99]. It is defined as:

$$E_m = \frac{RT}{zF} \times \ln \frac{c_{out}}{c_{in}} \quad (1.1)$$

Where charge  $E_m$  is the membrane potential,  $z$  is the ion charge,  $c$  is the concentration of an ion in that cell environment,  $R$  is the ideal gas constant,  $T$  is the temperature (Kelvin), and  $F$  is the Faraday constant per molecule.

However, the Nernst equation is rife with caveats caused by the assumptions of the simplified model. Such assumptions include ions having point charge and that the potential is constant throughout the solution. This issue is compounded because it assumes the constant potential is the same as the point of measurement which can be heavily influenced by, for example, a specific adsorption of either part of the redox pair or the competitive adsorption of a supporting ion in solution [99]. Considering that in biology the compartments always involve multiple ion channels and constant flux of biochemical environments, one should be cautious to understand the limitations and

variability when extrapolating experimentally determined  $E_0$  particularly when using such an idealised model in a biological context.

Several studies have attempted to quantify the various voltages across the intracellular membranes. Negativity was found in the ER, with a voltage between 75mV to 95mV in the ER membrane [100, 101]. Negativity was found in the mitochondrial matrix with a voltage across the mitochondrial membrane at 150mV [102]. No notable membrane potential has been identified in the Golgi [103, 104].

## 1.3 *$\alpha$ helices in the membrane; structure and function*

### 1.3.1 Transmembrane helix sequence composition

TMHs are  $\alpha$  helix structural elements of membrane proteins that span the membrane. Measurements of the TMH regions have found that they are roughly 20 residues in length;  $17.3 \pm 3.1$  from 160 TMHs [105],  $27.1 \pm 5.4$  residues based on 129 TMHs [106], 26.4 residues based on 45 TMHs [107],  $25.3 \pm 6.0$  residues based on 702 TMHs [108],  $24.6 \pm 5.6$  from 837 TMHs [109], and  $28.6 \pm 1.6\text{\AA}$  to  $33.5 \pm 3.1\text{\AA}$  from 191 proteins depending on membrane types [110]. There are a couple of reasons for this variation. Primarily is that the boundaries of TMHs are extremely hard to precisely identify since it is unclear exactly how far the TMH rises into the water interface region [38]. Secondly is that it is emerging that different membranes have different thicknesses [92] and that this is directly reflected in the hydrophobic lengths of the TMH [86, 110].

A study by Baeza-Delgado *et al.* from 2013 [109] looked at TMHs with known topology and structure in 170 integral membrane proteins from a manually maintained database of experimentally confirmed TMPs; MPTopo [112]. The group examined the distribution of residues along the TMHs. As expected, half of the natural amino acids are equally distributed along transmembrane TMHs whereas aromatic, polar, and charged amino acids along with proline are biasedly near the flanks of the TMHs [109]. It has been noted that transitions between the polar and non-polar groups at the ends of the hydrophobic core occur in a more defined edge on the cytoplasmic side than at the extracytoplasmic face when counting from the middle of the helix outwards [109].



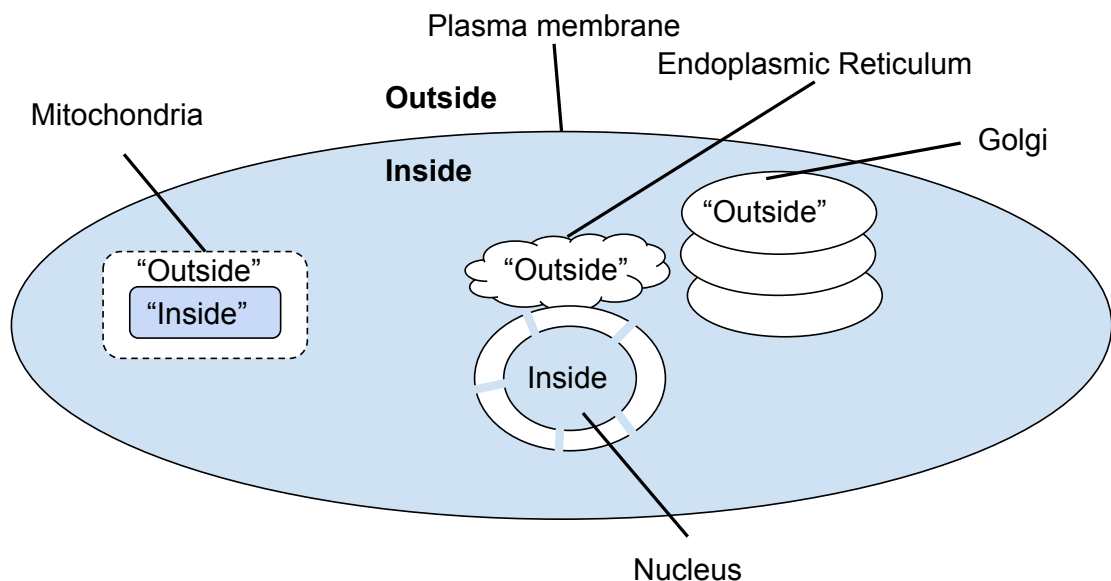
**Figure 1.4: A cartoon showing the general components of the membrane and a typical transmembrane helix.** The example used here for illustrative purposes is the transmembrane region of therein (PDB 2LK9) [111]. Dark grey areas denote the area of lipid head groups. The residues found in these areas are often described as flanking regions and are often in contact with the aqueous interface of the membrane. The helix core is mostly composed of hydrophobic residues. Although the regions labelled here generally hold true in terms of the statistical distribution of polar, non-polar, and charged groups, it is by no means absolute laws and many proteins break these “rules” [86, 109, 110].

This is probably reflecting the different lipid composition of both leaflets of biological membranes [109].

A previous study by Sharpe *et al.* from 2010 used 1192 human and 1119 yeast predicted TMHs that were not structurally validated to further explore the difference in TMH and leaflet structure by exploiting the evolutionarily conserved sequence differences between the TMH in the inner and outer leaflets [86]. The differences in consensus TMH structure implies that there are general differences between the membranes of the Golgi and ER. The abundance of serines in the region following the luminal end of Golgi TMSs probably reflects the fact that this part of many Golgi enzymes forms a flexible linker that tethers the catalytic domain to the membrane [86].

### The “positive-inside” rule

Two publications by von Heijne coined the “positive-inside” rule demonstrated the practical value of positively-charged residue sequence clustering in topology prediction of TMHs in bacteria [113, 114]. It was clearly defined and shown that positively-charged residues more commonly were found on the “inside” of the cytoplasm rather than the periplasm of *E. coli*. This holds true in the human, where the “inside” is the cytoplasm. In the case of the mitochondria, net positive charge was found to localise in the matrix [115] and so the intermembrane space is considered “outside” and the matrix can be considered “inside” (Figure 1.5).



Positively charged residues near the transmembrane regions of proteins cluster on the inside

**Figure 1.5:** A cartoon of the topological clustering of positively-charged residues near transmembrane helices in relation to subcellular location. First identified across the inner bacterial membrane from the periplasm to the cytoplasm, the “positive-inside” rule generally is in relation to inside the cytoplasm and outside the cell across the cellular membrane. The clustering pattern also applies to other cellular locations denoted by “inside” and their opposing environment across a membrane shown by the “outside” annotation. Throughout this thesis, “inside” and “outside” generally refer to inside and outside the cytoplasm unless explicitly stated otherwise.

More recently still, large-scale sequence analysis of TMHs from different organelle membrane surfaces in eukaryotic proteomes, show the clustering of positive charge being cytosolic [86, 109, 110].

### The aromatic belt

Tyrosine and tryptophan residues commonly are found at the interface boundaries of the TMH and this feature is called the “aromatic belt” [86, 109, 116–118]. Not all aromatic residues are found in the aromatic belt; phenylalanine has no particular preference for this region [117, 119]. However, it remains unclear if the aromatic belt is to do with anchoring or translocon recognition [109].

A study of conserved tryptophan residues during folding of integrin  $\alpha II\beta 3$  TM complex demonstrated the anchoring effects of tryptophan (0.4 kcal/mol contribution to membrane stability) in TMHs is greater than the other residues [120]. It was suggested that the wide amphiphilic range (the stabilising energetic contribution in either hydrophobic or polar sites) of tryptophan complements the heterogeneity and asymmetry of mammalian membrane lipids in particular.

Phenylalanine, although aromatic, is hydrophobic, and unlike tyrosine and tryptophan is typically found in the transmembrane part rather than the interfacial parts of TMHs.

The tyrosine side chain is a 6-carbon aromatic ring with an OH group attached. Tryptophan has two aromatic rings that contribute to a large hydrophobic ring-structure. The aromatic rings of tryptophan and tyrosine are buried close to, or within, the hydrophobic core, while the hydrophilic portion can interact with the polar lipid head-groups at the interface between the lipids and the water environment. Other factors such as the aromaticity, size, rigidity and shape of tryptophan, rather than its dipolar character, has also been suggested as the primary reasons for its interfacial preference and indeed interfacial localisation preference could be the result of a combination of all of these factors [121].

### Snorkelling

Broadly speaking, TMHs are non-polar. However, some contain polar and charged residues in the helix itself. Whilst this might seem thermodynamically unstable at first glance, a molecular dynamic feature called the “snorkel” effect explains in part how this is possible [122, 123]. Simply put, the snorkelling effect involves the long flexible side chain of lysine reaching out of the inner core of the membrane environment to the water interface region to interact with the polar head-groups of the bilayer even when

the  $\alpha$  helix backbone is pulled into the hydrophobic layer [124]. This has also been suggested to allow helices to adapt to varying thicknesses of the membrane [125]. More recently it was found that although in simulations the energetic cost of arginine at the centre of the TMH is large, *in vivo* experimentation with the Sec61 translocon reveals a much smaller penalty [126]. That same study also found that in MD simulations, snorkelling, bilayer deformation, and peptide tilting combined to be sufficient to lower the thermodynamic stability penalty of arginine insertion so that hydrophobic TMHs with a central arginine residue will readily insert into the membrane.

### 1.3.2 The hydrophobicity of transmembrane segments

Perhaps the most prevalent and important feature of the transmembrane regions is the membrane-spanning region which is composed mostly of non-polar residues. The importance of hydrophobicity on the effectiveness of membrane anchoring has been known for some time [127]. More recently the hydrophobic group region has been associated with cell localisation and a broad range of biochemical functions [45, 86, 128]. Once inserted the protein does not leave the membrane as a result of the TMH being very hydrophobic. This hydrophobicity of TMHs and the hydrophobicity of the lipid tails means that they self-associate and this association is entropically driven by water. Another way of describing it is that they dissociate from the water. The overall  $\Delta G$  for an ideal TMH in the membrane is -12 kcal/mol [40]; the association of the helix in the membrane is typically spontaneous but complex owing to interactions with other TMHs in the membrane as well as TMP-lipid interactions.

Over the last 50 years or so, there have been many attempts to use hydrophobicity scales of residues to predict structural classifications of proteins. Due to the vast amounts of scales, major efforts have been made to compare them to identify which ones are better for which tasks of identifying structural elements [129, 130]. Simm *et al.* 2016 [129] compared 98 scales and found that the accuracy of a scale for secondary structure prediction depends on the spacing of the hydrophobicity values of certain amino acids but generally that the methods behind the scales do not affect the separation capacity between  $\beta$  sheets or  $\alpha$  helices.

Throughout this thesis, several scales are used to evaluate and estimate the hydrophobic values of peptide chains. All the scales aim for quantifying the hydrophobic

values of each residue. There are several key differences in their methodology, assumptions, and aims. Ultimately, all the scales are attempting to allow estimation of  $\Delta G_{whf}$ ; the free energy of a folded helix ( $f$ ) from the water ( $w$ ) into the membrane core ( $h$ ). This free energy measurement is regarded as being currently experimentally inaccessible [40].

Although as a trend most of the scales agree, because of the methodological differences, there are indeed variations of values even after normalisation. Due to these discrepancies, it is preferable and typical amongst the literature to use several scales to verify the observable trends resulting from interpretation from an individual scale. Notably, one of the classic scales, Kyte & Doolittle Hydropathy scale shows a striking similarity to the modern Hessa's  $\Delta G_{app}^{aa}$  scale, and that generally the "better" scales for TMH prediction count proline as hydrophilic, and focus on helix recognition rather than amino acid analogues [130]. Several of the scales used throughout this thesis are overviewed below.

### Kyte & Doolittle hydropathy scale

The Kyte & Doolittle scale [73] is based on the water–vapour transfer free energy and the interior-exterior distribution of individual amino acids determined in previous investigation [131]. Kyte & Doolittle gave a composite score to each amino acid based on evidence from previous experiments in the literature, scaling them between -4.5 and +4.5. These experiments included the molal volumes of model compounds for the side-chain R groups [132–134], the water vapour partition coefficients [132, 135], and water-ethanol transfer free energies [136, 137]. However, alanine, tyrosine, leucine, and proline scores were subjectively modified. The authors found it difficult to accept that the single methyl group from alanine would have more hydrophobic force than leucine, which contains 4 methyl groups so the score was arbitrarily lowered to halfway between the originally determined score and the score of glycine. Tyrosine and leucine had their hydropathy values raised to one closer to the water vapour transfer free energy than experimental data suggested. In the case of proline, no suitable model existed and it tends to become buried, indicating that it is fairly hydrophilic. However, because it contains three methyl groups, the score considers it more hydrophobic than the experiments suggested. The authors stated: "None of these last 3 adjustments,

the result of personal bias and heated discussion between the authors, affects the hydropathy profiles in any significant way” [73]. Arginine represents the bottom of the scale, arbitrarily set at -4.5.

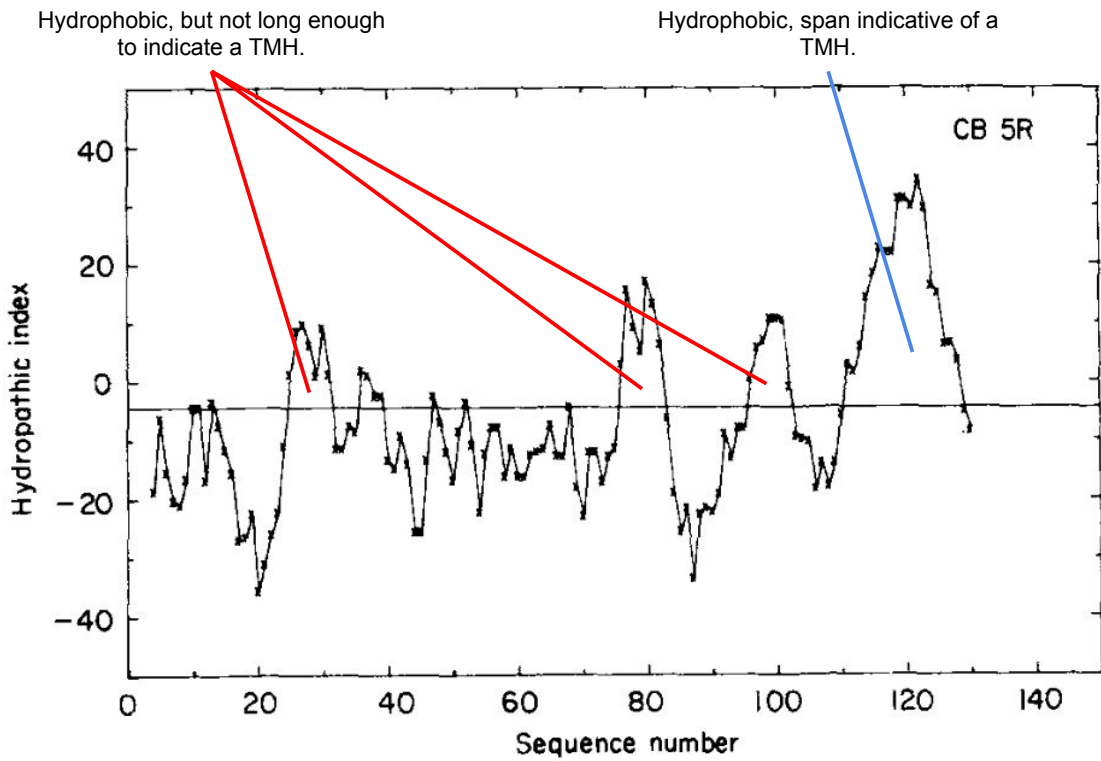


**Figure 1.6: The hydropathic index of rabbit cytochrome b5.** The hydropathic index according to the Kyte & Doolittle scale [73] is given on the vertical axis and the sequence number is on the horizontal axis. Whilst there are several peaks above 0, only one is sustained for around 20 residues near the c-terminal. Cytochrome b5 is a TA protein with an exceptionally polar TMH for an anchor [138], demonstrating the sensitivity of this method. Figure adapted from Kyte & Doolittle, 1982 [73].

An algorithm called SOAP was used to scan a window of  $\pm 10$  residues either side of each residue (allowing for half windows) across a protein to take the mean average of each position and plot them on a profile (Figure 1.6). Sustained areas of high hydrophobicity were indicative of a TMH [73].

### Hessa’s biological hydrophobicity scale

This is arguably the most biologically relevant scale [130] and is often called the  $\Delta G_{app}^{aaa}$  scale. The scale is based on an experimental method where the free energy exchange during recognition of designed poly-peptide TMH by the ER Sec61 translocon occurred [116]. These measurements were then used to calculate a “biological hydrophobicity scale.” The original study reported positional variance in some residues and is

strictly valid only for residues in the core of the TMH. A more refined study quantified the positional dependencies of each amino acid type [74].

### White and Wimley octanol – interface whole residue scale

This scale is calculated from two other scales; the octanol scale, and the interface scale [139]. This scale is fundamentally based on the partitioning of host-guest pentapeptides (acetyl-WL-X-LL-OH) and another set of peptides (AcWLm) between water and octanol, as well as water to Palmitoyloleoylphosphatidylcholine (POPC).

### The Eisenberg hydrophobic moment consensus scale

The Eisenberg scale is a consensus scale based on the earlier scales from Tanford [137], Wolfenden [140], Chothia [131], Janin [141], Wolfenden [142], and the von Heijne scale [143]. The scales are normalised according to serine [144]. The automatic TRANSMEM annotation currently used in UniProt is according to TMHMM [67], MemSat [66], Phobius [71] and the hydrophobic moment plot method of Eisenberg and co-workers [144].

### 1.3.3 Sequence complexity

Whilst identifying TMH presence in a protein is somewhat trivial with modern tools, the role a TMH plays within the membrane is more difficult to determine. Sequence properties that can be analysed by bioinformatics, the sequence information complexity and hydrophobicity, of the TMH have been used to predict the role of the TMH as either functional or structural, and as a discrete cluster from other SCOP-annotated helices [45]. Those findings demonstrated that the sequence of the TMH holds valuable information regarding biological roles, and forms the basis of our interest in the link between the polarity of a helix and functional activity beyond structural anchoring.

TMSOC's z-score is able to distinguish between functionally active TMHs and those only associated with anchoring [44, 45]. This was determined with the annotation of TMHs from the UniProt database (303 membrane anchors and 1741 functional TM helices) from UniProt [75] and tested with 181132 TMH sequences. Two peaks can be observed when stratifying the hydrophobicity and the sequence complexity of the

TMHs (Figure 1.7). These peaks correspond with the “simple” and “complex” TMH annotation.

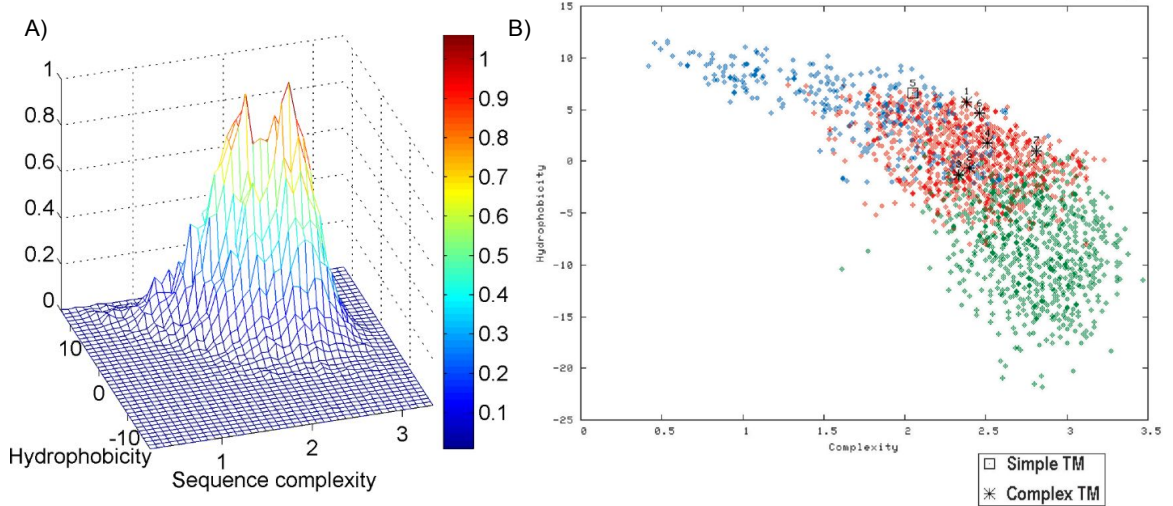


**Figure 1.7: The hydrophobic-complexity continuum distinguishes between transmembrane helix anchors and those with function beyond anchoring.** A) Two distinct points can be observed when plotting sequence complexity on the x-axis, frequency on the y-axis, and hydrophobicity on the z-axis of TMHs from UniProt. These peaks were shown to correspond to the membrane anchor and functional TMH populations. From Wong *et al.*, 2011 [44]. B) The  $\alpha$  helix hydrophobicity complexity continuum stratified by hydrophobicity (vertical axis) and complexity (horizontal axis). In blue are the membrane anchors, in red are the TMH with function, and in green are non-TM  $\alpha$ -helices from SCOP [145]. Clear distinctions can be made between the 3 groups and in fact, a composite z-score of the distance of these two factors from the functional TMH group allows prediction of which group a TMH belongs to [44, 45]. From Wong *et al.*, 2012 [45].

The z-score is a product of both hydrophobicity and a Shannon like sequence entropy [44, 45] of the character string in the TMH. This term is described below in equation 1.2.

$$z(x_\Phi, x_c) = (-1)^s \left[ \frac{(x_\Phi - \mu_\Phi)^2}{\sigma_\Phi^2} + \frac{(x_c - \mu_c)^2}{\sigma_c^2} \right] \quad (1.2)$$

Where  $x_c$  and  $x_\Phi$  are moving window averages of c, the sequence entropy [146].  $\Phi$  is the White and Wimley hydrophobicity [139] for a given segment and  $\mu$  and  $\sigma$  are the mean and standard deviation of the sequence entropy and hydrophobicity of the functional TMH set, that is those TMHs containing active residues.  $s$  is set to equal to one if equation 1.3 is true, and zero otherwise.

$$\frac{x_\Phi - \mu_\Phi}{\sigma_\Phi} \geq -\frac{1}{\rho_{c,\Phi}} \frac{x_c - \mu_c}{\sigma_c} \quad (1.3)$$

Where  $\rho_{c,\Phi}$  is the correlation between sequence complexity and normalised hydrophobicity. Equation 1.3, above, is the normal to the regression line between that

can be read as in equation 1.4.

$$\frac{x_\Phi - \mu_\Phi}{\sigma_\Phi} = \rho_{c,\Phi} \frac{x_c - \mu_c}{\sigma_c} \quad (1.4)$$

Sequence entropy is essentially an estimate of the linguistic entropy of a string. In the context of biology can be thought of as an estimation of the non-randomness of a sequence. Sequence complexity can be used to analyse DNA sequences [147–149], however here we will focus on the analysis of the complexity of a sequence in protein sequences.

The SEG algorithm [146, 150] finds stretches of non-random amino acids; sub-segment regions of the protein which have the lowest probability of occurring. It uses a Shannon entropy-like term [151] which identifies regions with high information entropy density. It can distinguish between globular and non-globular regions of a protein sequence [150]. Furthermore, by altering the window lengths and thresholds SEG can be optimised to search for subtle compositional deviations, such as coil-coiled regions [152]. However, sequence complexity alone fails to fully discriminate in the low complexity high hydrophobicity search space of TMHs [46], hence the requirement for the hydrophobic scoring contribution (Figure 1.7).

## 1.4 Biogenesis of transmembrane proteins

### 1.4.1 An overview of translocation

In this thesis we focus on cotranslational protein translocation and insertion via the Sec pathway, and on the post-translational pathway of TA proteins in eukaryotic systems (Figure 1.8).

The Sec pathway is conserved across all life [153] and is facilitated by the heterotrimeric SecYEG (prokaryotic) and Sec61 $\alpha\beta\gamma$  (eukaryotic) translocons. SecYEG targets proteins to the Plasma Membrane (PM) (inner membrane) of bacteria. In bacteria, nearly all TMPs are inserted by either the Sec pathway via SecYEG machinery, or by the structurally unrelated the 5-fold more abundant YidC machinery [154, 155], and proteins can often use either pathway. Sec61 targets proteins to the ER of eukaryotic cells. Broadly speaking, these proteins translocate hydrophilic peptides

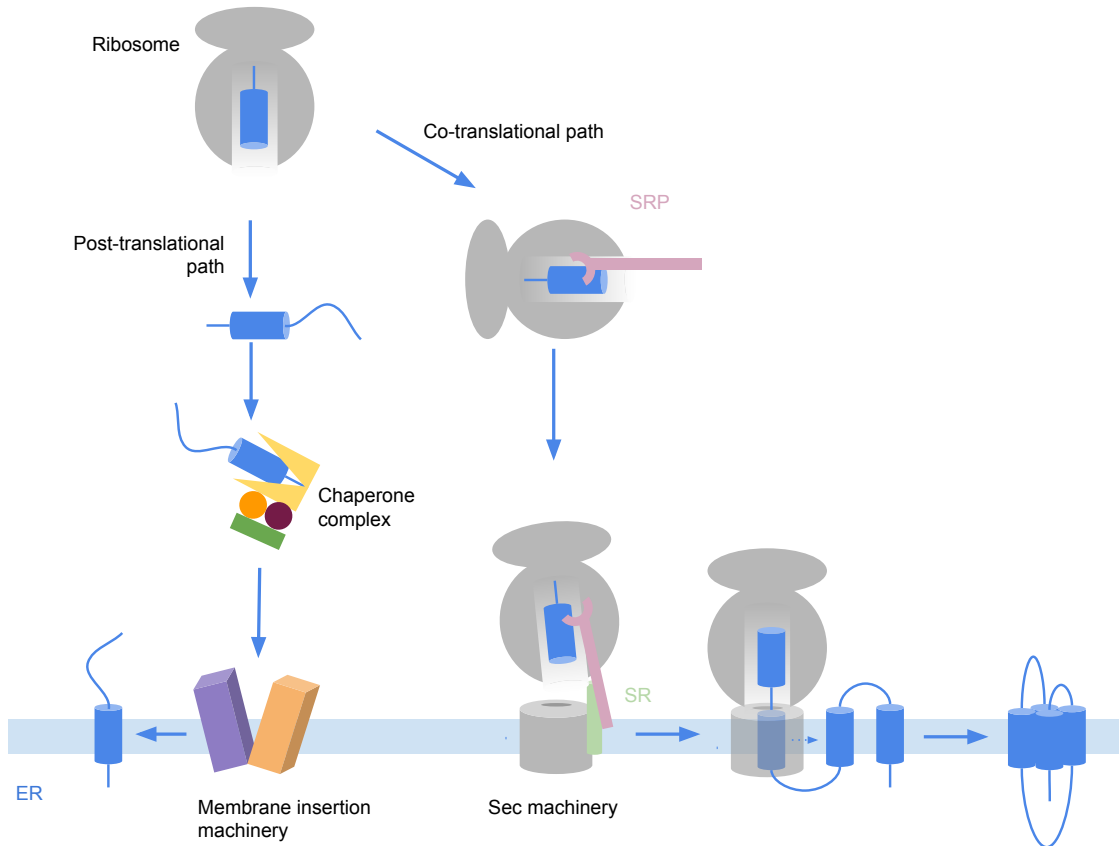


**Figure 1.8: A simplified schematic of the co-translational Sec pathway and the post-translational pathway.** The ribosome translates Ribonucleic Acid (RNA) to a nascent polypeptide chain. In the case of post-translational insertion (the left-hand-path), the nascent peptide is released, albeit briefly, to the cytosol. Chaperones of various types then shield the protein TMH and bring it into contact with various TM bound translocation machinery. In the case of co-translation (the right-hand-path), the Signal Recognition Particle (SRP) binds to the emerging signal sequence of the nascent peptide, which slows protein synthesis of the ribosome. SRP then targets the ribosome protein complex to the Signal Recognition Particle Receptor (SR), which then moves into contact with the translocon. As the nascent protein is inserted into the translocon, SR and SRP detach from the complex and translocation begins.

across a membrane whilst also integrating sufficiently hydrophobic sequences to the membrane [40, 128, 156, 157]. SecYEG and Sec61 also translocate soluble proteins. In bacteria, the SecY protein is partly encircled by SecE (Sec61 $\gamma$  in eukaryotes) which enhances its stability in the membrane [158]. SecG is made up of two TMHs and a cytosolic loop. It has been associated with SecA dependent translocation of secretory proteins [159, 160]. SecA is an ATPase and a membrane channel that can clamp translocating substrates above the SecY pore [161].

Whilst ultimately the translocon machinery is built of multiple subunits, the TM translocating protein itself is a 10 TMH protein with an hourglass-shaped interior pore [163] (SecY in prokaryotes or Sec61 $\alpha$  in eukaryotes). When translocation is not

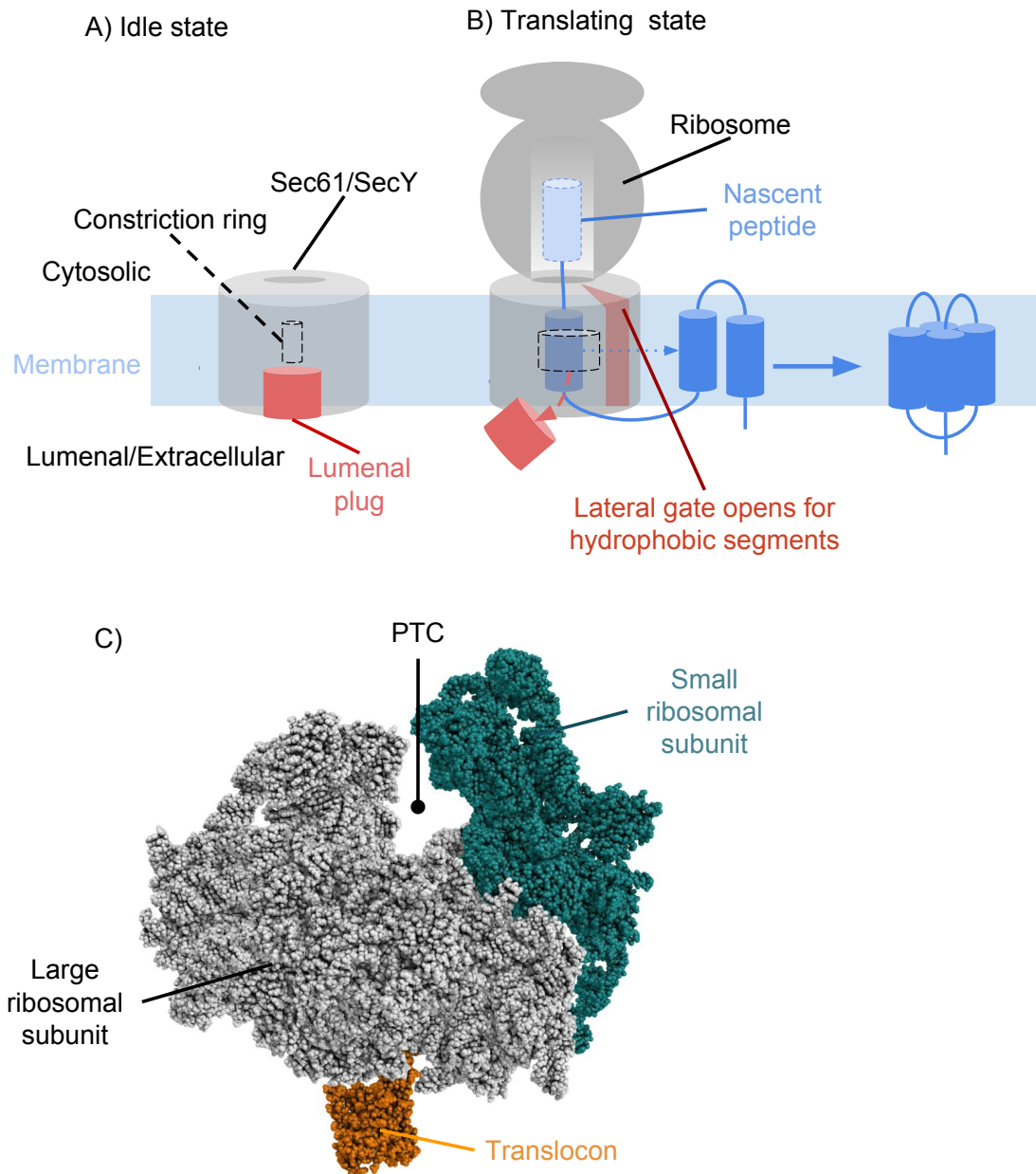


**Figure 1.9: The pore, the plug, and the lateral gate of the translocon.** A) The idle state of the translocon. The pore constriction ring is shown by a dashed transparent cylinder. The plug is in red and the translocon (SecY or Sec61) is in grey. B) The translocating state of the translocon coloured similarly to A, but the plug has moved to allow translocation through the channel, the constriction ring has widened, and the lateral gate opens to allow hydrophobic TMHs into the membrane environment. C) A sphere representation of the translocon-ribosome complex structure during translocation. Highlighted are the Sec61 translocon (orange) the ribosome made up of the large 60s subunit and the small 40S subunit and the peptidyl transferase centre (denoted by PTC), the site of translation (PDB 3J7R [162]). Part C redrawn from Voorhees *et al.*, 2014 [162].

occurring and the protein is idle, the hydrophobic core is constricted [128] and a luminal plug is in place over the pore resulting in a seal across the TMP pore [164,

165] that protects the membrane from ion flow [166] (Figure 1.9). SPs in elongation-stalled nascent chains crosslinked to the lipid and to the translocon machinery [167], showing that there may be a holding space which exposes the TMH to the membrane interfacial environment before insertion is complete and this was verified by more recent EM structural studies [156, 168].

During translation the 6-polypeptide single RNA ribonucleoprotein complex SRP binds to hydrophobic signal sequences, typically at the N-terminal of the nascent peptide, emerging from the ribosomal exit tunnel and translation elongation is slowed [169]. The SRP targets the ribosome-SRP complex to the target membrane (either the PM in bacteria or the ER in eukaryotes) [170, 171]. The SRP engages with the membrane-bound SR, which mediates the association of the ribosome and the translocon [172]. As the ribosome binds with the translocon and the signal sequence is released [173], SRP54 moves away from the ribosomal protein L23a [174], the nascent peptide is brought into proximity of the translocon [175] and translocation begins (Figure 1.8).

During translocation the plug exits the pore, the constriction ring is opened, and a lateral gate opens between TMH2 and TMH3, and TMH7 and TMH8 to integrate hydrophobic stretches of nascent peptide into the membrane [163, 168, 176–181] (Figure 1.9). Mutation experiments on these three features (the plug, constriction ring, and lateral gate) destabilised the closed state of the translocon and resulted in a protein localisation phenotype that suppressed inactivating mutations in signal sequences [182–185] and even caused transient channel openings in bacteria [186].

The EMC can act as a post-translational TA protein insertase [25]. Recently it was shown that the EMC was also able to act cooperatively with the Sec translocon during cotranslational insertion on a subset of multipass TMPs in both yeast and human cells [24]. Proximity specific ribosome profiling in yeast confirmed that the EMC engages the translocating multipass TMPs, especially those containing charged residues in the TMH. This would explain why it also interacts with TA protein TMHs [24, 25]. Pulldown experiments revealed that the EMC stabilised the synthesised TMPs and recruited chaperones (both substrate specific and general) that allowed unstable TMPs to achieve viable conformations allowing function in the ER and transport to the Golgi [24]. In the absence of the EMC, UPS (a proteasome) degrades the membrane proteins

[24]. This dual function of the EMC is analogous with YidC [24] in bacteria which has the role of an insertase [154, 155, 187] as well as interacting with SecYEG to stabilise translocated TMPs [188].

Additional proteins associated in cotranslational insertion during the TMP integration by Sec61 are the membrane-bound TRAP and TRAM protein complexes. TRAP, otherwise known as the translocon-associated protein complex, is a multi-subunit complex. The TRAP complex facilitates the translocation of TMHs by moderating the “positive-inside” rule, but does not seem to play a role in the integration of very hydrophobic TMHs [189]. TRAM, also called the translocating chain-associated membrane protein, is critical to the efficient translocation of TMPs [190], but has yet to be fully structurally solved [191]. During translocation, the association between TRAM, TRAP and the Sec61 translocon is strengthened [191].

Another group of proteins capable of Sec61 TMP integration are the membrane-bound Sec62 and Sec63 proteins. In mammals, these proteins associate with Sec61 and facilitate membrane integration independently from the SRP-ribosome complex [192]. Post translational translocation in this case involves ATP hydrolysis driven Hsp70 chaperones delivering the unfolded TMP [193, 194] to the Sec61-Sec62-Sec63 machinery [195]. It was shown using crosslinking and co-translational and post-translational translocation assays that SR displaces Sec62 which returns the Sec61 to the SRP dependent insertion pathway; Sec62 and ribosomal associations with Sec61 are mutually exclusive [196].

### 1.4.2 Signal peptides

SPs are short peptide sequences present at the N-terminus of most secretory pathway destined proteins in both prokaryotes and eukaryotes. Mutations to the length and composition of the SP revealed their composition is essential for effective localised transport, however, they have high compositional variability [197]. Like TMHs they translocate into the membrane due to their hydrophobic  $\alpha$  helix (albeit typically shorter than a TMH) and follow the positive-inside rule.

Once the protein is fully translocated and at the correct location within the cell, a three domain signal peptidase cleaves the SP from the rest of the protein. SPs can also be experimentally interchanged to proteins from different organisms to target them to

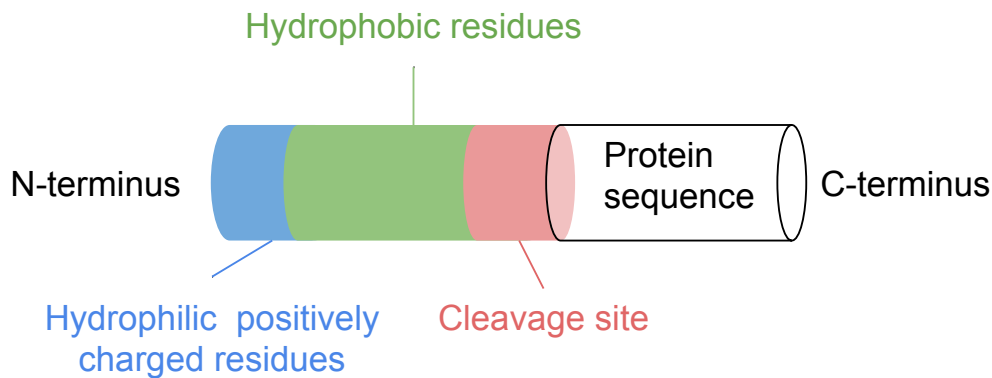


**Figure 1.10: The key components of a signal peptide.** Signal peptides consist of between 1-5 hydrophilic charged residues (in blue) at the N terminal, a 7-15 residue hydrophobic region (in green), and a c-region of 3-7 residues that invites cleavage by specific signal peptidase (in red). Redrawn from von Heijne, 1990 [198].

cellular locations [199, 200].

SPs are rarely used by TMPs with the exception of most type I TMPs, which are defined by the presence of an SP. Instead, TMPs use their first TMH and flanking region as a targeting signal. Many bioinformatic methods over the last twenty years have aimed to predict SPs and sort them from TMHs [201], however, these methods all struggle to distinguish SPs from N-terminal TMHs [76]. This is due to the similarities SPs have with TMHs, and that although TMHs are not cleaved, the cleavage site pattern alone cannot effectively separate SPs from TMHs. This results in many false positives for SP presence in genome-wide studies [76]. SignalP 4, a neural network based approach, is less effective at predicting cleavage sites or SP prediction in the absence of TMPs from the dataset, however currently is the most accurate method to distinguish the currently vague differences between TMHs and SPs [76].

### 1.4.3 $\beta$ sheets in the membrane

The membrane is critical in maintaining the separation of biochemically distinct compartments. However, there needs to be a flux of not only small molecules but also larger complex structures across these membranes in order to facilitate cellular life. Whilst the focus of this thesis is primarily on TMHs it is important to acknowledge that  $\beta$  sheets are another secondary structural element capable of spanning the membrane.

$\beta$  barrel proteins are present only in a few membrane types; the outer membrane of Gram-negative bacteria for which they constitute between 2-3% of the genome [205],

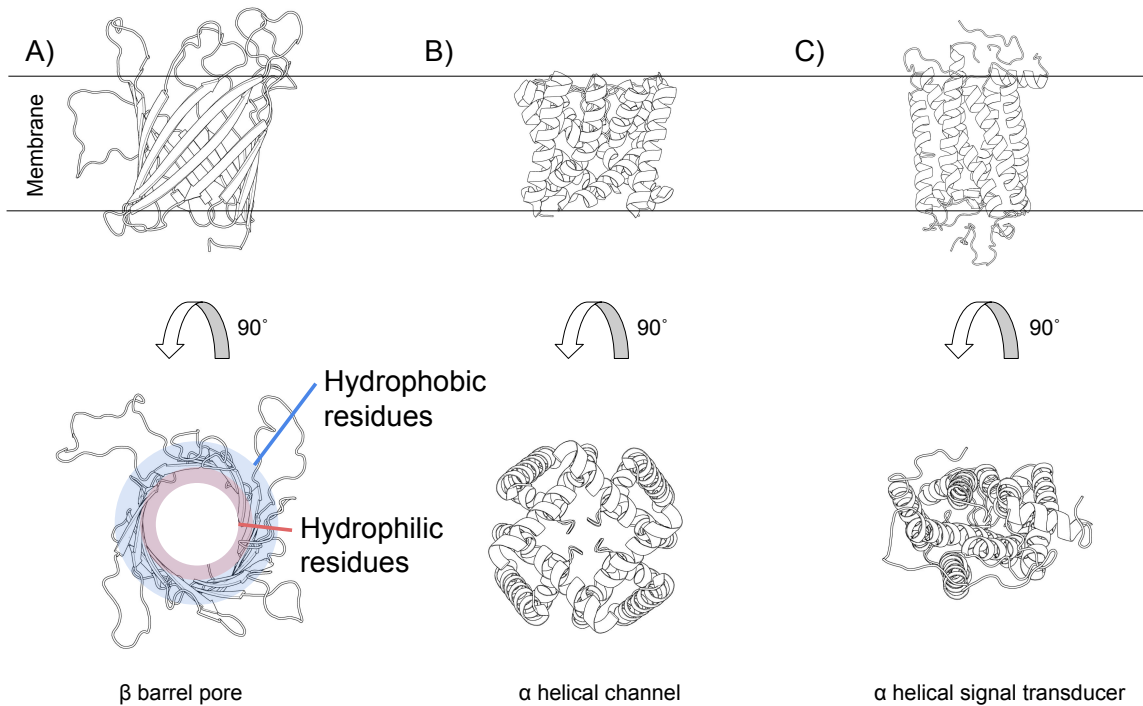


**Figure 1.11: Cartoons showing the structural differences of the outer membrane proteins, transmembrane helix channels, and transmembrane helix signal transducers in the membrane.** The top row shows the proteins traversing the membrane with the interfacial regions denoted by the black lines. A) A porous outer membrane protein using  $\beta$ -sheets to form a pore-forming protein structure. PDB code 2JQY [202]. B) A highly selective ion channel made up of membrane-spanning TMHs. PDB code 4HYO [203]. C) A 7-TMH GPCR that receives a signal on one side of the membrane which causes a conformational change influencing the structural arrangement of the tertiary structure on the opposing side of the membrane. PDB code 1F88 [204]. Note the pore in the  $\beta$  barrel protein not present in either the TMH channel or the TMH transducer.

and in the outer membranes of eukaryotic chloroplasts and the Mitochondrial Outer Membrane (MOM). Their restriction to these membrane types is the result of ancestral symbiogenesis [206–211].

These outer membrane proteins cause the membranes to be permeable, diminishing membrane potential between the outer and the inner membrane. Unlike the TMHs,  $\beta$  barrel proteins are permeable to water and many other small molecules often unspecifically due to their large pore (Figure 1.11). Integral  $\beta$  barrel proteins consist of between 8 and 26 amphipathic antiparallel  $\beta$  strands forming a cylindrical pore. They are capable of active and passive transport, molecule receptors, enzymatic catalysis, structural formation, and translocon machinery [205].

The biogenesis of  $\beta$  barrel membrane proteins also differs from that of TMHs, and there are differences between prokaryotic and eukaryotic cells. In Gram-negative

bacteria, the  $\beta$  barrel proteins are translated on cytoplasmic ribosomes (Figure 1.12). An N-terminal SP sequence allows the protein to pass through the inner membrane to the outer membrane [212, 213]. Instead of cotranslational insertion, SecB transports the nascent polypeptide chain to the Sec translocon on the inner membrane [214].  $\beta$ -sheets do not trigger the opening of the lateral gate [211]. Once in the periplasm, the SP is cleaved [215] and chaperones, such as the redundant SurA [216, 217], DegQ, and Skp [217], bind to the protein to prevent premature folding. Once at the inner surface, the BAM complex assembles and integrates the  $\beta$  barrel protein into the membrane [218, 219] via a lateral opening of one of the BAM subunits, BamA [220].

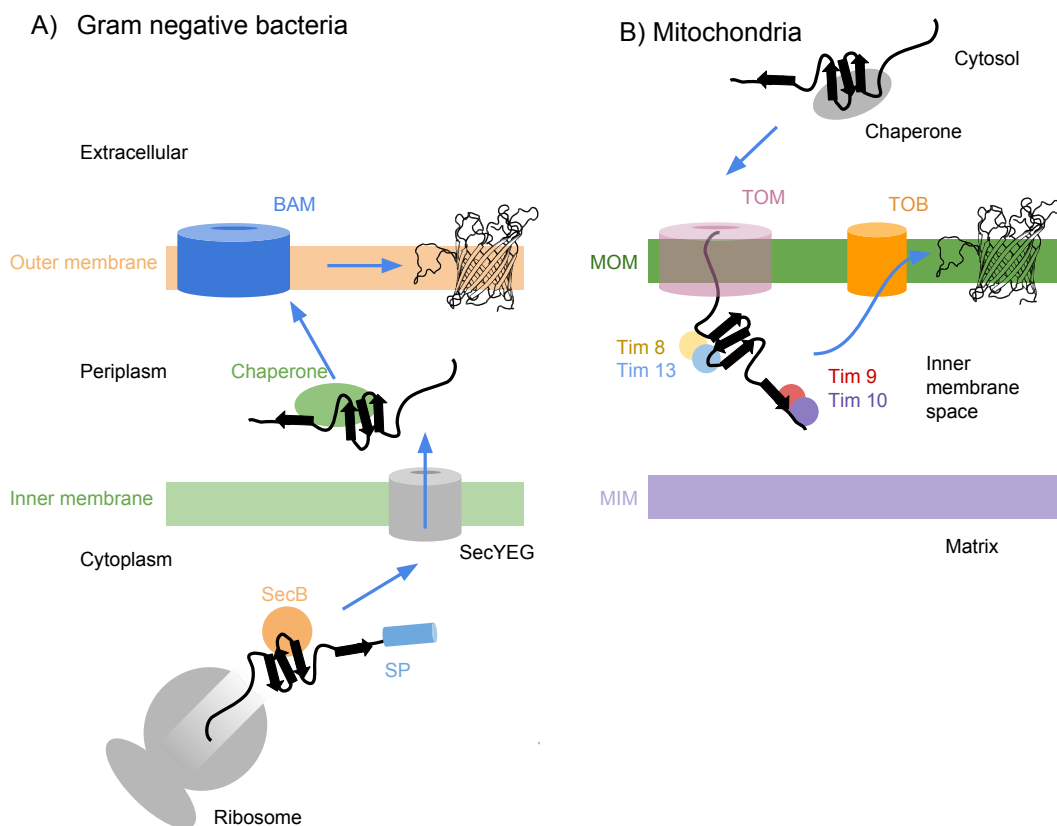


**Figure 1.12: A cartoon of the biogenesis of  $\beta$  barrel membrane proteins in mitochondria and Gram-negative bacteria.** This is an overview of the current model of  $\beta$ -barrel protein membrane integration. A) In bacteria, SecB chaperones the nascent peptide to SecYEG where it is transported across the inner membrane. Once the SP is cleaved, the protein is chaperoned to the BAM machinery by SurA, DegQ, or Skp. The BAM machinery integrates the protein into the membrane. B) After ribosomal translation, the nascent peptide is transported across the MOM by the Translocase of the Outer Membrane (TOM) machinery. Several Tim recognition molecules then attach to the protein and present it to the TOB insertion machinery, which integrates the protein into the membrane. Redrawn from Ulrich & Rapoport, 2015 [211].

Unlike in the bacterial outer membrane,  $\beta$ -barrel proteins are rare in the mitochondria [211]. There is Tom40, Tob55, two isoforms of a porin, and Mdm10 [211]. And

yet, indeed it was shown that a  $\beta$  barrel protein fragments not found in the eukaryotic proteome called trimeric autotransporter can be recognised and assembled by the mitochondria [221]. Since there is no need to cross the inner membrane, mitochondrial proteins do not have the cleavable SP or any other known targeting signal [211]. After cytosolic ribosomes complete the translation, the  $\beta$  barrel proteins are recognised on the mitochondrial surface by the TOM complex import receptors, handed to the  $\beta$  barrel protein Tom40 which is the central machinery for mitochondrial protein import [222]. After being processed through the TOM machinery, hexameric chaperone complexes of Tim8 in complex with Tim13, and Tim9 in complex with Tim10 transport the peptide to the TOB complex (also known as the SAM complex) also on the MOM which integrates the  $\beta$  barrel protein into the membrane [223–225].

Whereas mitochondria originated from the ancestral incorporation of  $\alpha$ -proteobacteria [207], chloroplasts were thought to originate from the incorporation of cyanobacterium [206]. Similarly to mitochondrial  $\beta$  barrel proteins, there is no cleavable targeting SP for the chloroplast since they integrate on the internal side of the membrane, however much less is known about the precise insertion machinery of  $\beta$  barrel proteins at a molecular level in chloroplasts [211].

Besides the differences in biogenesis between  $\beta$  barrel TMPs and TMPs with TMHs as the membrane-spanning units, there are also biophysical differences. Membrane-spanning  $\beta$  sheets exhibit a “positive-outside” distribution of positively-charged residues [110], as opposed to the much more typical positive-inside distribution [86, 109, 110, 113, 114]. Typically,  $\beta$  sheets are less hydrophobic than TMHs [226] as a result of their amphiphilic nature.

## 1.5 The aims of this thesis

In this thesis, we explore three ideas surrounding the role of TMHs in the membrane. Each chapter is presented in the general style of an article and contains a further introduction to the specific topic of study.

In chapter 2 we explore the sequence composition of large datasets of TMHs stratifying them by species, organelle, single-pass and multi-pass. After considering the rarity of certain amino acid types, we show a “negative-outside” tendency in concert

with the “positive-inside” rule. We go on to further divide the single-pass TMPs into complex and simple TMHs according to TMSOC. This reveals that simple TMHs have amino acid distribution features along the helix that would optimise the TMH for anchoring, however complex TMHs are more akin to TMHs from multi-pass TMPs. This indicates that TMH function beyond anchoring outweighs the evolutionary pressure to adhere to membrane constraints.

In chapter 3 we generate an up to date dataset of post-translationally inserted TA proteins based on previous methods and compare the TMHs within to a manually curated TA protein dataset from UniProt. This cross-examination revealed adaptations in the TMH sequences to mitochondrial membranes. This is likely to play a role in trafficking of the TA TMPs as well as being an adaptation to the differences in the biological composition of the mitochondrial membrane. We also generate homology models of two spontaneously inserting TMHs from TA proteins and show that they have an amphipathic surface which may be key to their spontaneous insertion into the amphiphilic lipids of the bilayer.

In chapter 4 we look at families of TMPs that exhibit a high hydrophobic discrepancy between sequentially adjacent TMHs. The conservation of these pairs across the families corroborates evidence of cooperative TMH insertion, showing that marginally hydrophobic TMHs could use typical TMHs as part of their biogenesis on a larger scale than previously thought.

# Chapter 2

## The “negative-outside” rule

The research presented in this chapter is published work presented in Baker *et al.*, 2017 titled ‘Charged residues next to transmembrane regions revisited: “Positive-inside rule” is complemented by the “negative inside depletion/outside enrichment rule”’ by James Alexander Baker, Wing-Cheong Wong, Birgit Eisenhaber, Jim Warwicker, and Frank Eisenhaber [227]. Here we include the supplementary tables and figures in the text.

### 2.1 Summary

#### 2.1.1 Background

Transmembrane helices frequently occur amongst protein architectures as means for proteins to attach to or embed into biological membranes. Physical constraints such as the membrane’s hydrophobicity and electrostatic potential apply uniform requirements to transmembrane helices and their flanking regions; consequently, they are mirrored in their sequence patterns (in addition to transmembrane helices being a span of generally hydrophobic residues) on top of variations enforced by the specific protein’s biological functions.

#### 2.1.2 Results

With statistics derived from a large body of protein sequences, we demonstrate that, in addition to the positive charge preference at the cytoplasmic inside (positive-inside

rule), negatively-charged residues preferentially occur or are even enriched at the non-cytoplasmic flank or, at least, they are suppressed at the cytoplasmic flank (negative-not-inside/negative-outside rule). As negative residues are generally rare within or near transmembrane helices, the statistical significance is sensitive with regard to details of transmembrane helix alignment and residue frequency normalisation and also to dataset size; therefore, this trend was obscured in previous work. We observe variations amongst taxa as well as for key organelles along the secretory pathway. The effect is most pronounced for transmembrane helices from single-pass transmembrane (bitopic) proteins compared to those with multiple transmembrane helices (polytopic proteins) and especially for the class of simple transmembrane helices that evolved for the sole role as membrane anchors.

### 2.1.3 Conclusions

The charged-residue flank bias is only one of the transmembrane helix sequence features with a role in the anchorage mechanisms, others apparently being the leucine intra-helix propensity skew towards the cytoplasmic side, tryptophan flanking as well as the cysteine and tyrosine inside preference. These observations will stimulate new prediction methods for transmembrane helices and protein topology from a sequence as well as new engineering designs for artificial membrane proteins.

## 2.2 Introduction

Two decades ago, the classic concept of a TMH was a rather simple story: typical TMPs were thought to be anchored in the membrane by membrane-spanning bundles of non-polar  $\alpha$ -helices of roughly 20 residues length, with a consistent orientation of being perpendicular to the membrane surface. Although this is broadly true, hundreds of high quality membrane structures have elucidated that membrane-embedded helices can adopt a plethora of lengths and orientations within the membrane. They are capable of just partial spanning of the membrane, spanning using oblique angles, and even lying flat on the membrane surface [38, 39]. The insertion and formation of the TMHs follow a complex thermodynamic equilibrium [40, 228, 229]. From the biological function point of view, many TMHs have multiple roles besides being just

hydrophobic anchors; for example, certain TMHs have been identified as regulators of protein quality control and trafficking mechanisms [43]. As these additional biological functions are mirrored in the TMHs’ sequence patterns, TMHs can be classified as simple (just hydrophobic anchors) and complex sequence segments [44–46].

The relationship between sequence patterns in and in the vicinity of TMHs and their structural and functional properties, as well as their interaction with the lipid bilayer membrane, has been a field of intensive research in the last three decades [1]. Besides the span of generally hydrophobic residues in the TMH, there are other trends in the sequence such as with a saddle-like distribution of polar residues (depressed incidence of charged residues in the TMH itself), an enriched occurrence of positively-charged residues in the cytosolic flanking regions as well as an increased likelihood of tryptophan and tyrosine at either flank edge [86, 109, 113, 117, 230, 231]. Such properties vary somewhat in length and intensity between various biological organelle membranes, between prokaryotes and eukaryotes [232] and even among eukaryotic species studied due to slightly different membrane constraints [86, 110]. These biological dispositions are exploitable in terms of TM region prediction in query protein sequences [233, 234] and tools such as the quite reliable TMHMM [67, 235], Phobius [71, 236] or DAS-TMfilter represent today’s prediction limit of TMHs’ hydrophobic cores within the protein sequence [237–239]. The prediction accuracy for true positives and negatives is reported to be close to 100% and the remaining main cause of false positive prediction are hydrophobic  $\alpha$ -helices completely buried in the hydrophobic core of proteins. To note, reliable prediction of TMHs and protein topology is a strong restriction for protein function of even otherwise non-characterised proteins [240–242] and thus, very valuable information.

The “positive-inside rule” reported by von Heijne [38, 113] postulates the preferential occurrence of positively-charged residues (lysine and arginine) at the cytoplasmic edge of TMHs. The practical value of positively-charged residue sequence clustering in topology prediction of TMH was first shown for the plasmalemma in bacteria [113, 243]. As a trend, the “positive-inside rule” has since been confirmed with statistical observations for most membrane proteins and biological membrane types [109, 118, 244, 245]. However, more recent evidence suggests that, in thylakoid membranes, the “positive-inside rule” is less applicable due to the co-occurrence of aspartic acid and

glutamic acid residues together with positively-charged residues [110].

The positive-inside rule also received support from protein engineering experiments that revealed conclusive evidence for positive charges as a topological determinant [113, 246–248]. Mutational experiments demonstrated that charged residues, when inserted into the centre of the helix, had a large effect on insertion capabilities of the TMH via the translocon. Insertion becomes more unfavourable when the charge was placed closer to the TMH core [116].

It remains unclear exactly why and how exactly the positive charge determines topology from a biophysical perspective. positively-charged residues are suggested to be stronger determinants of topology than negatively-charged residues due to a dampening of the translocation potential of negatively-charged residues. This dampening factor is the result of protein-lipid interactions with net zero charged phospholipid, phosphatidylethanolamine and other neutral lipids. This effect favours cytoplasmic retention of positively-charged residues [249].

The recent accumulation of TMP sequences and structures allowed revisiting the problem of charged residue distribution in TMHs (see also <http://blanco.biomol.uci.edu/mpstruc/>). For example, whilst  $\beta$ -sheets contain charged residues in the TM region,  $\alpha$ -helices generally do not [106]. Large-scale sequence analysis of TMH from various organelle membrane surfaces in eukaryotic proteomes confirm the clustering of positive charge having a statistical bias for the cytosolic side of the membrane. At the same time, there are many TMH exception examples to the positive-inside rule; however as a trend, topology can be determined by simply looking for the most positive loop region between helices [86, 109].

When the observation of positively-charged residues preferentially localised at the cytoplasmic edge of TMHs emerged, it was also asked whether negatively-charged residues work in concert with TMH orientation. It was shown that a single additional lysine residue can reverse the topology of a model *Escherichia coli* protein, whereas a much higher number of negatively-charged residues is needed to achieve the same [248]; nevertheless, a sufficiently large negative charge can overturn the positive-inside rule [250, 251] and, thus indeed, negative residues are topologically active to a

point. negatively-charged residues were observed in the flanks of TMHs [109], especially of marginally hydrophobic TM regions [252]. It is known that the negatively-charged acidic residues in TM regions have a non-trivial role in the biological context. In *E. coli*, negative residues experience electrical pulling forces when travelling through the SecYEG translocon indicating that negative charges are biologically relevant during the electrostatic interactions of insertion [42, 253].

Unfortunately, there is a problem with statistical evidence for preferential negative charge occurrence next to TMH regions. Early investigations indicated overall both positive and negative charge were influential topology factors, dubbed the charge balance rule. If true, one would also expect to see a skew in the negative charge distribution if a cooperation between oppositely charged residues orientated a TMH [243, 254]. It might be expected that, if positive residues force the loop or tail to stay inside, negative residues would be drawn outside and topology would be determined not unlike electrophoresis. Yet, there is plenty of individual protein examples but no conclusive statistical evidence in the current literature for a negatively-charged skew [86, 109, 110, 114, 117, 118].

There are many observations described in the literature that charged residues determine topology more predictably in single-pass proteins than in multi-pass TMH [251, 255]. It is thought that the charges only determine the initial orientation of the TMH in the biological membrane; yet, the ultimate orientation must be determined together with the totality of subsequent downstream regions [256].

With sequence-based hydrophobicity and volume analysis and consensus sequence studies, Sharpe *et al.* [86] demonstrated that there is asymmetry in the intramembranous space of some membranes. Crucially, this asymmetry differs among the membrane of various organelles. They conclude that there are general differences between the lipid composition and organisation in membranes of the Golgi and ER. Functional aspects are also important. For example, the abundance of serines in the region following the luminal end of Golgi TMHs appears to reflect the fact that this part of many Golgi enzymes forms a flexible linker that tethers the catalytic domain to the membrane [86].

A study by Baeza-Delgado *et al.* [109] analysed the distribution of amino acid

residue types in TMHs in 170 integral membrane proteins from a manually maintained database of experimentally confirmed TMPs (MPTopo [112]) as well as in 930 structures from the PDB. As expected, half of the natural amino acids are equally distributed along TMH whereas aromatic, polar and charged amino acids along with proline are biased near the flanks of the TM helices. Unsurprisingly, leucine and other non-polar residues are far more abundant than the charged residues in the TM region [86, 109].

In this work, we revisit the issue of statistical evidence for the preferential distribution of negatively-charged (and a few other) residues within and nearby TMHs. We rely on the improved availability of comprehensive and large sequence and structure datasets for TM proteins. We also show that several methodical aspects have hindered previous studies [86, 109, 110] to see the consistent non-trivial skew for negatively-charged residues disfavouring the cytosolic interfacial region and/or preferring the outside flank. First, we show that acidic residues are especially rare within and in the close sequence environment of TMHs, even when compared to positively-charged lysine and arginine. Second, therefore, the manner of normalisation is critical: Taken together with the difficulty to properly align TMHs relative to their boundaries, column-wise frequency calculations relative to all amino acid types as in previous studies will blur possible preferential localisations of negative charges in the sequence. However, the outcome changes when we ask where a negative charge occurs in the sequence relative to the total amount of negative charges in the respective sequence region. Thus, by accounting for the rarity of acidic residues with sensitive normalisation, the “non-negative inside rule/negative-outside rule” is clearly supported by the statistical data. We find that minor changes in the flank definitions such as taking the TMH boundaries from the database or by generating flanks by centrally aligning TMHs and applying some standardised TMH length does not have a noticeable influence on the charge bias detected.

Third, there are significant differences in the distribution of amino acid residues between single-pass and multi-pass TM regions in both the intra-membrane helix and the flanking regions with further variations introduced by taxa and by the organelles along the secretory pathway. Importantly, we find that it is critical to weigh down the effect of TMHs in multi-pass TMPs with no or super-short flanks to observe statistical

significance for the charge bias. To say it bluntly, if there are no flanks of sufficient length, there is also no negative-charge bias to be observed.

The charge bias effect is even clearer when a classification of TMHs into so-called simple (which, as a trend, are mostly single-pass and mere anchors) and so-called complex (which typically have functions beyond anchorage) is considered [44–46]. We also observe parallel skews with regard to leucine, tyrosine, tryptophan and cysteine distributions. With these large-scale datasets and a sensitive normalisation approach, new sequence features are revealed that provide spatial insight into TMH membrane anchoring, recognition, helix-lipid, and helix-helix interactions.

## 2.3 Results

### 2.3.1 Acidic residues within and nearby transmembrane helix segments are rare

In order to reliably compare the amino acid sequence properties of TMHs, we assembled datasets of TMH proteins from what are likely to be the best in terms of quality and comprehensiveness of annotation in eukaryotic and prokaryotic representative genomes, as well as composite datasets to represent larger taxonomic groups and with regard to sub-cellular locations (see Table 2.1). In total, 3292 single-pass TMH segments and 29898 multi-pass TMH segments were extracted from various UniProt [75] text files according to TRANSMEM annotation (download dated 20–03–2016). The UniProt datasets used only included manually curated records; however, it is still necessary to check for systematic bias due to the prediction methods used by UniProt for TMH annotation in the majority of cases without direct experimental evidence. Therefore, a fully experimentally verified dataset was also generated for comparison. The representative 1544 single-pass and 15563 TMHs were extracted from the manually curated experimentally verified TOPDB [257] database (download dated 21–03–2016) referred to as ExpAll here (Table 2.1). TMH organelle residency is defined according to UniProt annotation. To ensure reliability, organelles were only analysed from a representative redundancy-reduced protein dataset of the most well-studied genome: *Homo sapiens* (referred to as UniHuman herein). The several datasets from UniProt

are subdivided into different human organelles (UniPM, UniER, UniGolgi) and taxonomical groups (UniHuman, UniCress, UniBacilli, UniEcoli, UniArch, UniFungi) as described in Table 2.1 (see also Methods section). As will be shown below, these various datasets allow us to validate our findings for a variety of conditions, namely with regard (i) to experimental verification of TMHs, (ii) to origin from various species and taxonomic groups, (iii) to the number of TMHs in the same protein as well as (iv) to sub-cellular localisation. Data-sets and programs used in this work can be downloaded from <http://mendel.bii.a-star.edu.sg/SEQUENCES>NNI/>.

**Table 2.1: Acidic residues are rarer in transmembrane helices of single-pass proteins than in transmembrane helices of multi-pass proteins.** The statistical results when comparing the number of acidic residues in single-pass or multi-pass TMHs within their database-defined limits and excluding any flanks. The number of helices per dataset can be found in Table 2.2 for single-pass TMHs and Table 2.3 for multi-pass helices.  $\mu$  SP is the average number of the respective residues per helix in TMHs from single-pass proteins, while  $\mu$  MP is the average number of the respective residues per TMH from multi-pass proteins. The Kruskal-Wallis test scores (H statistics) were calculated for the numbers of aspartic acid and glutamic acid residues in each helix from single-pass and the number of aspartic acid and glutamic acid residues in each helix from multi-pass TMHs

Data-set	Acidic residues (D and E)			Aspartic acid (D only)			Glutamic acid (E only)		
	$\mu$ SP	$\mu$ MP	H statistic p-value	$\mu$ SP	$\mu$ MP	H statistic p-value	$\mu$ SP	$\mu$ MP	H statistic p-value
ExpAll	0.086	0.309	148.1 4.50E-34	0.045	0.157	40.3 2.13E-10	0.042	0.161	46.6 8.64E-12
UniHuman	0.076	0.398	316.5 8.31E-71	0.034	0.191	91.6 1.05E-21	0.042	0.207	100.3 1.33E-23
UniER	0.106	0.43	34.4 4.39E-9	0.061	0.161	8.0 4.72E-3	0.045	0.268	26.8 2.24E-7
UniGolgi	0.097	0.381	39.8 2.88E-10	0.043	0.18	19.4 1.05E-5	0.053	0.201	20.2 7.01E-6
UniPM	0.039	0.4	121.0 3.86E-28	0.016	0.187	32.7 1.06E-8	0.022	0.213	36.9 1.26E-9
UniCress	0.062	0.434	163.5 1.99E-37	0.036	0.198	32.5 1.20E-8	0.025	0.241	66.0 4.59E-16
UniFungi	0.177	0.349	43.1 5.14E-11	0.044	0.166	24.5 7.60E-7	0.133	0.183	4.6 0.033
UniBacilli	0.089	0.352	24.1 9.16E-7	0.048	0.185	11.2 8.27E-4	0.04	0.176	12.3 4.54E-5
UniEcoli	0.148	0.315	2.7 0.100	0.111	0.15	0.1 0.729	0.037	0.163	2.2 0.140
UniArch	0.438	0.606	1.8 0.183	0.083	0.344	11.2 8.33E-4	0.354	0.247	3.5 0.0624

The hydrophobic nature of the lipid bilayer membrane implies that, generally, charged residues should be rare within TMHs. For acidic residues, even the location in the sequence vicinity of TMHs should be disfavoured because of the negatively-charged head groups of lipids directed towards the aqueous extracellular side or the cytoplasm. In agreement with the biophysically justified expectations, the statistical data confirms that acidic residues are especially rare in TMHs and their flanking

regions. In Figure 2.1 where we plot the total abundance of all amino acid types in single-pass TMHs and multi-pass TMHs (including their  $\pm 5$  flanking residues), acidic residues were found to be amongst the rarest amino acids both in UniHuman and ExpAll.

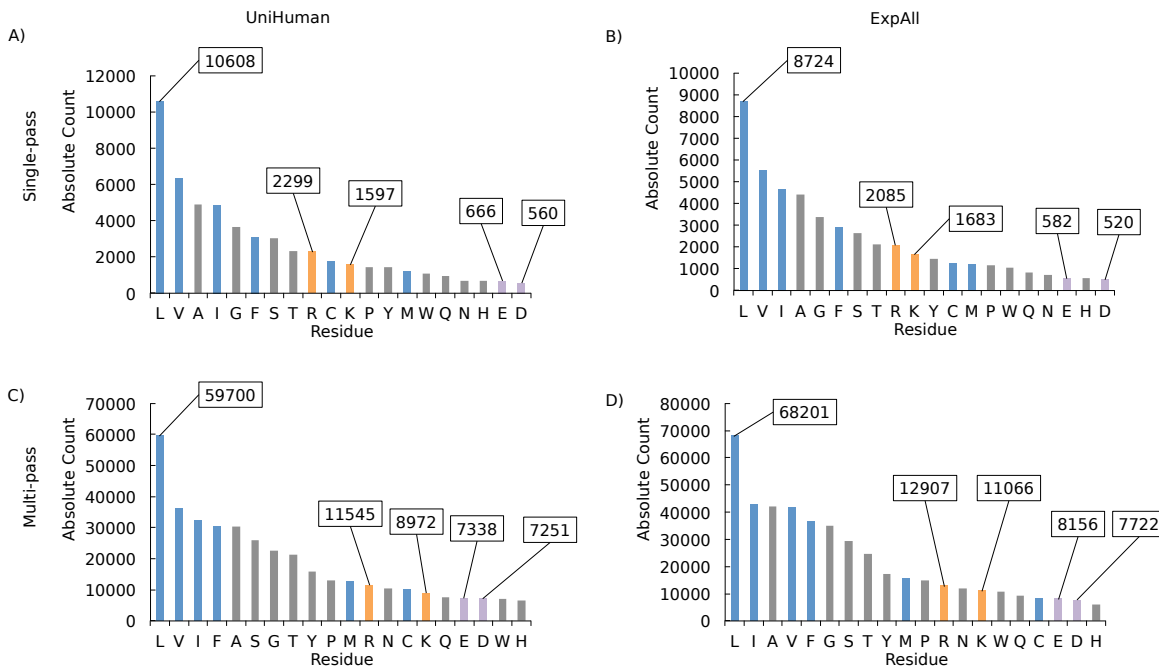


**Figure 2.1: Negatively-charged amino acids are amongst the rarest residues in transmembrane helices and  $\pm 5$  flanking residues.** Bar charts of the abundance of each amino acid type in the TMHs with flank lengths of the accompanying  $\pm 5$  residues from the (a) UniHuman single-pass proteins, (b) ExpAll single-pass proteins, (c) UniHuman multi-pass proteins, and (d) ExpAll multi-pass proteins. Amino acid types on the horizontal axis are listed in descending count. The bars were coloured according to categorisations of hydrophobic, neutral and hydrophilic types according to the free energy of insertion biological scale [116]. Grey represents hydrophilic amino acids that were found to have a positive  $\Delta G$  app, and blue represents hydrophobic residues with a negative  $\Delta G$  app, purple denotes negative residues and positive residues are coloured in orange. The abundances of key residues are labelled.

The effect is most pronounced in single-pass TMPs (Figure 2.1). There are only 666 glutamates (just 1.24% of all residues) and 560 aspartates (1.05% respectively) among the total set of 53238 residues comprised in 1705 TMHs and their flanks. Within just the TMH regions, there are 71 glutamates (0.20% of all residues in TMHs and flanks) and 58 aspartates (0.16% respectively). This cannot be an artefact of UniProt TMH assignments since this feature is repeated in ExpAll. There are only 582 glutamates (1.22%) and 520 aspartates (1.09%) among the 47568 residues involved. Within the TMH itself, there are 64 glutamates (0.19%) and 69 aspartates (0.21%). In both cases, the negatively-charged residues represent the ultimate end of

the distribution. To note, acidic residues are rare even compared to positively-charged residues which are about 3–4 times more frequent. On a much smaller dataset of single-spanning TMP, Nakashima *et al.* [258] made similar compositional studies. To compare, they found 0.94% glutamate and 0.94% aspartate within just the TMH region (values very similar to ours from TMHs with small flanks; apparently, they used more outwardly defined TMH boundaries) but the content of each glutamate and aspartate within the extracellular or cytoplasmic domains is larger by an order of magnitude, between 5.26% and 9.34%. These latter values tend to be even higher than the average glutamate and aspartate composition throughout the protein database (5–6% [258]).

In the case of multi-pass TMPs (Figure 2.1), glutamates and aspartates are still very rare in TMHs and their  $\pm 5$  residue flanks (1.94% and 1.92% from the total of 377207 in the case of UniHuman respectively, 1.79% and 1.70% from the total of 454700 in the case of ExpAll). Yet, their occurrence is similar to those of histidine and tryptophan and, notably, acidic residues are only about  $\sim 1.5$  times less frequent than positively-charged residues. The observation that acidic residues are more suppressed in single-pass TMHs compared with the case of multi-pass TMHs is statistically significant. In Table 2.1, the acidic residues are counted in the helices (excluding flanking regions) belonging to either multi-pass or single-pass helices. Indeed, single-pass helices appear to tolerate negative charge to a far lesser extent than multi-pass helices as the data in the top two rows of Table 2.1 indicates (for datasets UniHuman and ExpAll). The trend is strictly observed throughout sub-cellular localisations (rows 3–5 in Table 2.1) and taxa (rows 6–10). Statistical significance ( $P \leq 0.001$ ) is found in all but six cases. These are UniEcoli (D+E, D, E), UniArch (D+E, E) and UniFungi (E). The problem is, most likely, that the respective datasets are quite small. Notably, the difference between single- and multi-pass TMHs is greatest in UniPM; here, TMHs from multi-pass proteins have on average 0.400 negative residues per helix, whereas single-pass TMHs contained just 0.039 ( $P=3.86e-28$ ).

### 2.3.2 Amino acid residue distribution analysis reveals a “negative-not-inside/negative-outside” signal in single-pass transmembrane helix segments

The rarity of negatively-charged residues is a complicating issue when studying their distribution along the sequence positions of TMHs and their flanks. For UniHuman and ExpAll, we plotted absolute abundance of aspartic acid, glutamic acid, lysine, arginine, and leucine at each position (i.e., it scales as the equivalent fraction in the total composition of the alignment column) (Figure 2.2). To note, the known preference of positively-charged residues towards the cytoplasmic side is nevertheless evident. Yet, it becomes apparent that any bias in the occurrence of the much rarer acidic residues is overshadowed by fluctuations in the highly abundant residues such as leucine.

The trends become clearer if the occurrence of specific residues is normalised with the total number of residues of the given amino acid type in the dataset observed in the sequence region studied as shown for UniHuman and for ExpAll in Figure 2.2. For comparison, we indicated background residue occurrences (dashed lines calculated as averages for positions -25 to -30 and 25 to 30). The respective average occurrences in the inside and outside flanks (calculated from an average of the values at positions -20 to -10 and 10 to 20 respectively) are shown with wide lines.

The “positive-inside rule” becomes even more evident in this normalisation: Whereas the occurrence of positively-charged residues is about the background level at the outside flank, it is about two to three times higher both for the UniHuman and the ExpAll datasets at the inside flank. To note, the background level was found to be 1.7% (lysine) and 1.6% (arginine) in UniHuman and 1.4% (lysine and arginine) in ExpAll. The inside flank average is 4.3% (lysine) and 4.6% (arginine) in UniHuman and 4.2% (lysine) and 4.6% (arginine) in ExpAll. The outside flank is similar to the background noise levels: about 1.4% (lysine) and 1.5% (arginine) in UniHuman and about 1.5% (lysine) and 1.4% (arginine) in ExpAll.

Most interestingly, a “negative-inside depletion” trend for the negatively-charged residues is apparent from the distribution bias. The inside flank averages for glutamic acid were 1.1% and 1.4% in UniHuman and ExpAll respectively; for aspartic acid, 1.2% and 1.4% in UniHuman and ExpAll respectively. Meanwhile, the outside flanks

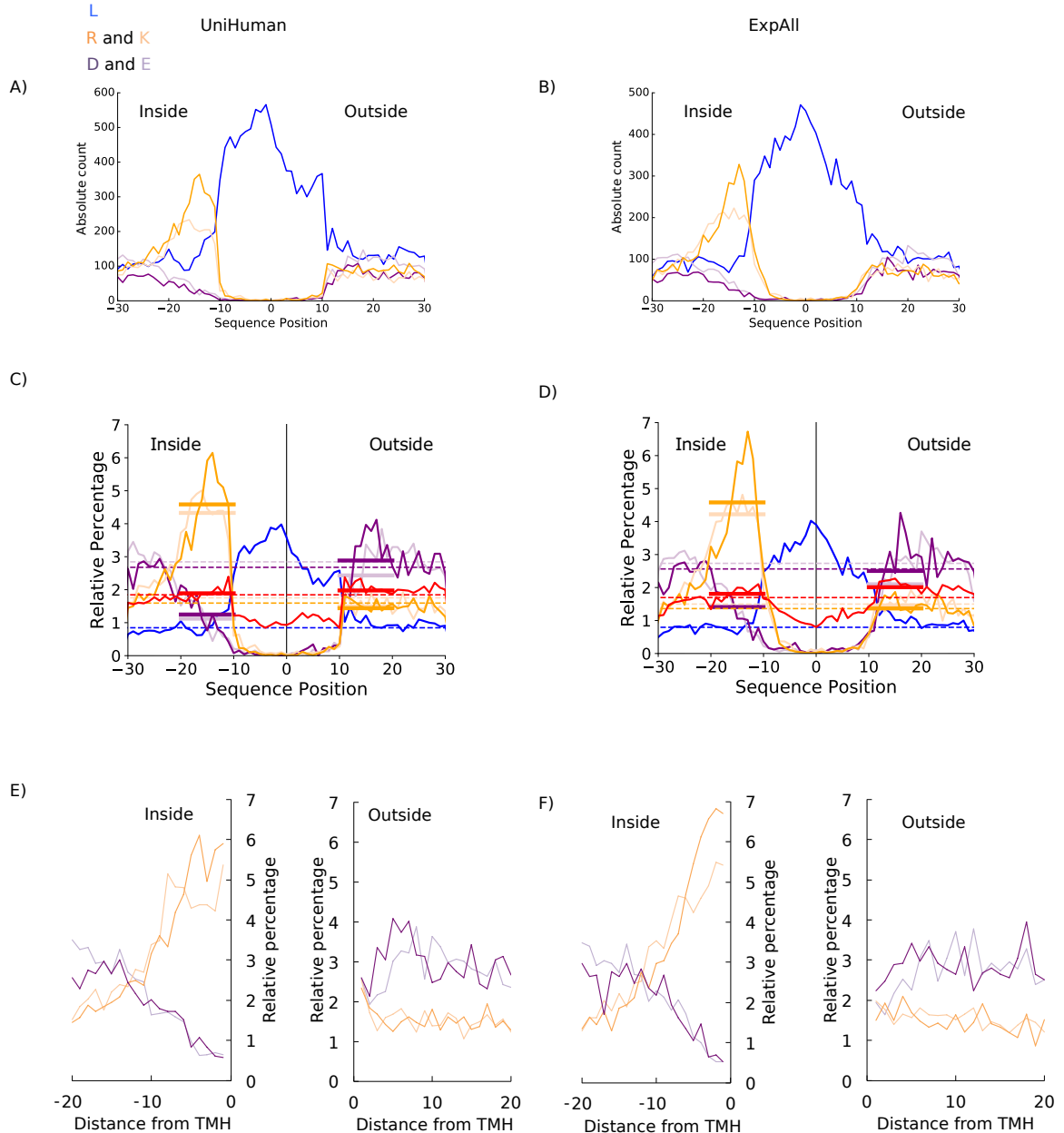


**Figure 2.2: Relative percentage normalisation reveals a negative-outside bias in transmembrane helices from single-pass protein datasets.** All flank sizes were set at up to  $\pm 20$  residues. We acknowledge that all values, besides the averaged values, are discrete, and connecting lines are illustrative only. On the horizontal axes (a-d) are the distances in residues from the centre of the TMH, with the negative numbers extending towards the cytoplasmic space. For (e) and (f), the horizontal axis represents the residue count from the membrane boundary with negative counts into the cytoplasmic space. Leucine, the most abundant non-polar residue in TMHs, is in blue. Arginine and lysine are shown in dark and light orange respectively. Aspartic and glutamic acid are showing in dark and light purple respectively. In red are the uncharged polar amino acids serine, asparagine, glutamine, threonine, tyrosine, and cysteine. (a) and (b) On the vertical axis is the absolute abundance of residues in TMHs from single-pass proteins from (a) UniHuman and (b) ExpAll. Note that no clear trend can be seen in the negative residue distribution compared to the positive-inside signal and the leucine abundance throughout the TMH. (c) and (d) On the vertical axis is the relative percentage at each position for TMHs from single-pass proteins from (c) UniHuman and (d) ExpAll. The dashed lines show the estimation of the background level of residues with respect to the colour; an average of the relative percentage values between positions 25 to 30 and -30 to -25. The thick bars show the averages on the inner (positions -20 to -10) and outer (positions 10 to 20) flanks coloured to the respective amino acid type. Note a visible suppression of acidic residues on the inside flank when compared to the outside flank in single-pass proteins when normalising according to the relative percentage. (e) and (f) The relative distribution of flanks defined by the databases with the distance from the TMH boundary on the horizontal axis. The inside and outside flanks are shown in separate subplots. The colouring is the same as in (a) and (b).

for aspartic acid and glutamic acid occurrences were measured at 2.9% and 2.4% respectively in UniHuman and, in ExpAll, these values for aspartic acid and glutamic acid were found to be 2.5% and 2.1% respectively. Against the background level of aspartic acid (2.8% and 2.9% in UniHuman) and glutamic acid (2.6% and 2.9% in ExpAll), the inside flank averages were found to be about 2–3 times lower than the background level while the outside flank averages were comparable to the background level (Figure 2.2). Taken together, this indicates a clear suppression of negatively-charged residues at the inside flank of single-pass TMHs and a possible trend for negatively-charged residues occurring preferentially at the outside flank. This is not an effect of the flank definition selection since the trend remains the same when using the database-defined flanks without the context of the TMH (Figure 2.2). For UniHuman, the negative charge expectancy on the inside flank doesn’t reach above 2% until position -10 (D) and position -11 (E), whereas, on the outside flank, both D and E start >2%. The same can be seen in ExpAll where negative residues reach above 2% only as far from the membrane boundary as at position -9 (D) and position -7 (E) on the inside but exceed 2% beginning with position 1 (D) and 3 (E) on the outside (Figure 2.2).

Residue presence is a zero-sum variable. If there is more likelihood of a positively-charged residue being present at an inside position, then there must be less probability of at least one type of amino acid at that position. To check if this probability was spread throughout non-charged amino acids as well as negatively-charged amino acids, we also examined non-charged polar residues for any inside versus outside preference (Figure 2.2B and Figure 2.2C). As expected there was an increased prevalence at the flanks (peaking at position +12 with 2.27% in Expall and 2.39 at position -10 in UniHuman), however, there was no clear difference between the inside and outside flank relative percentages. In ExpAll the inside flank (1.8% relative percentage average) to outside (1.9% relative percentage average) was between 5 to 10 times less than the negatively-charged residue inside-outside difference, and there was very little difference in the UniProt inside (1.88% relative percentage average) to outside (1.94% relative percentage average) relative abundance.

The observation of negative charge suppression at the inside flank, herein the “negative-inside depletion” rule, is statistically significant throughout most datasets in

this study. The inside-outside bias was counted using the Kruskal-Wallis (K-W) test comparing the occurrence of acidic residues within 10 residues of each TMH inside and outside the TMH (Table 2.2). We studied both the database-reported flanks as well as those obtained from central alignment of TMHs (see Methods). The null hypothesis (no difference between the two flanks) could be confidently rejected in all cases ( $p\text{-value} < 0.001$  except for UniBacilli), the sign of the H-statistic (K-W) indicating suppression at the inside and/or preference for the outside flank (except for UniArch). Most importantly, acidic residues were found to be distributed with bias in ExpAll ( $p\text{-value} < 3.47\text{e-}58$ ) and in UniHuman ( $p\text{-value} = 1.13\text{e-}93$ ). Whereas with UniBacilli, the problem is most likely the dataset size, the exception of UniArch, for which we observe a strong negative inside rule, is more puzzling and indicates biophysical differences of their plasma-membrane.

**Table 2.2: Statistical significances for negative charge distribution skew on either side of the membrane in single-pass transmembrane helices.** The “Helices” column refers to the total TMHs contained in each dataset (ExpALL, TMHs from TOPDB [257]; UniHuman, human representative proteome; UniER, human endoplasmic reticulum representative proteome; UniGolgi, human Golgi representative proteome; UniPM, human plasma membrane representative proteome; UniCress, *Arabidopsis thaliana* (mouse-ear cress) representative proteome; UniFungi, fungal representative proteome; UniBacilli, Bacilli class representative proteome; UniEcoli, *Escherichia coli* representative proteome; UniArch, Archaea representative proteome; see Methods for details). In the “Database-defined flanks” column, the “Negative residues” column refers to the total number of negative residues found in the  $\pm 10$  flanking residues on either side of the TMH and does not include residues found in the helix itself. In the “Flanks after central alignment” column, the “Negative residues” column refers to the total number of negative residues found in the  $-20$  to  $-10$  residues and the  $+10$  to  $+20$  residues from the centrally aligned residues of the TMH. Unlike the other tables, the global averages are derived from the  $\pm 20$  datasets. The K-W scores were calculated for negative residues by comparing the number of negatively-charged residues that were within the 10 inside residues and the 10 outside residues in either case

single-pass		Database-defined flanks				Flanks after central alignment			
Data-set	Helices	Negative residues		H statistic	p-value	Negative residues		H statistic	p-value
		Inside	Outside			Inside	Outside		
ExpAll	1544	848	1648	258.59	3.47E-58	735	1541	262.29	5.44E-59
UniHuman	1705	780	1922	421.53	1.13E-93	652	1865	501.86	3.74E-111
UniER	132	78	156	23.76	1.09E-06	76	150	21.62	3.33E-06
UniGolgi	206	60	240	104.45	1.61E-24	54	239	107.18	4.06E-25
UniPM	493	197	578	177.68	1.56E-40	161	569	215.18	1.02E-48
UniCress	632	314	450	18.23	1.96E-05	231	444	55.8	8.01E-14
UniFungi	729	449	631	28.15	1.12E-07	413	627	38.08	6.79E-10
UniBacilli	124	90	113	3.73	5.35E-02	86	106	2.53	1.12E-01
UniEcoli	54	32	77	17.24	3.30E-05	30	74	14.74	1.24E-04
UniArch	48	113	8	49.66	1.83E-12	96	7	45.62	1.43E-11

### 2.3.3 Amino acid residue distribution analysis reveals a general negative-charge bias signal in outside flank of multi-pass transmembrane helix segments — the negative outside enrichment rule

As a result of the rarity of negatively-charged residues, any distribution bias is difficult to be recognised in the plot showing the total abundance (or alignment column composition) of residues in multi-pass TMHs and their flanks from UniHuman and ExpAll (Figure 2.3). Yet, as with single-pass helices, the dominant general leucine enrichment, as well as positive inside signal, can be identified with certainty. When the residue occurrence is normalised by the total occurrence of this residue type in the sequence regions studied (shown as a relative percentage of at each position for multi-pass helices from UniHuman and ExpAll in Figure 2.3), the bias in the distribution of any type of charged residues becomes visible.

With regard to the positive-inside preference, positively-charged residues have a background value of 2.0% for arginine and 2.2% for lysine in UniHuman, and 1.7% for arginine and 1.9% for lysine in ExpAll. At the inside flank, this rises to 4.6% for arginine and 4.1% for lysine in UniHuman and 4.6% for arginine and 4.2% for lysine in ExpAll. The mean net charge at each position was calculated for multi-pass and single-pass datasets from UniHuman and ExpAll (Figure 2.4). The positive inside rule clearly becomes visible as the net charge has a positive skew approximately between residues -10 and -25. What is noteworthy is that the peaks found for single-pass helices were almost three times greater than those of multi-pass helices. For single-pass TMHs, the peak is +0.30 at position -15 in UniHuman and +0.31 at position -14 in ExpAll, whereas TMHs from multi-pass proteins had lower peaks of +0.15 at position -13 in UniHuman and +0.10 at position -14 in ExpAll. Thus, there is a positive charge bias towards the cytoplasmic side; yet, it is much weaker for multi-pass than for single-pass TMHs.

Notably, a “negative outside enrichment” trend also can be seen from the distribution of the negatively-charged residues, though with some effort (Table 2.3) as the effect is also weaker than in the case of single-pass TMHs. We studied the flanks under four conditions: (i) database-defined flanks without overlap between neighbouring TMHs,

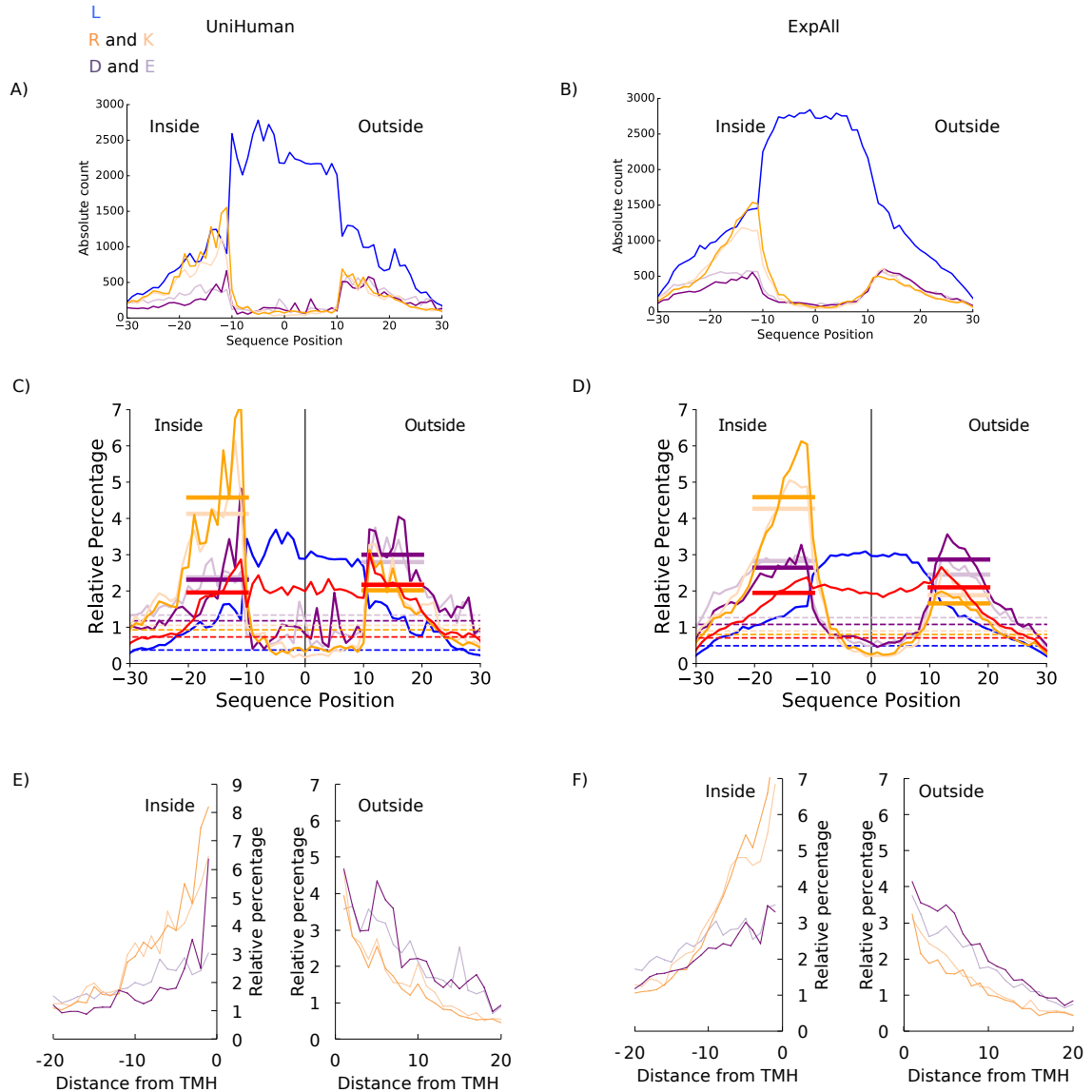


**Figure 2.3: Negative-outside bias is very subtle in transmembrane helices from multi-pass proteins.** The meaning for the horizontal axis is the same as in Figure 2.2, with the negative sequence position numbers extending towards the cytoplasmic space. Leucine is in blue. Arginine and lysine are shown in dark and light orange respectively. Aspartic and glutamic acid are shown in dark and light purple respectively. In red are the uncharged polar amino acids serine, asparagine, glutamine, threonine, tyrosine, and cysteine. All flank sizes were set at up to  $\pm 20$  residues. (a) and (b) On the vertical axes are the absolute abundances of residues from TMHs of multi-pass proteins from (a) UniHuman and (b) ExpAll. c and d On the vertical axes are the relative percentages at each position for TMHs from multi-pass proteins from (c) UniHuman and (d) ExpAll. As in Figure 2.2(c) and (d), the dashed lines show the estimation of the background level of residues with respect to the colour, and the thick bars show the averages on the inner and outer flanks coloured to the respective amino acid type. e and f The relative distribution of flanks defined by the databases with the distance from the TMH boundary on the horizontal axis for both the inside and outside flanks. The colouring is the same as in (a) and (b).

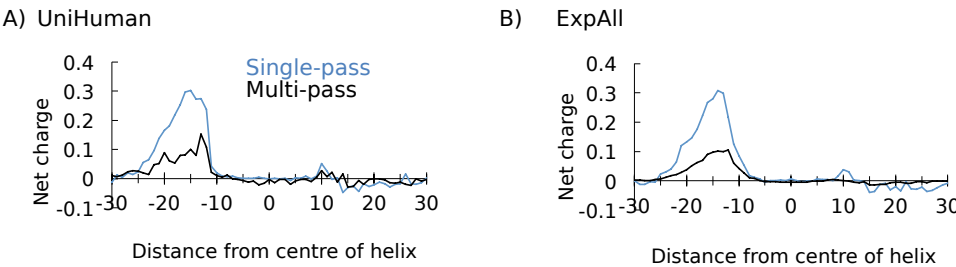


**Figure 2.4:** The net charge across multi-pass and single-pass transmembrane helices shows a stronger positive inside charge in single-pass transmembrane helices than multi-pass transmembrane helices. The net charge per TMH plotted at each position; the positive-inside rule is stronger in TMHs from single-pass proteins than TMHs from multi-pass proteins. The net charge was calculated at each position as described in the Methods section for the (A) UniHuman and (B) ExpAll datasets. Net charge for TMHs from multi-pass proteins is shown in black, and the profile of TMHs from single-pass proteins is drawn in blue.

(ii) flanks after central alignment of TMHs without flank overlap, (iii) database-defined flanks but allowing overlap of flanks shared among neighbouring TMHs, (iv) same as condition (ii) but only the subset of cases where there is at least half of the required flank length at either side of the TMH. In UniHuman as calculated under condition (i), aspartic acid is lower on the inside flank (2.3%) than on the outside flank (3.0%). Glutamic acid is also lower at the inside flank (2.4%) than the 2.8% on the outside flank (Figure 2.3C). Slight variations in defining the membrane boundary point do not influence the trend (compare figures 2.3C and 2.3E). We find that, in all studied conditions, the UniHuman dataset delivers statistical significances (p-values: (i) 6.10e-34, (ii) 5.43e-41, (iii) 3.00e-57, (iv) 5.60e-41) strongly supporting negative-charge bias (inside suppression/outside preference; see Table 2.3).

As with the single-pass proteins, we checked if this probability was spread throughout non-charged amino acids as well as negatively-charged amino acids by examining non-charged polar residues for inside versus outside preference (Figure 2.3B and Figure 2.3C). There was no clear difference between the inside and outside flank relative percentages for ExpAll since the inside flank was 1.9% (relative percentage average) and the outside flank was 2.0% (relative percentage average). There was some small difference in the UniHuman dataset with the inside average being 1.9% and the outside average being 2.2%. This however is much less of a difference than the negatively-charged residue flank differences in the UniHuman dataset.

Surprisingly, the result could not straightforwardly be repeated with the considerably smaller ExpAll. Under condition (i), we find with ExpAll that aspartic acid has

**Table 2.3: Statistical significances for negative charge distribution skew on either side of the membrane in multi-pass transmembrane helices.** The “Helices” column refers to the total TMHs contained in each dataset (ExpALL, TMH from TOPDB [257]; UniHuman, human representative proteome; UniER, human endoplasmic reticulum representative proteome; UniGolgi, human Golgi representative proteome; UniPM, human plasma membrane representative proteome; UniCress, Arabidopsis thaliana (mouse-ear cress) representative proteome, UniFungi, fungal representative proteome; UniBacilli, Bacilli class representative proteome; UniEcoli, Escherichia coli representative proteome; UniArch, Archaea representative proteome; see Methods for details). In (A) the “Database-defined flanks” and in (B) the “Database-defined viable\* flanks” and the “Overlapping flanks” columns, the “Negative residues” column refers to the total number of negative residues found in the  $\pm 10$  flanking residues on either side of the TMH and does not include residues found in the TMH itself. (A) In the “Flanks after central alignment” column, the “Negative residues” column refers to the total number of negative residues found in the -20 to -10 residues and the +10 to +20 residues from the centrally aligned residues with a maximum database defined flank length of 20 residues. The total number of proteins is given in the IDs column. The “Helices” column contains the total number of TMHs in the dataset (n), the average number of TMHs per protein in that population ( $\mu$ ) and the standard deviation of that average ( $\sigma$ ). The K-W scores were calculated for negative residues by comparing the number of negatively-charged residues that were within 10 residues inside and 10 residues outside the TMH.

\*Here, “viable” indicates that in each TMH used for both flanks either side of the TMH has a flank length of at least half the maximum allowed flank length, in this case 10 (the viable length is 5)

multi-pass				Database-defined flanks				Flanks after central alignment					
Data-set	IDs	Helices			Negative residues		H statistic	p-value	Negative residues		H statistic	p-value	
		n	$\mu$	$\sigma$	Inside	Outside			Inside	Outside			
(A)	ExpAll	2205	15,563	7.07	3.95	9709	9598	0.04	8.43E-01	9648	9659	0.35	5.56E-01
	UniHuman	1789	12,353	6.93	3.2	7196	9164	147.5	6.10E-34	6740	8968	179.77	5.43E-41
	UniER	155	898	5.85	3.2	630	584	0.44	5.08E-01	578	576	0.03	8.58E-01
	UniGolgi	61	383	6.28	2.97	274	261	0.02	8.75E-01	266	259	0.09	7.65E-01
	UniPM	427	3079	7.22	3.3	1945	2499	47.98	4.30E-12	1791	2440	64.42	1.01E-15
	UniCress	507	3823	7.55	3.32	2567	2426	0.73	3.93E-01	2398	2433	1.11	2.93E-01
	UniFungi	1338	8685	6.5	3.75	5560	5266	5.83	1.57E-02	5140	5214	0	9.62E-01
	UniBacilli	140	822	5.94	3.98	470	468	0.07	7.92E-01	450	471	0.92	3.38E-01
	UniEcoli	529	3888	7.39	3.76	1990	1902	0.26	6.07E-01	1875	1887	0.18	6.71E-01
	UniArch	59	327	5.97	2.73	245	175	7.98	4.72E-03	235	181	7.08	7.81E-03
multi-pass				Database-defined viable* flanks									
(B)	Negative residues				Negative residues								
	Data-set	Inside	Outside	H statistic	p-value	N	Inside	Outside	H statistic	p-value			
	ExpAll	11,969	12,615	22.54	2.05E-06	8808	6082	6916	59.93	9.81E-15			
	UniHuman	8645	11,181	254.3	3.00E-57	8183	5169	6915	179.71	5.60E-41			
	UniER	750	763	1.16	2.81E-01	516	398	441	3.16	7.55E-02			
	UniGolgi	333	369	7.12	7.64E-03	195	162	186	3	8.30E-02			
	UniPM	2319	3107	99.68	1.79E-23	1977	1343	1960	98.63	3.05E-23			
	UniCress	3142	3298	9.21	2.41E-03	2110	1626	1741	6.4	1.14E-02			
	UniFungi	6724	6814	0.46	4.96E-01	4581	3340	3411	0.41	5.22E-01			
	UniBacilli	585	636	2.65	1.04E-01	382	230	306	12.73	3.61E-04			
	UniEcoli	2574	2800	17.88	2.35E-05	1596	951	1114	16.57	4.69E-05			
	UniArch	342	248	14.67	1.28E-04	132	120	104	0.28	5.97E-01			

a background level of 1.0%, an average of 2.6% on the inside flank, and of 2.9% on the outside flank but glutamic acid’s background is 1.2% but 2.8% on the inside flank and 2.5% on the outside flank. Statistical tests do not support finding a negative-charge bias in conditions (i) and (ii). Apparently, the problem is TMHs having no or almost no flanks at one of the sides. Statistical significance for the negative-charge bias is detected as soon as this problem is dealt with – either by allowing extension of flanks overlap among neighbouring TMHs as in condition (iii) or by removing examples without proper flank lengths from the dataset as in condition (iv). The respective p-values are 2.05e-6 and 9.81e-15 respectively.

The issues we had with ExpAll raised the question that, maybe, sequence redundancy in the UniHuman set could have played a role. Therefore, we repeated all calculations but with UniRef50 instead of UniRef90 for mapping into sequence clusters (see Methods section for detail). We were surprised to see that harsher sequence redundancy requirements do not affect the outcome of the statistical tests in any major way. For the conditions (i)- (iv), we computed the following p-values: (i) 1.31e-28 (5940 negatively residues inside versus 7492 outside), (ii) 1.38e-36 (5516 versus 7320), (iii) 5.60e-53 (7089 versus 9233) and (iv) 4.18e-41 (4232 versus 5730).

So, the amplifying effect of some subsets in the overall dataset on the statistical test that might be caused by allowing overlapping flanks (condition (iii)) is not the major factor leading to the negative charge skew. Similarly, the trend is also not caused by sequence redundancy. Thus, we have learned that the negative-charge bias does also exist in multi-pass TMPs but under the conditions that there are sufficiently long loops between TMHs. Bluntly said: no loops equals to no charge bias. As soon as the loops reach some critical length, there are differences between single-pass and multi-pass TMHs with regard to occurrence and distribution of negative charges and the inside-suppression/outside-enrichment negative-charge bias appears. Not only are there more negative charges within the multi-pass TMH itself (in fact, negative charges are almost not tolerated in single-pass TMHs; see Table 2.1), but also, there is a much stronger negative outside skew in the TMHs of single-pass proteins than those of multi-pass proteins.

### 2.3.4 Further significant sequence differences between single-pass and multi-pass helices: distribution of tryptophan, tyrosine, proline and cysteine

Amino acid residue profiles along the TM segment and its flanks differ between single- and multi-pass TMHs also in other aspects. The relative percentages of all amino acid types (normalisation by the total amount of that residue type in the sequence segment) from single-pass helices of the UniHuman (Figure 2.5A; from 1705 TMHs with flanks having 68571 residues) and ExpAll (Figure 2.5B; from 1544 TMHs with flanks having 60200 residues) were plotted as a heat-map. The amino acid types were listed on the Y axis according to Kyte & Doolittle hydrophobicity [73] in descending order.

In accordance with expectations, enrichment for hydrophobic residues in the TMH, for the positively-charged residues on the inside flank as well as a distribution the negative distribution bias was found in both datasets. Additionally, the inside interfacial region showed consistent enrichment hotspots for tryptophan (e.g., 7.1% at position -11 in ExpAll, 6.2% at position -10 in UniHuman with flanks after central TMH alignment) and tyrosine (6.4% at -11 in ExpAll, 7.1% at -11 in UniHuman), and some preference can also be seen for the outer interfacial region (e.g., 5.2% at position 11 for tryptophan in ExpAll, and 5.8% at position 10 for tryptophan in UniHuman) albeit the “hot” cluster of the outer flank covers fewer positions than that of the inner flank. Further, there is an apparent bias of cysteine on the inner flank and interfacial region (e.g., 5.5% at position -10 in ExpAll, 5.9% at position -11 in UniHuman), and a depression in the outer interfacial region and flank (up to a minimum of 0.3% in both ExpAll and UniHuman). Proline appears to have a depression signal on the outer flank. Note that, in a similar way to Figures 2.2 and 2.3, the distributions of the flanks derived from centrally aligned TMHs are corroborated by the distributions from the database defined TMH boundary flanks (see outside bands in Figures 2.5A-D).

A similar heatmap was generated for UniHuman multi-pass (Figure 2.5C; from 12353 TMHs with flanks having 452708 residues) TMHs and ExpAll multi-pass (Figure 2.5D; from 15563 TMHs with flanks having 535599 residues). Whereas Figures 2.5A-C appear quite noisy, the plot for ExpAll multi-pass TMHs appears almost Gaussian-like

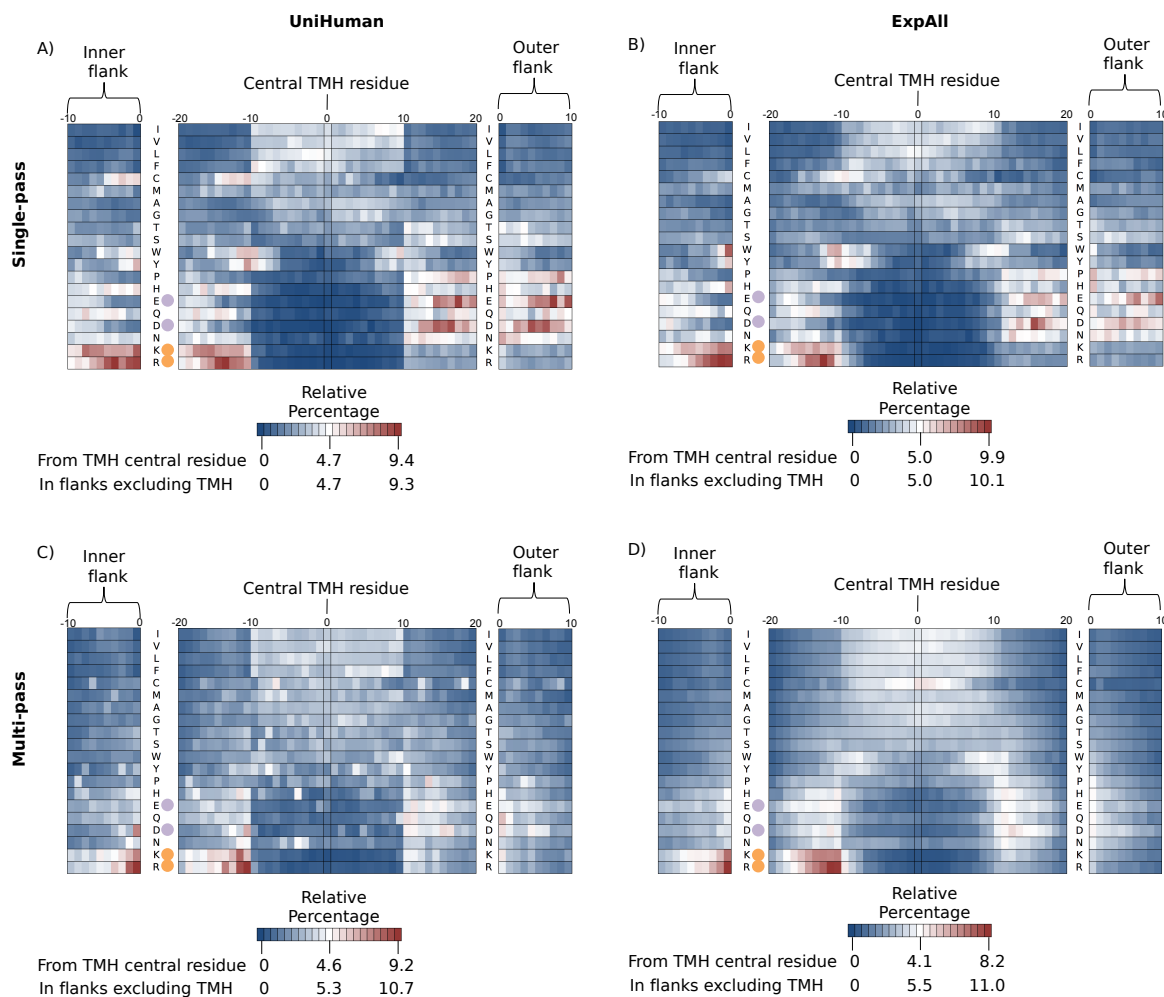


**Figure 2.5: Relative percentage heat-maps from predictive and experimental datasets corroborate residue distribution differences between transmembrane helices from single-pass and multi-pass proteins.** The residue position aligned to the centre of the TMH is on the horizontal axis, and the residue type is on the vertical axis. Amino acid types are listed in order of decreasing hydrophobicity according to the Kyte and Doolittle scale [52]. The flank lengths in the TMH segments were restricted to up to  $\pm 10$  residues. The scales for each heat-map are shown beneath the respective subplot. The darkest blue represents 0% distribution, whilst the darkest red represents the maximum relative percentage distribution that is denoted by the keys in each subplot, with white being 50% between “cold” and “hot”. The central TMH subplots extend from the central TMH residue, whereas the inner and outer flank subplots use the database-defined TMH boundary and extend from that position. a TMHs from the single-pass UniHuman dataset. b single-pass protein TMHs from the ExpAll dataset. c TMHs from the proteins of the multi-pass UniHuman dataset. d TMHs from ExpAll multi-pass proteins. The general consistency in relative distributions of every residue type between single-pass and multi-pass of either dataset including flank/TMH boundary selection allows us to infer biological conclusions from these distributions that are independent of methodological biases used to gather the sequences. The only residue that displays drastically differently between the datasets is cysteine in multi-pass TMHs only. The most striking differences in distributions between residues from TMHs of single-pass and multi-pass proteins include a more defined Y and W clustering at the flanks, a suppression of E and D on the inside flank, a suppression of P on the outside flank and a topological bias for C favouring the inside flank.

smoothed, thus, indicating the quality of this dataset. Tyrosine and tryptophan in the multi-pass case do not appear as enriched in the interfacial regions of single-pass TMHs from both UniHuman and ExpAll. Prolines are only suppressed in the TMH itself and are not suppressed in the outer flank as in the single-pass case but, indeed, are tolerated if not slightly enriched in the flanks.

### 2.3.5 Hydrophobicity and leucine distribution in transmembrane helices in single- and multi-pass proteins

Generally, we see in Figure 2.5 that compositional biases appear more extreme in the single-pass case, particularly when it comes to polar and non-polar residues being more heavily suppressed and enriched. To investigate this observation, we calculated the hydrophobicity at each sequence-position averaged over all TMHs considered (after having window-averaged over 3 residues for each TMH) using the Kyte & Doolittle hydrophobicity scale [73] (Figure 2.6A) and validated using White and Wimley octanol-interface whole residue scale [139], Hessa's biological hydrophobicity scale [116], and the Eisenberg hydrophobic moment consensus scale [144] (Figure 2.7). The total set of TMHs was split into 15 sets of membrane-spanning proteins (1 set containing single-pass proteins, 13 sets each containing TMHs from 2-, 3-, 4...14-TMPs and another of TMHs from proteins with 15 or more TMHs). In Figure 2.6B, we show the p-value at each sequence position by comparing the respective values from multi-pass and single-pass TMHs using the 2-sample t-test (Figure 2.6B). Strikingly, the inside flank of the single-pass TMHs is much more hydrophilic (e.g., see the Kyte & Doolittle score=-1.3 at position -18) than that of multi-pass TMHs (p-value=5.64e-103 at position -14). Most likely, the positive inside rule, along with the interfacial clustering of tryptophan and tyrosine, contribute to a strong polar inside flank in single-pass helices that is not present in multi-pass helices en masse. Further, multi-pass TMHs cluster remarkably closely within the TM core; the respective hydrophobicity is apparently not dependent on the number of TMHs in a given multi-pass TMP. On average, single-pass TMHs are more hydrophobic in the core than multi-pass TMHs (p-value<1.e-72 within positions -5...5 and p-value=5.92e-190 at position 0). On the other hand, hydrophobicity differences between TMHs from single- and multi-pass proteins fade somewhat at the

transition towards the flanks (p-value=1.85e-4 at position -10, and p-value=3.35e-31 at position 10).

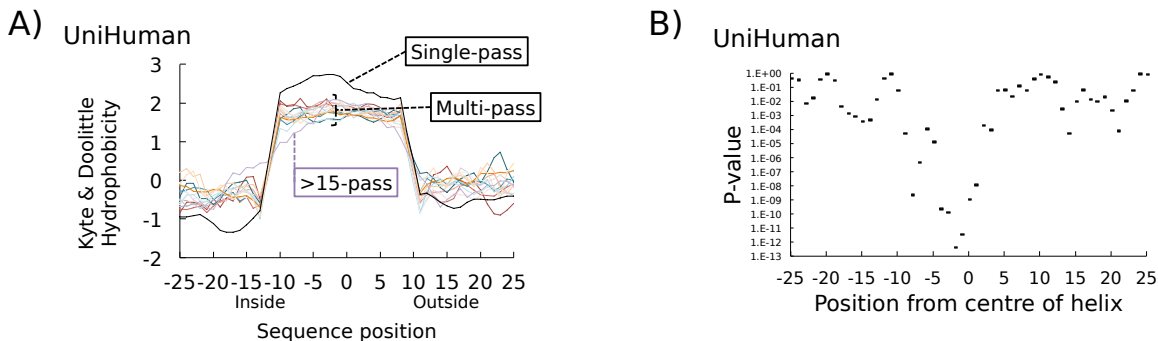


**Figure 2.6: There is a difference in the hydrophobic profiles of transmembrane helices from single-pass and multi-pass proteins.** a The hydrophobicity of single-pass TMHs compared to multi-pass segments from the UniHuman dataset. The Kyte and Doolittle scale of hydrophobicity [73] was used with a window length of 3 to compare TMHs from proteins with different numbers of TMHs. This scale is based on the water-vapour transfer of free energy and the interior-exterior distribution of individual amino acids. The same datasets also had different scales applied (Figure 2.7). The vertical axis is the hydrophobicity score, whilst the horizontal axis is the position of the residue relative to the centre of the TMH, with negative values extending into the cytoplasm. In black are the average hydrophobicity values of TMHs belonging to single-pass TMHs, whilst in other colours are the average hydrophobicity values of TMHs belonging to multi-pass proteins containing the same numbers of TMHs per protein. In purple are the TMHs from proteins with more than 15 TMHs per protein that do not share a typical multi-pass profile, perhaps due to their exceptional nature. b The Kruskal-Wallis test (H statistic) was used to compare single-pass windowed hydrophobicity values with the average windowed hydrophobicity value of every TMH from multi-pass proteins at the same position. The vertical axis is the logarithmic scale of the resultant p-values. We can much more readily reject the hypothesis that hydrophobicity is the same between TMHs from single-pass and multi-pass proteins in the core of the helix and the flanks than the interfacial regions, particularly at the inner leaflet due to leucine asymmetry (Table 2.4)

Leucine is the most abundant residue in TMHs (Figure 2.1) and is considered one of the most hydrophobic residues by all hydrophobicity scales. Therefore, it plays a very influential role in TMH helix-helix and lipid-helix interactions in the membrane and recognition by the insertion machinery. When looking at the difference in the abundance of leucine between the inner and outer halves, we find that TMHs from single-pass proteins have a trend to contain more leucine residues at the cytoplasmic side of TMHs, particularly in the case of TMHs from single-pass proteins (see Figures 2.2 and 2.5).

This trend is statistically significant for TMHs in many biological membranes (Table 2.4, Figure 2.8). In the most extreme case of UniCress (single-pass), we see 49% more leucine residues on the inside leaflet than the outside leaflet (p-value=5.41e-24). This contrasts with UniCress (multi-pass), in which the skew is far weaker, albeit

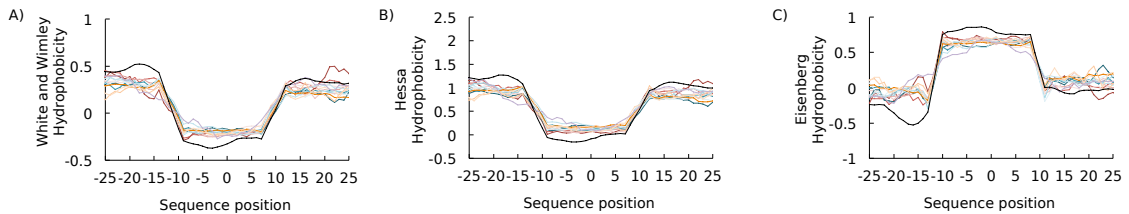


**Figure 2.7: There is a difference in the hydrophobic profiles of transmembrane helices from single-pass and multi-pass proteins.** The difference in hydrophobicity between the single-pass and multi-pass datasets stratified by number of TMHs is not due to the choice of scale. As with Figure 2.6, UniHuman was stratified according to the number of TMHs in each protein. The mean amino acid hydrophobicity values of TMHs with a sliding unweighted window of 3 residues from UniHuman proteins at each position were plotted. To validate the findings presented in Figure 2.6A, several scales of hydrophobicity were used. (A) The White and Wimley whole residue scale [139] is based on the partitioning of peptides between water and octanol as well as water to POPC. A positive score indicates a more polar score. (B) The Hessa biological scale [116]. The hydrophobicity values represent the free energy exchange during recognition of designed peptide TMHs by the endoplasmic reticulum Sec61 translocon and, therefore, negative values indicate an energetic preference for the interior of a lipid bilayer. (C) The Eisenberg consensus scale [144] is a scale based on the earlier scales from Nozaki and Tanford [137], Wolfenden *et al.* [142], Chothia [131], Janin [141] and the von Heijne and Blomberg scale [143]. The scales are normalised according to serine. A positive score indicates a generally more hydrophobic score.

yet statistically significant. There are 6% more leucine residues at the inside half ( $p\text{-value}=2.08\text{e-}4$ ). The trend of having more leucine residues at the cytoplasmic half of the TMH is observed for all datasets (both single- and multi-pass) except for UniArch (single-pass). The phenomenon is statistically significant with  $p\text{-value}<1.\text{e-}3$  for Ex-pAll, UniHuman, UniPM and UniCress (both single- and multi-pass). As with negative charge distribution, UniArch presents a reversed effect compared to other single-pass protein datasets with a 57% reduction in leucine on the inside leaflet compared to the outside leaflet ( $p\text{-value}=7.25\text{e-}6$ ). However, leucine of TMHs from UniArch multi-pass proteins have no discernible preference for the inside leaflets (4% more on the inside leaflet,  $p\text{-value}=0.625$ ).

### 2.3.6 A negative-outside (or negative-non-inside) signal is present across many membrane types

We explored the presence of amino acid residue compositional skews described above for human TMPs for those in other taxa and also specifically for human proteins with regard to membranes at various subcellular localisations. Acidic residues for TMHs from single-pass and multi-pass helices were plotted according to their relative percentage distributions (of the total amount of this residue type in the respective segment) for

**Table 2.4: Leucines at the inner and outer leaflets of the membrane in transmembrane helices.** The statistical results when comparing the number of leucine residues from the inner and outer leaflets in each protein in the dataset. The number of helices per dataset can be found in Table 2.1. The Kruskal-Wallis test scores (H statistics) were calculated for leucine residues by comparing the number of leucine residues that were in the inner half of the leaflet with those in the outer half of the leaflet of the database-defined TMH

Dataset	single-pass					multi-pass				
	Inside	Outside	Percentage	H statistic	p-value	Inside	Outside	Percentage	H statistic	p-value
ExpAll	4020	3403	118.13	40.07	2.44E-10	27,986	27,008	103.62	14.13	1.70E-04
UniHuman	4982	3697	134.76	193.02	6.99E-44	25,199	22,365	112.67	195.24	2.29E-44
UniER	359	297	120.88	8.41	3.72E-03	1863	1764	105.61	3.98	4.61E-02
UniGolgi	604	513	117.74	10.74	1.05E-03	753	677	111.23	5.61	1.79E-02
UniPM	1485	1006	147.61	98.9	2.65E-23	6221	5577	111.55	35.21	3.00E-09
UniCress	1495	1005	148.76	102.05	5.41E-24	6491	6099	106.43	13.76	2.08E-04
UniFungi	1389	1308	106.19	3.41	6.48E-02	14,505	14,099	102.88	6.74	9.41E-03
UniBacilli	260	251	103.59	0.03	8.72E-01	1488	1335	111.46	7.59	5.89E-03
UniEcoli	130	100	130	2.78	9.53E-02	7251	6975	103.96	5.92	1.50E-02
UniArch	51	118	43.22	20.13	7.25E-06	636	612	103.92	0.24	6.25E-01

five taxon-specific datasets UniCress (Figure 2.8A), UniFungi (Figure 2.8B), UniEcoli (Figure 2.8C), UniBacilli (Figure 2.8D), UniArch (Figure 2.8E) and for three organelle-specific datasets UniER (Figure 2.8F), UniGolgi (Figure 2.8G), UniPM (Figure 2.8H).

For single-pass proteins in all taxon-specific datasets (with the exception of UniArch), there are more negative residues at the outside than at the inside. The skew is statistically significant (see Table 2.2,  $P<0.001$ ) except for UniBacilli. Despite statistical significance found for UniFungi ( $p\text{-value}=1.12\text{e-}7$  for database-defined and  $p\text{-value}=6.79\text{e-}10$  for flanks after central alignment; Table 2.2), however, the trend is not very strong in this case (Figure 2.8B). Whereas the skew is just a suppression of negatively-charged residues at the inside flank for ExpAll and UniHuman (as well as in UniCress), the bias observed for UniEcoli involves also a negative charge enrichment at the outside flank. In the case of UniArch (Figure 2.8E), we see a negative inside preference that is 6.0% in the case of aspartic acid, and 6.3% for glutamic acid (not shown), with much lower values close to 0% on the outside. Whilst the difference is statistically significant for both TMHs (Table 2.2) from single-pass proteins ( $p\text{-value}=1.83\text{e-}12$  and  $p\text{-value}=1.43\text{e-}11$  for two versions of flank determination) and multi-pass proteins ( $p\text{-values } 4.72\text{e-}3, 7.81\text{e-}3, 1.28\text{e-}4$  for three versions of flank determination, see Tables 3A and 3B), the distribution along the position axis is heavily fluctuating, maybe as a result of the small size of the dataset. However, one can assuredly assign a “negative-inside” tendency to the flanking regions of Archaean TMHs.

In the human organelle datasets, we see trend shifts at different stages in the

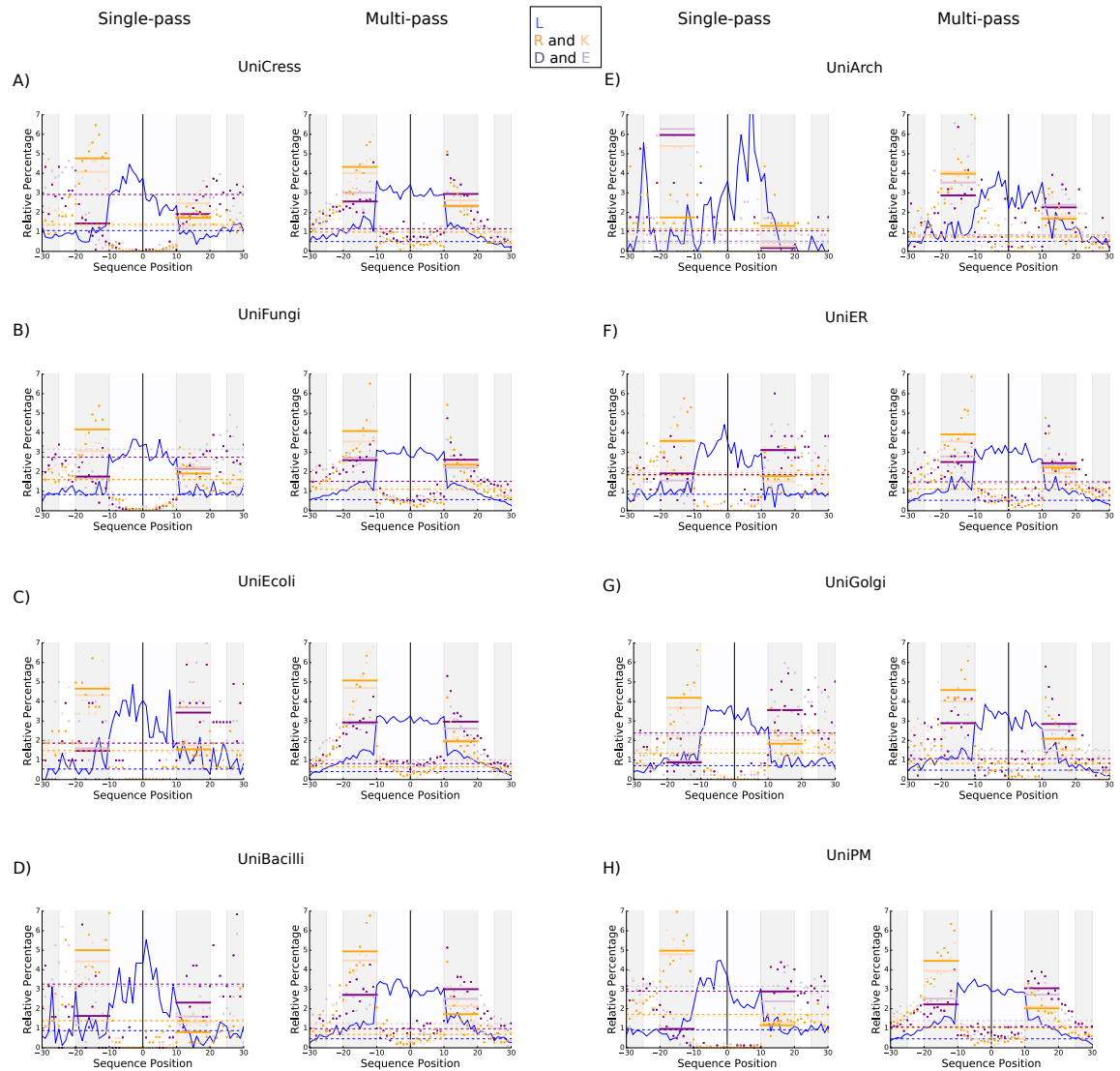


**Figure 2.8: Comparing charged amino acid distributions in transmembrane helices of multi-pass and single-pass proteins across different species and organelles.** The relative percentage distribution of charged residues and leucine was calculated at each position in the TMH with flank lengths of  $\pm 20$  in different datasets. The distributions are normalised according to relative percentage distribution. Aspartic acid and glutamic acid are shown in dark purple and light purple respectively. Leucine, the most abundant non-polar residue in TMHs, is in blue. Arginine and lysine are shown in orange. TMHs from single-pass proteins are on the left and TMHs from multi-pass proteins are on the right for different taxonomic datasets: a UniCress, b UniFungi, c UniEcoli, d UniBacilli, e UniArch, and different organelles: f UniER, g UniGolgi, h UniPM. As a trend, the negative-outside skew is more present in TMHs from single-pass proteins than multi-pass proteins (Tables 2 and 3). Another key observation is that in single-pass TMHs there is a propensity for leucine on the inner over the outer leaflet (Table 2.4)

secretory pathway. In UniER, there is an enrichment of negative charge on the outside flank of 1–1.5% that is comparable to the magnitude of the positive inside signal. In UniGolgi, there is a suppression of negatively-charged residues on the inside flank as well as an enrichment on the inside flank resulting in ~2% distribution difference. For UniPM, there is a negative-inside suppression (but no outside enrichment) as well as

a positive-inside signal. All observed trends are statistically significant (see Table 2.2,  $P < 1.e-5$ ).

For multi-pass TMH proteins, we see either the same trends but in a weaker form or no skews are observed at all as inspection of the graphs in Figure 2.8 shows. For datasets UniER, UniGolgi, UniCress, UniFungi, and UniBacilli, the hypothesis of equal distribution of negatively-charged residues cannot be rejected ( $p\text{-value} > 0.001$ , see Table 2.3); thus, a skew is statistically non-significant. Although UniPM has a statistically significant bias ( $p\text{-value} < 4.30e-12$ , Table 2.3), the trends are more subtle and most present for aspartic acid of UniPM. We see many more negative and positive charges tolerated within the multi-pass TMHs themselves throughout all datasets (Table 2.1). To note, there is a positive-inside rule for all multi-pass datasets studied herein.

To conclude, we find that negative-charge bias distribution is a feature of single-pass protein TMHs that is present across many membrane types and it can have the form of a negative charge suppression at the inside flank or an enrichment of those charges at the outside flank.

### 2.3.7 Amino acid compositional skews in relation to trans-membrane helix complexity and anchorage function

In previous work, we studied the relationship of TMH composition, sequence complexity and function [44–46] and concluded that simple TMHs are more probably responsible for simple membrane anchorage, whereas complex TMHs have a biological function beyond just anchorage. We wished to see how the skews observed in this work relate to that classification. Therefore, the single-pass TMHs from UniHuman and ExpAll were separated into subsets of simple, twilight, and complex TMHs using TMSOC [44, 45]. The relative percentages of eight residue types (L, D, E, R, K, Y, W, C; normalisation with the total amount of residues of that amino acid type in all sequence segments considered) were plotted along the sequence position for simple and complex helices (Figure 2.9). Of UniHuman single-pass proteins, there were 889 records with simple TMHs and 570 with complex TMHs (Figure 2.9B). In ExpAll, 769 TMHs from single-pass proteins were simple TMHs and 570 were complex TMHs.

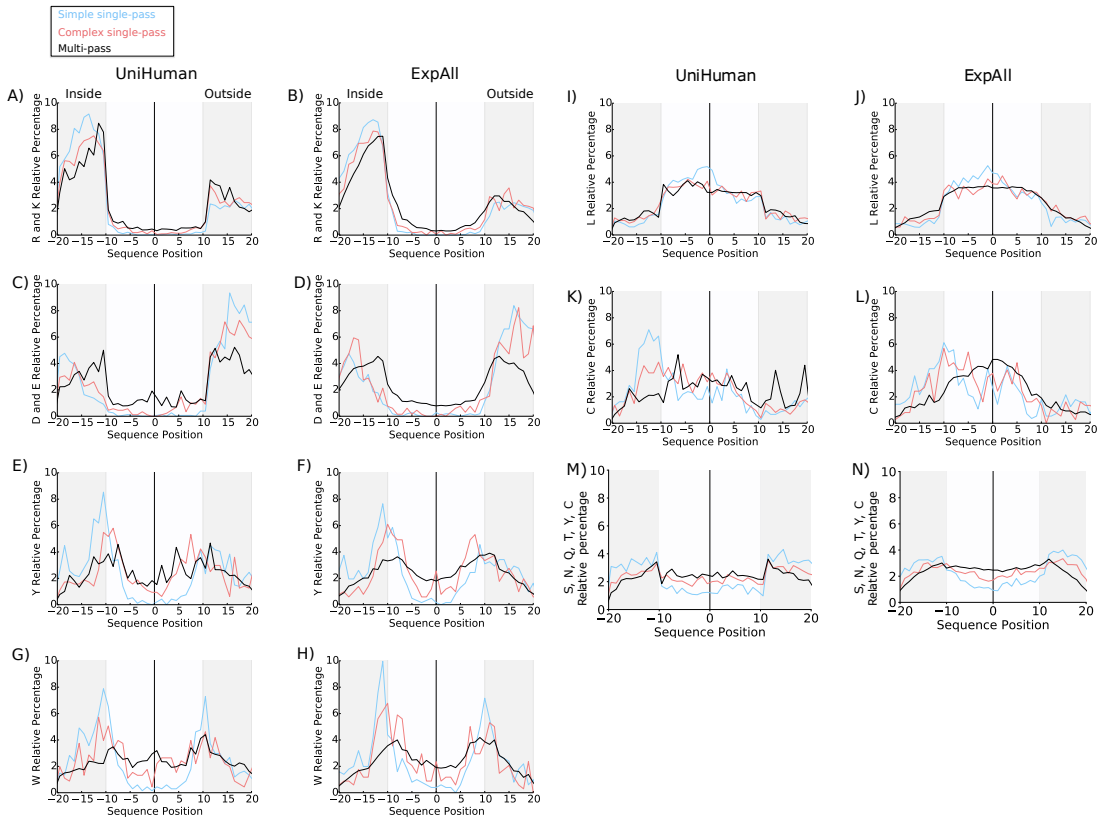


**Figure 2.9: Comparing the amino acid relative percentage distributions of simple and complex transmembrane helices from single-pass proteins and transmembrane helices from multi-pass proteins.** Comparing the amino acid relative percentage distributions of simple and complex TMHs from single-pass proteins and TMHs from multi-pass proteins. TMSOC was used to calculate which single-pass TMHs were complex and which were simple from ExpAll and UniHuman datasets. Simple TMHs are typically anchors without necessarily having other functions (Wong *et al.* [46]). The relative percentages from single-pass simple (shown in light blue), single-pass complex (red), and multi-pass protein TMHs (black) were plotted for (a, c, e, g, i and k) UniHuman and (b, d, f, h, j and l) ExpAll for (a and b) positive residues, (c and d) negative residues, (e and f) tyrosine, (g and h) tryptophan, (i and j) leucine and (k and l) cysteine (m and n) uncharged polar amino acids; serine, asparagine, glutamine, threonine, tyrosine, and cysteine. The slopes are statistically compared in Tables 2.5 and 2.6, and as a trend, the profiles of complex TMHs are more similar to multi-pass TMH profiles than simple TMHs are to multi-pass TMHs

It is visually apparent (Figure 2.9) that there are (i) stronger skews and more inside-outside disparities in simple single-pass TMs than in complex single-pass TMs and (ii) greater similarities between single-pass complex TM regions and those from multi-pass proteins compared with simple single-pass TMs in comparison with either of the other two distributions. To examine the statistical significance of these observations, we compared the amino acid distributions (K, R, K+R, D, E, D+E, Y, W, L, C) across the range of TMHs with flank lengths  $\pm 10$  residues using the Kolmogorov-Smirnov (K-S), K-W and the  $\chi^2$  statistical tests. To note, the K-S test scrutinises for significant maximal absolute differences between distribution curves; the glskw test is after skews between distributions and the  $\chi^2$  statistical test checks the average difference between distributions. Calculations were carried out over single-pass complex, single-pass simple and multi-pass TMH datasets from both ExpAll and UniHuman (for p-values and Bahadur slopes, Table 2.5 (dataset UniHuman) and Table 2.6 (dataset ExpAll)).

There is also a visual difference between simple single-pass proteins, complex single-pass proteins, and multipass proteins with regard to uncharged polar amino acids (serine, asparagine, glutamine, threonine, tyrosine, and cysteine), with complex single-pass TMHs being between multipass TMHs and simple single-pass TMHs in terms of relative percentage profile across the membrane (Figure 2.9M and Figure 2.9N). TMSOC uses hydrophobicity as part of the scrutinisation between simple and complex TMHs, so it is not surprising that there are differences in polar residues between simple and complex TMHs. However, it is interesting to note that the reduction in polar residues is not reduced through the TMH and flanks of simple and complex TMHs evenly; simple TMHs have less uncharged polar residues in the core of the TMH than the complex TMHs relative to the flanking areas. Because there was no observable inside-outside flank skews in the distributions, no further statistical analysis was carried out on this set.

Many low p-values in Tables 2.5 and 2.6 indicate significant differences between the three distributions studied. For the UniHuman dataset (Table 2.5), we find most striking, significant differences between charged residue distributions (R, K, D, E) of simple and complex single-pass TMH+flank regions ( $\chi^2$  p-value $<2.23\text{e-}3$  for single

**Table 2.5: Simple transmembrane helices are less similar than complex transmembrane helices to transmembrane helices from multi-pass proteins in UniHuman.** The statistical results were gathered by comparing complex single-pass TMHs, simple TMHs from single-pass proteins and TMHs from multi-pass proteins in UniHuman. The abundance of different residues at each position when using the centrally aligned TMH approach was compared with several statistical tests (the K-S, K-W and the  $\chi^2$  statistical tests) and the Bahadur slope values of those results

Residues	p-values for $\chi^2$			Bahadur slopes for $\chi^2$		
	Simple-vs-complex	Simple-vs-multi	Complex-vs-multi	Simple-vs-complex	Simple-vs-multi	Complex-vs-multi
R	3.20E-06	7.38E-02	1.24E-01	6.61E-03	2.20E-03	1.27E-04
K	2.23E-03	4.99E-02	2.14E-01	3.99E-03	3.70E-03	1.18E-04
D	1.67E-09	3.06E-01	3.02E-01	3.34E-02	3.24E-03	1.20E-04
E	3.80E-07	2.34E-01	2.31E-01	1.81E-02	3.05E-03	1.36E-04
Y	3.86E-01	3.97E-01	2.11E-01	1.06E-03	1.47E-03	8.25E-05
W	3.77E-03	2.97E-01	3.84E-01	8.52E-03	2.73E-03	1.13E-04
L	3.59E-01	2.88E-01	3.21E-01	1.52E-04	3.92E-04	1.69E-05
C	6.44E-01	3.97E-01	3.41E-01	4.29E-04	1.29E-03	8.57E-05
R+K	2.19E-02	2.83E-01	2.52E-01	1.11E-03	6.33E-04	4.68E-05
D+E	1.47E-03	2.86E-01	2.79E-01	4.59E-03	1.49E-03	6.15E-05
p-values for Kolmogorov-Smirnov				Bahadur slopes for Kolmogorov-Smirnov		
	Simple-vs-complex	Simple-vs-multi	Complex-vs-multi	Simple-vs-complex	Simple-vs-multi	Complex-vs-multi
	2.31E-01	3.57E-04	1.08E-02	7.66E-04	6.71E-03	2.76E-04
R	4.31E-02	2.18E-03	8.93E-01	2.06E-03	7.56E-03	8.68E-06
K	1.39E-01	5.02E-06	1.08E-02	3.26E-03	3.34E-02	4.52E-04
D	7.96E-02	1.58E-05	1.08E-02	3.10E-03	2.32E-02	4.20E-04
E	7.96E-02	2.22E-02	2.31E-01	2.81E-03	6.07E-03	7.78E-05
Y	2.31E-01	9.06E-04	4.31E-02	2.24E-03	1.58E-02	3.70E-04
W	2.31E-01	2.31E-01	5.31E-01	2.17E-04	4.61E-04	9.42E-06
L	1.39E-01	3.61E-01	3.61E-01	1.93E-03	1.42E-03	8.10E-05
C	7.96E-02	1.33E-04	7.96E-02	7.35E-04	4.48E-03	8.60E-05
R+K	4.31E-02	1.58E-05	4.98E-03	2.21E-03	1.31E-02	2.55E-04
p-values for Kruskal-Wallis				Bahadur slopes for Kruskal-Wallis		
	Simple-vs-complex	Simple-vs-multi	Complex-vs-multi	Simple-vs-complex	Simple-vs-multi	Complex-vs-multi
	2.19E-01	5.06E-02	2.37E-01	7.92E-04	2.52E-03	8.79E-05
R	2.90E-01	1.33E-01	7.00E-01	8.11E-04	2.49E-03	2.73E-05
K	3.50E-01	1.81E-02	2.81E-01	1.74E-03	1.10E-02	1.27E-04
D	2.59E-01	5.65E-02	1.78E-01	1.65E-03	6.04E-03	1.60E-04
E	6.03E-01	4.53E-01	4.41E-01	5.62E-04	1.26E-03	4.34E-05
Y	4.19E-01	1.84E-01	5.70E-01	1.33E-03	3.81E-03	6.62E-05
W	6.37E-01	4.88E-01	9.77E-01	6.68E-05	2.25E-04	3.47E-07
L	5.00E-01	2.22E-01	9.62E-01	6.76E-04	2.10E-03	3.11E-06
C	1.87E-01	8.67E-02	4.08E-01	4.86E-04	1.23E-03	3.05E-05
R+K	1.68E-01	4.52E-02	1.91E-01	1.25E-03	3.68E-03	7.97E-05

**Table 2.6: Simple transmembrane helices are less similar than complex transmembrane helices to transmembrane helices from multi-pass proteins in ExpAll.** As in Table 2.5, the statistical results were gathered by comparing complex single-pass TMHs, simple TMHs from single-pass proteins and TMHs from multi-pass proteins; however, in this case only ExpAll is used. The abundance of different residues at each position when using the centrally aligned TMH approach was compared with several statistical tests (the K-S, K-W and the  $\chi^2$  statistical tests) and the Bahadur slope values of those results

Residues	p-values for $\chi^2$			Bahadur slopes for $\chi^2$		
	Simple-vs-complex	Simple-vs-multi	Complex-vs-multi	Simple-vs-complex	Simple-vs-multi	Complex-vs-multi
R	5.10E-06	2.98E-01	5.10E-06	9.17E-03	1.61E-03	6.23E-05
K	2.35E-03	1.85E-01	2.35E-03	4.81E-03	3.88E-03	9.78E-05
D	2.61E-08	1.84E-01	2.61E-08	4.15E-02	7.90E-03	1.41E-04
E	2.38E-10	2.04E-01	2.38E-10	3.88E-02	7.08E-03	1.22E-04
Y	3.03E-01	3.11E-01	3.03E-01	2.01E-03	2.49E-03	5.51E-05
W	4.21E-03	4.29E-01	4.21E-03	1.11E-02	4.76E-03	6.46E-05
L	3.79E-01	3.04E-01	3.79E-01	2.28E-04	4.66E-04	1.50E-05
C	3.87E-01	2.52E-01	3.87E-01	1.75E-03	3.28E-03	1.48E-04
R+K	7.16E-04	2.52E-01	7.16E-04	2.80E-03	1.28E-03	3.76E-05
D+E	3.58E-05	2.94E-01	3.58E-05	1.03E-02	1.94E-03	4.90E-05
p-values for Kolmogorov-Smirnov			Bahadur slopes for Kolmogorov-Smirnov			
	Simple-vs-complex	Simple-vs-multi	Complex-vs-multi	Simple-vs-complex	Simple-vs-multi	Complex-vs-multi
	3.61E-01	4.31E-02	3.61E-01	7.66E-04	7.79E-03	1.62E-04
K	4.31E-02	8.93E-01	4.31E-02	2.49E-03	1.05E-02	6.57E-06
D	1.39E-01	2.18E-03	1.39E-01	4.68E-03	3.61E-02	5.10E-04
E	5.31E-01	1.33E-04	5.31E-01	1.11E-03	2.81E-02	6.87E-04
Y	2.31E-01	9.06E-04	2.31E-01	2.47E-03	6.26E-03	3.30E-04
W	5.31E-01	4.98E-03	5.31E-01	1.29E-03	1.13E-02	4.04E-04
L	2.31E-01	2.31E-01	2.31E-01	3.45E-04	2.12E-03	1.85E-05
C	5.31E-01	3.61E-01	5.31E-01	1.16E-03	8.91E-04	1.09E-04
R+K	1.39E-01	2.31E-01	1.39E-01	7.61E-04	4.82E-03	4.00E-05
D+E	1.39E-01	9.06E-04	1.39E-01	1.99E-03	1.41E-02	2.80E-04
p-values for Kruskal-Wallis			Bahadur slopes for Kruskal-Wallis			
	Simple-vs-complex	Simple-vs-multi	Complex-vs-multi	Simple-vs-complex	Simple-vs-multi	Complex-vs-multi
	4.37E-01	3.92E-01	4.37E-01	6.24E-04	2.52E-03	4.82E-05
K	3.83E-01	6.93E-01	3.83E-01	7.62E-04	2.88E-03	2.13E-05
D	4.49E-01	1.81E-01	4.49E-01	1.90E-03	1.06E-02	1.42E-04
E	7.64E-01	1.94E-01	7.64E-01	4.71E-04	9.05E-03	1.26E-04
Y	8.32E-01	3.36E-01	8.32E-01	3.09E-04	9.63E-04	5.15E-05
W	7.25E-01	1.36E-01	7.25E-01	6.53E-04	5.44E-03	1.52E-04
L	7.15E-01	7.95E-01	7.15E-01	7.90E-05	3.41E-04	2.90E-06
C	8.47E-01	9.54E-01	8.47E-01	3.05E-04	4.26E-05	5.06E-06
R + K	2.89E-01	5.13E-01	2.89E-01	4.79E-04	1.41E-03	1.82E-05
D+E	4.94E-01	2.07E-01	4.94E-01	7.11E-04	4.14E-03	6.29E-05

amino acid types). Similarly, simple single-pass TMH+flank segments differ significantly from multi-pass TMH+flank segments (K-W test p-values<3.e-2 for R, K, D, E, Y, W amino acid types as well as for K+R and D+E). The trends are the same for the ExpAll dataset (Table 2.6): simple and complex single-pass TMH+flank regions differ in charged amino acid type distributions ( $\chi^2$  p-value<4.21e-3 for all cases), as well as simple single-pass and multi-pass ones, do (K-W test p-values<5.e-2 for R, D, E, Y, W amino acid types and D+E).

Whereas p-value tests for significant differences between distributions depend strongly on the amount of data, the more informative Bahadur slopes that measure the distance from the zero hypothesis are independent of the amount of data [259–261]. As we can see in Tables 2.5 and 2.6, the absolute Bahadur slopes for the simple single-pass to multi-pass comparison are always larger (even by at least an order of magnitude): (ii) for all three statistical tests applied ( $\chi^2$ , K-S and K-W), (ii) for all amino acid types, for K+R and E+D and (iii) for both datasets UniHuman and ExpAll. Thus, complex single-pass TMH+flanks have compositional properties that are indeed very similar to those of multi-pass ones (which are known to have a large fraction of complex TMHs [44, 45]). This strong evidence implies that the actual issue is not so much about single- and multi-pass TMH segments but between simple and complex TMHs where the first are exclusively guided by the anchor requirements whereas the latter have more complex restraints to fulfil.

Several distribution features of simple TMHs from single-pass proteins when compared to complex TMHs from single-pass proteins and TMHs from multi-pass proteins that contribute to the statistical differences (Figure 2.9) are especially notable. There is a more pronounced trend for positively-charged residues and tyrosine to be preferentially located on the inside flanks and for negatively-charged residues to be on the outside flanks. The symmetrical peaks in the percentage distribution of tyrosine in complex single-pass TMHs are more akin to multi-pass TMHs, whereas in simple TMHs the distribution resembles a more typical single-pass helix (compare with Figure 2.2). Furthermore, the depression of charged residues within the TMH itself is strongest in simple single-pass TMHs.

To emphasise, tryptophan is essentially not tolerated within the simple TMHs and there are higher peaks of tryptophan occurrence at either flank. We also see a strong

inside skew for leucine clustering within the core of simple TMHs which is not present in the “flatter” distributions of complex single-pass TMHs and TMHs from multi-pass proteins.

There is obviously a cysteine-inside preference for simple, single-pass TMHs but less in complex, multi-pass TMHs (Figure 2.9). This conclusion is contrary to a previous study [258] but that deduction was drawn from a much smaller dataset of 45 single-pass TMHs and 24 multi-pass TMPs.

## 2.4 Discussion

The “negative-outside/non-negative inside” skew in TMHs and their flanks is statistically significant We have seen that, consistently throughout the datasets, there is a trend for generally rare negatively-charged residues to prefer the outside flank of a TMH rather than the inside (and to almost completely avoid the TMH itself); be it by suppression on the inside and/or enrichment on the outside. The trend is much stronger in single-pass protein datasets than in multi-pass protein datasets. However as we elaborated on further, the real crux of the bias appears to be associated with the TMH being simple or complex [44, 45], thus, whether or not the TMH has a role beyond anchorage. The existence of this bias has implications for topology prediction of proteins with TMHs, engineering membrane proteins as well as for models of protein transport via membranes and protein-membrane stability considerations.

It should be noted that the controversy in the scientific community about the existence of a negative-charge bias at TMHs was mainly with regard to multi-pass TMPs. Despite having access to much larger, better annotated sequence datasets and many more 3D structures than our predecessors, we also had our share of difficulties here (see Results section 2.3.3 and Table 2.3). The straightforward approach results in inconclusive statistical tests if datasets become small (for example, if selections are restricted to subcellular localisations, 3D structures or if very harsh sequence redundancy criteria are applied) and, especially, if TMHs with very short or no flanks are included. Therefore in the case of multi-pass proteins, we studied flanks as taken from the TM boundaries in the databases under several conditions: (i) without allowing flank overlap between neighbouring TMHs, (ii) as subset of (i) but with requiring

some minimal flank length at either side, (iii) with overlapping flanks. We also studied flanks after central alignment of TMHs and assuming standardised TMH length. multi-pass TMHs (without overlapping flanks) do not show statistically significant negative-charge bias under condition (i) but, apparently, due to many TMHs without any or super-short flanks at least at one side. Significance appears as soon as subsets of TMHs with flanks at both sides are studied. Not surprisingly, there is no charge bias if there are no flanks in the first place. It is perhaps worth noting that the results from multi-pass TMHs with overlapping flanks may involve amplification of skews since it involves multiple counting of the same residues. Given the redundancy threshold of UniRef90, we cannot rule out that these statistical skews are the result of a trend from only a small sub-group of TMPs which is being amplified. Hence, we also needed to observe if these same observed biases were true in condition (ii), which is indeed the case.

As the “negative-outside/negative-not-inside” skew is widely observed among varying taxa and subcellular localisations with statistical significance, it appears to, at least to a certain extent, be caused by physical reasons and be associated with the background membrane potential. Several earlier considerations and observation support this thought: (i) Firstly, a concert between the negative and positive charge on the TMH flanks drives anchorage and the direction of insertion of engineered TMHs [243, 254]. (ii) The inner leaflet of the plasmalemma tends to be more negatively-charged [262]. Specifically, phosphatidylserine was found to distribute in the cytosolic leaflets of the plasma membrane and it was found to electrostatically interact with moderately positive-charged proteins enough to redirect the proteins into the endocytic pathway [263]. The negative charge of proteins at the inside of the plasma-membrane would decrease the anchoring potency of the TMH via electrostatic repulsion. (iii) Thirdly in membranes that maintain a membrane potential, there are inevitably electrical forces acting on charged residues during chain translocation as this influences the translocon machinery when orienting the TMH. Therefore, it is no surprise that we see an inside-outside bias for negatively-charged residues that is opposite to the one for positively-charged residues. The negative charges in TMH residues have been shown to experience an electrical pulling force as they pass through the bacterial SecYEG translocon import [42, 253]. Also, they are known to be involved in

intra-membrane helix-helix interactions [264]. For example, aspartic acid and glutamic acid can drive efficient di- or trimerisation of TMHs in lipid bilayers and, furthermore, that aspartic acid interactions with neighbouring TMHs can directly increase insertion efficiency of marginally hydrophobic TMHs via the Sec61 translocon [264]. In support of this, less acidic residues are found in single-pass TMHs, among which only some will undergo intra-membrane helix-helix interactions. As the mutation studies have shown negative charge as a topological determinant [248], therefore, it is perhaps no surprise that we observe a skew in negatively-charged residues in a similar manner to the skew in positively-charged residues.

Whereas the “negative-outside/negative-not-inside” skew is observed for distantly related eukaryotic species and it is also present in Gram-negative bacteria such as *E. coli*, this sequence pattern was not observed for the Gram-positive bacteria in which there is no observable bias. In contrast, Archaea have a statistically significant “negative-inside” propensity both for single- and multi-pass TMPs. It is known that Archaea have remarkably different membranes compared to other kingdoms of life due to their extremophile adaptations to stress [265]. Whilst it is unclear why negative charge is distributed so differently in UniArch to the other taxonomic datasets, one must appreciate that a much more nuanced approach would be needed to draw formal conclusions about Archaea, which current databases cannot provide due to the relatively limited information and annotation of Archaean proteomes.

Methodological issues made previous studies struggle to identify negatively-charged skews with statistical significance

Whereas the influence of a negative-charge bias in engineered proteins with TM regions on the direction of insertion into the membrane was solidly established [114, 248, 250, 251, 266], the search for the negative charge distribution pattern in the statistics of sequences of TM proteins from databases failed to find significance for the expected negative charge skew [86, 109, 110, 114, 117, 118].

Generally speaking, the datasets from previous studies have been considerably smaller compared with those in our work (only Sharpe *et al.* had a similar order of magnitude [86]), especially those with experimental information about 3D structure and membrane topology that we used for validation. And they might not have had the luxury of using UniProt’s improved TRANSMEM consensus annotation based on

a multitude of TM prediction methods and experimental data, but this is also not the major issue. We found that there are other factors that are critical for observing sequence bias such as negative charge skew in the case of TMHs.

- i Acidic residues are rare near and within TMH and biases in their distribution are easily blurred by minor fluctuations of much more frequent amino acid types, most notably leucine. Therefore, the method of normalisation is critical. We have shown that normalising by the total amount of residues of the amino acid type studied within the sequence region under consideration is appropriate to answer the question where to find a negatively-charged residue if there is any at all (called “relative percentage” in this work).
- ii The alignment of the TMHs is critical. It was common practice to align TMH according to the most cytosolic residue [86] although it is known that the membrane/cytosol boundary of the TMH is not well defined (and the exact boundary is even less well understood at the non-cytosolic side). Aligning the TM regions and their flanks from the center of the TMH was first proposed by Baeza-Delgado *et al.* [109]. Since we know now that acidic residues are often suppressed in the cytosolic flank and within the TMH, this implies that the few acidic residues found in the cytosolic interface would appear more comparable to those in the poorly defined non-cytosolic interface as the respective residues are spread over more potential positions, diminishing any observable bias.
- iii We find that separation into single- and multi-pass TM datasets (or, even better, simple and complex TMHs [44, 45]) is critical to study the inside/outside bias. As many TMHs in multi-pass TMPs have essentially no flanks or very short flanks if the condition of non-overlap is applied to flanks of neighbouring TMHs, this might also obscure the observation of the negative-charge bias. If there are no flanks, then there will be no residue distribution bias in these flanks. The problem can be alleviated by either studying only subsets with minimal flank lengths on both sides (although datasets might become too small for statistical analysis) or by allowing flank overlaps between neighbouring TMHs.
- iv This classification is even more justified in the light of previous reports about the “missing hydrophobicity” in multi-pass TMHs [74, 248, 267, 268]. Otherwise, the

distribution bias well observed among the exclusive anchors could be lost to noise. This addresses the more biologically contextualised issue that there are different evolutionary pressures on different types of TMHs. The negative charge skew is most pronounced for dedicated anchors frequently found with simple TMHs typically observed in single-pass TM proteins. These TMHs are pressured to exhibit residue biases that may aid anchorage in a topologically correct manner. Complex TMHs, typically within multi-pass membrane proteins that have a function beyond anchorage, comply with a multitude of restraints structural and functional constraints and the negative charge skew is just one of them.

The most representative precedent papers are those of Sharpe *et al.* [86] from 2010 (with 1192 human and 1119 yeast single-pass TMHs), Baeza-Delgado *et al.* [109] (with 792 TMHs mixed from single- and multi-pass TMPs) and Pogozheva *et al.* [110] (TMHs from 191 mixed from single- and multi-pass TMPs with structural information) both from 2013. Whereas the first analysis would have benefited from the central alignment approach and the first two studies from another normalisation as described above, the third study did come close to our findings. To note, their dataset mixed with single- and multi-pass proteins was too small for revealing the negative-charge bias with significance; yet, they observed total charge differences at either sides of the membrane varying for both single- and multi-pass proteins. Membrane asymmetry due to positively-charged residues occurring more frequently on the cytosolic side causes net charge unevenness at both sides of the membrane. This observation has been known to correlate with orientation for decades [109, 113, 264]. Our data shows that the negative charge skew contributes to this asymmetry.

There are differences in charged amino acid residue biases in TMH flanks through each stage of the secretory pathway

Here, we observe differences throughout sub-cellular locations along the secretory pathway. We found that negative charges are enriched at the outside flank (in the ER), both enriched outside and suppressed inside for the Golgi membrane, and suppressed on the inside flank in the PM. It has been suggested that the leaflets of different membranes have different lipid compositions throughout the secretory pathway [92] and this has led to general biochemical conservation in terms of TMH length and amino acid composition in different membranes [86, 110]. However, herein only the organelles with

the most protein record annotation were used. Further investigation into the TMPs of lysosomes, endosomes, and other ER-Golgi transition vesicles would yield more information on this. Furthermore, there could be study into TMPs not associated with the signal peptide TMPs destined for the secretory pathway such as those TMPs embedded in the membranes of the mitochondrion, apicoplast, chromoplast, chloroplast, cyanelle, thylakoid, amyloplast, peroxisome, glyoxysome, and hydrogenosome.

Lipid asymmetry in the Golgi and PM (in contrast to the ER) has been known about for over a decade [269, 270]. To note, the Golgi and PM have lipid asymmetry with sphingomyelin and glycosphingolipids on the non-cytosolic leaflet, and phosphatidylserine and phosphatidylethanolamine enriched in the cytosolic leaflet. Although the ER is the main site for cholesterol synthesis, it has markedly low concentrations of sphingolipids [271]. Golgi synthesises sphingomyelin, a lipid not present in the ER, but present in both the Golgi [272] and in the PM [184, 273]. The PM is also enriched with densely packed sphingolipids and sterols [274]. Another factor influencing the sequence patterns of TMHs and their along the secretory pathway appears to be the variation in membrane potentials [100, 101, 103].

Several sequence features can be assigned to anchor TMHs: Charged-residue flank biases, leucine intra-helix asymmetry, and the “aromatic belt”.

We investigated the difference between TMHs from single-pass and multi-pass proteins and found significant differences in sequence composition that are reflective of the biologically different roles the TMHs play. To emphasise and validate these findings, we separated TMHs from single-pass proteins into simple and complex TMHs [44, 45]; ones that likely contains mostly TMHs that act as exclusive anchors, and another that have roles beyond anchorage. This leaves us with “anchors” (simple TMHs from single-pass proteins) and “non-anchors” (complex TMHs from single-pass proteins, and TMHs from multi-pass proteins). If there are strong sequence feature differences between anchors and non-anchors, it is likely that the sequence feature has a role in satisfying membrane constraints to act as an energetically optimally stable anchor.

Future studies in the area would desirably directly include a comprehensive analyses of datasets oligomerised TMHs from single-pass proteins and ascertain if they appear to be more similar to simple anchors, multi-pass, or generally neither. Currently, no sufficiently complete set of intra-membrane oligomerised single-pass proteins exists

that can be compared to a large set of known non-oligomerising proteins. The current work sidesteps this issue by comparing single-pass proteins with simple TMHs, which tend to be simple anchors (as shown in previous work [44, 45]), against datasets that contain TMHs that will form intra-membrane bundles. Bluntly, the simple/complex status of a TMH can be easily computed from its sequence with TMSOC whereas the oligomerisation state of most membrane proteins still needs to be experimentally determined.

Unsurprisingly, both positively and negatively-charged residues can be seen to be more strongly distributed with bias in anchors than non-anchors. Both the “positive-inside” rule as well as the “negative-outside/non-negative-inside” bias are mostly observable in simple single-pass TMHs (although they are statistically significant elsewhere). It is perhaps true that where a bias is clearly present in both non-anchors and anchors alike, it is a strong topological determinant, whereas if the residue is only distributed with topological bias in exclusively anchoring TMHs, we can attribute these features more specifically to biophysical anchorage. This being said, we should not rule out that the same features aid topological determination since negative charge has been shown to be a weaker topological determinant than positively-charged residues (35).

Tyrosine and tryptophan residues commonly are found at the interfacial boundaries of the TMH and this feature is called the “aromatic belt” [86, 109, 116–118] and this was thought to be caused by their affinity to the carbonyl groups in the lipid bilayer [275]. Not all types of aromatic residues are found in the aromatic belt; phenylalanine has no particular preference for this region [117, 119]. It is still unclear if the aromatic belt has to do with anchorage or with translocon recognition [109]. Here, TMHs with exclusively anchorage functions showed stronger preferences for the W and Y in the aromatic belt region, otherwise known as the water-lipid interface region than TMHs with function beyond anchorage. This is strong evidence that the aromatic belt indeed assists with anchorage, and is less conserved where the TMH must conform to other restraints beyond membrane anchorage. Furthermore, we see that the tyrosine’s preference for the inside interface region also appears to be to do with anchorage and this trend is somewhat true for tryptophan, too.

Finally, our findings corroborate earlier reports that many multi-pass TMHs are

much less hydrophobic than typical single-pass TMH and about 30% of them fail the hydrophobicity requirements of  $\Delta G$  TMH insertion prediction (“missing hydrophobicity”) [74, 116, 267, 268]. We also find that the leucine skew and the hydrophobic asymmetry towards the cytosolic leaflet of the membrane is more pronounced in simple, single-pass TMHs than in complex or multi-pass ones; thus, it appears to be another anchoring feature. It was found previously that the hydrophobic profiles of TMHs of multi-pass proteins share similar hydrophobicity profiles on average irrespective of the number of TMHs and TMHs from single-pass proteins have been found to be typically more hydrophobic than TMHs from multi-pass proteins [44]. Sharpe *et al.* [86] report an asymmetric hydrophobic length for single-pass TMHs. Our study reiterates the hydrophobic asymmetry and attributes it mainly to the leucine distribution. The leucine asymmetry might be linked to the different lipid composition of either leaflet of biological membranes.

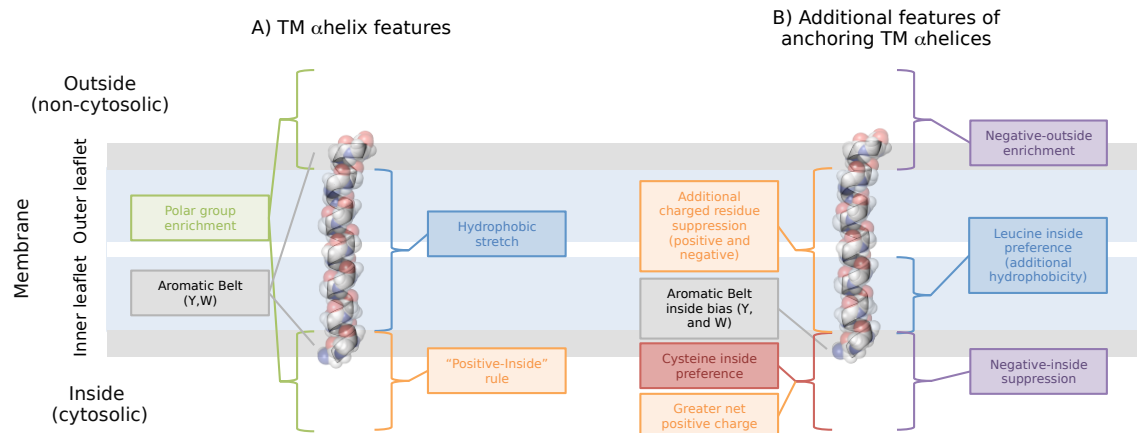


**Figure 2.10: Residue distributions of transmembrane anchors.** A view showing additional residue distribution features that transmembrane helices with an anchorage function display. a The more classic model of a TMH showing the “positive-inside” rule [113], the hydrophobic core [73], the polar enrichment that flanks the hydrophobic stretch [109] and the aromatic belt [117]. b Simple anchors may display additional features that conform to the membrane biophysical constraints: further suppression of charge in the hydrophobic core (Table 2.1), intra-membrane leucine asymmetry that likely causes hydrophobic skew [86] (Table 2.4, Figure 2.6), a higher preference for cysteine on the inside flanking region (Figure 2.9K and L), a higher net “positive-inside” charge (Figure 2.4), asymmetric skew of the hydrophobic belt favouring the inner leaflet interface (Figure 2.9E, F, G, and H) and a negative-outside bias via suppression on the inside flanking region or enrichment on the outside flanking region (Figure 2.9C and D, Tables 2.2 and 2.3)

In summary, three key features can be assigned to aiding TMH stability in the membrane (Figure 2.10): (i) charge, (ii) the aromatic belt, and (iii) leucine leaflet preference. What is most novel here is that each of these features are furthermore

distributed with preference for a particular side of the bilayer in the case of anchoring TMHs. These differences in inside-outside topology that are most present in anchoring TMHs further supports the notion that there are broad lipid compositional differences between the inner and outer leaflets of the bilayers [86]. Furthermore, while some TMHs conform and complement to the properties of the bilayer, other TMHs with function beyond anchorage are less constrained to biophysically complement the bilayer. For these TMHs, any advantage gained by adhering to the membrane restrictions is outweighed by more complicated protein dynamics, topological frustration and protein functional requirements.

To conclude, the large fraction of functionally uncharacterised genomic sequences is the great bottleneck in life sciences at this moment that hinders many biomedical and biotechnological applications, some with tremendous societal need [241, 276]. Among these uncharacterised genomic regions, there is  $\sim$ 10000 protein-coding genes, especially many membrane-embedded proteins. It is hoped that the NNI/NO-rule as well as the other sequence properties of membrane anchoring TMHs described in this article will add new insights for membrane protein function discovery, design and engineering.

## 2.5 Methods

### 2.5.1 Datasets

#### Databases.

All datasets used for analysis are listed in Table 2.1. Transmembrane protein sequences and annotations were taken from TOPDB [257] and UniProt [75]. UniProt derived datasets are the most comprehensive datasets built with (i) robust transmembrane prediction methods providing the limit of today’s achievable accuracy with regard to hydrophobic core localisation and (ii) subcellular location annotation that can be used for orientation determination. However, they mostly rely on predicted transmembrane regions. TOPDB has experimental verifications of the orientation from the literature that are independent of prediction algorithms [257]. Unfortunately, this dataset is much smaller with too few entries to have it divided with regard to taxonomy or subcellular locations.

UniProt database files were downloaded by querying the server for different taxonomic groups as well as different subcellular membrane locations; UniHuman (human representative proteome), UniCress (*Arabidopsis thaliana*, otherwise known as mouse eared cress, representative proteome), UniER (human endoplasmic reticulum representative proteome), UniPM (human plasma membrane representative proteome), UniGolgi (human Golgi representative proteome). To enforce a level of quality control, the queries were restricted to manually reviewed records and transmembrane proteins with manually asserted TRANSMEM annotation [75]. Proteins were then sorted into multi-pass and single-pass groups according to having more than one or exactly one TRANSMEM region respectively. TRANSMEM regions are validated by either experimental evidence [75], or according to a robust transmembrane consensus of the predictors TMHMM [67], MemSat [66], Phobius [71, 236] and the hydrophobic moment plot method of Eisenberg and co-workers [144]. TMHs and flanking regions were oriented according to UniProt TOPO\_DOM annotation according to the keyword “cytoplasmic”. If a “cytoplasmic” TOPO\_DOM was found in the previous TOPO\_DOM relative to the TRANSMEM region then the sequence remained the same. If “cytoplasmic” was found in the next TOPO\_DOM, relative to the TRANSMEM section then the sequence was reversed. Proteins without the “cytoplasmic” keyword in their TOPO\_DOM annotation were omitted from further analysis.

The TOPDB database [257] is a manually curated database composed of experimental records from the literature that allow determination of the protein topology. Experiments include fusion proteins, posttranslational modifications, protease experiments, immunolocalization, chemical modifications as well as revertants, sequence motifs with known mandatory membrane-embedded topologies, and tailoring mutants (Table 2.7).

Length cut-offs for the TMH were set at 16 as the shortest length and 38 as the longest.

To note, we are aware that proteome datasets are a moving target that have dramatically changed over the years and, probably, will continue to do so to some extent in the future[83]. Yet, we think that currently available protein sequence sets are sufficiently good for the purpose as we search for statistical properties in the TMH context only.

**Table 2.7:** The experimental evidences of TOPDB. The total number of experimental evidences that contribute to ExpAll according to the TOPDB database (More information at <http://topdb.enzim.hu/?m=exptype&mid=14>). “\*” refers to the total number of a subsection being larger than the total of the subcategories, likely due to lack of annotation where ambiguous literature evidence is counted toward the total, but cannot be categorised further.

	Experiment	Bitopic (single-pass)	Polytopic (multi-pass)
<b>Fusion</b>	PhoA	97	2332
	PhoAS	0	90
	LacZ	20	433
	PhoALacZ	0	224
	BlaM	162	570
	BAD	0	2
	PL	0	47
	GFP	18	591
	HIS	4	2
	SplitUbiquitin	0	11
	Suc2	0	96
<b>PostTransMod</b>	Other	1	137
	Total Fusion	316*	4600*
	NGlyc	4634	1130
	Cman	0	6
	Phosphorylation	4	1
<b>Protease</b>	Ubiquitination	47	102
	Total PostTransMod	4685	1239
	Partial Proteolysis	51	264
	Signal Peptidase	1	0
<b>Immunolocalisation</b>	TID	13	15
	Total Protease	64	279
	Epitope Insertion	33	313
<b>Chemical modification</b>	Endogen Epitope	8	41
	Total Immunolocalisation	53*	451*
<b>Structure</b>	Cys	0	361
	Lys	0	3
	Quenching	0	2
	Total Chemical Modification	0	368*
<b>Other</b>	PDBTM TMDET	5968	41977
	Revertants	0	14
	SeqMotif	2	32
	Tailoring	1	67
	Total other	3	115*

The following datasets are used throughout this work:

### ExpAll

TOPDB contained 4190 manually annotated transmembrane proteins at the time of download [257]. CD-HIT [277] identified 3857 representative sequences using sequence clusters of >90% sequence identity. This choice of similarity threshold was chosen since CD-HIT ultimately underlies the clustering behind UniRef. Unlike the other datasets, which by definition contain reasonably typical TMHs, many of the transmembrane segments annotated in TOPDB are extremely short or long and this would cause severe unrealistic hydrophobic mismatches. Especially, the short segments could be the result of miss-annotation, TMHs broken into pieces due to kinks or segments that peripherally insert only into the interface of the membrane bilayer. To remove the atypical lengths, cut-offs were set at 16 as the lower cut-off and 38 as the upper cut-off after inspecting the length histogram. We found that, for the single-pass TMHs in TOPDB, 1215 out of 1544 are within the length limits (78.7%). Among the 17141 multi-pass TMHs, we find 15563 within our global length limits (from 2205 TOPDB records corresponding to 2281 UniProt entries). This removed 1578 very short TMHs and none of the long TMHs. Our cut-off selection is very similar to the one by Baeza-Delgado *et al.* [109].

To get an idea of the taxonomical breakdown in the ExpAll dataset, the UniProt ID tags were extracted and mapped to UniProtKB. The combined dataset of multi-pass (single-pass) proteins was mapped to 1288 (1343) eukaryotic records, 404 (776) of which were human records, 926 (191) bacterial records, 46 (5) archaea records, and 14 (22) viral records.

### UniHuman

This is a set of mostly human TMH-containing proteins or their close mammalian homologues. UniProtKB contains 5187 human protein records that are manually annotated with TRANSMEM regions (query = “annotation:(type:transmem) AND reviewed:yes AND organism:“Homo sapiens (Human) [9606]” AND proteome:up000005640”). To reduce sequence redundancy, these sequences were submitted to UniRef90 [278]. To note, UniRef90 was chosen over UniRef50 to maintain a viable

size of datasets for statistical analysis of occurrence of negatively-charged residue, which are very rare in the vicinity of TMHs. 5015 UniRef90 clusters represented the 5187 sequences. A list of sequences representing those clusters was submitted back to UniProtKB resulting and 5014 representative entries were recovered. There is a small issue in that the list of representatives from UniRef includes non-canonical isoforms, while the batch retrieve query of UniProtKB only supports complete entries, i.e. canonical isoforms. This resulted in the loss of one record at this point is due to two splice isoforms acting as representative identifiers. Of those 5014 records, 4714 were records from human entries, 197 were from mice, 94 from rats, 5 from bovine, 2 from chimps, 1 from Chinese hamsters, and 1 from pigs. Although the TMH length variations within the UniHuman dataset are much smaller than for ExpAll, we applied the same length cut-offs for the sake of comparability. Out of the 1709 single-pass cases, 1705 entered the final dataset. Of those, 1596 were from human records, 87 were from mouse, 19 were from rat, and 2 were from chimpanzee. Among the 12390 multi-pass TMHs, 12353 were included into UniHuman. The other, multi-pass record identifiers were mapped to 1789 UniProtKB entries. 1660 of these were human entries, 63 from rat, 61 from mouse, 4 from bovine, and 1 from Chinese hamster. This clustered human dataset was then queried for subcellular locations to make the UniER, UniGolgi, and UniPM datasets (detailed below).

## UniER

The clustered UniHuman dataset was queried using UniProtKB for endoplasmic reticulum subcellular location (locations:(location:“Endoplasmic reticulum [SL-0095]” evidence:manual)). This returned 487 protein entries, 457 of which belonged to human, 24 to mouse and 6 to rat. 287 of these records contained sufficient annotation for orientation determination. 132 were single-pass entries of which 120 records were from humans, 11 from mouse, and 1 from rat. 155 were multi-pass entries containing 898 transmembrane helices. 144 were records from human, 8 were from mouse and 3 were from rat.

### UniGolgi

The clustered human dataset was queried using UniProtKB for Golgi subcellular location (locations:(location:“Golgi apparatus [SL-0132]” evidence:manual)). This returned 323 protein entries, 301 of which belonged to human, 19 to mice, 2 to rat and 1 to pig. 269 of these records contained sufficient annotation for orientation determination. 206 were single-pass entries of which 195 records were from human, 9 from mouse, and 1 from rat. 61 were multi-pass entries containing 383 transmembrane regions. 54 were records from human, 6 were from mouse and 1 was from rat.

### UniPM

The clustered human dataset was queried using UniProtKB for the cell membrane subcellular location (locations:(location:“Cell membrane [SL-0039]” evidence:manual)). This returned 1036 protein entries, 948 of which belonged to humans, 62 to mice, and 26 to rats. 920 of these records contained sufficient annotation for orientation determination. 493 were single-pass entries of which 451 records were from human, 37 from mouse, and 5 from rat. 427 were multi-pass entries containing 3079 transmembrane regions. 394 were records from human, 17 were from mouse and 16 were from rat.

### UniCress

For the mouse ear cress, a representative proteome dataset was acquired with the query annotation:proteomes:(reference:yes) AND reviewed:yes AND organism:“Arabidopsis thaliana (Mouse-ear cress) [3702]” AND proteome:up000006548. This returned 3174 records in UniProtKB. UniRef90 identified 3111 clusters. 3110 of the representative sequences were mapped back to UniProtKB. Of those, 3090 were from Arabidopsis thaliana, 2 from Hornwort, 1 from cucumber, 1 from tall dodder, 1 from soybean (*Glycine max*), 2 from Indian wild rice, 2 from rice, 2 from garden pea, 1 from potato, 4 from spinach, 1 from *Thermosynechococcus elongatus* (thermophilic cyanobacteria), 1 from wheat, and 2 from maize. Of those there were 1146 with suitable TOPO\_DOM annotation for topological orientation determination. 632 of those records were identified as single-pass, all of which were from *Arabidopsis thaliana*. 507 protein records were from multi-pass records, which contained 3823 transmembrane helices. 506 of

those records were from *Arabidopsis thaliana*, whilst 1 was from *Thermosynechococcus elongatus*.

### **UniFungi**

For the Fungi dataset, the query “annotation:(type:transmem) taxonomy:“Fungi [4751]” AND reviewed:yes” was used. This returned 5628 records that were submitted to UniRef90. UniRef90 identified 4934 representative records, all of which were successfully mapped back to UniProtKB. Of those, 2070 had suitable annotation for orientation. 1990 records belonged to Ascomycota including 1243 Saccharomycetales. 73 were Basidiomycota, and 6 were Apansporoblastina. 729 records contained a single TMH region, 702 of which belonged to Ascomycota, 26 to Basidiomycota and one to *Encephalitozoon cuniculi*, a Microsporidium parasite. 8698 helices were contained in 1338 records of multi-pass proteins. Of these records 1285 were Ascomycota, 47 were Basidiomycota, and 5 were Apansporoblastina. One TMH from UniFungi was discounted from P32897 due to an unknown position.

### **UniEcoli**

This dataset was generated by querying UniProt with “reviewed:yes AND organism:”*Escherichia coli* (strain K12)[83333]”” which returned 941 hits. The hits were submitted to UniRef90, which returned 935 clusters. The representative IDs were then resubmitted to UniProtKB, all of which returned successfully. 934 were from Bacteria, whilst one were from lambda-like viruses. Of the bacterial records, 862 were from various *Escherichia* species of which 565 were from *E. coli* strain K12, 28 were from *Salmonella choleraesuis*, 25 were from *Shigella* and the rest all also fell under Gammaproteobacteria class. This dataset contains 54 single-pass proteins and 3888 helices from 529 multi-pass proteins with sufficient annotation for topological determination.

### **UniBacilli**

The Bacilli dataset was constructed by querying UniProt for “reviewed:yes AND taxonomy:”*Bacilli*””. This returned 5044 records, which were submitted to UniRef90. 2,591 clusters were found in UniRef from these records. The representative IDs were

successfully resubmitted to UniProtKB. 2031 of these were of the genus *Bacillales* whilst 560 were also of the genus *Lactobacillales*. This dataset contains 124 single-pass proteins and 822 helices from 140 multi-pass proteins.

## UniArch

The Archaea dataset was constructed by querying UniProt for “reviewed:yes AND taxonomy:”Archaea [2157]””. This returned 1,152 records, which were submitted to UniRef90. 1,054 clusters were found in UniRef from these records. The representative IDs were successfully resubmitted to UniProtKB. 946 records belonged to the Euryarchaeota, 101 to Thermoprotei, 4 to Thaumarchaeota, and 3 to Korarchaeum *cryptoflum*. This dataset contains 48 single-pass proteins and 59 multi-pass proteins containing 327 helices from 59 proteins.

### 2.5.2 On the determination of flanking regions for transmembrane helices and the transmembrane helix alignment

The determination of the boundary point at the sequence between the TMH in a membrane and the sequence immersed in the cytoplasm, extracellular space, vesicular lumen, etc. is not that trivial as it initially appears. There is a lot of dynamics in the TMH positioning and the actual boundary point will be represented by various residues at different time points. Whilst the TMH core region detection from a sequence is trivial with modern software, the exact determination of TMH boundaries remains difficult since it is unclear exactly how far in or out of the membrane a given helix extends [232]. Previous studies have dealt with this issue in various ways [86, 109, 110, 279].

Here in this work, we explore two boundary definitions. First, we assign TMH boundary locations as described in the respective databases. These flanks are the ones that are reported in our TMH data files that are available at the WWW-site associated with this paper. We studied flank lengths of  $\pm 5$ ,  $\pm 10$ , and  $\pm 20$  residues preceding and following the inside and outside TMH boundaries. In these cases, the flanks are aligned relative to the residue closest to the TMH.

In cases where the loops before and after the TMH are shorter than the predefined

flank lengths, further precautions are necessary. In the multi-pass datasets particularly (Figure 2.11 & Figure 2.4), the flanks overlap with other membrane region flanks. We explore several variants. On the one hand, we work with data files where the flank residue stretches are equally truncated so that no overlap occurs. If the loop length was uneven, the central odd residue was not included into any flank. We find surprisingly, that a large number of TMH has no or just a super-short flank, a circumstance that should disturb any statistical analysis due to the absence of objects. Therefore, we also work with alternative datasets (i) with flanks overlapping between consecutive TMH (e.g., in Table 2.3B; yet, it leads to some residues being counted more than one time) as well as (ii) with subsets of the data where the flanks at both sides have a defined minimal length (50% or 100% of the required flanks; unfortunately, some of them become too small for analysis).

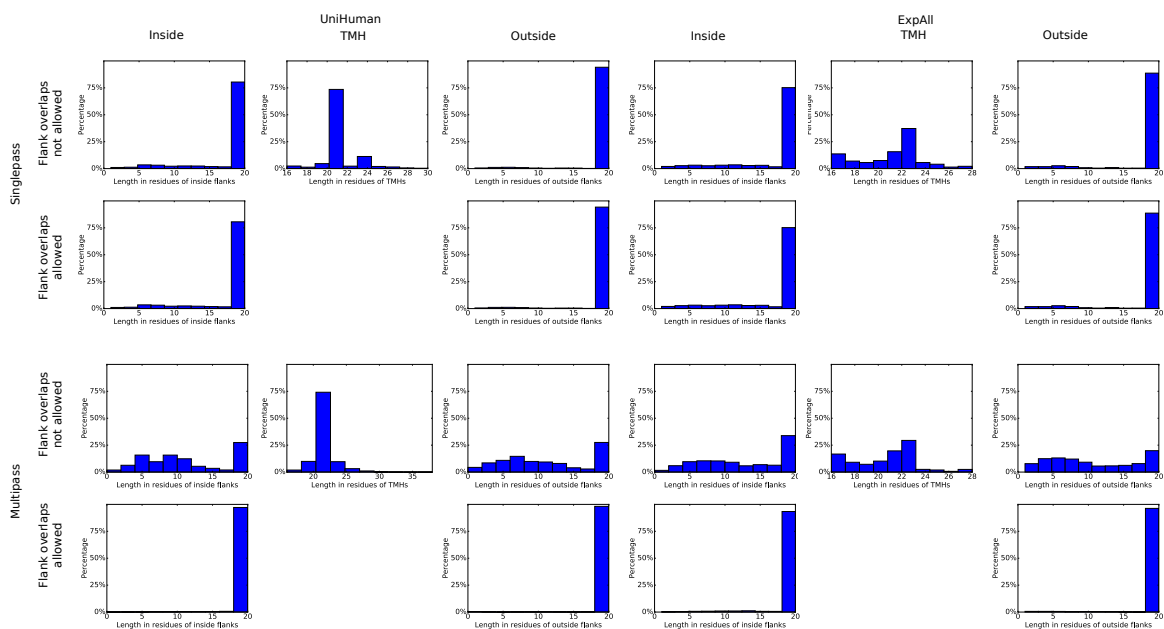


**Figure 2.11: The lengths of flanks and transmembrane helices in multi-pass and single-pass proteins in the UniHuman and ExpAll dataset.** On the horizontal axis are the lengths of the TM segment regions in residues. On the vertical axis are the percentages of the population. There are three regions: the inside flank, the TMH and the outside flank. These regions are acquired according to the TMH boundary of the respective database. Where no overlap is permitted, if the flank encroaches the flank of another TMH, the flank length becomes half the number of residues in the loop region between the two features. Where they are allowed to overlap, flanking residues may include other flanks, or indeed other TMHs.

The problem of flanks overlapping does affect also some single-pass and multi-pass TMH proteins with INTRAMEM regions as described in some UniProt entries. We do not include INTRAMEM regions in the datasets as TMHs but, sometimes,

the flanking regions of TMHs were truncated to avoid overlap with INTRAMEM flanking regions (Table 2.8). The identifiers affected for single-pass TMH proteins are Q01628, P13164, Q01629, Q5JRA8, A2ANU3 (UniHuman), P13164, Q01629, A2ANU3 (UniPM) and Q5JRA8 (UniER).

**Table 2.8: Records with INTRAMEM and TRANSMEM flanking region overlap.** The total number of TMHs from UniProt datasets with flanking region overlap between INTRAMEM and TRANSMEM regions. The number of multi-pass records that the TMHs belong to are shown in brackets.

Dataset	Flank length					
	5		10		20	
	single-pass	multi-pass	single-pass	multi-pass	single-pass	multi-pass
UniHuman	0	96 (80)	1	151 (90)	5	204 (96)
UniER	0	6 (6)	1	13 (8)	1	16 (8)
UniGolgi	0	1 (1)	0	2 (2)	0	4 (2)
UniPM	0	57 (46)	0	93 (51)	3	113 (52)
UniCress	0	17 (17)	0	24 (18)	0	46 (18)
UniFungi	0	0	0	0	0	0
UniBacilli	0	11 (3)	0	12 (3)	0	13 (3)
UniEcoli	0	22 (8)	0	25 (9)	0	31 (9)
UniArch	0	0	0	8 (8)	0	17 (9)

The second form of boundary point definition for flank determination was achieved with gaplessly aligning all TMHs relative to their central residue at the position equal to half the length of the TMHs at either side. Though there is some length variation among TMHs, most of them are centred around a length of 20-22 residues. In this case, flanks are the sequence extensions beyond the standardised-length 21-residues TMHs. We define the inside flanking segments as the positions -20 to -10 and the outside flanking regions to be +10 to +20 from the central TMH residue (with the label “0”). Instead of emphasising some artificially selected boundary residue, this definition allows the average TMH boundary transition to become apparent.

### 2.5.3 Separating simple and complex single-pass helices

Single-pass helices from ExpAll and UniHuman datasets helices were split into two groups: simple and complex following a previously described classification [44, 45]

to roughly distinguish simple hydrophobic anchors and TMHs with additional structural/functional roles. Simple and complex helices were determined using TM-SOC [45]. The complexity class is determined by calculating the hydrophobicity and sequence entropy. The resulting coordinates cluster with anchors being more hydrophobic and less complex whilst more complex and more polar TMHs are associated with non-anchorage functions. In UniHuman there were 889 simple helices and 570 complex TMHs. In ExpAll there were 769 simple helices and 570 complex helices.

### 2.5.4 Distribution normalisation

In this work, we have used normalisation techniques described in previous investigations as well as new approaches designed to more sensitively identify biases of rare residues. Baeza-Delgado and co-workers used LogOdds normalisation column-wise in TMH alignments. Critically, this is based on their definition of probability, which takes into account the total number of amino acids in the dataset as a denominator [109]. Since aliphatic residues such as leucine and other highly abundant slightly polar residues dominate the denominator, the distribution of the rare acidic residues will be easily lost in the “background noise” of those highly abundant residues. Pogozheva and co-workers used two approaches, (i) the total accessible surface area (ASA<sub>total</sub>) and (ii) total number of charged residues ( $N_{total}$ ) as a denominator in their distribution normalisation [110].

In this work, two methods for measuring residue occurrence in the TMH and its flanks were used. Similarly to previous work, we compute the occurrence of an amino acid type at a certain sequence position in a set of aligned sequences TMHs and their flanks. Following [86], the absolute relative occurrence of this amino acid type at the sequence position is then given by Equation 2.1 as:

$$p_{i,r} = \frac{a_{i,r}}{\max_r(a_r)} \quad (2.1)$$

Here, the denominator is the maximal number of all residues in any alignment column (i.e., the number of sequences in the alignment) and, to emphasise, this will make mostly dependent on the most abundant residue types. This type of normalisation reveals the most preferred residue types at given sequence positions.

Our second normalisation method is independent of the abundance of any amino acid types other than the studied one; it answers the question: “If there is a residue of type in the TMH-containing segment, where would it most likely be?” This relative occurrence calculated in Equation 2.2 as:

$$q_{i,r} = \frac{100 \cdot a_{i,r}}{a_i} \quad (2.2)$$

The value  $a_i$  is the total abundance of residues of just amino acid type  $i$  in a given alignment of TMH-containing segments (i.e., in the TMH together with its two adjoining flanks summed over all cases of TMHs in the given dataset). Peaks in  $q_{i,r}$  as function of  $r$  reveal the preferred positions of residues of type  $i$ . The difference in  $q_{i,r}$  and  $p_{i,r}$  normalisation is visualised in Figure 2.12.

### 2.5.5 Hydrophobicity calculations

Hydrophobicity profiles were calculated using the Kyte & Doolittle hydrophobicity scale [73] and validated with the Eisenberg scale [144], the Hessa biological scale [116], and the White and Wimley whole residue scale [139](Figure 2.7). The hydrophobicity profile uses un-weighted windowing of the residue hydrophobicity scores from end to end of the TMS slice. Three residues were used as full window lengths and partial windows were permitted.

### 2.5.6 Normalised net charge calculations

Charge was calculated at each position by scanning through each position of the transmembrane helices and flanking regions and subtracting one from the position if an acidic residue (D or E) was present, or adding one if a positively-charged residue (K or R) was present. The accumulative net-charge was then divided by the total number of transmembrane helices that were used in calculating the accumulative net-charge. Thus, the charge distribution is calculated by:

$$c_r = \frac{(a_{K,r} + a_{R,r}) - (a_{D,r} + a_{E,r})}{N} \quad (2.3)$$

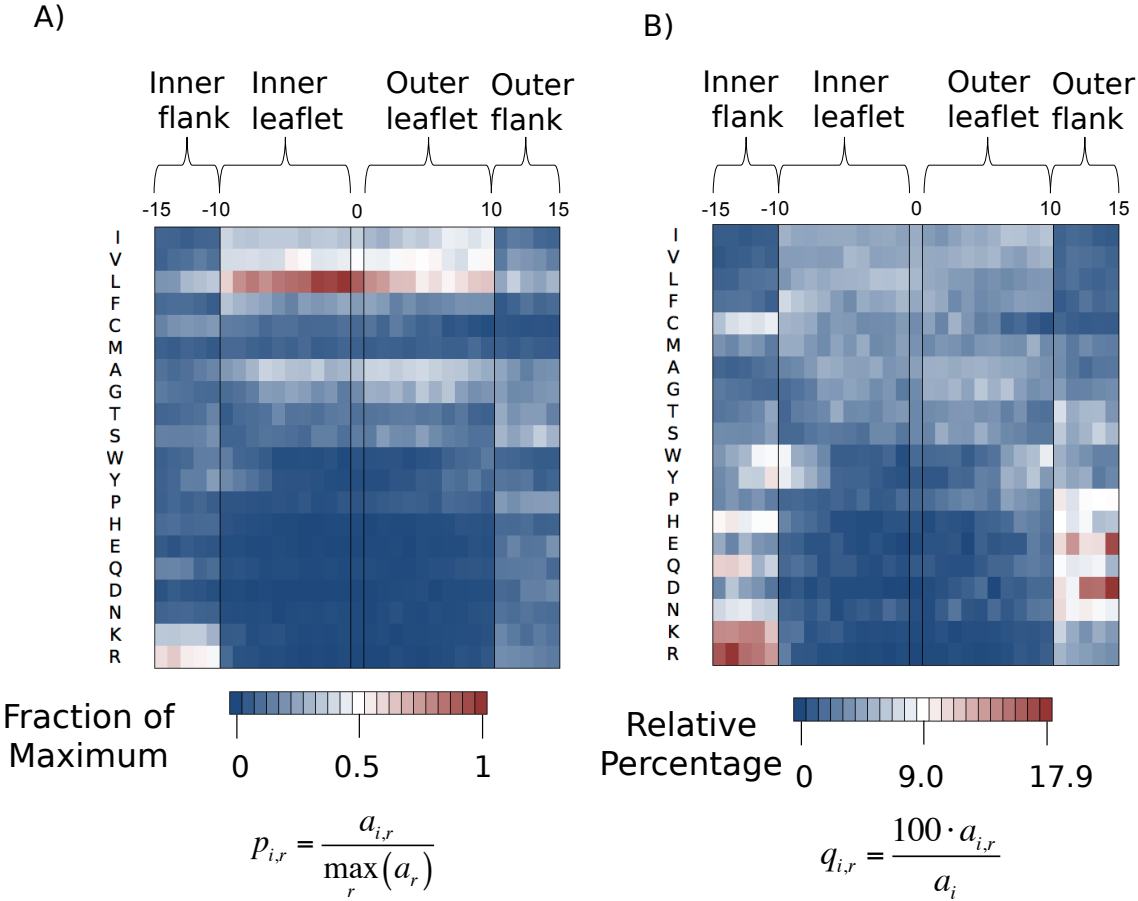


**Figure 2.12:** Relative percentage heatmaps from the predictive datasets calculated by fractions of the absolute maximum and by the relative percentage of a given amino acid type. The residue position aligned to the centre of the TMH is on the horizontal axis, and the residue type is on the vertical axis. Amino acid types are listed in order of decreasing hydrophobicity according to the Kyte and Doolittle scale [73]. The flank lengths in the TMH segments were restricted to up to  $\pm 5$  residues. The scales for each heatmap are shown beneath the respective subfigure. All TMHs and flank lengths are from the UniHuman dataset. (A) The heatmap has been coloured according to a scale that uses column-wise normalisations used in previous studies [86]. See Equation 2.1. As an illustrative example, we show how the value for E at position  $\pm 12$  is obtained. There are in total 91/22 Es at these positions in 1705 sequences; thus, the represented value is 0.013 at  $-12$  and 0.053 at 12. Note that L is clearly a hotspot as well as trends for other hydrophobic residues, I and V, as is to be expected. A positive inside effect can also be seen. (B) The heatmap has been coloured according to the relative percentage of each amino acid type (Equation 2.2). Here, 91/22 Es at position  $\pm 12$  are compared with 615 Es seen within the flanks and the TMH section itself amongst all sequences in the alignment. So, the expectation of an E at position  $\pm 12$  if there is any E in the TMH + flanks region at all is 0.036 at  $-12$  and 0.148 at position 12. With this type of normalisation, not surprisingly, we see the positive-inside rule is hotter than in subfigure A. There are also hotspots in the flanks for the negatively-charged residues on the outside flank. The leucine hotspot is no longer very pronounced, as the leucines are quite evenly spread over many positions.

## 2.5.7 Statistics

The inside/outside bias of negative residues was quantified by computing the independent K-W and the 2-sample t-test statistical method from the Python scipy stat package v0.15 python package [280]. This test answers the question whether two means

are actually different in the statistical sense. The p-values in Table 2.2 and Table 2.3 are calculated by comparing two lists of the number of the given residues in either the inside and outside flank with each entry belonging to an individual TMH. The p-values in Table 2.1 compare a list of the total number of negatively-charged residues in TMHs from either single-pass or multi-pass TMHs. For the leucine residues, each TMH region was divided into two sections, representing the inner and outer leaflets (Table 2.4) and the leucine residues in the inner and outer leaflets were compared similarly to the negatively-charged residues in the inside and outside flanks in Table 2.2 and Table 2.3.

For the hydrophobicity plot, 3 window values of hydrophobicity were taken for each TMH at each position. The statistical analyses were separately performed for single-pass and multi-pass transmembrane proteins. At each position, the two groups were compared using the K-W test.

The zero hypothesis of homogeneity of two distributions was examined with the K-S, the K-W and the  $\chi^2$  statistical tests. To note, the K-S test scrutinises for significant maximal absolute differences between distribution curves; the K-W test is after skews between distributions and the  $\chi^2$  statistical test checks the average difference between distributions. As the statistical significance value (“p-value”) is a strong function of N, the total amount of data used in the statistical test (for example, Table 2.5 and Table 2.6 N would be the total number of TMHs from both datasets in the comparisons), we rely on the (absolute) Bahadur slope (B) as a measure of distance between two distributions [259, 260]:

$$B = \frac{\ln(p\ value)}{N} \quad (2.4)$$

The larger the absolute Bahadur slope, the greater the difference between the two distributions.

# **Chapter 3**

## **Collation and analysis of tail-anchored protein transmembrane helices reveals subcellular variation in flanking charged residue distribution and the transmembrane helix core hydrophobicity**

### **3.1 Abstract**

Tail-anchored proteins are a functionally diverse group of post-translationally inserted membrane proteins that have a cytosolic N-terminal, a transmembrane  $\alpha$  helix, and a short C-terminal tail. The transmembrane helix and flanking regions of the tail-anchored protein have been shown to contain sufficient information for subcellular targeting. Here, we built datasets based on sequence definitions of plausible tail-anchored proteins using the UniProt database. We show that any statistical differences between the hydrophobicity of the transmembrane helix between tail-anchored proteins

belonging to mammalian, plant, or yeast organisms are, if at all present, small. Yet, the hydrophobicity of transmembrane helices from different subcellular locations is, on average, different between the mitochondria and other membranes along the secretory pathway. Notably, in the case of mitochondria, this appears to be a difference in the hydrophobic residue preference of alanine instead of leucine or isoleucine and does not seem to be an increase of intramembrane polar residues. In the endoplasmic reticulum, Golgi, and plasma membrane there are positively charged residues inside the cytoplasm and negatively charged residues outside. Yet we identify a charge skew reversal of the “positive-inside” and “negative-outside” rules in the mitochondrial tail-anchored proteins to negative-inside and positive-outside. It is unclear to what extent these differences are the result of membrane environment adaptations or biological features useful for the biogenesis and accurate localisation of the protein. Furthermore, structural homology modelling of the spontaneously inserting transmembrane helices of PTP1b and cytochrome b5 revealed that tail-anchored proteins may gain their ability to integrate into the membrane unaided due to a strip of conserved relatively polar residues and strong flanking charge that would allow effective membrane coupling and anchoring.

## 3.2 Introduction

TA proteins are defined by their single carboxy-terminal TMH with a cytosolic facing amino-terminus and are a topologically distinct class of intracellular proteins. The integration of TA proteins into the membrane is post-translational rather than co-translational; the ribosome is not in complex with the membrane bound insertion machinery. TA proteins are involved in a range of key cellular functions such as translocation (Sec61 $\beta$  and Sec61 $\gamma$ ) [281] and apoptosis (Bcl-2 apoptotic protein family) [282]. Additionally, within the TA class of proteins are a set of vesicle fusion proteins called Soluble N-ethylmaleimide-sensitive factor attachment protein receptor (SNARE) proteins [283], which contain typically hydrophobic TMHs [284]. The idea that SNARE proteins are modular and capable of spontaneous insertion has significant implications for biomedical application in liposome-based drug delivery. Furthermore, this could aid future research for testing complex biological molecular networks [285,

286].

The TA protein's TMH is both the anchor and the targeting factor for the ER [287]. Furthermore, the hydrophobicity of the TMH appears to be a determining factor in the delivery pathway that TA proteins use for insertion [288, 289], for which there is evidence demonstrating that there are several mechanisms of protein-membrane integration [289, 290](Figure 3.1).

TA proteins have several pathways for biogenesis in the ER membrane. TA proteins were originally thought to be inserted into the membrane via different machinery than the co-translational machinery, but unexpectedly SRP was found to be a factor for post-translational targeting confirmed by both cross-linking studies [291] and an *in vitro* pull-down experiment [292]. It was shown that SRP could deliver the TA protein to the membrane-bound SR in association with a highly conserved Sec translocon. Further cross-linking experiments confirmed Sec61 is also involved during TA protein membrane insertion [293]. Previous studies had shown the Sec61 translocon is not necessary for TA protein membrane integration by biochemical reconstitution experiments [287] and conditional mutants in yeast [294, 295]. So whilst it is hard to determine if Sec61 can be part of the post-translational pathway, we can conclude that it is certainly not essential, indeed almost no observable impact on biogenesis is had when it is removed [287, 294, 295]. Nevertheless, this suggests the possibility of at least one insertion mechanism that is related to the co-translational method of insertion. Most likely is that SRP binds to the TA protein after it is released from the ribosome and chaperones it until it is close enough to the established post translational machinery [296] (Figure 3.1iii).

A second redundant system is also known to be involved in TA protein biogenesis and is referred to as the TRC40 (also known as Asna1) pathway in mammals (Figure 3.1i). A conserved homologue was found in *Saccharomyces cerevisiae*, Get3 [297], named after the action it has in the GET pathway. Unlike co-translational insertion, the post-translational chaperone proteins do not couple with the ribosome, so the TA protein must be exposed to the cytosolic environment for at least some time [78]. At some point after the TA protein emerges from the ribosomal exit tunnel, the TA protein TMH associates with Sgt2 (SGTA in mammals). An *in vitro* assay revealed that Sgt2 associates with Get5 [298] (UBL4A) as part of a dimerised Get4 (TRC35)

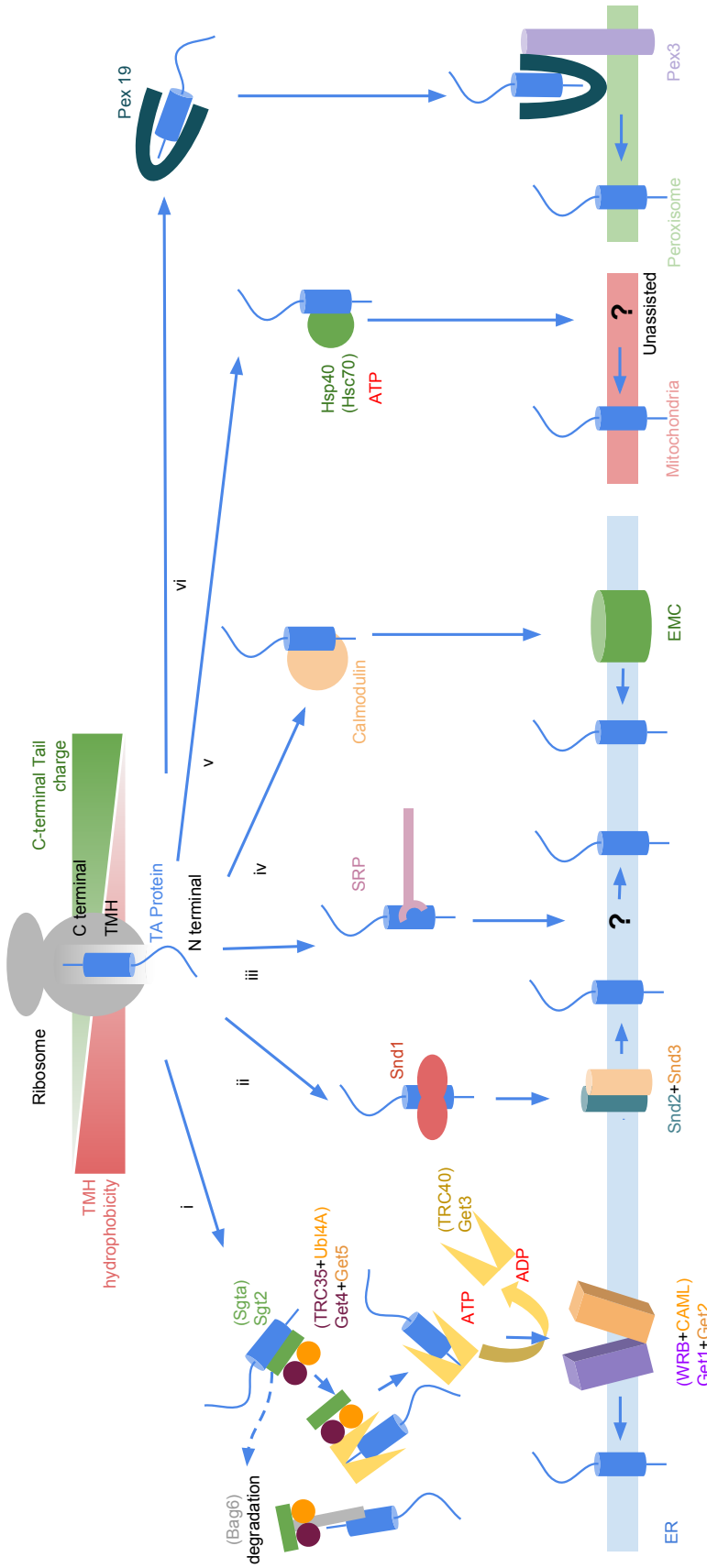


**Figure 3.1: An overview of the biogenesis of tail-anchored proteins.**

(i) The intensively studied Get (yeast) or TRC40 (mammalian) pathway can target either for membrane integration or degradation of the TA protein. Text in brackets indicates mammalian proteins. (ii) In yeast, a novel mechanism was identified in which Snd1 binds to the folded TA protein and delivers it to the membrane-bound Snd2 and Snd3 complex. (iii) SRP of the co-translational insertion mechanism has been shown to be able to integrate TA proteins. Sec61s role in this is disputed, and it is likely other proteins are involved in membrane partitioning instead. (iv) A recently identified insertase, the EMC, can integrate TA proteins with relatively polar TMHs into the ER. (v) A handful of TA proteins with relatively polar TMH regions have been observed spontaneously integrating into the membrane using Hsp40 and Hsc70 as chaperones. This system may be employed for mitochondrial localisation. (vi) Peroxisomal proteins with an abundance of charge in the tail region are chaperoned by Pex19 into association with the membrane-bound Pex3.

and Get5 (Ubl4A) complex (two copies of each)[299–302].

In mammals, at this point SGTA either associates with preferential TRC40 which targets the TA protein for ER membrane biogenesis or if there are excess TA proteins SGTA also associates with Bag6 which targets the TA protein for degradation [303]. This “race” between Bag6 and TRC40 ensures a level of quality control within the system.

Get3 associates first with the Sgt2-Get4-Get5 complex via an interaction with the N-terminal of Get4 [298]. A dimerised ADP-bound Get3 [304–308] associates with and shields the C-terminal region of the TA protein [297, 309, 310]. This shielding may be especially important since Get3 is involved in reducing the misfolding of any nascent TA proteins, the TMH of which would be unviable in the cytosol due to their hydrophobicity [311]. Fluorescence studies revealed that tagged Get3 appears at both the cytosol and the ER membrane so apparently shuttles the TA protein between the transmembrane complex of Get1 and Get 2 (WRB and CAML in mammalian cells), that contains cytosolic domains that receive the Get3, Get4, Get5, Sgt2 complex [312, 313]. Yet it is an interesting note that a single molecule fluorescence study revealed that the minimum machinery required for TA protein insertion from this system is a Get1 and Get2 heterodimer [313]. The Get pathway exclusively delivers TA proteins to the ER membrane, and indeed has been recently shown to be responsible for some of the mislocalisation of mitochondrial TA proteins during overexpression or signal masking to the ER [314]. The significance of this is that the Get machinery can recognise and tolerate integration of non-ER proteins. Yet there is also evidence that the deep groove of Get3 [315, 316] predisposes it to only effectively integrating the more hydrophobic TMHs of TA proteins [298, 317]. As an example, increasing the hydrophobicity of the TMH in squalene synthase (an ER TA TMP involved in sterol synthesis) in a TRC40 inhibited system reduced the biogenesis of the protein, where the wild-type was unaffected by TRC40 inhibition [25]. Around a half of TA proteins are estimated to not use the TRC40 pathway [25].

Redundancy of the GET/TRC40 pathway and SRP pathway may be explained in part by a novel SRP and Get independent pathway. This pathway utilises the Snd pathway and was discovered in yeast [318] (Figure 3.1ii). Snd1 binds to the TA

protein after it exits the ribosome and delivers it to the Snd2 and Snd3 membrane-bound complex which integrates the TA protein into the membrane. So far only the human homologue of Snd2 has been identified (hSnd2) with relatively low sequence identity [319]. However, it is suspected that functional mammalian homologues exist for Snd1 and Snd3 also, albeit with low sequence similarity.

Even more recently identified as a TA protein insertase was the EMC [25] (Figure 3.1iv). In the interaction study, squalene synthase did not effectively crosslink with any TRC pathway machinery. Calmodulin (a eukaryotic highly conserved calcium-sensing globular protein with a flexible symmetrical structure that performs a variety of functions) sufficiently prevented aggregation and acted as a chaperone in ER microsomes in a chaperone free *E. coli* translation system with purified translation factors. In this system, calmodulin acted similarly to the mammalian chaperone protein SGTA, and although in native cytosol calmodulin was preferred, SGTA could also be used by the protein. By contrast VAMP2 (a TA protein involved in vesicle binding), which is known to interact with TRC40 as a chaperone [303], was unable to insert in this system. Abolition by knock-outs of the EMC components greatly reduced the insertion potential of squalene synthase, along with five mutants thereof, and six other TRC40 independent proteins in ER membranes from semi-permeabilised cultured cells, but not that of VAMP2. Insertion of Sec61 $\beta$  (a post-translationally inserted protein) was partially dependent on both systems, perhaps indicating the midway point between the two [25] (Figure 3.1).

Some TA proteins, for example BCL-2 involved in apoptosis, are targeted to the MOM instead of the ER, however the mitochondrial mechanism of membrane integration works independently from the TOM [320, 321]. In the absence of the mitochondrial inner and outer translocons and their associated machinery, insertion machinery and GET/TRC machinery, heat shock proteins Hsp40 and Hsc70 chaperones along with ATP are also sufficient for enough biogenesis of TA proteins for viable cell growth [288, 289, 320–324] (Figure 3.1v). Synaptobrevin, one of the first identified SNARE proteins, is capable of spontaneous insertion if the naturally occurring TA domain is replaced by the TM that is known to be able to spontaneously insert into the ER. One can, therefore, conclude that spontaneous insertion is a property of the TMH, not of the rest of the protein [286]. Molecular dynamics simulations showed that direct

insertion TMHs thermodynamically mimics the energies of TMHs integrated by the translocon [325] so in theory, no integration machinery is strictly necessary if the TMH can “correctly” interact with the membrane interface. Furthermore, it was revealed that scrambling the TMH sequence, but maintaining hydrophobicity, reduced the insertion potential of spontaneously inserting TMHs [138]. This phenomenon cannot, therefore, be explained entirely by the marginal hydrophobicity of the TMH.

The few peroxisomal TA proteins first associate with Pex19 which forms a complex with the membrane-anchored Pex3 protein from which the TA protein is integrated into the membrane [326–328](Figure 3.1vi).

Given a “choice”, it is speculated that hydrophobicity determines the integration pathway [288, 289, 329]. Altering the hydrophobicity, at least in the case of the spontaneously inserting PTP1b, also determines the localisation of the TA protein to either the mitochondrial membrane or the ER membrane, or rather a more hydrophobic TA protein TMH is less likely to localise to the mitochondrial membrane [330]. Broader analysis has shown that hydrophobicity [139] stratified by TM tendency score [234] can distinguish between the ER and mitochondrial localised TA proteins [78]. However, the diversity and known biosynthetic redundancy of these proteins may mean that no single factor applied en masse is able to distinguish the TMH recognition factors and investigation into this area is becoming increasingly complex [78].

By regenerating a list of likely TMHs [284] and using a manually curated list of TA proteins [75], this investigation aims to find relationships between biochemical factors and a disposition to a certain insertion mechanism and terminal localisations. Here, we also present evidence for a conserved polar strip along the spontaneously inserting TA protein TMHs, which may be the key to the initial interaction of these TMHs with the membrane interface.

## 3.3 Methods

### 3.3.1 Building a list of tail-anchors

Steps carried out by Kalbfleisch *et al.* (Traffic 8: 16871694) to generate a list of all TA proteins in the human proteome [284] were recreated using up to date tools and applied to other model representative species. Whilst their study focused on the human

proteome, here we take into account the entire TrEMBL and SwissProt database and then stratify the datasets by the organism at the end of the pipeline. An overview of the generation of these datasets is shown in Figure 3.2.

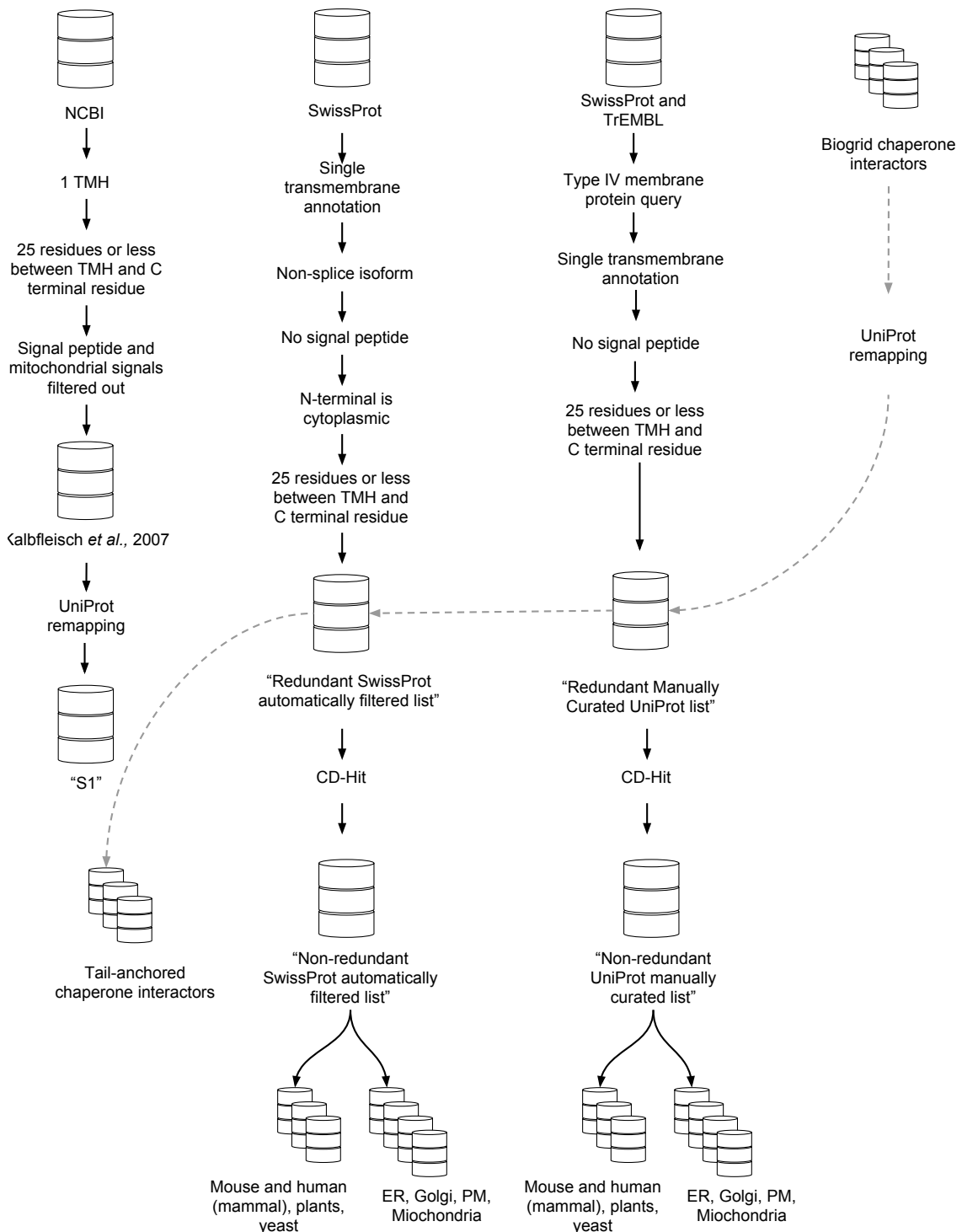


**Figure 3.2: The sources, methods, and filters applied to the sequences in the tail-anchored protein datasets.** From top to bottom are the sources of the sequences and the filters and methods applied to each of the datasets of sequences. The database symbol is used to denote when the dataset was used to capture results and is available as supplementary material. For the dataset size and more information, see the methods section text.

### SwissProt tail anchored dataset according to filters

There were 557012 protein records downloaded from SwissProt via UniProt [75] (downloaded 24–04–2018). 106149 TMHs (TRANSMEM annotation) were found between 76953 records (`annotation:(type:transmem)ANDreviewed:no`). This keyword is contained in a record according to either experimental evidence [75] or a conservative meta-analysis of TMH prediction using TMHMM [67], Memsat [66], Phobius [71, 236] and the hydrophobic moment plot method of Eisenberg and co-workers [144]. 11141 of those records had only a single TMH. 11110 of those TMHs were within the length thresholds of 16 to 30 residues (None of those had the annotation for splice isoforms according to `NON_TER` annotation). 5548 of those had had no SP annotation (`SIGNAL`). 4332 of those had annotation (based on `TOPO_DOM` annotation) that the N terminal was cytoplasmic. 615 of those had the TMH within 25 residues of the C-terminal, the same threshold used by Kalbfleisch *et al.*, [284]. Running CD-Hit 4.5.3 on the WebMGA web-server [277, 331] at 90% identical sequence at 90% coverage thresholds resulted in 443 representative proteins. This threshold was chosen as a compromise between avoiding over-representation of a certain protein and maintaining a viable sample size.

From this representative list, 46 were Archaeal, 66 were bacterial, and 320 were eukaryotic and 11 came from dsDNA viruses. When counting proteomes with greater than 20 records, 49 belonged to the *A. thaliana* proteome, 48 to *Mus musculus* (Mouse), 46 to the *Homo sapiens* proteome, 24 to *S.cerevisiae*.

65 were annotated under the mitochondrion location (query locations: `(location:"Mitochondrion[SL-0173]"')`), 157 in the PM (query locations: `(location:"Cellmembrane[SL-0039]"')`), 82 in the Golgi (query locations: `(location:"Golgiapparatus[SL-0132]"')`), and 98 in the ER (query locations: `(location:"Endoplasmicreticulum[SL-0095]"')`). Only 16 records were found for the peroxisome (query locations: `(location:"Endoplasmicreticulum[SL-0204]"')`) which is not high enough a sample size for accurate statistical analysis.

### TrEMBL tail anchored dataset according to filters

111425234 records were stored in the TrEMBL database at the time of download (downloaded 25–04–2018). 22107826 of those contained TRANSMEM annotation (`annotation:(type:transmem)ANDreviewed:no`). 18053 of these were single-pass

proteins. All of these were within the length restrictions of between 16 and 35 residues for the TMH region. 17973 of those did not contain a signal sequence when looking for SIGNAL annotation. 5157 of those contained a cytoplasmically located N terminal according to TOPO\_DOM annotation. 155 records had a TMH within 25 residues of the C-terminal residue. When considering which species these records come from, no more than 1 record belonged to any given species. To avoid representing a well annotated SwissProt record that includes species annotation by a poorly annotated TrEMBL record without species annotation, these TrEMBL records were omitted from the sequence redundancy protocol and further analysis.

### UniProt curated list

A query for locations:(location:"Single\--passtypeIVmembraneprotein[SL-9908]") was used in UniProt which returned 2633 UniProtKB IDs; 463 SwissProt results and 2170 TrEMBL results. Type IV anchors are sometimes split into two topological groups; A (A cytosolic facing N terminal domain) and B (The N terminal is targeted to the lumen), however, the UniProt nomenclature is strictly N terminal being cytosolic. This manually created list contained some TA proteins that did not exactly fit the generally accepted definition of a TA protein and were excluded from further analysis. These could be examples of misannotation in the databases or exceptional TA proteins that behave as post-translationally inserted TA proteins despite not matching the exact criteria. 101 exceeded the TA length restrictions of 25 residues between the TMH and the terminal residue. 8 contained annotation for SIGNAL, indicating an SP, inconsistent with the TA protein definition. 20 were multipass proteins. A full list of which records exceeded these limits and by how much is included in the supplementary files. Running these records through CD-HIT at 90% redundancy yielded 956 clusters; 269 SwissProt records and 687 TrEMBL records [277, 331]. No further filters were applied to this list. Proteomes represented by more than 20 records include *A. thaliana* (53 records), Human (30), *Mus musculus* (30), and *S. cerevisiae* (27).

426 were annotated under the mitochondrion location (query locations:(location:"Mitochondrion[SL-0173]")) 47 from SwissProt and 379 automatically assigned in TrEMBL. 397 in the ER (query locations:(location:

"Endoplasmic reticulum[SL-0095]")), 88 from SwissProt and 308 automatically annotated in TrEMBL. 1 TrEMBL record (UniProt ID A0A1E5RT24) in the ER set contained an "X" residue in the C-terminal flank and was omitted from the analyses. Two subcellular location datasets had no automatically ascribed records and only contained manually annotated SwissProt records; 31 in the PM (query locations: (location:"Cellmembrane[SL-0039]"), and 83 in the Golgi (query locations: (location:"Golgiapparatus[SL-0132]")). There were only 8 TA proteins located in the peroxisome (locations:(location:"Golgiapparatus[SL-0204]")), making them an unsuitable dataset for statistical analysis.

### Remapping the previous dataset

189 of the 411 proteins from the previous Kalbfleisch *et al.*, 2007 study [284] were successfully mapped to 222 UniProtKB IDs using the UniProt mapping tools with the RefSeq Protein to UniProtKB option [75].

### Tail anchor protein chaperone interactors

As discussed in the introduction text, there is evidence surrounding the TMH biochemical factors that determine which chaperone will interact with a given TA protein. To gain a more quantitative understanding of the relationship between the TA protein TMH and the potential chaperones, it would be ideal to have a large TA dataset stratified by known chaperone interactions.

Known interactor lists from BioGrid from the chaperones were checked against the SwissProt automatically filtered and the UniProt curated TA protein datasets. There were 91 interaction pairs for Hsp40 (Biogrid ID 119699) which mapped to 206 UniProt records. Hsc70 (Biogrid ID 109544) had 534 interaction pairs 61 of which were mapped to 91 UniProt records. Hsp40 and Hsc70 both returned 0 record hits after filtering the UniProt records IDs through the UniProt manually curated list and the automatically generated SwissProt list both before redundancy removal.

Snd1 (Biogrid ID 32240) had 237 interaction pairs which mapped to 239 records. Snd1 returned 15 hits when filtering it through the TA datasets.

Sgt2 (BioGrid ID 34410) had 260 BioGrid interactor ids which mapped to 264 UniProt records. SGTA (BioGrid ID 112347) had 155 interactor ids from BioGrid,

153 of which were mapped to 274 records. Sgt2 and SGTA returned 14 and 5 hits respectively.

50 BioGrid ids from TRC40 (Biogrid ID 106931) interaction pairs were mapped to 90 UniProt records. Get3 (BioGrid ID 31962) had 456 Biogrid interactor ids, which mapped to 465 UniProt records. After filtering those records through the TA anchor datasets TRC40 and Get3 returned 7 and 22 hits respectively.

In yeast, Pex19 (BioGrid ID 31994) contained 466 interactor pairs which mapped to 384 UniProt IDs. The *Homo sapiens* Pex19 (BioGrid ID 111782) contained 230 interaction pairs which successfully mapped to 218 UniProt records. When the TA list filters were applied, 2 *Homo sapiens* and 7 *Saccharomyces cerevisiae* records were found.

For SRP54, ideally the plant version of the protein was required, for which there is more precedent for post-translational protein interaction and biogenesis into the chloroplasts [291], however, of the 3 plant SRPs available on Biogrid, between them only 10 interactor pairs were available, none of which were common with our TA lists. It is also worth noting that plants have two forms of SRP; one for the chloroplastic and one cytoplasmic which would have to be compared separately. The human SRP54 (Biogrid ID 112607) had 37 interactors which mapped to 85 UniProt IDs, but again, none of which were in our TA lists. On the other hand, the yeast SRP54 (BioGrid ID 36258) had 270 interactors which mapped to 273 UniProt records. 4 of those were found in our TA lists.

### 3.3.2 Calculating hydrophobicity

Windowed hydrophobicity was calculated using a window length of 5 residues, and half windows were permitted. Average hydrophobicity takes the total of the raw amino acid hydrophobicity values and divides them by the number of amino acids in the slice. Unless explicitly stated, values reported in the results are based on the Kyte & Doolittle scale [73] which is based on the water–vapour transfer free energy and the interior-exterior distribution of individual amino acids.

### 3.3.3 Calculating sequence information entropy

Information entropy is essentially an estimate of the entropy of a string of characters. In the context of biology, it can be thought of as an estimation of the non-randomness of a sequence. Sequence complexity can be used to analyse DNA sequences [147–149] and is a component of the TMSOC z-score which can predict function beyond anchoring of a TMH; an increase in complexity is associated with increased likelihood of function [44, 45, 227]. Here we focus on the analysis of the complexity of a string of characters in protein sequences.

Broadly speaking, the entropy of a string of characters in information theory can be defined as in equation 3.1, and we treat the protein sequence TMH as a string with or without its flanking regions.

$$H(S) = - \sum_{i=1}^n P(s_i) \log_2 P(s_i) \quad (3.1)$$

Where  $H$  is the entropy of a sequence  $S$  with values  $\{s_1, \dots, s_n\}$ , and  $P(s_i)$  is the probability ( $P$ ) of a character  $i$  through each position in  $S$ . This allows us to quantify the average relative information density held within a string of information [151].

### 3.3.4 Statistics

The null hypothesis of homogeneity of two distributions was examined with the Kolmogorov Smirnov, the Kruskal-Wallis, and the 2-sampled Student’s T-test statistical tests. These tests were all ran through the Python SciPy stat v0.17 package [280]. To note, the K-S test scrutinises for significant maximal absolute differences between distribution curves; the K-W test is after skews between distributions and the student T-test statistical test checks the average difference between distributions.

Since the  $p$ -value is a product of a fraction of test statistics obtained from a permuted set of the samples, it exponentially increases as  $N$  increases; the  $p$ -value is a strong function of  $N$ . We rely on the Bahadur slope ( $B$ ) as a measure of distance between two distributions [227, 259–261]. A larger Bahadur slope shows a greater difference between the two distributions.

$$B = \frac{|\ln(p \text{ value})|}{N} \quad (3.2)$$

In the heatmaps (Figure 3.6, Figure 3.7), the relative percentage normalisation was used rather than a fraction of the absolute value. This aims to answer the question of “if we have a certain amino acid, which position is it likely to be in?” and are able to sensitively identify clusters of skewed preference [227].

$$q_{i,r} = \frac{100 \cdot a_{i,r}}{a_i} \quad (3.3)$$

$a_i$  is the total abundance of residues of a specific amino acid type ( $i$ ) of an aligned set of TMH-containing segments. Peaks in  $q_{i,r}$  as a function of  $r$  (the position index) reveal the preferred positions of residues of type  $i$ . TMHs are oriented according to “inside” to “outside” from left to right respectively where “inside” refers to the cytoplasm.

### 3.3.5 Modelling cytochrome b5 and PTP1b

In order to assess the 3D arrangement of residues, the HHpred web server was used to query homologues of and model templates for Cytochrome b5 (UniProt accession code P00167) and PTP1b (UniProt accession code P18031) [332]. Homologues were queried using three iterations of HHblitscd against the sequence database version uniprot20\_2016\_02 to generate the query Hidden Markov Model. For cytochrome b5, a multiple alignment was generated from PDB accession codes and residues positions were approximated for the TMH regions based on those of PDB accession codes 5NAO, 5DOQ, 5NAM, and 2MMU covering the TMH. Modeller was run from within the HH-PRED server to generate the homology model [333, 334]. Similarly for PTP1b, the TMS was modelled using a homology model derived from a single sequence alignment of 5NAO based on the TMH $\pm$ 6 (the length of the C-terminal tail) residues of PTP1b.

Both the TMH regions for that of PTP1b and cytochrome 1b were verified by a consensus of sequence TMH predictions (Scampi seq [72], Phobius [71], TMHMM [67], MEMSAT3 [66], TMpred [335], HMMTOP [68], DAS-TMfilter [238], MINNOU [336], OCTOPUS [70], PRODIV [69], PRO-S [69], S-TMHMM [69], and proteus [337]). However, it should be noted that not all these predictions unanimously agreed. For PTP1b, several methods identified more than 1 TMH (HMMTOP, TMPred) whilst Memsat identified a short TMH in a completely different region for the TMH (35A to 45R). Besides that, only S-TMHMM and PRO agreed on the exact start and stop

positions, and it so happens that these are also the majority consensus positions [338] (409F to 429F).

APBS as a PyMol plugin was used to map the electrostatic surface of the model [339]. Consurf [340] was used to map the conservation scores based on 5 iterations of PSI-BLAST [341] with an E-value cut-off of 0.0001. Hydrophobicity was mapped according to the Eisenberg aggregated hydrophobicity scale [144] using a script accessed at [https://pymolwiki.org/index.php/Color\\_h](https://pymolwiki.org/index.php/Color_h).

### 3.3.6 Availability of materials

The scripts and datasets associated with this study can be accessed at <https://github.com/JamesABaker/TA-protein-seq>.

## 3.4 Results and discussion

### 3.4.1 A comparison of up-to-date tail-anchored protein datasets

Here, we use two sources for TA protein datasets. One dataset is based on a previous method [284] to obtain TA datasets and consists of 9296 TMH residues (13279 including up to  $\pm 5$  flanking residues) from 443 SwissProt entries with 90% redundancy removal. Another dataset contains the UniProt curated set of Type IV membrane proteins again with 90% redundancy removal. This dataset contains 20528 TMH residues (27950 including up to  $\pm 5$  flanking residues) from 956 UniProt protein records.

In order to get an understanding of the consistency of the datasets, before removing redundant proteins, we compared these two datasets to a remapped set of proteins from a previous 2007 method by Kalbfleisch *et al.*, which aimed to predict TA proteins from the NCBI database using predictive tools [284] (see Figure 3.2 for an overview of these methods). The S1 dataset was built with an aim to gather TA proteins in the human genome from the NCBI. The greatest source of uncertainty here is that the original S1 list includes 411 records, however, only 222 of these were successfully mapped to the UniProt dataset. This figure is closer to the 202 proteins from the original S1 list that excluded proteins that were either hypothetical or splice isoforms. That being said,

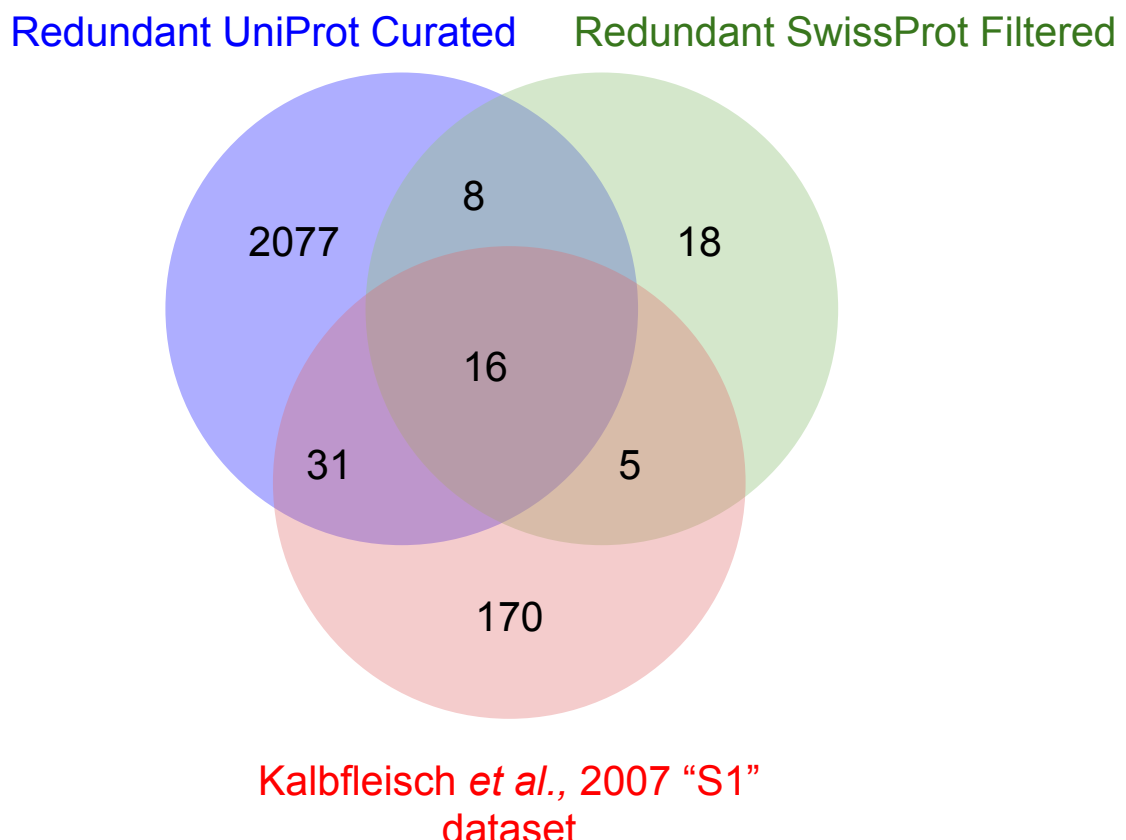


**Figure 3.3:** A Venn diagram showing tail-anchored protein UniProt ids present in each of the datasets as well as those present in multiple datasets. The number of ids present in redundant versions of i) the supplementary materials table of a previous study by Kalbfleisch *et al.*, predicting the complete set of human tail-anchored proteins was mapped to UniProtKB and is denoted by “S1” [284] is in red, ii) and in green is the SwissProt dataset filtered according to typical TA features limited to the *Homo sapiens* proteome [75], and iii) in blue is the UniProt curated list of TA proteins [75]. Note that to avoid losing IDs to redundancy reduction this diagram was generated without the use of CD-HIT [277, 331], which is applied in the later statistical analysis.

this mapping step prevents us from directly comparing the entire original S1 dataset. We compared the up-to-date datasets to S1 to see how many records are shared, how many are now obsolete, and how many are unique.

Figure 3.3 shows that S1 has 175 record ids of 222 records (78.8%) which do not share overlap the up-to-date manually curated UniProt dataset [75]. Of the 170 unique records of that S1 dataset, 4 were manually annotated as not belonging to the *Homo sapiens* proteome, 20 have the C-terminal as annotated being cytoplasmic, only 125 had TRANSMEM annotation indicating a bona fide TMH. If we apply equivalent filters, only 42 have annotation verifying that they are TA proteins.

Equivalent criteria to the original Kalbfleisch *et al.*, 2007 [284] study was applied to the entire SwissProt database and then restricted to the human proteome dataset. 24 of these 47 records (51.1%) are in the curated UniProt TA dataset. 21 of the 49 (44.7%) records from SwissProt filtered *Homo sapiens* dataset can be found in the original S1 list.

The same method applied to an up-to-date dataset overlaps more with a manually curated dataset. There is also a large degree of what we now believe to be mistakes that occurred in the older prediction tools and datasets, even when using similar methods. As a trend, this shows that up-to-date datasets improve the reliability of this automated predicted method. These automated criteria still do not fully align with the manually curated list. Of 2633 records in the manually curated list, only 2241 have the TRANSMEM annotation. Furthermore, it is not only the transmembrane annotation itself but also the type of transmembrane protein. Small integral membrane protein 1 is a blood group antigen (UniProt ID B2RUZ4) that is just one example of a protein we know to be a post-translationally inserted TA protein, and yet in UniProt it is annotated as a type II, not a type IV, transmembrane protein. As a result of which it appears in the SwissProt automatically filtered list and not the manually curated list. In an ideal database, where there are instances of discrepancy, a note on post-translational or co-translational biogenesis would address this issue. Ultimately, this points to the idea that datasets are a moving target as they are constantly updated with more accurate information using evermore reliable tools and methods.

### 3.4.2 It is difficult to observe any hydrophobic variation of tail-anchored protein transmembrane helices from different species

In single-pass proteins of eukaryotic species, there are typically various adaptations of the TMH to adhere to the membrane constraints of the specific membrane. For single-pass proteins, previous studies have observed differences in terms of TMH hydrophobicity between *Saccharomyces cerevisiae* and *Homo sapiens* TMPs [86], or in cress, yeast, bacteria, and *Homo sapien* datasets [227]. We would expect to see a similar trend between the TMHs of TA proteins from different species. However, when assuming a zero-difference hypothesis, in these TMH TA protein datasets we cannot observe any species-level differences between the datasets at this sample size for TMH hydrophobicity.

When comparing the average Kyte & Doolittle [73] hydrophobicity values for the TMHs from *Homo sapiens* and *Mus musculus*, *A. thaliana*, and *S. cerevisiae*, we can see little difference between the mean values. All of the mean values lie between 2.3-2.6 when we only consider the TMH and at 1.3-1.6 when also considering flanking residues in close proximity to the TMH ( $\pm 5$  residues) (Figure 3.4). Indeed, we see no strong observable statistical differences in hydrophobicity ( $P > 3.35E - 1$  in the SwissProt automatically filtered list Table 3.1, and  $P > 2.40E - 1$  in the UniProt curated list Table 3.2). There are also no consistent trends among the absolute Bahadur slopes; no datasets are greatly different from any other.

**Table 3.1: Hydrophobicity statistical comparisons between mouse and human, yeast, and plants in the SwissProt Filtered Dataset.** Here, we compare a mammalian set of TA proteins (*Homo sapiens* N=46 and *Mus musculus* N=48) to *A. thaliana* (N=49) representing plants and *S. cerevisiae* (N=24) representing yeasts. The hydrophobicity was predicted as the mean average of the values of the sequences of the TMH, as well another group including up to  $\pm 5$  flanking residues, since predicting the boundary of TMHs is difficult, according to the Kyte & Doolittle hydrophobicity scale [73]. The Test column refers to the statistical score obtained from the test; H statistic for the Kruskal Wallis, the KS statistic for the Kolmogorov Smirnov test, and the t-statistic for the T-test.  $p$  is the p-value of that statistical score.  $B$  refers to the Bahadur slope, an interpretation of the p-value that accounts for the sample size powering the test [259, 260].

		Mammal and Plant			Mammal and Yeast			Plant and Yeast		
		Test	$p$	$B$	Test	$p$	$B$	Test	$p$	$B$
TMH	KW	0.93	3.35E-1	7.64E-3	0.10	7.56E-1	2.37E-3	0.84	3.60E-1	1.40E-2
	KS	0.13	6.36E-1	3.17E-3	0.12	9.24E-1	6.69E-4	0.19	5.28E-1	8.76E-3
	T-test	-0.86	3.90E-1	6.58E-3	0.21	8.31E-1	1.57E-3	0.79	4.33E-1	1.15E-2
TMH and flanks	KW	0.04	8.52E-1	1.12E-3	0.12	7.28E-1	2.69E-3	0.04	8.33E-1	2.51E-3
	KS	0.11	7.72E-1	1.81E-3	0.13	8.79E-1	1.09E-3	0.11	9.80E-1	2.81E-4
	T-test	-0.22	8.23E-1	1.37E-3	-0.38	7.04E-1	2.97E-3	-0.19	8.50E-1	2.22E-3

Here, we are dealing with datasets at least an order of magnitude smaller than

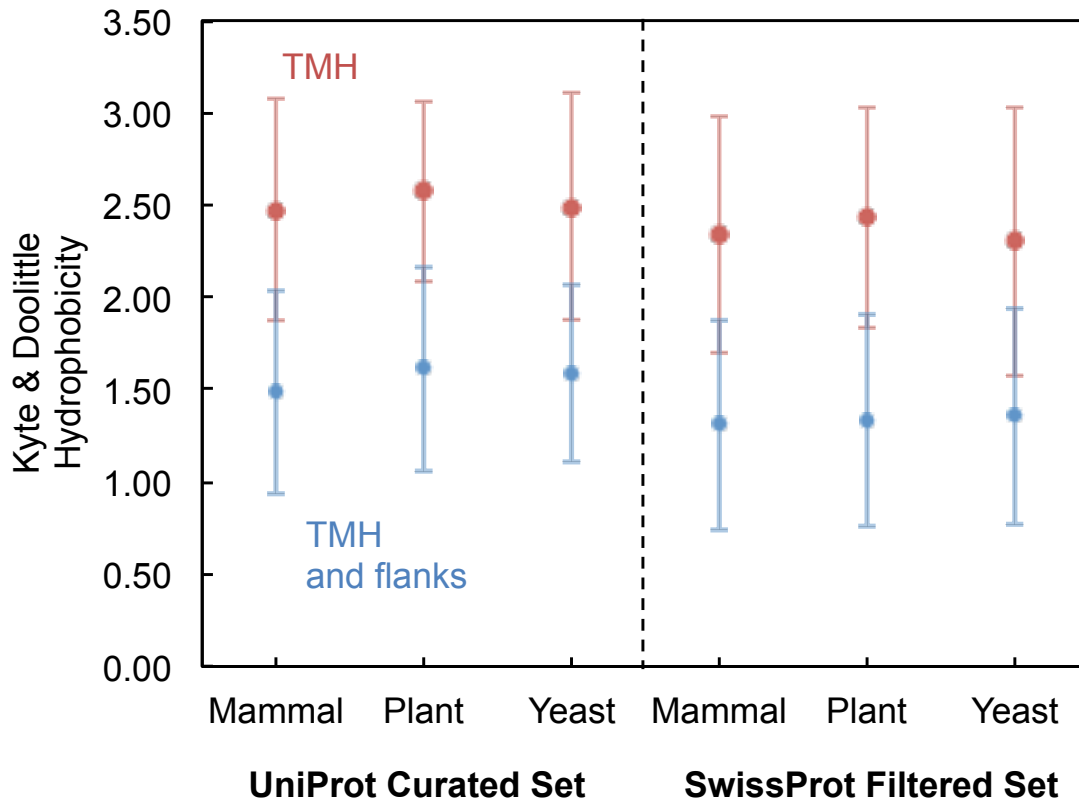


**Figure 3.4: Average values of species datasets from UniProt manually curated set and SwissProt automatically filtered dataset.**

The average hydrophobicity values from the Kyte & Doolittle scale [73] for both the TMH and the TMH±5 residues. Values are shown for both the UniProt manually curated set and the SwissProt filtered set. In the UniProt manually curated set we compare the mammalian set of TA proteins (*Homo sapiens* N=30 and *Mus musculus* N=30) to *A. thaliana* (N=57) representing plants and *S. cerevisiae* (N=27) representing yeasts. For the SwissProt filtered set we compare the mammalian set of TA proteins (*Homo sapiens* N=46 and *Mus musculus* N=48) to *A. thaliana* (N=49) representing plants and *S. cerevisiae* (N=24) representing yeasts. Error bars are shown at  $\pm 1\sigma$  from the mean of the respective dataset.

those broad studies [86, 227] which could explain the absence of the effect. However, this only goes to show that if there is a biochemically distinct effect in TA proteins in terms of hydrophobicity between species, it is indeed weak.

**Table 3.2: Hydrophobicity statistical comparisons between mouse and human, yeast, and plants in the UniProt Curated Dataset.** Here, we compare a mammalian set of TA proteins (*Homo sapiens* N=30 and *Mus musculus* N=30) to *A. thaliana* (N=53) representing plants and *S. cerevisiae* (N=27) representing yeasts. The hydrophobicity was predicted as the mean average of the values of the sequences of the TMH, as well another group including up to  $\pm 5$  flanking residues, since predicting the boundary of TMHs is difficult, according to the Kyte & Doolittle hydrophobicity scale [73]. The Test column refers to the statistical score obtained from the test; H statistic for the Kruskal Wallis, the KS statistic for the Kolmogorov Smirnov test, and the t-statistic for the T-test. *p* is the p-value of that statistical score. *B* refers to the Bahadur slope, an interpretation of the p-value that accounts for the sample size powering the test [259, 260].

		Mammal and Plant			Mammal and Yeast			Plant and Yeast		
		Test	P	B	Test	P	B	Test	P	B
TMH	KW	0.71	4.01E-01	8.09E-03	0.03	8.72E-01	1.57E-03	0.57	4.48E-01	1.00E-02
	KS	0.13	6.93E-01	3.24E-03	0.13	9.11E-01	1.08E-03	0.20	4.16E-01	1.10E-02
	T-test	-0.93	3.55E-01	9.15E-03	-0.11	9.13E-01	1.04E-03	0.64	5.22E-01	8.12E-03
TMH and flanks	KW	1.37	2.42E-01	1.26E-02	0.38	5.36E-01	7.17E-03	0.08	7.80E-01	3.11E-03
	KS	0.19	2.40E-01	1.26E-02	0.14	8.13E-01	2.38E-03	0.09	9.97E-01	3.21E-05
	T-test	-1.17	2.45E-01	1.24E-02	-0.79	4.35E-01	9.58E-03	0.20	8.43E-01	2.14E-03

### 3.4.3 There are biochemical differences between tail-anchored transmembrane helices from different organelles

Although the species datasets appeared to have no significant differences between them in terms of hydrophobicity, we also investigated the subcellular membranes. We see clear differences in the biochemistry of the TMH (Figure 3.5).

In the UniProt manually curated dataset, the Kyte & Doolittle hydrophobicity scores range from 1.7 in mitochondria to 2.7 in the PM (Figure 3.5A).

**Table 3.3: Statistical comparisons between TMH sequences from organelles in the UniProt Curated Dataset.** Here, we compare an organelle subset from the UniProt curated dataset of TA proteins. We compare ER (N=397) to Golgi (N=83), PM (N=31), and the mitochondria (N=426). The hydrophobicity was predicted as the mean average of the values of the sequences of the TMH, as well another group including up to  $\pm 5$  flanking residues, since predicting the boundary of TMHs is difficult, according to the Kyte & Doolittle hydrophobicity scale [73]. The linguistic information entropy was calculated according to the methods section [151]. The Test column refers to the statistical score obtained from the test; H statistic for the Kruskal Wallis (KW), the KS statistic for the Kolmogorov Smirnov test (KS), and the t-statistic for the student's T-test (T-test). *p* is the p-value of that statistical score. *B* refers to the Bahadur slope, an interpretation of the p-value that accounts for the sample size powering the test [259, 260].

		ER and Golgi			ER and PM			ER and mito		
		Test	P	B	Test	P	B	Test	P	B
Hydrophobicity of TMH	KW	21.83	2.98E-06	2.66E-02	28.53	9.21E-08	3.80E-02	377.02	5.54E-84	2.34E-01
	KS	0.34	1.61E-07	3.27E-02	0.57	5.32E-09	4.47E-02	0.67	4.22E-82	2.28E-01
	T-test	-6.45	2.72E-10	4.61E-02	-8.86	2.30E-17	8.99E-02	23.53	6.58E-94	2.61E-01
... and flanks	KW	0.21	6.48E-01	9.07E-04	17.53	2.83E-05	2.46E-02	490.46	1.13E-108	3.03E-01
	KS	0.19	1.10E-02	9.44E-03	0.50	4.69E-07	3.42E-02	0.82	5.58E-123	3.43E-01
	T-test	0.32	7.48E-01	6.07E-04	-4.85	1.75E-06	3.11E-02	34.60	2.19E-162	4.53E-01
Sequence Entropy of TMH	KW	4.66	3.09E-02	7.28E-03	27.54	1.54E-07	3.68E-02	24.03	9.48E-07	1.69E-02
	KS	0.24	4.78E-04	1.60E-02	0.46	4.20E-06	2.91E-02	0.18	2.10E-06	1.59E-02
	T-test	3.22	1.37E-03	1.38E-02	6.42	3.71E-10	5.10E-02	-4.55	6.28E-06	1.46E-02
... and flanks	KW	0.52	4.70E-01	1.58E-03	19.50	1.01E-05	2.70E-02	40.11	2.40E-10	2.70E-02
	KS	0.13	2.06E-01	3.31E-03	0.41	7.97E-05	2.22E-02	0.23	5.53E-10	2.60E-02
	T-test	1.08	2.82E-01	2.65E-03	4.47	1.00E-05	2.70E-02	-5.84	7.51E-09	2.28E-02

In the UniProt curated list, there are clear hydrophobic differences between all the organelle TMH datasets excluding flanks ( $P < 2.98E-6$ ) which as a trend becomes less

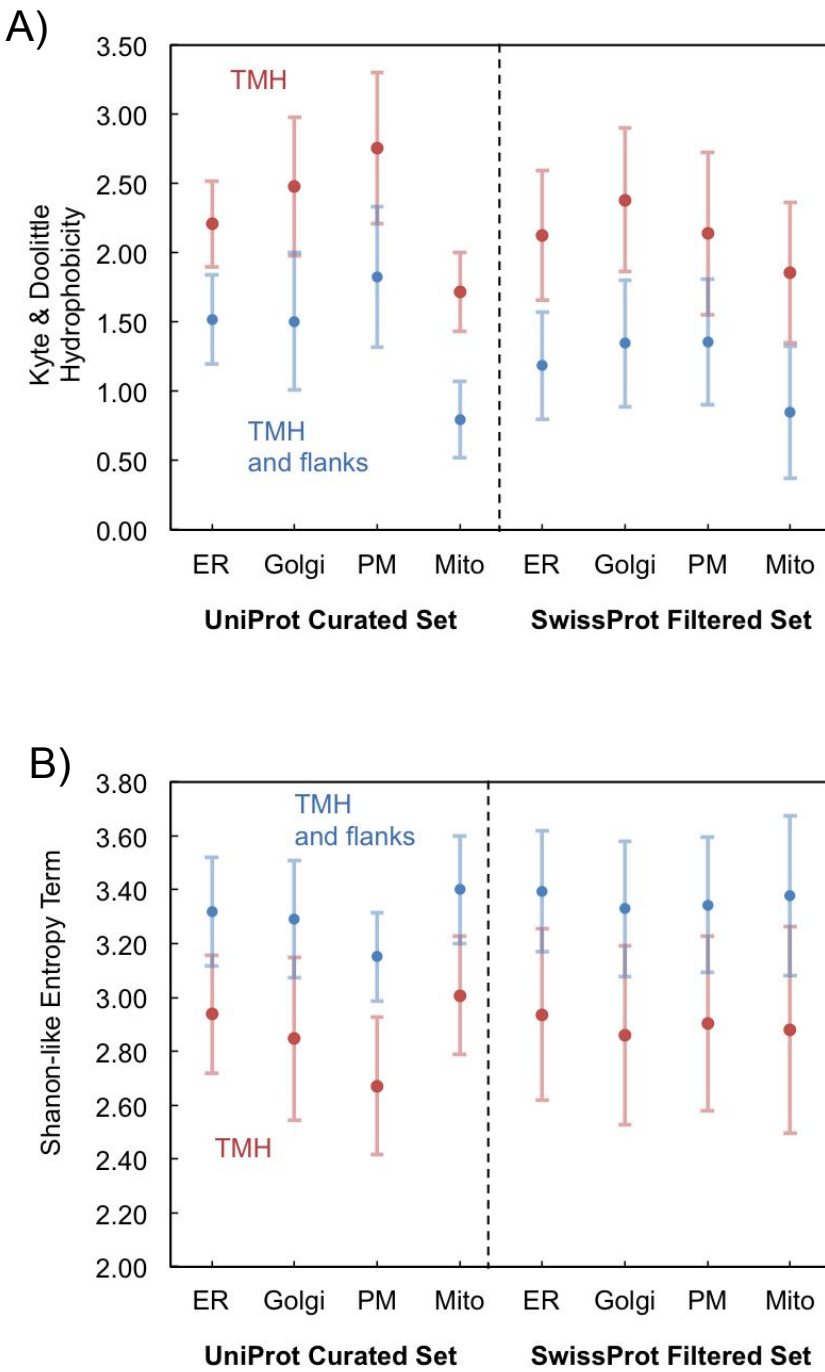


Figure 3.5: Average sequence-based biochemical values of organelle datasets from UniProt manually curated set and SwissProt automatically filtered dataset.

A) The average hydrophobicity values from the Kyte & Doolittle scale [73], B) the average information entropy [151] (see methods) for both the TMH and the TMH $\pm$ 5 residues. Values are shown for both the UniProt manually curated set and the SwissProt filtered set. In the UniProt manually curated set we compare TA proteins from the ER (N=400) to the Golgi (N=82), the PM (N=37), and the mitochondria (N=401). For the SwissProt filtered set we compare TA proteins from the ER (N=98) to the Golgi (N=82), the PM (N=157), and the mitochondria (N=65). Error bars are shown at  $\pm 1\sigma$  from the mean of the respective dataset.

clear when considering the  $\text{TMH} \pm 5$  flanking residues except for mitochondria which increases in significance when considering the flanks also (Table 3.3). The ER and mitochondrial tests are very significant ( $P < 4.22E - 82$ ). Consistently the Bahadur slope is at least an order of magnitude greater in the ER and mitochondrially located protein comparison than for the other considerations, so these differences cannot be accounted for by the larger sample size. This gap in hydrophobicity appears to be due to a trend of the ER, PM, and Golgi using isoleucine, valine, and leucine as their most common TMH residues, whereas in the case mitochondrially located TA proteins, the most common residue type is alanine in the UniProt manually curated dataset (16.3% of total residues) followed by valine (12% total residues)(Figure 3.6). Similarly, alanine is the second most common residue in mitochondrial located TA proteins from the SwissProt automatically generated dataset at 11.9% of the total residues after leucine which is 13.4% of the total residues(Figure 3.7).

Analysis from 16 TA proteins with known subcellular locations showed that both the C-terminal tail charge and hydrophobicity are determinants of the terminal destination to the ER, mitochondria, and the peroxisome intracellular subcellular locations [328]. They found that less hydrophobicity and more charge in the “tail” determined the TA protein for the mitochondria rather than the ER. This corroborates what we see in terms of hydrophobicity (Figure 3.5A). When we consider charge difference between organelles on larger datasets, we see trends that reinforce this idea, however, rather than net charge, we see differences in charge distribution along the TMH and the neighbouring flanks. In the SwissProt automatically filtered dataset, in the ER 9.4% of the residues are positively charged, and 2.5% are negatively charged. Most of the positively charged residues cluster following the “positive-inside” rule between positions -15 and -10 for R and K, but so do the negatively charged residues D and E, effectively reducing this local charge by 2.5%. In mitochondria, we find that the proportion of charge is similar (10.4% R and K, 3.3% D and E) however the negatively charged residues cluster on the N flank (-15 to -8) and the positively charged residues cluster more strongly on the outside flank (positions 9 to 15) (Figure 3.7).

In the UniProt manually curated ER set, 6.6% of residues are positively charged and 3.3% of residues are negatively charged. K clusters strongly on the inside flank as expected, yet R clusters strongly between positions 7 to 15 and rather weakly at

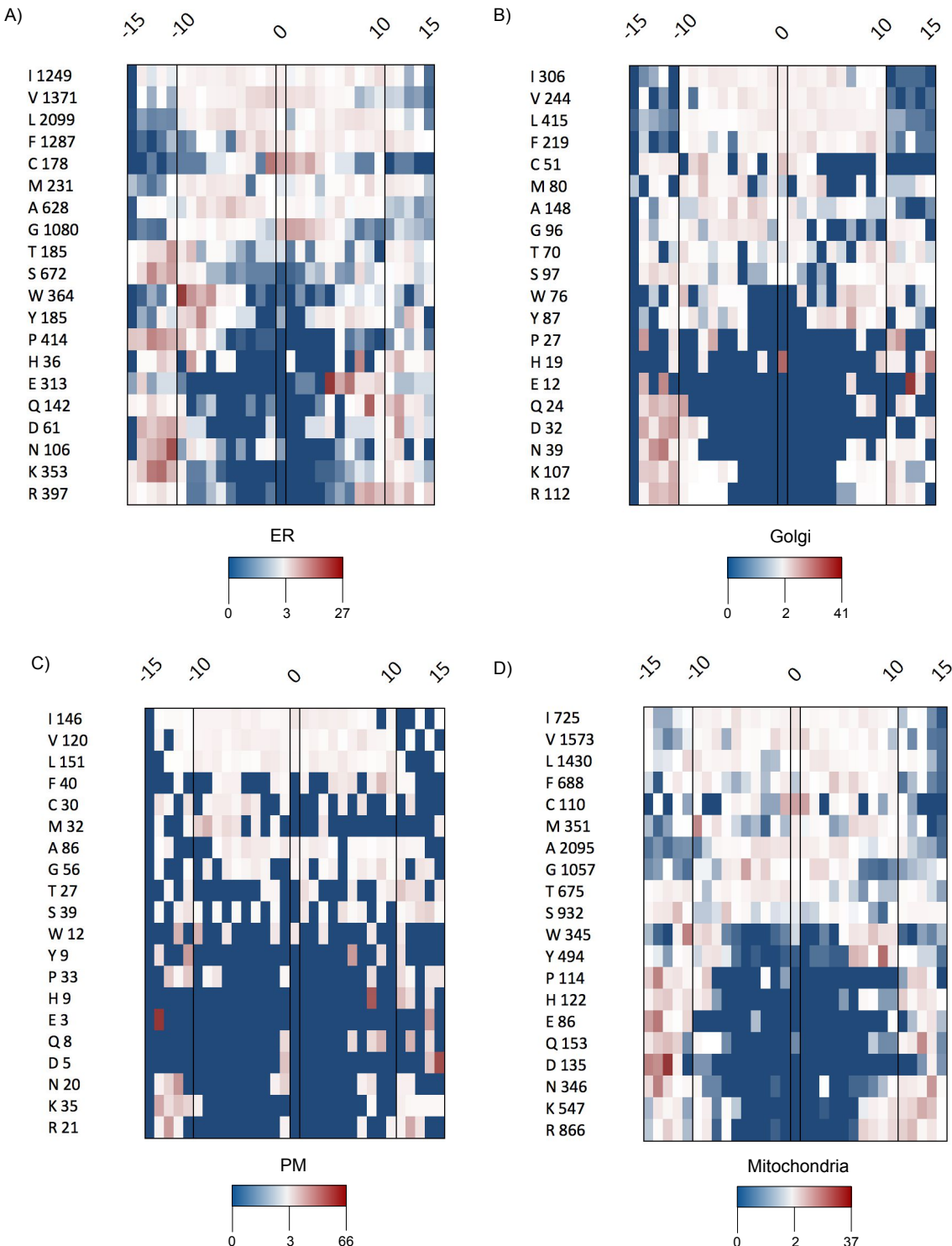


**Figure 3.6:** The normalised skews of each amino acids from tail-anchored proteins grouped by localisation from the UniProt manually curated dataset.

The residue position aligned with the centre of the TMH is on the horizontal axis, and the residue type is on the vertical axis. Amino acid types are listed in order of decreasing hydrophobicity according to the Kyte and Doolittle scale [73]. Flank lengths were restricted to  $\pm 5$  residues. The edge residues from proteins with flank lengths and TMH lengths that exceeded the plotted 31 residues were still included in the normalisation calculations despite not being plotted. The colour scale represents the relative percentage of a particular amino acid and is shown with dark blue as 0, white as the 50th percentile value of the entire heatmap, and dark red as the highest percentage on the heat map. The panels are constructed from TA proteins derived from the SwissProt automatic method with redundancy removal applied detailed in the methods section. The datasets were further separated by subcellular locations: (a) the ER, (b) the Golgi, (c) the cell membrane, (d) the mitochondria. These datasets are more thoroughly outlined in the methods section.

the inside flank (positions -15 to -10) (Figure 3.6). Similarly to the SwissProt sets, D prefers the inside flank but is tolerated in the outside flank. The more abundant E residues behave very unusually and cluster at positions 5-10. Generally, charged residues are suppressed in the TMH core [86, 109], especially in anchoring TMHs [227]. It is unclear why this is observed, yet, altogether the 313 glutamic acid residues and 397 arginine residues that appear unusually deep in the TMH core may be to an extent neutralising one another in the compacted TMH arrangement, but are ultimately not that abundant compared to the total number of residues in this organelle dataset (11351 total residues).

In mitochondria, 1413 positively charged residues (11% of the total residues in the mitochondrial dataset) were preferentially located at the outside flank and somewhat into the core (positions 6 to 15) than the expected “inside” flank (positions -15 to -5). The 221 negatively charged residues (1.7%) unusually cluster at the inside. This results in a strong net positive-outside charge signal since there are more positively charged residues on the outer flank un-countered by the negatively charged residues, which are skewed with a preference for the inside flank.

Information entropy has been known to identify cryptic function in TMHs when considered along with hydrophobicity [44, 45]. In terms of information entropy, there is a marked decrease in entropy in the PM subset (mean entropy = 3.15 in the TMH, 2.67 including  $\pm 5$  flanking residues) from the UniProt curated dataset compared to the other organelle datasets (entropy > 3.29 and > 2.85 including the flanks). However, this stark difference in TMHs from PM-bound TA proteins and the other organelle datasets cannot be observed in the SwissProt set (Figure 3.5).

No clear significant differences can be observed for the information entropy ( $P > 6.33E - 2$ ). This is unsurprising given that the hydrophobic nature of the TMHs demands that certain residues must be over-represented, which lowers the information entropy. In this case, we have a highly hydrophobic set, the PM UniProt set, which likely contains a higher proportion of the most hydrophobic residues. As a trend, the information entropy mirrors the hydrophobicity albeit with less range between dataset means (2.67-3.15 in the TMH for information entropy, 1.72-2.74 for hydrophobicity) (Figure 3.5).

Similarly, in the SwissProt filtered dataset, the mean TMH hydrophobicity for

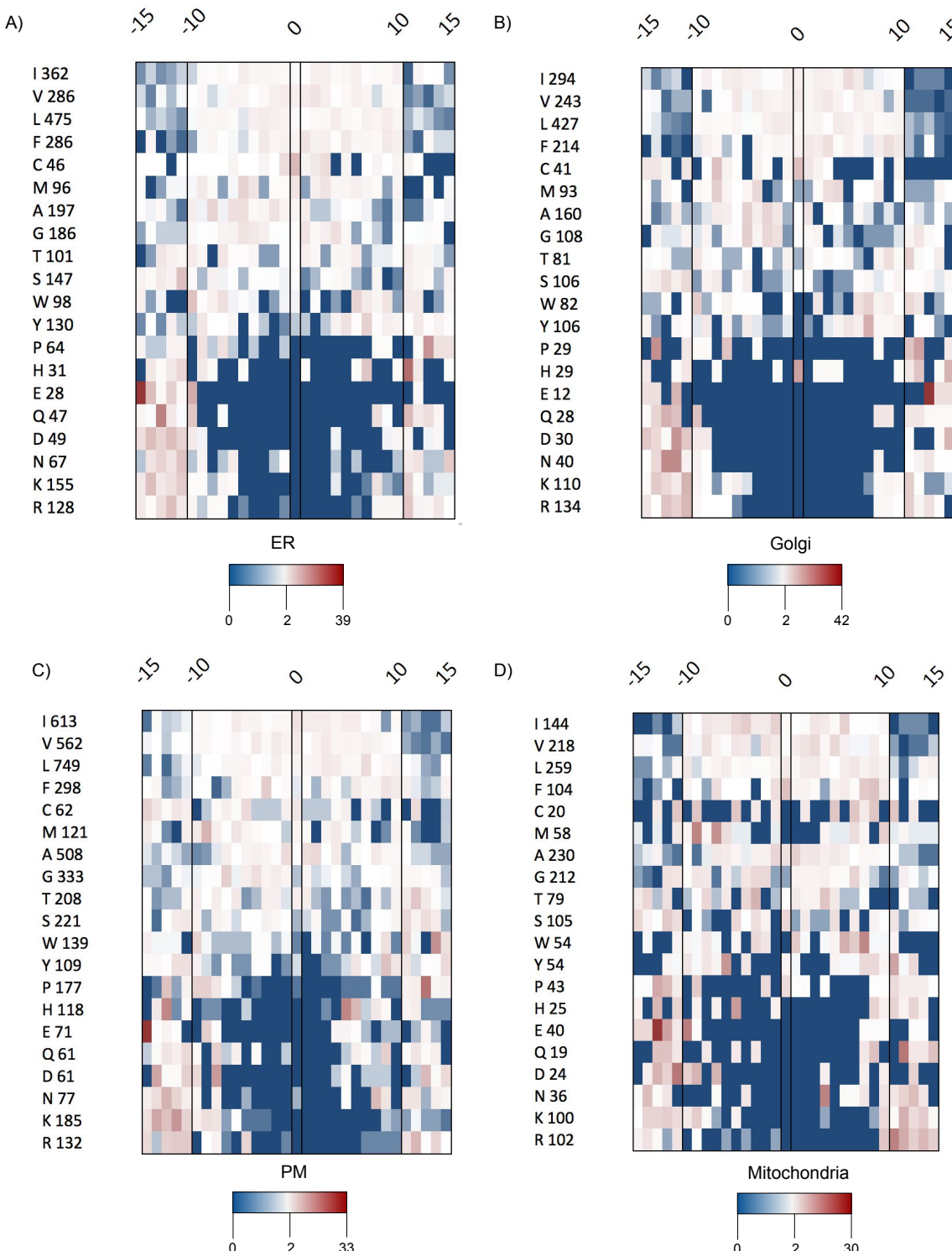


**Figure 3.7:** The normalised skews of each amino acids from tail-anchored proteins grouped by localisation from the SwissProt automatically filtered dataset

Similarly to figure 3.6, the residue position aligned with the centre of the TMH is on the horizontal axis, and the residue type is on the vertical axis. Amino acid types are listed in order of decreasing hydrophobicity according to the Kyte and Doolittle scale [73]. Flank lengths were restricted to  $\pm 5$  residues. The edge residues from proteins with flank lengths and TMH lengths that exceeded the plotted 31 residues were still included in the normalisation calculations despite not being plotted. The colour scale represents the relative percentage of a particular amino acid and is shown with dark blue as 0, white as the 50th percentile value of the entire heatmap, and dark red as the highest percentage on the heat map. The panels are constructed from TA proteins derived from the SwissProt automatic method with redundancy removal applied detailed in the methods section. The datasets were further separated by subcellular locations: (a) the ER, (b) the Golgi, (c) the cell membrane, (d) the mitochondria. These datasets are more thoroughly outlined in the methods section.

**Table 3.4: Statistical comparisons between transmembrane helix sequences from organelles in the SwissProt Filtered Dataset.** Here, we compare organelle subsets from the SwissProt automatically filtered dataset of TA proteins. We compare ER (N=98) to Golgi (N=82), PM (N=157), and the mitochondria referred to as “mito” (N=65). The hydrophobicity was predicted as the mean average of the values of the sequences of the TMH, as well another group including up to  $\pm 5$  flanking residues, since predicting the boundary of TMHs is difficult, according to the Kyte & Doolittle hydrophobicity scale [73]. The linguistic information entropy was calculated according to the methods section [151]. The Test column refers to the statistical score obtained from the test; H statistic for the Kruskal Wallis (KW), the KS statistic for the Kolmogorov Smirnov test (KS), and the t-statistic for the student’s T-test (T-test).  $p$  is the p-value of that statistical score.  $B$  refers to the Bahadur slope, an interpretation of the p-value that accounts for the sample size powering the test [259, 260].

		ER and Golgi			ER and PM			ER and mito		
		Test	$p$	$B$	Test	$p$	$B$	Test	$p$	$B$
TMH Hydrophobicity	KW	11.96	5.43E-4	4.18E-2	0.02	8.77E-1	5.14E-4	8.46	3.64E-3	3.45E-2
	KS	0.27	1.98E-3	3.46E-2	0.08	8.48E-1	6.44E-4	0.27	4.62E-3	3.30E-2
	T-test	-3.47	6.50E-4	4.08E-2	-0.17	8.67E-1	5.60E-4	3.45	7.24E-4	4.44E-2
... including flanks	KW	5.92	1.50E-2	2.33E-2	9.14	2.50E-3	2.35E-2	26.42	2.75E-7	9.27E-2
	KS	0.21	2.85E-2	1.98E-2	0.26	4.88E-4	2.99E-2	0.43	4.93E-7	8.91E-2
	T-test	-2.52	1.25E-2	2.43E-2	-3.09	2.23E-3	2.40E-2	4.95	1.87E-6	8.09E-2
TMH entropy	KW	2.96	8.56E-2	1.37E-2	0.66	4.17E-1	3.43E-3	0.69	4.05E-1	5.54E-3
	KS	0.13	4.32E-1	4.66E-3	0.10	5.27E-1	2.51E-3	0.18	1.40E-1	1.20E-2
	T-test	1.58	1.15E-1	1.20E-2	0.79	4.32E-1	3.29E-3	1.03	3.06E-1	7.26E-3
... including flanks	KW	2.62	1.06E-1	1.25E-2	2.87	9.04E-2	9.42E-3	0.05	8.31E-1	1.14E-3
	KS	0.15	2.48E-2	7.75E-3	0.17	6.56E-2	1.07E-2	0.21	6.33E-2	1.69E-2
	T-test	1.84	6.75E-2	1.50E-2	1.66	9.84E-2	9.09E-3	0.42	6.72E-1	2.44E-3

mitochondria is the lowest at 1.9. It appears to be the Golgi apparatus that is the peak at 2.4. In the SwissProt dataset, when we compare each subset of only the TMH to the ER subset, we find significance between the ER and the Golgi ( $p < 1.98E - 3$ ), and the ER and the mitochondria ( $p < 4.62E - 3$ ), however, the ER and PM are more similar considering the Bahadur values are  $< 6.44E - 4$ , two orders of magnitude smaller than the other sets (Bahadur values  $> 3.3E - 2$ ) (Table 3.4). When we take into account the flanks, the ER and PM dataset can be distinguished ( $P < 2.50E - 3$ ), however, as a trend the other two comparisons, ER and Golgi become less significant, and ER and mitochondria become more significant.

The information entropy of the TMH string was also examined. No significance was observed in any consideration of the information entropy, but similarly to the UniProt subset, as a trend, the entropy mirrors the hydrophobicity (Figure 3.5).

Lipid asymmetry is caused by sphingomyelin and glycosphingolipids on the non-cytosolic leaflet and phosphatidylserine and phosphatidylethanolamine in the cytosolic leaflet in the Golgi and PM, however, this asymmetry is not present in the ER [269, 270]. Another consideration is that sphingomyelin is not present in the ER but is present in the Golgi [272] and PM [184, 273]. Furthermore, the PM contains densely packed sphingolipids and sterols [274]. Mitochondria have bacterial lipids in their

membrane and uniquely contain cardiolipin [342], which is also confirmed to be present in the MOM [343]. The compositional differences of the membrane environments inevitably places different constraints on the TMHs, which may drive the observed variations in their biochemistry.

The hydrophobicity of TMHs in TA proteins is lower in proteins targeted to the mitochondria compared to those targeted to the ER [344]. Here we observe that average biochemical features are evidently of significance. Furthermore, we see that the typically positive-inside negative outside tandem in positively and negatively charged residues is reversed in the mitochondria to positive-outside negative-inside. This variation in TMH hydrophobicity and the charged residue skew reversal may be yet another nuance of the system which goes some way to explaining how signals are maintained in local environments even when the average values are ambiguous. We also identify that alanine is a key reason behind the hydrophobic difference between subcellular organelles, with alanine being highly selected, if not favoured over other hydrophobic residues like leucine, in mitochondrial TA proteins compared to the ER, the Golgi, and the PM. This could be an adaptation to the mitochondrial membrane, which contains a higher level of cardiolipins than other membranes [92, 343]. Regarding the charged residue distribution, there should also be a consideration of membrane potential. Although membrane potentials are in flux, typically, the PM has a potential of 70mV with the negativity being on the cytoplasmic side. It has been shown that the ER is again between 75-95mV with negativity on the luminal side [100, 101]. There is no detectable potential across the Golgi [103], and the mitochondrial inner membrane has a potential of 150-180 with negativity on the matrix side [102]. However, whilst those numbers go some way to satisfy the flanking charge reversal we see, they do not apply to the MOM in which the TA proteins are localised;  $\beta$  barrel porins on the MOM allow passive ion and water transfer across the membrane effectively diminishing the membrane potential. Furthermore, these observed membrane potential values are by their nature not fixed values. Not only would this be most striking in the nerve and muscle cells of course, but also would contrast between resting and stimulated secretory cells.

It has been known for some time that both the charge and the hydrophobic length of the TA protein TMH region are indicative of subcellular targeting of the protein [344]. ER localised TA proteins typically have a more hydrophobic TMH than those

targeted to the MOM [298]. The C-terminal tail charge is particularly important for determining subcellular localisation, and can even override the hydrophobic signal if strong enough [328]. Here we see that while hydrophobicity is statistically different between the subcellular membranes, there is overlap. Whilst there are differences in total average charge at the C-terminal flank, this is not an absolute rule. Perhaps these TA protein anchor TMHs are mechanistically similar to those of the signal anchor proteins, a group of singlepass TMPs containing an uncleaved SP that remains in the membrane. The single hydrophobic segment in mitochondrial signal-anchored proteins serves as both a mitochondrial targeting signal and a membrane anchor. Signal-anchored proteins, along with some TA proteins, have been shown to be able to spontaneously insert into the membrane independently from the translocon [41, 323, 345].

Nevertheless, it is tempting to conclude that these biochemical differences between differently localised TA proteins are an adaptation to the membrane composition and environment. But this must be tempered by noting that the spontaneously inserting cytochrome b5 localises to the mitochondrial membrane in the absence of cytosol, and to the ER in the presence of cytosol [329]; there are also biological factors determining localisation.

In summary, the mitochondria located TA protein TMHs typically have a preference for alanine over leucine unlike their secretory counterparts and have a negative-inside positive-outside tendency counter to the overwhelming majority of TMPs. It is unclear if these features are a biophysical adaptation or part of a biological sorting process.

#### **3.4.4 More annotation is required to identify chaperone interaction factors of the transmembrane helix.**

TA proteins known to interact with certain chaperones were acquired by filtering the interactor partner IDs for chaperones from BioGrid through the redundant versions of these UniProt manually curated lists and SwissProt automatically generated lists.

Hsp40, Hsc70, SRP54 (both plant and human) returned 0 hits, indicating a lack

of annotation regarding TA proteins with these chaperons probably due to the relatively polar, and non-trivially predictable, TMHs of TA proteins that these chaperones interact with.

Snd1 has 15 records that were in our TA lists. The average Kyte & Doolittle hydrophobicity of these records was 2.60 in the TMH itself and 1.58 including  $\pm$  5 flanking residues. Sgt2, with 14 records, had a TMH hydrophobicity of 2.47 and 1.51 including the flanks. 5 records were captured for SGTA with a TMH hydrophobicity of 2.27 and 1.19 including the flanks. TRC40 had the highest TMH hydrophobicity of 2.77 and 1.82 including flanks. However, TRC40 also only had 7 records. Get3 had 22 TA interactor records with an average TMH hydrophobicity of 2.36 and 1.48 including the flanks. The 2 records for human Pex19 had an average hydrophobicity of 1.33 for the TMH and 0.70 including the flanking residues. The yeast Pex19 had a TMH average hydrophobicity of 2.48 and 1.41 including the flanking residues. The 4 yeast SRP54 interactors had an average TMH of 2.43 and 1.98 including the flanking residues.

At the time of the investigation, these sample sizes are not statistically viable for analysis. Whilst it appears TRC40 interactors have notably hydrophobic TMHs, TRC40s yeast homologue Get3 has interactors with much more polar TMHs, yet SGTA was lower than Sgt2 on average. So although these average values differ and overlap between various chaperone systems, we tried to identify clearer patterns from the TMH hydrophobic profiles (Figure 3.8). Similarly, whilst a clear dip in hydrophobicity at position +5 in Get3 from between 2-3 across the rest of the TMH core to 0.32, there is no such spike for TRC40 meaning this is probably not of any functional importance, but rather an artefact of overrepresented proteins in the Get3 dataset. Snd1 also lies among these values, reinforcing Snd1 as a biological redundancy system [289, 290, 297].

As expected, the human Pex19 interactors are as a trend among the most polar throughout the TMH core, however, when we consider the yeast Pex19, this trend is less clear (Figure 3.8). In figure 3.8, at least at a handful of locations (-3, 3, 4 and 5) the SRP54 interactors have the most hydrophobic TMH cores.

TRC40 has the highest TMH mean average hydrophobicities at a given point at 3.9 at position -1. However, the yeast homologue Get3 does not appear to have any preference for especially hydrophobic TMHs (Figure 3.8).

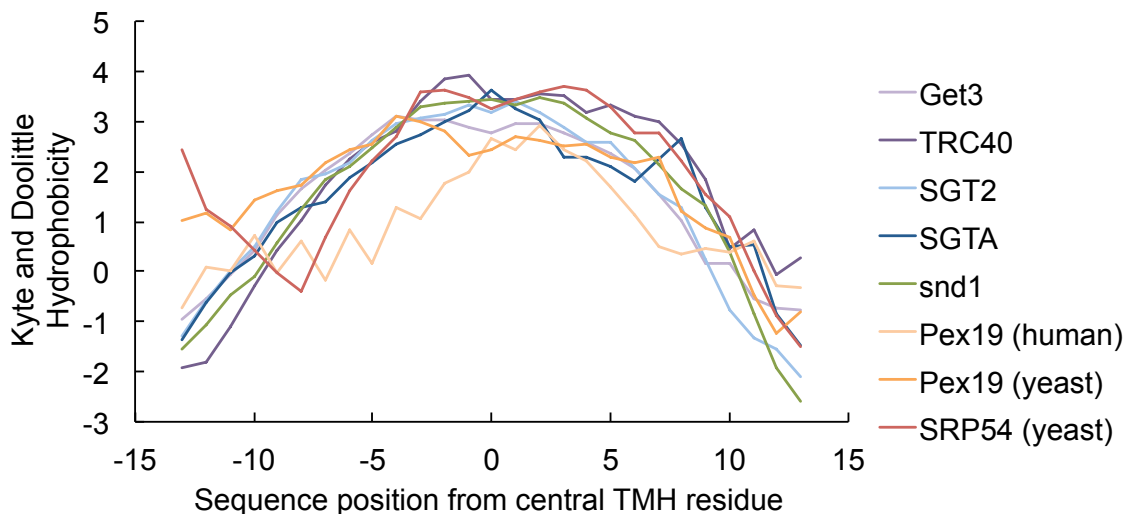


**Figure 3.8:** The profile of transmembrane helix and flanks hydrophobicity from tail-anchored protein groups stratified by chaperone interactors. On the horizontal axis is the position relative to the central TMH residue defined by UniProt. On the vertical axis is the Kyte & Doolittle hydrophobicity windowed across 5 residues allowing for half windows. The chaperone interactors are colour coded according to the key.

In order to remove redundant proteins and investigate this further, more records with greater levels of accurate annotation need to be available to both BioGrid and UniProt. We also observe a great deal of overlap between the profiles, indicating that as a trend this is more complex than hydrophobicity alone and that net/average TMH polarity is not the absolute determinant of chaperone association.

However, this method demonstrates a potential way that this chaperone-interaction problem can be investigated to verify that indeed hydrophobicity plays a deterministic role in chaperone selection.

### 3.4.5 Spontaneous insertion may be achieved by polar strips in the transmembrane helix of tail-anchored proteins

The TMHs of cytochrome b5 and PTP1b are among the least hydrophobic of the TA proteins [288, 289]. Indeed the TMH is so polar that it is not trivial to predict and is not found in either dataset prepared herein. Structural modelling and analysis thereof reveal features that may explain the “missing hydrophobicity” [74, 116, 267, 268] of these particular TMHs.

A positive patch can be seen on the cytoplasmic side of either protein TMH, and

a negative patch on the luminal tip at the C-terminus. There are large “positive-inside” patches [86, 109, 110, 113, 114, 227] and a strong “negative-outside” charge [227] (Figure 3.9C) at the respective flanks of the TMH. Such a distribution of charge is typical of a TMH anchor. Once in the membrane, this may allow the TMH to be an effective anchor despite such poor hydrophobicity since it satisfies electrostatic coupling to the membrane potential.

Furthermore, there is the question of overcoming the unfavourable interaction most TMHs would hypothetically face when coming into contact with the highly polar membrane interface without the presence of membrane integration machinery. We observe a highly conserved strip of relatively polar / non-hydrophobic residues on one side of the TMH core (in cytochrome b5 these are N112, P116, A120, A124 Y127, and R128). Similarly, a polar face exists for the PTP1b TMH (R430, N434, Y426, T422, and T419). These polar faces would not be as repulsed by the interfacial environment as either a more hydrophobic TMH or an equally hydrophobic TMH with a different sequence and structure order (Figure 3.9 and Figure 3.10). Scrambling the cytochrome b5 TMH sequence whilst maintaining the same hydrophobicity (DSNSS W W T N W V I P A I S A L I V A L M YR to DSNSS W W A S A I I A T M I P L L V N V W YR) reduces the insertion potential [138]. Therefore we can conclude that there is more to this phenomenon than hydrophobicity alone. It becomes apparent that the 3D arrangement of these relatively polar TMH residues is conserved and is probably the key to spontaneous insertion of TMHs.

We speculate that this polar face allows the unassisted approach to the membrane’s polar phospholipid head groups, and once in sufficiently close proximity, the hydrophobic side of the helix is entropically driven by the water environment into the membrane core (Figure 3.11). This close proximity is less likely to be achieved if there is no side of the TMH to favourably interact with the lipid head groups, even though average hydrophobicity could be similar. Once integrated, the charged TMH flanking regions help sustain integration in lieu of a more hydrophobic TMH core.

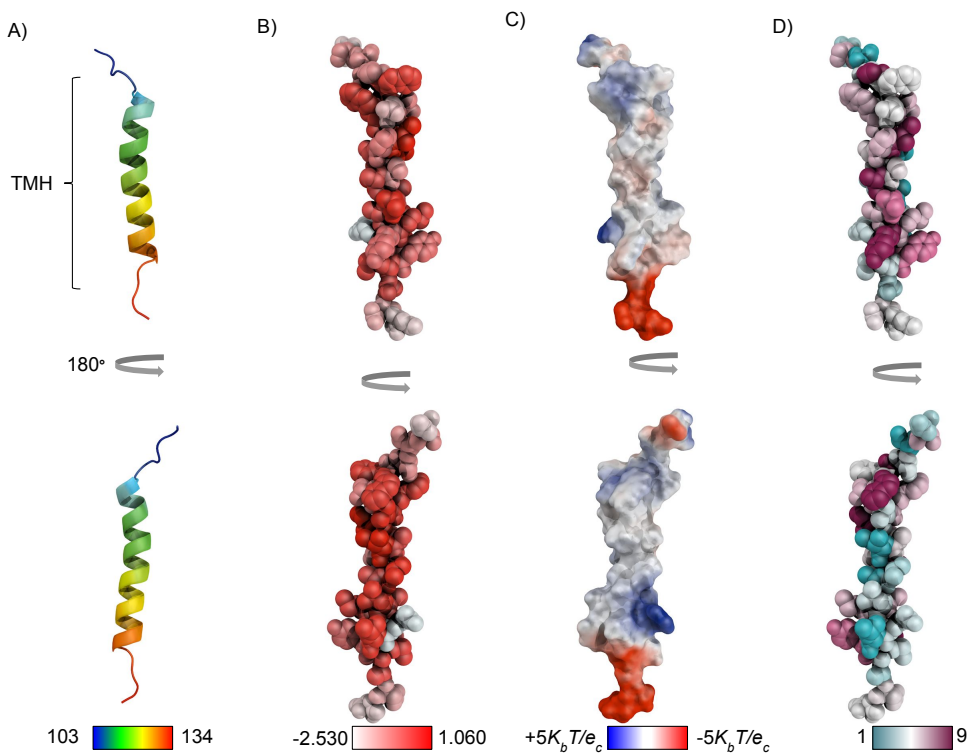


**Figure 3.9: Structural biochemical analysis of a homology model of cytochrome b5.** (A) The secondary structure of the protein coloured from the N terminus in blue to the C terminus in red coloured through the rainbow according to the residue number. (B) The hydrophobicity of the TMH from white representing relatively polar residues to red showing relatively hydrophobic residues [144]. (C) The electrostatic surface with a threshold of  $\pm 5 \text{ KT/e}$  calculated by APBS in PyMol [339]. Red patches are negatively charged whilst blue is positively charged. (D) The consurf scores on a scale of 1-9 (all residues had sufficient data) [340]. Purple represents the most conserved whilst blue is the least. Note the correlation between the highly and modestly conserved TMH residues and the relatively polar residues. Another observable feature is the very strong “positive inside” [86, 109, 110, 113, 114] and “negative outside” features which are associated with anchoring [227].

## 3.5 Summary

Here, we have observed a clear biochemical distinction between TA proteins with different terminal subcellular destinations. Previously it was known that both hydrophobicity and charge are involved in targeting to distinct subcellular locations [328]. In this study, we find that the location of the charge along and around the TMH of TA proteins differs among subcellular compartments. Crucially, there is a shift in the charged residue inside-outside tandem in the TMH flanking residues in different organelles. In the secretory pathway, the “positive-inside” “negative-outside” skew adheres to the membrane-potential for electrostatic coupling, but in the MOM where there is no membrane potential, positively charged residues are skewed to be

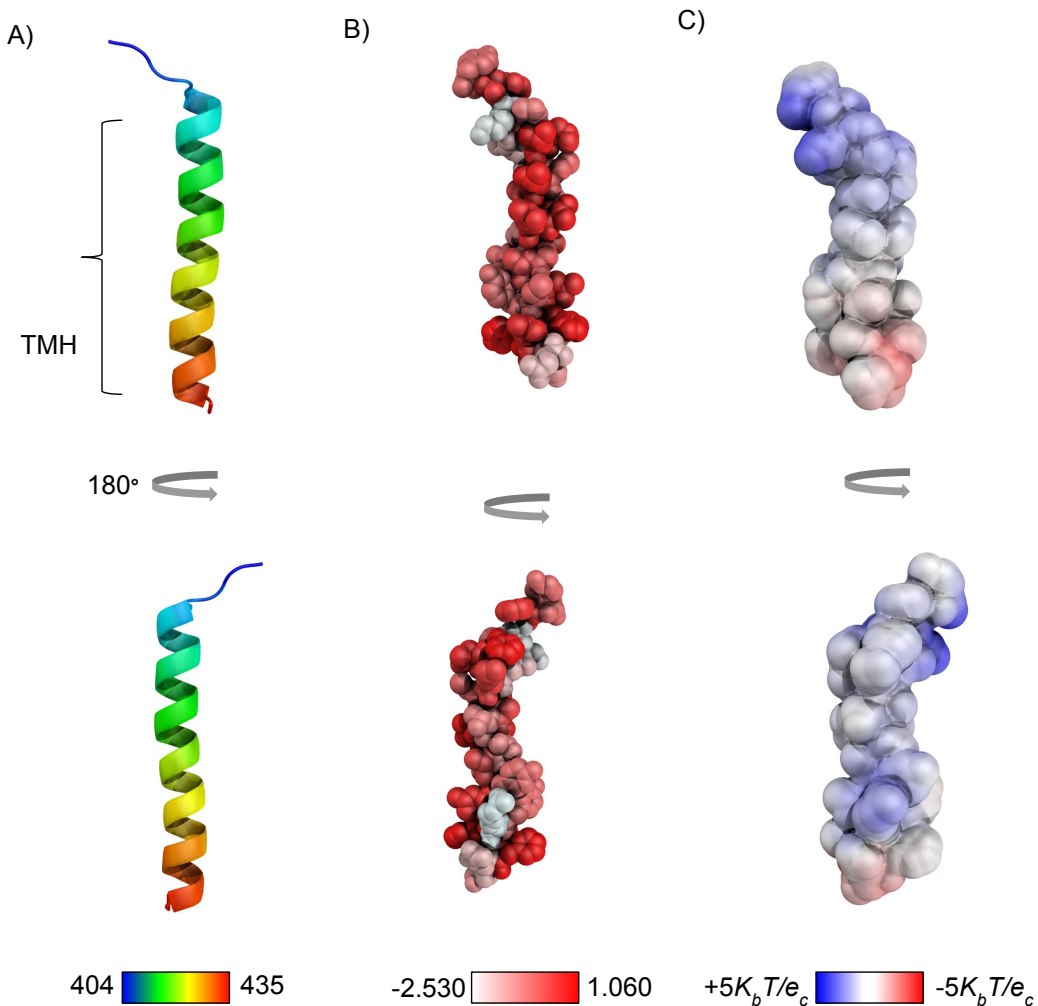


**Figure 3.10: Structural biochemical analysis of a homology model of PTP1b.** (A) The secondary structure of the protein coloured from the N terminus in blue to the C terminus in red coloured through the rainbow according to the residue number. (B) The hydrophobicity of the TMH from white representing relatively polar residues to red showing relatively hydrophobic residues [144]. (C) The electrostatic surface with a threshold of  $\pm 5 \text{ KT}/\text{e}_c$  calculated by APBS in PyMol [339]. Red patches are negatively charged whilst blue is positively charged. Note the one hydrophobic face of the TMH and the opposing relatively polar face. Another observable feature is the “positive inside” [86, 109, 110, 113, 114] and “negative outside” features which are associated with anchoring [227].

located outside the cytoplasm similarly to  $\beta$  barrels [110] which are also located on the MOM, and the negatively charged residues are preferentially found inside the cytoplasm. Furthermore, the missing hydrophobicity of mitochondrial TA proteins can be in part attributed to the high abundance of alanine rather than leucine or isoleucine in the TMH; it is not solely the tolerance of polar residues in the TMH. We expected to see evolutionary adaptations of TMH hydrophobicity to species-specific membranes, even within eukaryotes [86, 227]. In this study using both a manually curated dataset

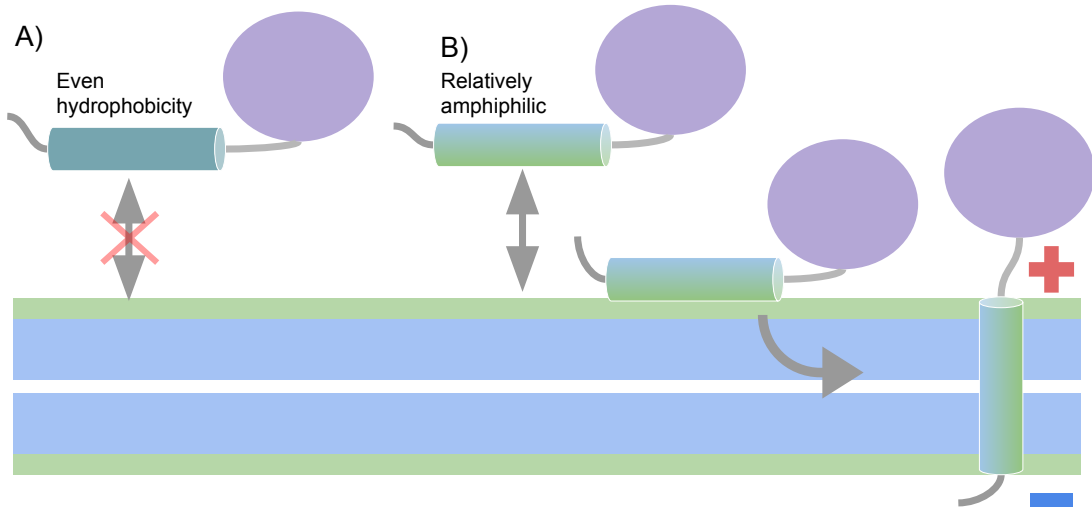


**Figure 3.11:** A cartoon of a potential method the cytochrome b5 and PTP1b transmembrane helix could integrate spontaneously into the membrane. A) The marginally hydrophobic TMH in teal cannot approach the membrane interface. B) Although the average hydrophobicity is the same as the teal TMH, by having a more hydrophobic side (blue), and a more polar side (green), the TA protein now has a TMH surface that may interact more favourably with the interfacial region. Once interacting with the membrane sufficiently close to the interfacial region, the hydrophobic face is still being entropically driven by water molecules from the cytosol, which would lead to partitioning into the membrane. Once integrated, the strong “positive-inside” “negative-outside” charges on the TMH flanks compensate for the lack of hydrophobicity in the core of the TMH.

from UniProt and an automatically filtered list using SwissProt annotation, we do not observe any strong differences. Since we could not scrutinise a difference in the species, the strong hydrophobic differences between organelle TMHs are indicative of a stronger adaptation pressure than between species as a whole. These differences are likely to be partially adaptations to the organelle location membrane type and also possible cryptic biological factors that play a role in their targeting via chaperone-binding affinity. We could not find any clear trends or perform statistical work on the chaperone interactor datasets due to the small sample sizes, however, as the databases are enriched, this same method will be able to answer the questions about chaperone affinity with more accuracy in the future.

Furthermore, the spontaneously inserting TA proteins PTP1b and cytochrome b5 appear to share a polar face that emerges in structural models and a strong “positive-inside” “negative-outside” electrostatic surface. The polar face may be responsible

for the promotion insertion potential in the absence of insertion proteins since when the sequence is scrambled, the insertion potential is reduced [138]. The positively and negatively charged residues are distributed like an ideal anchoring TMH [227], which could allow the marginally hydrophobic TMH to perform as a suitable membrane anchoring feature.

# Chapter 4

**Sequence analysis of polarity in transmembrane helices suggests that translocation of marginally hydrophobic helices could be facilitated by neighbouring typically hydrophobic helices**

## 4.1 Abstract

Marginally hydrophobic transmembrane helices perform a variety of essential for life intra-membrane molecular biochemistry. However, due to their relatively polar composition, they often lack sufficient hydrophobicity by themselves to incorporate into the membrane efficiently via the translocon. In some cases other elements of the sequence context, such as other transmembrane helices or flexible loop regions, allow the marginally hydrophobic transmembrane regions to integrate into the membrane environment. Here we analyse large numbers of multipass transmembrane protein sequences stratified by protein families and molecular functions to show that there are conserved stark differences between sequentially adjacent transmembrane helices in

terms of hydrophobicity and TMSOC complexity. Not all classes of transmembrane protein have these highly polar-hydrophobic pairs. In the instances of GPCRs and ion channels, there is evidence in the literature to support cooperative insertion between these highly polar-hydrophobic transmembrane helix pairs highlighted in our results.

## 4.2 Introduction

Translocation is the process of incorporating a TMP into the membrane. A ribosome translates the RNA to a nascent peptide chain which is handed directly (co-translational insertion) or indirectly (post-translational insertion) to the translocon insertion machinery. This translocon assembly then threads the chain through the membrane and releases hydrophobic TMHs into the membrane environment (Figure 4.1).

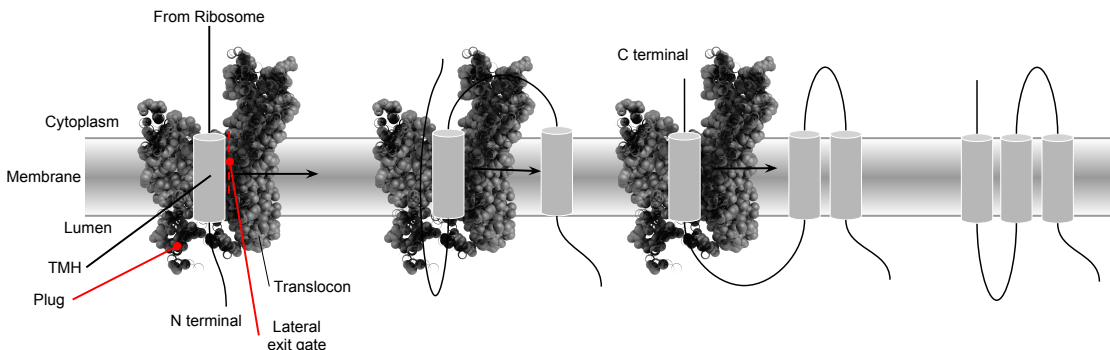


**Figure 4.1: A cartoon showing the generally accepted schematic of sequential multipass transmembrane helix insertion into the membranes.** The two key concepts are that one at a time, the TMHs emerge from the ribosome into the translocon. This appearance of hydrophobicity triggers the lateral gate to open. As the nascent TMH is exposed to the membrane, it begins to partition. The downstream protein from the TMH is then threaded through the translocon until the next TMH is recognised. This implies that the TMHs ultimately have no meaningful interactions with one another until the protein has been threaded into the membrane and the multiple TMHs form a bundle.

The overwhelming majority of TMPs use the co-translational method of translocation. It has long been understood that this method is essentially the SRP recognising and attaching to the nascent peptide chain whilst it is still associated with the ribosome, which targets the peptide and ribosome to an SR in association with the membrane insertion machinery on the ER membrane [116, 171].

Crystal structures showed the SRP targets the nascent peptide chain for membrane insertion via a GTPase in both the SRP and the membrane bound translocon

associated SR [175]. The SRP-ribosome-nascent peptide complex associates with the translocon-SR complex thus bringing the nascent peptide chain in proximity to the translocon [175]. Mutant studies of SRP revealed key discrete conformational stages [175]. These are the specific recognition of signal sequences on cargo proteins, the targeting of the package to the membrane, the handing over of the cargo to the translocation machinery all the while maintaining precise spatial and temporal coordination of each molecular event [346].

The prevailing view of membrane insertion by the translocon is that the TMHs partition in the membrane one at a time as the translocon lateral gate opens, exposing the TMH to the membrane (Figure 4.1) [40].

#### 4.2.1 The ribosome-translocon complex in the biogenesis of membrane proteins

A ribosome translates the mRNA into amino acid chains and are present in all living cells. Indeed the ribosomal complexes presence and activity is considered an important distinction in biology between ribosome-encoding organisms and capsid encoding organisms [347]. They are a highly conserved RNA-protein complex with a multitude of accessory proteins and targetting factors.

During translation of a TMP protein, the SRP binds to the ribosome after recognising the nascent protein as a TMP [169]. This complex then binds to the SR in association with the membrane-bound translocon [172]. The nascent peptide is then fed into the translocon as it is being translated; hence “co-translational insertion”. The journey of the TMH through this machinery has been studied using both cross-linking experiments and the relatively new technique of Arrest Peptide (AP)s [40].

APs are typically 10-15 residues long that bind to the upper end of the ribosomal exit tunnel. Once a specific mRNA codon is recognised, ribosomal stalling is induced [352] and the translation is halted unless a strong enough pulling force from the downstream insertion is acting on the nascent chain at that time [353]. Several “strengths” of AP have been identified. For example, SecM from *E. coli* is 17 residues long and relatively weak, whereas a mutated SecM from *Mannheimia succiniciproducens* (Ms-Sup1) is much stronger and 8 residues long ending in a proline which will halt translation

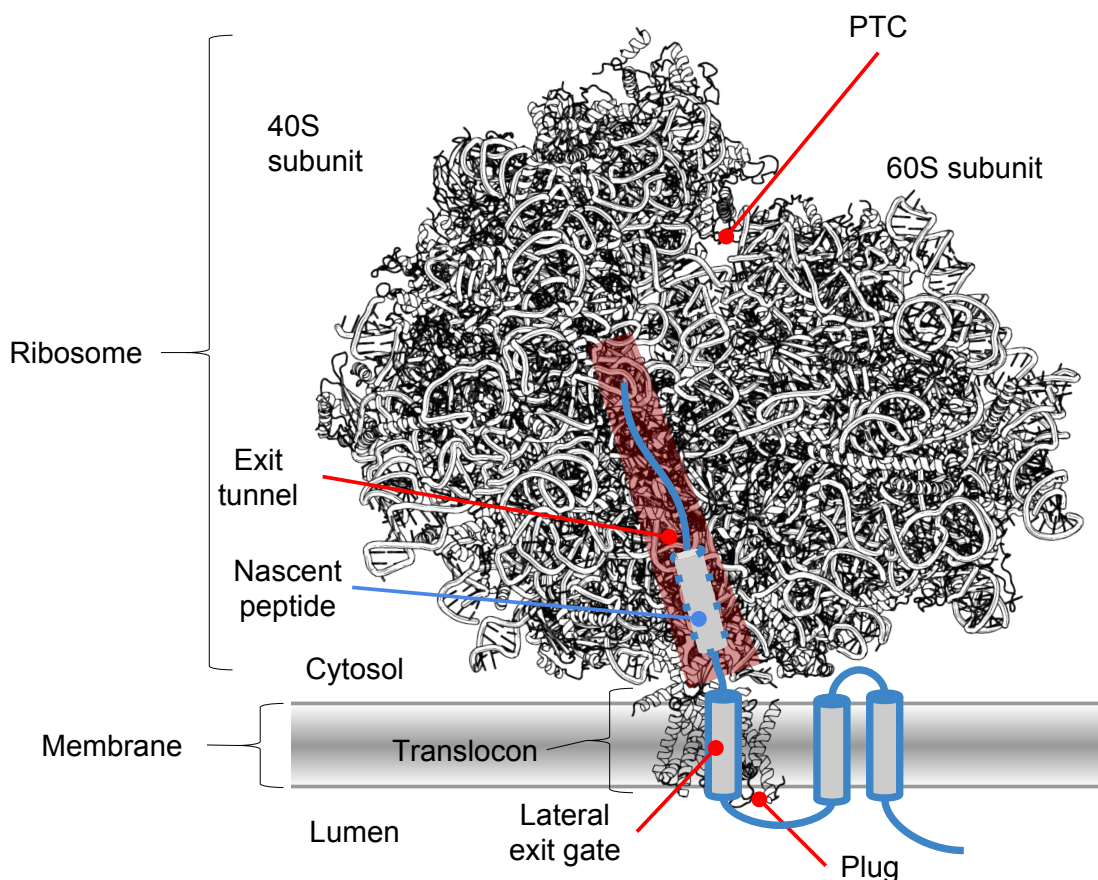


**Figure 4.2: A cartoon of the ribosome in association with the translocon during insertion.** The structure used is of a translating mammalian ribosome-Sec61 translocon complex (PDB code 3j7r [162]). The Sec61 translocon is the membrane-embedded element of the structure that feeds the protein into the membrane. The ribosome is made of two elements; 60s and 40s. These vary in composition and size between eukaryotes and prokaryotes. PTC refers to the peptidase transferase centre, a high conserved catalytic site across all the kingdoms of life that performs the translation of RNA to amino acid polypeptides. After translation, the nascent peptide moves down the exit tunnel located in the larger ribosomal subunit (a simplified version of this channel is highlighted in red). There is evidence that the secondary structural elements of TMHs in ion channels are pre-folded in the ribosomal exit tunnel [348–351]. The ribosome hands the nascent chain to the translocon. Once the plug moves to expose the translocon pore, the translocon has a hydrophobic core which regulates the integration of the TMH via the lateral gate [128].

[253]. There are several other SecM proteins of other strengths from various bacterial species [354]. Therefore APs are a technique that can be used to measure precise forces acting on a specific part of the nascent chain during co-translational membrane protein integration allowing the study of TMP kinetics during insertion and folding. The force profile of a single residue can now be obtained *in vivo* [253]. In an idealised TMH segment composed of alanine and leucine being inserted into *E. coli* membrane

through SecM AP with SDS-PAGE, hydrophobicity is more able to overcome the arrest peptide when it is near the N-terminal of a TMH with N-terminal-inside topology [253]. This could be either the TMH finally coming into contact with the cytoplasmic face of the lipid bilayer, or an interaction between the N-terminal and the tip of the lateral gate as previously shown in Sec61; part of a pre-integration TMH interrogation [355].

The ribosome passes the nascent chain to the Sec translocon machinery. Like the ribosome, the Sec pathway is widely conserved across life [153]. Sec61 (in eukaryotes) and SecYEG (in prokaryotes) translocate hydrophilic peptides across a membrane whilst also integrating sufficiently hydrophobic sequences to the membrane [40, 128, 156, 157]. SecY in prokaryotes or Sec61 $\alpha$  in eukaryotes are TMPs with 10 TMHs that perform the translocation. These proteins have a luminal plug [164, 165] and a constricted core to prevent permeability whilst the protein is idle [128]. During translocation the plug moves out of the pore [356], the channel is in an open unconstricted state [128], and a lateral gate of TMH2 and TMH7 [181] periodically opens to release a TMH to the membrane environment if sufficient hydrophobicity is present in the nascent peptide chain [128, 179, 180](Figure 4.1).

#### 4.2.2 Cooperative transmembrane helix insertion by the translocon-ribosome complex

Early evidence of secondary structure folding of the  $K_v$  ion channel showed that the S6 TMH (referred to later in this study as TMH6) is indeed compacted in the ribosomal tunnel by using pegylation and calmodulation of the tagged cysteine-scanned S6 TMS [348]. Furthermore, accessibility assays and an improved intramolecular cross-linking assay showed that the helical transmembrane S3-S4 hairpin (the “paddle”) of a voltage-gated potassium ( $K_v$ ) forms in the ribosome tunnel [350]. Ribosomal folding of the TMHs in  $K_v$ 1.3, a potassium channel, is maintained in the translocon [349]. Therefore, some of the final structural folding of the voltage sensor domain occur within the ribosomal exit tunnel.

Furthermore, it has recently been suggested that larger structures fold as the ribosomal exit tunnel widens [351]. This size-dependent folding was observed by using the

SecM translational AP. Two ribosome mutants of deleted uL23 and a uL24 variant that does not contain the hairpin loop were compared to the wild-type (uL23 is a globular domain buried within the ribosome that is close to the exit tunnel and uL24 contains a hairpin loop that obstructs the tunnel exit). These mutants resulted in reduced space for folding in the ribosomal exit tunnel at separate points. ADR1a, a 29-residue zinc finger motif, was found to fold deeper in uL23 mutant than the wild-type and the uL24. Two domain folds of 109 and 89 residues in length folded deeper in the uL24 mutant than in the wild-type and the uL23 mutant. This shows that cotranslational folding can occur in the ribosomal exit tunnel once sufficient space is available [351].

The ribosomal tunnel also slows down elongation of positively charged peptide segments. This is attributed to the sporadic negative patches within the ribosomal exit tunnel [357].

The ribosome clearly has the potential to pre-fold secondary structures and some motifs before translocon insertion into the membrane.

Multiple TMHs in a nascent protein can be associated with the eukaryotic translocon simultaneously. It was shown that TMHs can stay in association with the translocon in order to mediate integration of downstream TMHs demonstrated by cross-linking analysis in Aquaporin-4 [358] and a ligand-gated ion channel, the P2X2 receptor channel [359]. Not only this, but it was shown that there is a direct interaction between the TMHs; more recently APs were used to show pulling forces between a TMH and more C-terminally located TMH during the C-terminal TMH membrane partitioning from the translocon *in vivo* [360]. This could be facilitated during the probing of a TMH from the translocon as the lateral gate “cracks” open in an intermediate stage before the TMH satisfies the full hydrophobic requirements to open the gate fully, an intermediate stage observed in a SecY crystal structure [179].

Sixteen marginally hydrophobic TMHs were screened and revealed that independently they did not efficiently insert via the translocon into the ER [267]. The study showed that in the presence of the neighbouring loops and TMHs, insertion often became sufficient with the exception of two of the marginally hydrophobic TMHs. The orientational preference of neighbouring TMHs was shown to increase insertion efficiency into the ER of a marginally hydrophobic TMH [268]. A glycosylation study

of three relatively polar TMHs revealed that proteins have even evolved to exhibit stronger “positive-inside” tendencies when following another TMH [361]. Subsequent TMHs with a strong topological preference (increased arginine presence) increase the insertion potential of marginally hydrophobic TMHs, however, no specific interaction between the TMHs was responsible. The nascent polypeptide in the cavity between the ribosome and the translocon can alter the hydrophobic threshold of the translocon which therefore is dynamic and influenced by downstream flexible sequences [362]. Sequence context is clearly an important factor for the efficient insertion of marginally hydrophobic TMHs. These TMHs rely on other components of their protein in order to incorporate into the membrane.

### 4.2.3 Aims

Marginally hydrophobic TMHs often miss the energetic requirements of insertion via the translocon [74]. In the literature, there are examples of cooperative TMH interactions during insertion of marginally hydrophobic TMHs in 6TMH ion channels and GPCRs [40, 268, 350, 358–361, 363–367].

In this chapter, we investigate the relationship between biochemical sequence derived properties such as TMH hydrophobicity and TMSOC z-score [44, 45] of marginally hydrophobic TMHs and their sequential neighbouring TMHs to identify family wide patterns that may use a cooperative TMH insertion folding mechanism.

## 4.3 Methods

### 4.3.1 Datasets

#### Membrane protein families

Datasets were attained by querying the UniProt database for controlled vocabulary keywords (Table 4.1) [75]. After filtering out redundant proteins using UniRef50, the datasets were stratified according to the total number of TMHs per protein. Only families with a total  $N > 20$  were included in the analysis, for example, there are ion channels with 12 TMHs, but only 16 examples fitted the criteria and were omitted from the study. Analysis can only be done if the number of TMHs is conserved across

the family.

**Table 4.1: Dataset sizes of common transmembrane protein families of transporters and channels.** The type column refers to the family name. The keyword identifier column refers to the specific query term that UniProt uses as the controlled vocabulary identifier. UniProt hits refers to the number of SwissProt hits, which are manually curated, however, the SwissProt and TrEMBL hits are also given in the brackets. The UniRef column denotes how many representative sequences resulted from the UniProt hits, again with the number in the brackets including the TrEMBL hits. Because UniRef often returns representatives of splice isoforms as a separate hit, the lists were re-uploaded to UniProtKB to get the final hit. The lists are then stratified by the total number of TMHs.

Type	KW	UniProt Hits	UniRef	Records	TMHs	Final hits
Ion channel	0407	2452 (176417)	912 (21024)	882	4	234
					6	188
					24	34
Ligand-gated ion channel	1071	452 (14051)	189 (3055)	185	6	33
Voltage-gated channel	0851	683 (27,662)	285 (3876)	267	6	97
Calcium channel	0107	272 (5056)	128 (1003)	120	6	38
Potassium channel	0631	337 (11852)	160 (1893)	152	6	88
Sugar transport	0762	1217 (107721)	467 (16748)	464	12	134
Chloride channel	0869	303 (3697)	117 (1039)	117	4	50
Ion transport	0406	10264 (443600)	3070 (42259)	3023	4	338
					6	390
					8	162
					10	189
					12	292
					24	35

## GPCR subfamilies

The 7TMR list is a list distributed by UniProt containing GPCRs available at <http://www.uniprot.org/docs/7tmrlist.txt> [75]. The entire list contains 3115 UniProt IDs which mapped to 3092 records on the date of download (12/9/2017). After removing redundant records using UniRef50 to identify cluster representatives, 1142 records made the final dataset. The original list is also sub categorised by function. Here, we also looked at opsins, the T2R taste receptors, frizzled/smooth GPCRs, metabotropic glutamate receptors (Family C), and fungal mating proteins.

218 opsin records were mapped through UniRef50 to 40 records. 211 T2R taste receptors were mapped to 45 records after UniRef50. There were 82 records for frizzled/smooth, of which 41 were cluster representatives after querying with UniRef50. 114 were metabotropic glutamate receptors which became 44 after redundancy removal. In serotonin, 91 original records were represented by 28 records. There were 13 fungal mating proteins, represented by 9 after UniRef50. 560 olfactory records were mapped to 274 records after UniRef50.

After limiting all these sets to records containing 7 TRANSMEM features, there were 39 opsins, 38 frizzled smooth GPCRs, 9 fungal mating GPCRs, 41 metabolic glutamate receptors, 45 t2r taste receptor proteins, and 263 olfactory receptor GPCR proteins. TRANSMEM is an annotation by UniProt denoting a TMH evidenced by experimental documentation or a robust TMH prediction method [75].

### 4.3.2 Gene ontology

77153 protein records matched the query `annotation:(type:transmem)` `ANDreviewed:yes` in UniProt [75]. 30045 records of these represented those proteins after submitting the list to UniRef50. To gain an approximate idea of what proteins may have cooperative TMHs, we submitted that non-redundant SwissProt transmembrane dataset to PANTHER and used their pie chart visualisation [368]. We also submitted a constricted list of the non-redundant SwissProt transmembrane dataset to PANTHER by sorting the list according to proteins with sequentially adjacent TMHs that had the greatest difference in Kyte & Doolittle hydrophobicity [73]. This consisted of the top 102 pairs from a list of 101604 (the top 0.1%) TMH pairs from 87 unique UniProt records. In PANTHER, these hit 59 genes with 58 functions.

### 4.3.3 Complexity and hydrophobic estimation

Primarily we used the Kyte & Doolittle scale in this work [73]. We verified this scale with the Eisenberg scale [144], the Hessa biological scale [116], and the White and Wimley scale [139]. The Eisenberg scale is potentially double counted for many of these proteins since it is used by UniProt during their automatic TMH annotation where experimental evidence is not available. The Hessa biological scale originally reported positional dependencies that affected the hydrophobicity values which were refined in a later version of the scale [74], however, this later version was not programmatically available to us.

When stratifying TMHs by hydrophobicity and sequence information entropy, there is a clear distinction between anchoring TMHs and those with a function beyond anchoring. The TMSOC z-score quantifies this relationship and is calculated by equation

## 4.1.

$$z(x_\Phi, x_c) = (-1)^s \left[ \frac{(x_\Phi - \mu_\Phi)^2}{\sigma_\Phi^2} + \frac{(x_c - \mu_c)^2}{\sigma_c^2} \right] \quad (4.1)$$

$x_c$  and  $x_\Phi$  are moving window averages of c, the sequence entropy determined by SEG [146, 150].  $\Phi$  is the White and Wimley hydrophobicity [139] for a given segment and  $\mu$  and  $\sigma$  are the mean and standard deviation of the sequence entropy and hydrophobicity of the functional TMH sets.  $s$  is set to either zero or one depending on the the normal to the regression line between normalised hydrophobicity and complexity [44] (Equation 1.3, equation 1.4)

Broadly speaking, the information theory entropy of a string of characters can be defined as in equation 4.2, which we use to calculate the sequence information entropy of TMH sequences.

$$H(S) = - \sum_{i=1}^n P(s_i) \log_2 P(s_i) \quad (4.2)$$

Where  $H$  is the entropy of a sequence ( $S$ ) with values  $\{s_1, \dots, s_n\}$ , and  $P(s_i)$  is the probability of a character  $i$  through each position in  $S$ . This allows us to quantify the average relative information density held within a string of information [151].

### 4.3.4 Statistics

We used the Welch's t-test to scrutinise the means of the datasets without assuming equal variance. To examine any differences in the skew of the datasets, the Kruskal Wallis, and the Kolmogorov Smirnov tests were used. All these tests were performed using the Python scipy package [369].

### 4.3.5 Availability of materials

The scripts and datasets associated with this study can be accessed at [https://github.com/JamesABaker/multipass\\_tmh\\_analysis](https://github.com/JamesABaker/multipass_tmh_analysis).

## 4.4 Results and discussion

### 4.4.1 Large contrasts in transmembrane helix hydrophobicity occur in channels and receptors

Large differences in sequentially adjacent TMHs could indicate cooperative insertion between a marginally hydrophobic TMH and a more typically hydrophobic TMH. In order to identify which type of TMP may contain cooperative TMHs, the hydrophobicities for TMHs from 30045 records in a non-redundant version of SwissProt were calculated according to the Kyte & Dolittle hydropathy scale [73]. The absolute difference between each sequentially adjacent TMH was calculated. The full list, alongside a list of the 0.1% highest hydrophobic discrepancy TMH pairs, were submitted to PANTHER [368]. We found that transporters were by far the most abundant in the 0.1% sub-list relative to the global TMP list, however, it should be considered that “transporters” in this sense also includes both ion transporters and ion channels (Figure 4.3). Among the other prevalent functions are receptors, binding proteins, and signal transducers. All these lists were predominantly made up of GPCRs.

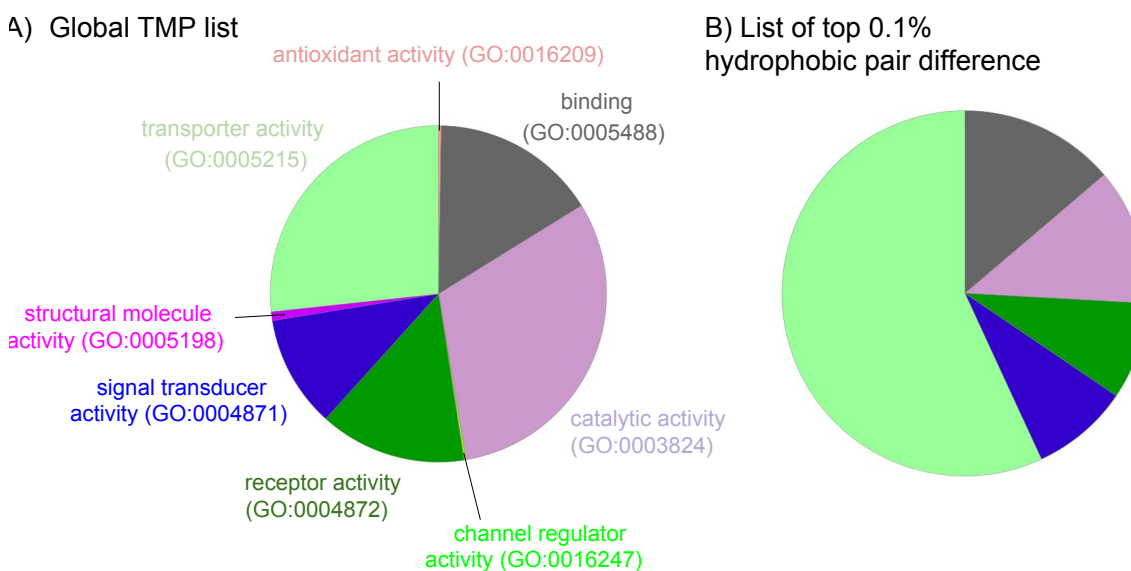


**Figure 4.3: Pie charts of a non-redundant list of transmembrane proteins compared to a list of transmembrane proteins containing the most hydrophobically different transmembrane helix pairs.** The output of PANTHER Gene ontology server of A) a non-redundant list of all TMPs in SwissProt and B) a list of the TMPs with the highest (0.1%) hydrophobic discrepancy between adjacent TMHs. Note that the proportions of binding TMPs stay roughly the same, receptors and signal transducers reduce slightly, catalytic proteins are reduced by two thirds and transporter activity proteins more than double in proportion.

The relative proportion of GO terms for catalytic function decreased when considering the top 0.1% of hydrophobic difference between sequential TMH pairs. This trend suggests that a catalytic function of the TMP may not be associated with a high hydrophobic discrepancy between TMHs within the protein. Figure 4.3 gives us an idea of search space where highly polar TMHs are proximally adjacent to typically hydrophobic TMHs; GPCRs and membrane transporters.

#### 4.4.2 GPCRs contain conserved relatively polar TMH7, which follows the typically hydrophobic TMH6

GPCRs are a diverse family of membrane surface receptors with 7 TMH segments. GPCRs have long been known to be overrepresented among genomes [370]. They have adapted to respond to a wide range of specific signals ranging from macromolecules to photons. The specific signal triggers a conformational change of the GPCR that is translated across the membrane. GPCRs have been associated with tumorigenesis [371], metastasis [372] and in cancers [373] and are a potential target for therapies [374]. Their ubiquitous presence in cellular life and medical relevance makes them an important topic of study.

Here, we structurally aligned 7 structures of monomeric GPCRs using PyMol [375]; PDB codes 1u19 (rhodopsin) [376], 2z73 (rhodopsin) [377], 2vt4 ( $\beta$ 1-adrenergic receptor) [378], 2lnl (CXCR1, rhodopsin-like) [156], 4mbs (CCR5, chemokine receptor) [379], 4xt1 (viral chemokine) [380], and 4ea3 (opioid receptor) [381] (Figure 4.4A).

Even in a relatively small dataset of functionally varied GPCRs, we can see structural conservation of the TMH arrangement (Figure 4.4A Figure 4.4C). Hydrophobic patterns are hard to identify structurally beyond the clear membrane boundary where we would expect to see hydrophobic residues in the TMH (Figure 4.4B). TMSOC [44, 45] is an algorithm that takes into account the White and Wimley hydrophobicity [139] and the information entropy of the TMH sequence. Note that the scale is the inverse of the Kyte & Doolittle scale, i.e a more negative TMSOC z-score indicates a higher hydrophobic contribution to the TMSOC z-score. The resulting z-score has been shown to be able to scrutinise between TMHs that serve as anchors and those that have a function beyond TMP anchoring. The lower the z-score (low sequence

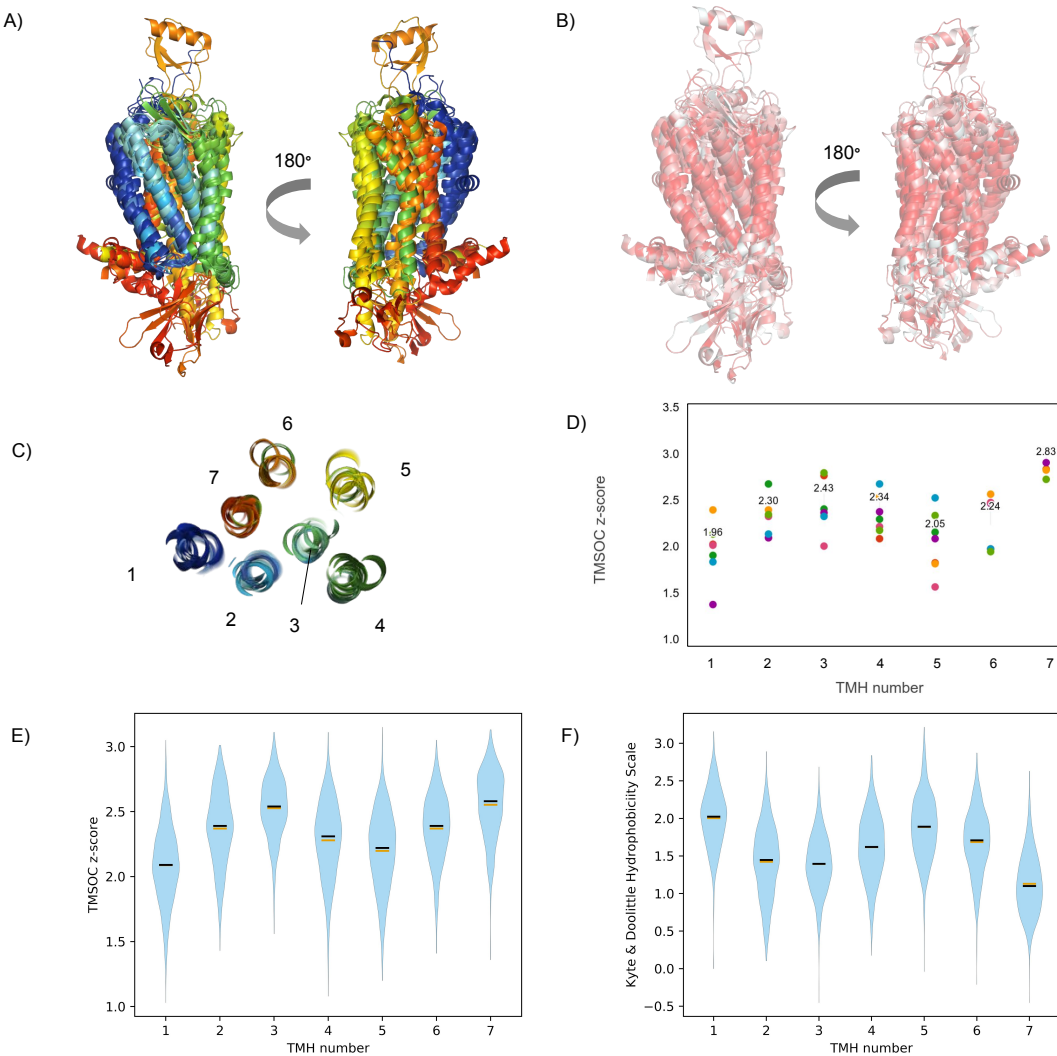


**Figure 4.4: The hydrophobicity and complexity of GPCR transmembrane helices.** A) A cartoon of 7 structurally aligned GPCRs of various molecular functions coloured according to the residue sequence position. Blue is the N terminal residue, working through the rainbow until red at the C terminal position. B) The same 7 GPCRs aligned structurally but instead coloured by the Eisenberg hydrophobic scale [144] at 50% transparency with red being hydrophobic and white being polar. C) A top-down (birds-eye) version of the alignment coloured similarly to A taken at a slice halfway through the TMHs. D) On the vertical axis is the TMSOC z-score of each of the helices and on the horizontal axis is the TMH number. The points are coloured by the corresponding structure. E) The axes are similar to D, however, the datasets are from non-redundant UniProt GPCR sequence datasets from 1016 GPCR records that contained the annotation for 7 TMHs. The data is represented by a violin plot, the thickness indicating the distribution of the data. The mean average is the dash in black, and the median is the dash in orange. F) As in E, however, the vertical axis is Kyte & Doolittle hydrophobicity [73].

information entropy and high hydrophobicity), the more likelihood of the TMH being solely a membrane anchor. When considering the functional/anchoring potential of these GPCR TMHs using TMSOC, we see trends among the structures with an average of 1.96 for TMH1, 2.30 for TMH2, 2.43 for TMH3, 2.34 for TMH4, 2.05 for TMH5,

2.24 for TMH 6 and 2.83 for TMH7 (Figure 4.4D). TMH3 and TMH7 are therefore the most likely to contain function beyond anchorage, whilst the low z-scores of TMH1 and TMH5 indicate they are more optimal anchors [227].

When we consider much larger sequence datasets containing 1016 TMHs at each TMH number from non-redundant GPCRs obtained from UniProt, the trend remains the same; that TMH3 (mean z-score of 2.52) and TMH7 (mean z-score of 2.55) have the highest z-score, whilst TMH1 (mean z-score of 2.09) and TMH5 (mean z-score of 2.20) have the lowest (Figure 4.4E). To investigate the statistical differences between the z-score of the TMHs, we applied the Kruskal Wallis and 2-sample Kolmogorov Smirnov tests from each TMH number to each other TMH number. TMH5 and TMH7 are statistically significantly distinct in terms of TMSOC z-score (Welch's t-test p-value = 1.57E-146, Kruskal Wallis p-value = 1.66E-132, Kolmogorov Smirnov p-value = 1.38E-105) as are TMH6 and TMH7 (p-value = 1.48E-51, Kruskal Wallis p-value = 4.96E-52, Kolmogorov Smirnov p-value = 1.74E-37). This is also mirrored in the relationship between the preceding TMHs of TMH3. TMH1 and TMH3 are distinct (Welch's t-test p-value = 3.12E-229, Kruskal Wallis p-value = 1.06E-192, Kolmogorov Smirnov p-value = 1.06E-174) and so are TMH2 and TMH3 (Welch's t-test p-value = 3.66E-39, Kruskal Wallis p-value = 2.70E-36, Kolmogorov Smirnov p-value = 1.06E-31). We also find it difficult to observe any significant differences between TMH2 and TMH6 (Welch's t-test p-value >0.99, Kruskal Wallis p-value = 0.99, Kolmogorov Smirnov p-value = 0.07).

As expected, these trends are mirrored in the Kyte & Doolittle [73] hydrophobicity plots. Where there is a high TMSOC z-score, there is a low hydrophobicity score. However, whereas TMH6 (mean hydrophobicity = 1.69) to TMH7 (mean hydrophobicity = 1.13) are very different (Welch's t-test p-value = 3.95E-163), the difference between TMH2 (mean hydrophobicity = 1.42) and TMH3 (mean hydrophobicity = 1.39) is less stark (Welch's t-test p-value = 0.12). Even though there is a discrepancy between the scales, the significant change in hydrophobicity between TMH6 and TMH7 can be seen consistently across the Eisenberg consensus scale [144] (Welch's t-test p-value = 5.61E-130), the White and Wimley biophysical scale [139] (Welch's t-test p-value = 5.21E-62), and the von Heijne/Hessa biological scale [116] (Welch's t-test p-value = 3.56E-210) emphasising the significance of this particular TMH pair

(Figure 4.5).

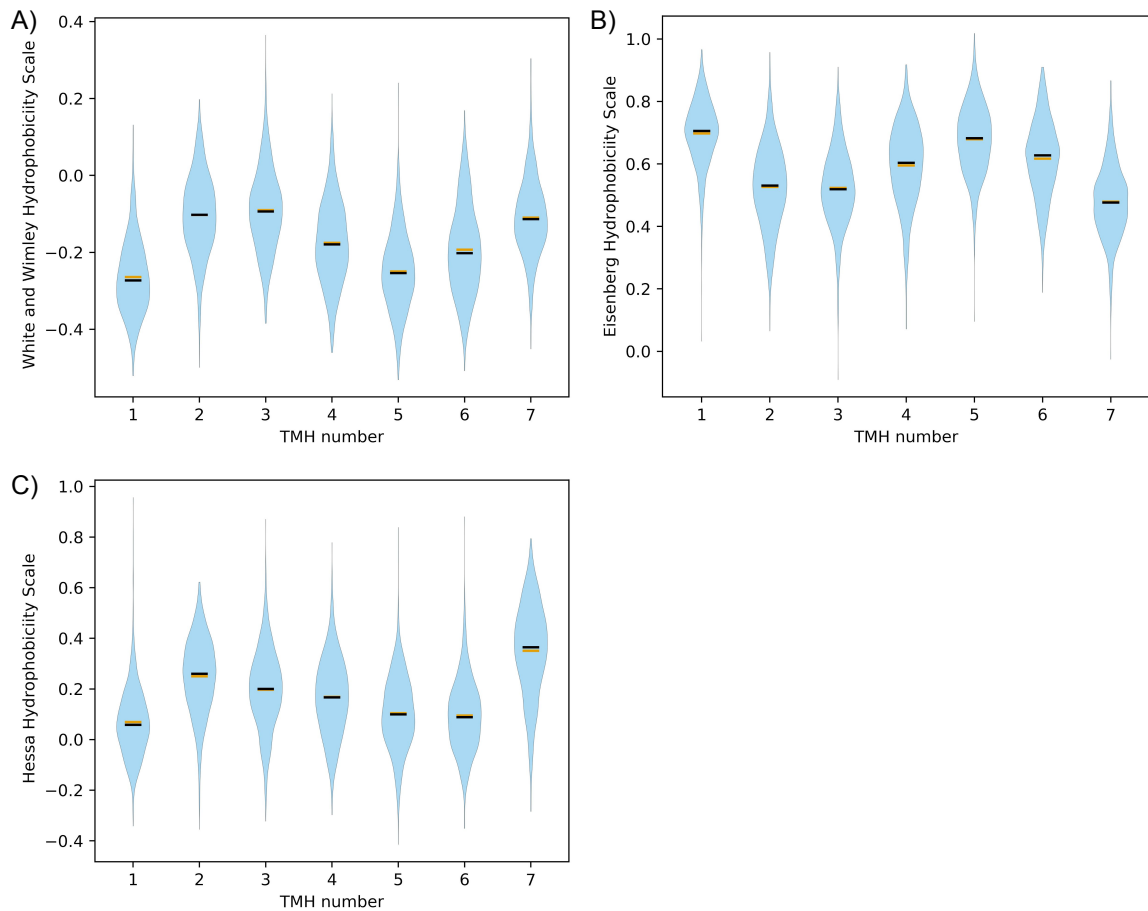


**Figure 4.5: The hydrophobic difference observed between TMH6 and TMH7 in GPCRs is not due to the choice of hydrophobic scale.** Three different scales were applied to the same dataset used in figure 4.4F to verify the observed differences were not caused by the choice of scale. A) The White and Wimley biophysical scale [139] B) The Eisenberg consensus scale [144]. C) The von Heijne/Hessa biological scale [116].

In order to determine if this is conserved through the GPCR subfamilies, a variety of GPCRs with different functions were examined in terms of Kyte & Doolittle hydrophobicity [73]. When considering different GPCR subfamilies, we see a consistent difference between the TMH hydrophobicities of TMH6 and TMH7 besides metabolic glutamate GPCRs (Welch's t-test p-value = 0.90) and Frizzled-smooth GPCRs (Welch's t-test p-value = 0.07) (Figure 4.6). For opsins, Welch's t-test p-value is 5.62E-15 between TMH6 and TMH7. After restricting the dataset to only those records with 7 TMHs, fungal mating GPCRs were reduced to a set of 9 proteins, however as a trend, they appear to be very typical GPCRs in terms of TMH hydrophobicity. They follow a very similar pattern to the much more popular olfactory GPCRs ( $N=263$ ) for which the TMH6 to TMH7 Welch's t-test p-value was 4.73E-35.

For taste receptors, there are much bigger step changes between sequentially adjacent TMHs than between TMH6 to TMH7. But there is still a real statistical difference between TMH6 and TMH7 (Welch's t-test p-value = 2.89E-12).

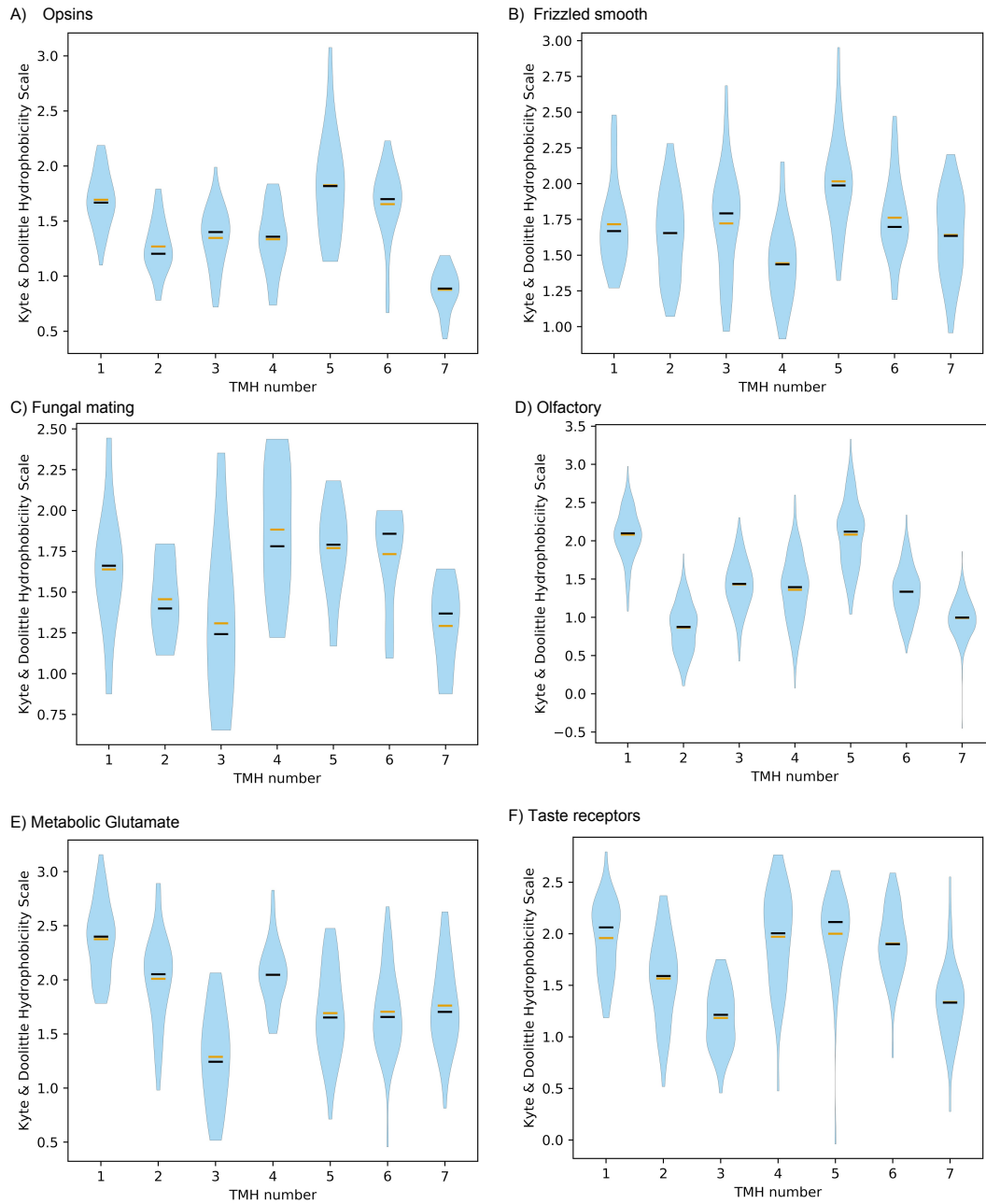


**Figure 4.6: The hydrophobicity of transmembrane helices in GPCR subfamilies.** Violin plots of the Kyte & Doolittle hydrophobicity [73] of TMHs of GPCRs after selecting a non-exhaustive sample of GPCR subfamilies with a wide variety of molecular functions. A) Opsins (N=39). B) Frizzled-smooth GPCRs (N=38). C) Fungal mating GPCR proteins (N=9). D) Olfactory receptor proteins (N=263). E) Metabolic glutamate receptor (N=41). F) T2R taste receptors (N=45)

Opsins are a group of light-sensitive GPCRs that exhibit the TMH6-TMH7 hydrophobic discrepancy (Figure 4.6A). It was shown by cross-linking studies that opsin

TMHs 5-7 are retained in the ER translocon and only partition into the membrane once biosynthesis is complete [363]. The timing of this partitioning is controlled by the hydrophobicity of the TMH, not protein length or the relative position of the TMH within the protein. Although artificially extending the C-terminal did not result in the release of the TMHs, by replacing native TMH7 with a more hydrophobic TMH, the speed of insertion was decreased. TMHs 1-4 are inserted independently, and the 5-7 TMHs partition into the membrane at the same time [363].

Lowering the difference in hydrophobicity between TMH6 and TMH7 impedes efficient insertion of the GPCR [363], however, one would expect the terminal TMH to be more hydrophobic rather than relatively polar [361]. This hydrophobic difference is highly conserved throughout GPCRs generally (Figure 4.4F), and especially in many of the subfamilies (Figure 4.6A, C, D, F). We believe that the hydrophobic difference of TMH6 and TMH7 is highly important to the biogenesis of GPCRs. This could be evidence for widespread biologically employed TMH cooperation during translocation. A typically hydrophobic TMH remains in association with the translocon until the relatively polar TMH is processed by the insertion machinery.

#### **4.4.3 6TMH ion channels contain polar-hydrophobic transmembrane helix pairs/groups indicative of conserved cooperative insertion**

Another group of proteins that featured heavily on the list of top TMH pairs with a high hydrophobic discrepancy were ion channels (Figure 4.3B). Ion channels are a much more structurally varied class of TMP than GPCRs, varying greatly in their number of TMHs, so a summary structural alignment equivalent to Figure 4.4A, B, and C was not possible.

Voltage-gated ion channels are another example of cooperative TMH insertion. The 3rd and 4th TMH of the potassium channel (shaker family) has been shown to insert either sequentially or cooperatively [40, 366]. This is especially notable in the case of KAT1, that is a plant  $K_v$  channel that is thought to mediate long-term potassium influx into guard cells causing the stomata to open. In the case of KAT1, N-glycosylation of various mutant fusion KAT1 constructs revealed that

there is no choice of sequential insertion since TMH3 and TMH4 have no insertion potential and no topogenic functions themselves [364, 365]. In TMH4 this is due to the charged residues making it relatively polar. However, previous experimentation in *Kv*1.3 had found that while TMH4 did not initiate insertion, it did have insertion potential and that when constructs contained multiple TMHs, membrane insertion efficiency increased [367]. Without the ability to stop the translation through the translocon and form a TMH, it was suggested that a different mechanism was needed than classic sequential insertion, and even that TMH3 and TMH4 are integrated by the translocon at the same time post-translationally, i.e the TMHs are folded prior to insertion [365]. They achieve this in part because the previous TMHs, TMH1 and TMH2, form a firm “base” within the membrane environment [365].

In the 6TMH class of ion channels, we observe a conserved difference in the relatively polar TMH4 known to carry charged residues (Figure 4.7A). When using the Kyte & Doolittle hydrophobic scale, the hydrophobic step change between TMH3 (mean hydrophobicity of 1.34) and TMH4 (mean hydrophobicity of 1.01) is statistically significantly different (Welch’s t-test p-value = 1.83E-8). This is the most significant step change besides TMH4 to TMH5 (mean hydrophobicity of 1.77, Welch’s t-test p-value = 1.88E-31). TMH5, the pore-forming region, and TMH6 can be integrated independently into the membrane, but TMH3 and TMH4, at least in the case of KAT1, cannot [364]. However, there is strong evidence that TMH3 and TMH4 cooperate with one another during membrane integration and are inserted at the same time [40, 364–366]. With this in mind, the hydrophobic gap here indicates a conserved cooperative role between TMH3 and TMH4 rather than TMH4 and TMH5.

This statistical difference between the hydrophobicity of TMH3 and TMH4 holds true for voltage-gated ion channels (Welch’s t-test p-value = 1.57E-17) (Figure 4.7C). However, the pattern is more obscure in ligand-gated ion channels (Welch’s t-test P-value = 5.32E-2). The difference does appear to match the general pattern, however, albeit as a trend, in the 33 records; there is a decrease in the mean hydrophobicity from 1.31 to 1.03 (Figure 4.7D).

The TMH3 TMH4 hydrophobic step also appears to be independent of the ion being transported. For calcium ion channels the drop from TMH3 (mean hydrophobicity 1.52) to TMH4 (mean hydrophobicity 1.21) is significant (Welch’s t-test p-value

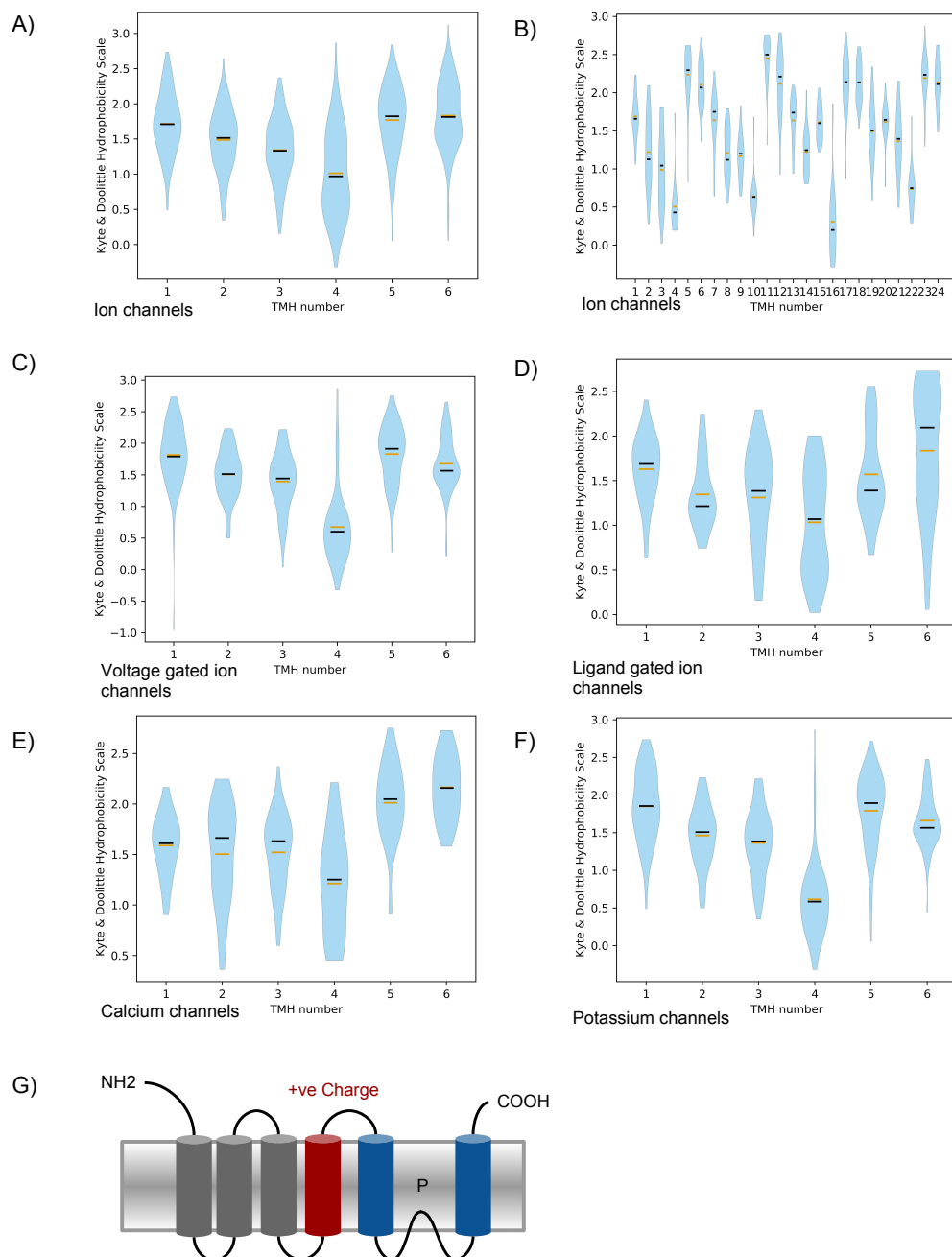


**Figure 4.7: The hydrophobicity of transmembrane helices in ion channels.** A) The Kyte & Doolittle TMH hydrophobicity of TMHs according to their TMH number of the 6TMH class of ion channels. N=188 (The total number of TMHs analysed is 1128). The data is presented as a violin plot. The thickness of the bar indicates a higher density of points at that hydrophobic value. B) A similar violin plot as in (A), however with the 24 TMH class of ion channel. N=35 (A total of 840 TMHs analysed). C) A subset of (A) with the keyword of ion channels restricted to voltage-gated ion channels. N=97. D) A subset of (A) with the keyword of ion channels restricted to ligand-gated channels. N=33. E) A subset of (A) with the keyword of ion channels restricted to calcium channels. N=38. F) A subset of (A) with the keyword of ion channels restricted to potassium channels. N=88. G) The general schematic of an ion channel. P indicates the pore-forming area of the protein, which is integrated into the membrane but is not a membrane-spanning unit. In the case of the 24 class, this pattern is repeated 4 times.

= 3.57E-3) given the relatively low sample size (38 protein records) (Figure 4.7E). In potassium channels, the difference is even greater between TMH3 (mean hydrophobicity of 1.37) and TMH4 (mean hydrophobicity of 0.61) (Welch's t-test p-value = 2.52E-19) in potassium ion channels (Figure 4.7F).

The observed difference between TMH3 and TMH4 is somewhat independent of the scale chosen (Figure 4.8), however, the Kyte & Doolittle scale is the most sensitive to the hydrophobic differences between TMH3 and TMH4. Statistical significance was found in the difference between TMH3 and TMH4 in the Eisenberg scale (Welch's t-test p-value = 4.74E-23) and the White and Wimley scale (Welch's t-test p-value = 1.26E-3). The Hessa/von Heijne biological scale was particularly insensitive to the mean difference (Welch's t-test p-value = 7.56E-2), but can scrutinise some difference in the skews of the data (Kolmogorov Smirnov test p-value = 1.56E-4, Kruskal Wallis p-value = 4.00E-2) indicating that whilst biophysically the TMHs are distinct, the translocon may not readily scrutinise the hydrophobicity between the two. All the scales however corroborate the large hydrophobic difference between TMH4 and TMH5 (Welch's t-test p-values for Hessa = 1.23E-35, White and Wimley = 4.82E-23, Eisenberg = 5.72E-41)

The 24TMH class is essentially a modular variant of the 6TMH class and has even more extreme discrepancies between the equivalent 4 TMHs (Figure 4.7B). In the first cluster, TMH3 (mean Kyte & Doolittle hydrophobicity = 0.96) to TMH4 (mean hydrophobicity = 0.47) is different (Welch's t-test p-value = 5.16E-6), but even more so is the step up from TMH4 to TMH5 (hydrophobicity = 2.26, Welch's t-test p-value = 5.16E-32). The preceding step is weaker, and the proceeding step is greater throughout the 6TMH “modules”. A similar step change is found between TMH9 and TMH10 (p-value = 3.02E-13) and TMH10 to TMH11 (p-value = 5.51E-44), TMH15 to TMH16 (p-value = 1.79E-23), TMH16 to TMH17 (p-value = 1.67E-27), TMH21 to TMH22 (p-value = 1.64E-9), and TMH22 to TMH23 (p-value = 3.42E-31).

As a trend, the TMSOC z-score was not sensitive to detecting function in the extremely hydrophobic TMH4 (Figure 4.9). This is due to the other component of the z-score, the sequence information entropy from SEG [44, 45, 146, 150]. The relative probability of a polar/charged residue is so high in TMH4 that it apparently has the same expectancy as the hydrophobic residues, and the “simple” entropy mutes

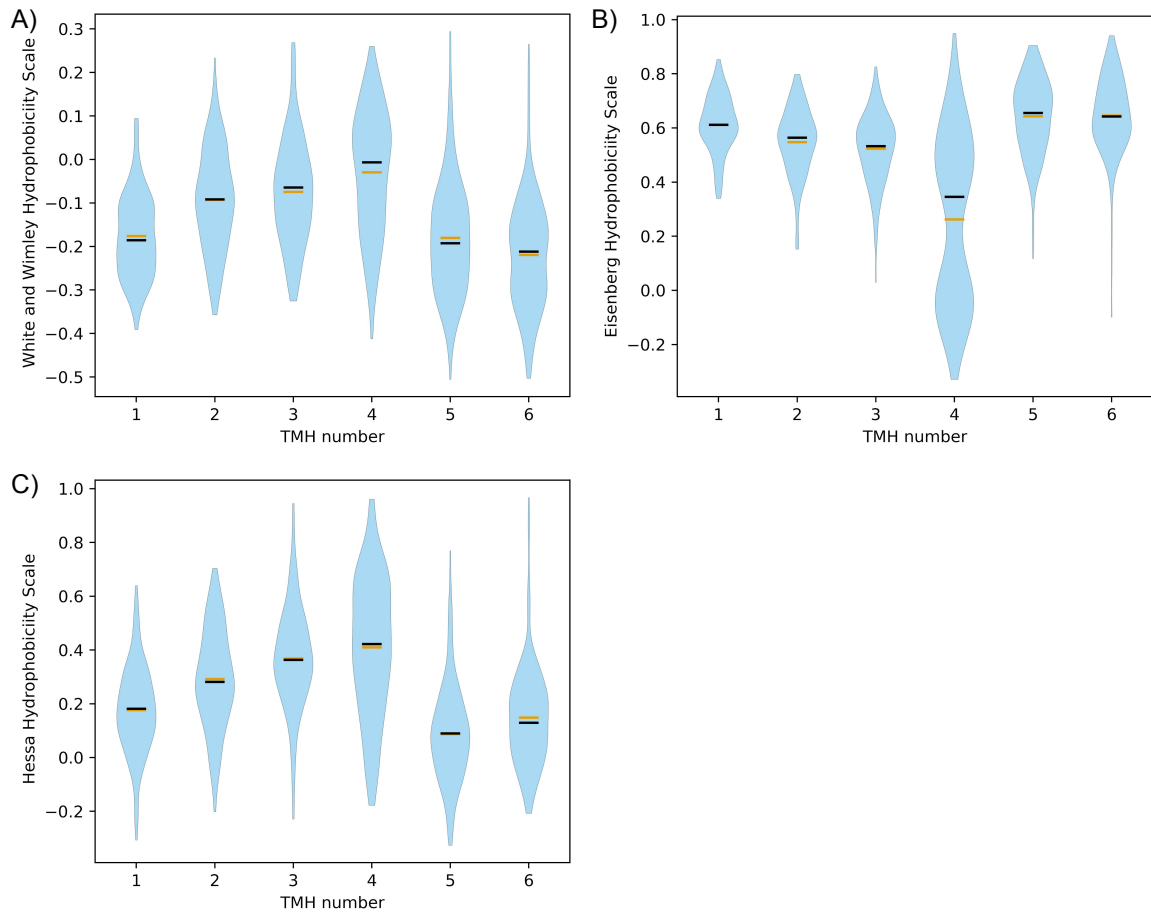


**Figure 4.8:** The hydrophobic difference observed between TMH4 and the neighbouring transmembrane helices in 6TMH ion channels is not due to the choice of hydrophobic scale. Three different scales were applied to the same dataset used in figure 4.7A to verify the observed differences were not caused by the choice of scale. A) The White and Wimley biophysical scale [139] B) The Eisenberg consensus scale [144]. C) The von Heijne/Hessa biological scale [116].

somewhat the effect of the extreme hydrophobicity. This is compounded by the fact that the White and Wimley scale (used to generate the z-score) is already less sensitive to the relative polarity difference between TMH3 and TMH4 than the Kyte & Doolittle scale (Figure 4.7A, Figure 4.8A).

#### 4.4.4 The prevalence of the high hydrophobic discrepancy of transmembrane helices amongst other common ‘transporter’ transmembrane protein classes

Whilst the gene ontology recognises “transporters” as having disproportionately more highly different hydrophobic sequential pairs, the list is predominantly ion channels, which are molecularly and functionally different from ion transporters. It also appears

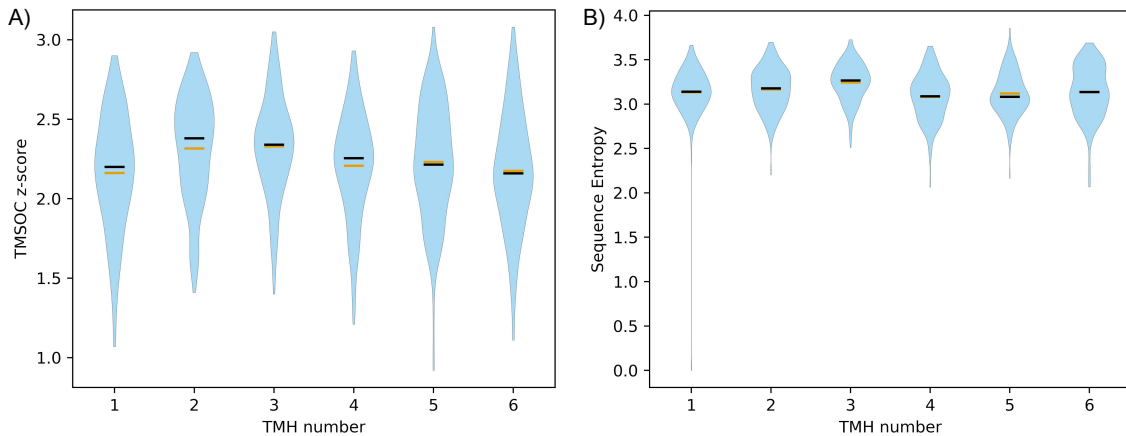


**Figure 4.9: Sequence entropy is unsuitable for assessing function in TMH4 of ion channels.** A) The TMSOC z-score [44, 45] of TMHs from the ion channel dataset used in Figure 4.7A. B) The sequence information entropy of those same TMHs.

that ion transporters have no conserved hydrophobicity discrepancy between any of their TMHs for the 4TMH, 6TMH, 8TMH, or 10TMH classes (Figure 4.10 C, D, E, F, G).

Another large family of transporters are the sugar transporters. In terms of the hydrophobic discrepancy between sequentially adjacent TMH pairs, sugar transporters also have a few peaks and dips at TMH6 and TMH11 (Figure 4.10A). TMH5 (mean hydrophobicity = 1.32) to TMH6 (mean hydrophobicity = 1.81) (Welch's t-test P-value = 3.09E-19) was less significant than TMH6 to TMH7 (mean hydrophobicity = 1.23) (Welch's t-test p-value = 8.75E-29). TMH10 (mean hydrophobicity = 1.66) to TMH11 (mean hydrophobicity = 1.23) (Welch's t-test p-value = 1.03E-14) was also less significant than TMH11 to TMH12 (mean hydrophobicity = 1.84) (Welch's t-test p-value = 3.22E-22).

The ion channel 4TMH class also has a discrepancy between TMH2 (Kyte & Doolittle hydrophobicity = 1.49) and TMH3 (hydrophobicity = 1.81) (Welch's t-test P-value = 4.42E-10, from 234 records) (Figure 4.10C). The largest family within the 4TMH class is the chloride channel 4TMH family. A jump of hydrophobicity is observed in TMH2 (hydrophobicity = 1.05) to TMH3 (hydrophobicity = 1.50) (Welch's t-test P-value = 5.34E-5, from 50 records) (Figure 4.10B).

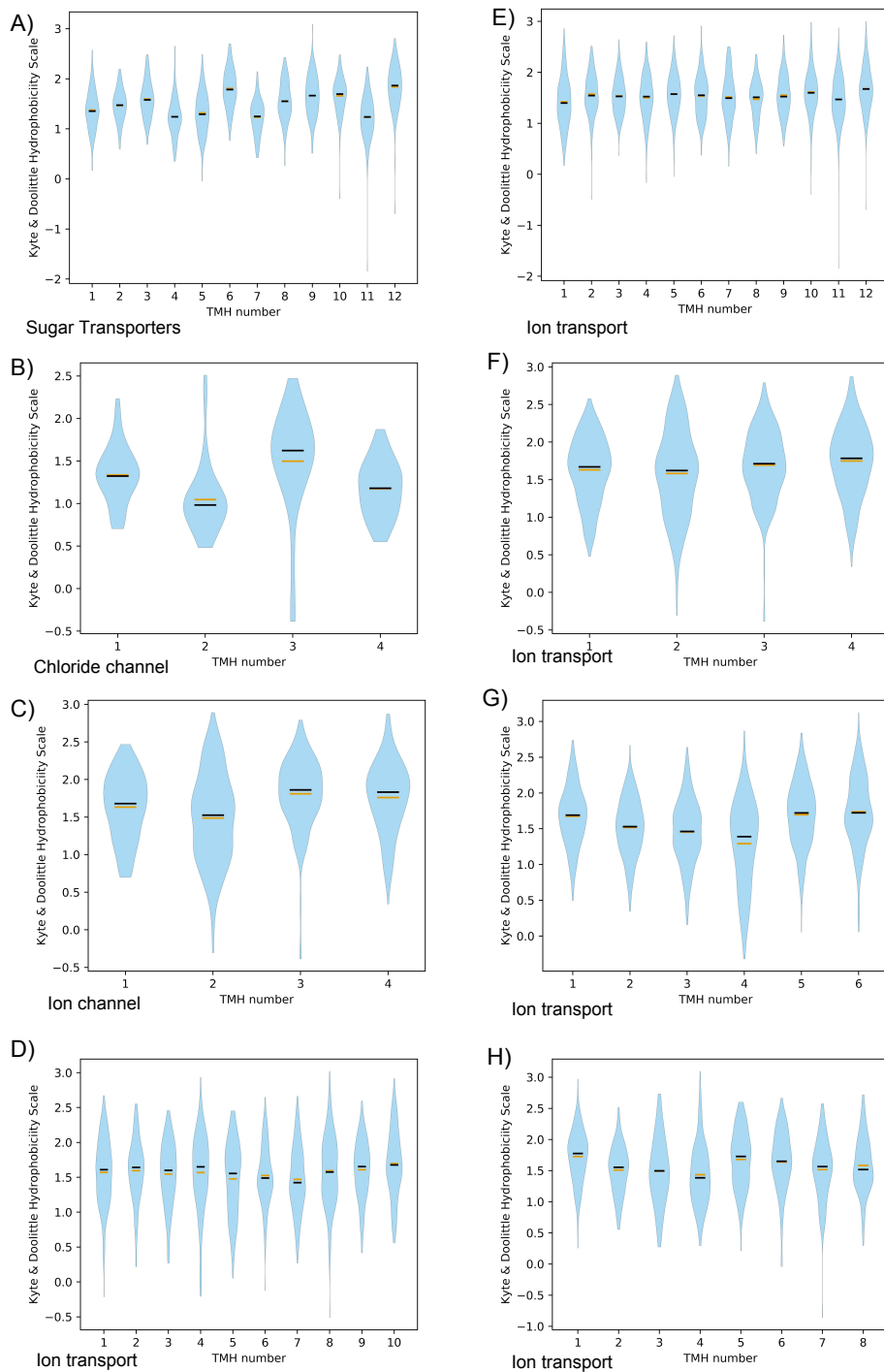


**Figure 4.10: High polarity discrepancy between sequentially adjacent transmembrane helices is not present in all transmembrane protein transporter families.** The mean average Kyte & Doolittle hydrophobic scores of a TMHs from various families and classes of membrane transporter proteins. Datasets are represented as a violin plot where thickness denotes the relative density of the population distribution. A) A dataset of 134 sugar transporters containing 12 TMHs. B) A dataset of 50 chloride channels containing 4 TMHs. C) 234 ion channels with 4 TMHs. D-H) Ion transporters restricted to the number of TMHs on the horizontal axis. Sample sizes can be found in table 4.1

## 4.5 Summary

M marginally hydrophobic TMHs are often essential physiological components for carrying out complex intra-membrane tasks beyond membrane anchorage, and widely

prevalent among TMPs [74]. However, this presents a significant biophysical and biological challenge; how to incorporate and maintain such necessarily relatively polar TMHs into the membrane. We show that among certain classes of TMPs that this is a conserved issue. It was recently discovered that the EMC protein assists the translocon with the marginally hydrophobic TMHs, particularly those containing charged residues [24]. There is also evidence to suggest that multipass TMH arrangements work cooperatively during translocation and insertion to achieve correct folding of marginally hydrophobic TMHs [40, 268, 350, 358–361, 363–367] (Figure 4.11).

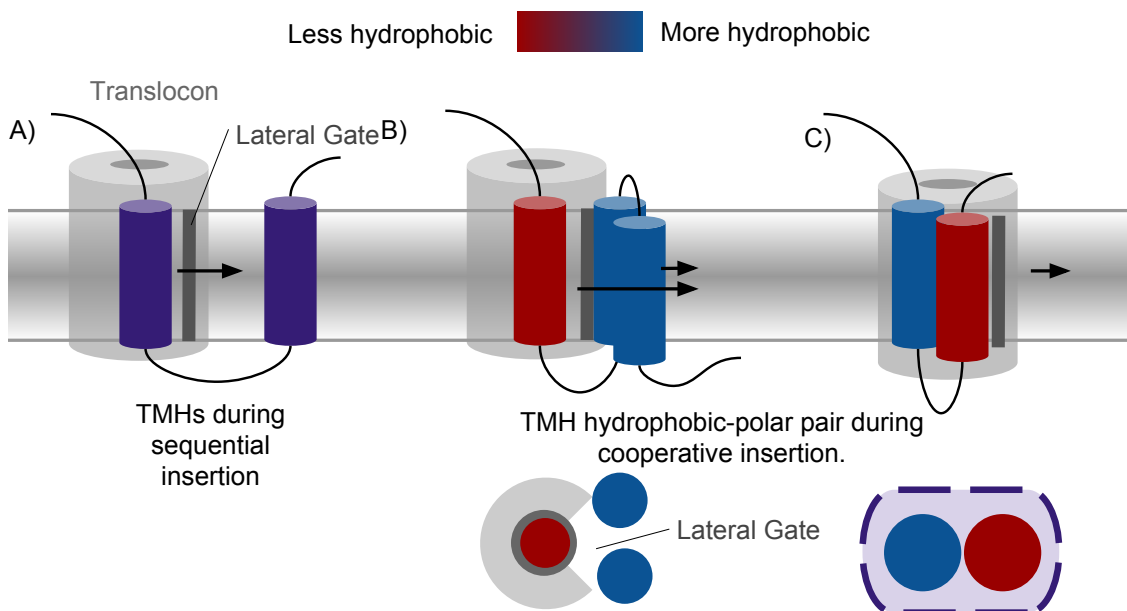


**Figure 4.11: A cartoon of potential cooperative transmembrane helix insertion methods.** A) Typically hydrophobic TMHs remain in association with the translocon machinery until the marginally hydrophobic TMH is released into the membrane. This was observed in an opsin protein [363]. B) TMH-TMH interactions allow the marginally hydrophobic TMH to shield the polar residues. The marginally hydrophobic TMH can associate with the typical hydrophobic TMH in the ribosomal exit tunnel [350] or in the translocon tunnel [366]. This was observed in a potassium ion channel [40, 350, 366].

Here, we have shown that high discrepancy of TMSOC z-score (simple-complex score) [44, 45], and several hydrophobicity scales [73, 116, 139, 144], between sequentially adjacent TMHs corroborates TMH groups known to insert cooperatively [40, 363, 365, 366]. The hydrophobic relationships between these cooperatively inserted TMHs may be conserved throughout their larger families indicating that cooperative insertion may be a routine mechanism for the insertion of some families of TMPs. So far, this method has shown that the TMH7 of GPCRs is a conserved marginally hydrophobic TMH with the typically hydrophobic TMH6 preceding it. In opsins,

TMH5-TMH7 are incorporated into the membrane together simultaneously by staying in association with the translocon until TMH7 emerges [363]. We see this pattern across several GPCR sub-families and the GPCR family as a whole.

Furthermore, we found that the charged TMH4 of 6TMH ion channels has a typically hydrophobic TMH3 preceding it and a more hydrophobic TMH5 following it. Indeed there is evidence that TMH3 and TMH4 cannot incorporate alone [365], that TMH3 and TMH4 can insert as a pair from the translocon simultaneously [40, 366].

Advanced cross-linking experiments, single molecule cryoEM, and APs can probe energetics and TMH-TMH interactions and associations dynamically during ribosomal translation and membrane insertion. These methods could explore the TMH-TMH relationships such as cooperation during insertion in more detail with temporal contextualisation. Understanding the biogenesis of TMPs is essential to solving misfolding in disease phenotypes, and for developing viable TMP chassis in synthetic biology [382].

# Chapter 5

## Conclusions and outlook

As the evidence of positive residues preferentially localising to the inside the cytoplasm emerged during the late 1980s [113], so did the idea of negative residues working in concert with the positive residues for TMH orientation. It was shown that removing a single lysine residue reversed the topology of a model *E. coli* protein, whereas much higher numbers of negatively charged residues are needed to reverse topology [248]. However, there was no conclusive evidence in the literature for an opposing negatively charged skew [86, 109, 110, 117, 118]. Yet these previous studies in various ways did not account for the rarity of the negatively charged residues relative to the more abundant residues. In *E. coli* negative residues do experience electrical pulling forces when travelling through the SecYEG translocon indicating that negative charges are biologically relevant [42], and as mentioned, they did to an extent have the ability to reverse topology [248]. In this thesis, we have demonstrated that the “negative-outside” skew exists in anchoring TMHs. Additionally, we have made observations regarding how anchoring TMHs are optimised to their membranes. This new insight into the behaviour of TMHs will not only help us understand specific cases in biology, but can also inform synthetic biology regarding TMPs [382–384].

Post-translationally inserted TA proteins integrate into the membrane independently of the co-translational ribosome-translocon complex insertion machinery. They are also of interest as a liposome drug delivery system due to the role of TA SNARE proteins in membrane fusion [283, 285, 286]. We found compositional differences between the mitochondrial and secretory localised TMHs of TA proteins. Alanine is used more commonly in the mitochondrial TMHs, perhaps even more so than isoleucine and

leucine. We also observed a reversal of the positive-inside and negative-outside distributions of charged TMH flanking residues in mitochondrially localised TA proteins. This re-emphasises the notion that there is more to TA protein trafficking than the hydrophobicity of the TMH alone [78], and could inform more specific studies of individual proteins. Still, several important questions remain unanswered that limit our understanding of TA protein biosynthesis. How truly redundant are the different pathways? What are the precise biophysical and biological signatures of TA proteins that determine their path? Why do some post-translationally inserted TA proteins have C-terminal tail lengths exceeding the traditional 25 residue length, whereas other proteins with far shorter tails than this cut-off are co-translationally inserted? Ultimately, as we have demonstrated, annotation of the protein databases must be completed for these questions to be more thoroughly answered.

We have identified amphipathic TMHs that may contribute to the spontaneous insertion of some TA proteins. However, MD simulations of the interactions between the membrane and the anchoring TMH of spontaneously inserting TA proteins would be needed to reveal the molecular energetic contributions involved in the spontaneous insertion.

The biological scale of hydrophobicity revealed that many TMHs do not make the energetic requirements of insertion by the translocon [74]. It is now understood that these so-called marginally hydrophobic TMHs rely on sequence context for correct topology [268] and efficient insertion [267, 361, 362]. Here we show that marginally hydrophobic TMHs located sequentially adjacent to typically hydrophobic TMHs is a conserved feature throughout some families of TMP such as ion channels and GPCRs. In these two cases, there is evidence demonstrating that these hydrophobic discrepancy pairs are capable of inserting cooperatively [40, 363–366]. It remains unclear as to what extent the newly discovered role of the EMC integration of marginally hydrophobic TMHs [24] works in respect to cooperatively inserted TMHs.

Understanding cooperative TMH insertion and the integration of marginally hydrophobic TMHs will require a much more thorough understanding of the temporal and energetic aspects of the process. It appears that the relatively new technologies of single molecule EM and APs may be able to grant insight into the energetics and dynamics of the structures throughout the process of TMP integration. Understanding

the relationship TMHs have with one another, particularly the temporal and spacial contextualisation, is critical for developing complex synthetic TMPs.

More generally, there are several challenges still facing our understanding of TMPs. The description of a TMH remains incomplete. Therefore, it remains difficult to interpret the role of a TMH in the membrane beyond anchoring. Furthermore, the prediction of TMP topology is often erroneous and requires experimental validation. Despite a wealth of structures the general model of helix-helix and helix-lipid interactions remains speculative and requires intensive analysis to generate a working model of a particular TMP. Nevertheless, progress is being made in our general understanding of TMPs.

# Bibliography

1. Ladokhin, A. S. Membrane Protein Folding & Lipid Interactions: Theory & Experiment. *Journal of Membrane Biology* **248**, 369–370 (2015).
2. Koshland Jr., D. E. Special essay: The seven pillars of life. en. *Science* **295**, 2215–2216 (2002).
3. Donaldson, I. Robert Hooke's Micrographia of 1665 and 1667. *The Journal of the Royal College of Physicians of Edinburgh* **40**, 374–376 (2010).
4. Hooke, R. *Micrographia: Or Some Physiological Descriptions of Minute Bodies Made by Magnifying Glasses. With Observations and Inquiries Thereupon. By R. Hooke, Fellow of the Royal Society* (Jo. Martyn, and Ja. Allestry, printers to the Royal Society, 1961).
5. Henderson, R. & Unwin, P. N. Three-dimensional model of purple membrane obtained by electron microscopy. *Nature* **257**, 28–32 (1975).
6. Deisenhofer, J., Epp, O., Miki, K., Huber, R. & Michel, H. X-ray structure analysis of a membrane protein complex: Electron density map at 3 Å resolution and a model of the chromophores of the photosynthetic reaction center from Rhodopseudomonas viridis. *Journal of Molecular Biology* **180**, 385–398 (1984).
7. Singer, S. J. & Nicolson, G. L. The fluid mosaic model of the structure of cell membranes. *Science (New York, N.Y.)* **175**, 720–31 (1972).
8. Gorter, E & Grendel, F. On bimolecular layers of lipoids on the chromocytes of the blood. *The Journal of experimental medicine* **41**, 439–443 (1925).
9. Danielli, J. F. & Davson, H. A contribution to the theory of permeability of thin films. *Journal of Cellular and Comparative Physiology* **5**, 495–508 (1935).
10. Lonsdale, K. The structure of the benzene ring. *Nature* **122**, 810 (1928).

11. Dickinson, R. G. & Raymond, A. L. The crystal structure of hexamethylene-tetramine. *Journal of the American Chemical Society* **45**, 22–29 (1923).
12. Carlisle, C. H. & Crowfoot, D. The crystal structure of cholesteryl iodide. *Proceedings of the Royal Society A: Mathematical, Physical and Engineering Sciences* **184**, 64–83 (1945).
13. Hodgekin, D. C. The X-ray analysis of the structure of penicillin. *Advancement of science* **6**, 85–9 (1949).
14. Hodgkin, D. G., Pickworth, J., Robertson, J. H., Trueblood, K. N., Prosen, R. J. & White, J. G. The crystal structure of the hexacarboxylic acid derived from B12 and the molecular structure of the vitamin. *Nature* **176**, 325–328 (1955).
15. Nobel Media. *Dorothy Crowfoot Hodgkin - Nobel Lecture: The X-ray Analysis of Complicated Molecules* 2018.
16. Bernstein, F. C., Koetzle, T. F., Williams, G. J., Meyer, E. F., Brice, M. D., Rodgers, J. R., Kennard, O., Shimanouchi, T. & Tasumi, M. The protein data bank: A computer-based archival file for macromolecular structures. *Archives of Biochemistry and Biophysics* **185**, 584–591 (1978).
17. Nobel Media. *Hartmut Michel - Biographical* 2018.
18. Carpenter, E. P., Beis, K., Cameron, A. D. & Iwata, S. Overcoming the challenges of membrane protein crystallography. *Current Opinion in Structural Biology* **18**, 581–586 (2008).
19. Hopkins, A. L. & Groom, C. R. The druggable genome. *Nature Reviews Drug Discovery* **1**, 727–730 (2002).
20. Almén, M. S., Nordström, K. J., Fredriksson, R. & Schiöth, H. B. Mapping the human membrane proteome: A majority of the human membrane proteins can be classified according to function and evolutionary origin. *BMC Biology* **7**, 50 (2009).
21. Wang, X., Wang, R., Zhang, Y. & Zhang, H. Evolutionary survey of druggable protein targets with respect to their subcellular localizations. *Genome Biology and Evolution* **5**, 1291–1297 (2013).

22. Overington, J. P., Al-Lazikani, B. & Hopkins, A. L. How many drug targets are there? *Nature Reviews Drug Discovery* **5**, 993–996 (2006).
23. Ruggiano, A., Foresti, O. & Carvalho, P. Quality control: ER-associated degradation: protein quality control and beyond. *The Journal of cell biology* **204**, 869–79 (2014).
24. Shurtleff, M. J., Itzhak, D. N., Hussmann, J. A., Schirle Oakdale, N. T., Costa, E. A., Jonikas, M., Weibe Zahnh, J., Popova, K. D., Jan, C. H., Sinitcyn, P., Vembar, S. S., Hernandez, H., Cox, J., Burlingame, A. L., Brodsky, J. L., Frost, A., Borner, G. H. & Weissman, J. S. The ER membrane protein complex interacts cotranslationally to enable biogenesis of multipass membrane proteins. *eLife* **7** (2018).
25. Guna, A., Volkmar, N., Christianson, J. C. & Hegde, R. S. The ER membrane protein complex is a transmembrane domain insertase. *Science* **359**, 470–473 (2018).
26. Sanders, C. R. & Myers, J. K. Disease-related misassembly of membrane proteins. *Annual Review of Biophysics and Biomolecular Structure* **33**, 25–51 (2004).
27. Partridge, A. W., Therien, A. G. & Deber, C. M. Polar mutations in membrane proteins as a biophysical basis for disease. *Biopolymers* **66**, 350–358 (2002).
28. Riordan, J. R., Rommens, J. M., Kerem, B, Alon, N, Rozmahel, R, Grzelczak, Z, Zielenski, J, Lok, S, Plavsic, N, Chou, J. L. & et Al. Identification of the cystic fibrosis gene: cloning and characterization of complementary DNA. *Science (New York, N.Y.)* **245**, 1066–73 (1989).
29. Roa, B. B., Garcia, C. A., Suter, U., Kulpa, D. A., Wise, C. A., Mueller, J., Welcher, A. A., Snipes, G. J., Shooter, E. M., Patel, P. I. & Lupski, J. R. Charcot-Marie-Tooth disease type 1A – Association with a spontaneous point mutation in the PMP22 gene. *New England Journal of Medicine* **329**, 96–101 (1993).

30. Fairweather, N., Bell, C., Cochrane, S., Chelly, J., Wang, S., L.Mostacciulo, M., P.Monaco, A. & E.Haites, N. Mutations in the connexin 32 gene in X-linked dominant Charcot- Marie - Tooth disease (CMTX1). *Human Molecular Genetics* **3**, 29–34 (1994).
31. Van Lieburg, A. F., Verdijk, M. A., Knoers, V. V., van Essen, A. J., Proesmans, W, Mallmann, R, Monnens, L. A., van Oost, B. A., van Os, C. H. & Deen, P. M. Patients with autosomal nephrogenic diabetes insipidus homozygous for mutations in the aquaporin 2 water-channel gene. *American journal of human genetics* **55**, 648–52 (1994).
32. Dryja, T. P., McGee, T. L., Reichel, E., Hahn, L. B., Cowley, G. S., Yandell, D. W., Sandberg, M. A. & Berson, E. L. A point mutation of the rhodopsin gene in one form of retinitis pigmentosa. *Nature* **343**, 364–366 (1990).
33. Gelsthorpe, M. E., Baumann, N., Millard, E., Gale, S. E., Langmade, S. J., Schaffer, J. E. & Ory, D. S. Niemann-Pick type C1 I1061T mutant encodes a functional protein that is selected for endoplasmic reticulum-associated degradation due to protein misfolding. *The Journal of biological chemistry* **283**, 8229–36 (2008).
34. Park, W. D., O'Brien, J. F., Lundquist, P. A., Kraft, D. L., Vockley, C. W., Karnes, P. S., Patterson, M. C. & Snow, K. Identification of 58 novel mutations in Niemann-Pick disease type C: Correlation with biochemical phenotype and importance of PTC1-like domains in NPC1. *Human Mutation* **22**, 313–325 (2003).
35. Scott, C. & Ioannou, Y. The NPC1 protein: structure implies function. *Biochimica et Biophysica Acta (BBA) - Molecular and Cell Biology of Lipids* **1685**, 8–13 (2004).
36. Fernandez-Valero, E., Ballart, A, Iturriaga, C, Lluch, M, Macias, J, Vanier, M., Pineda, M & Coll, M. Identification of 25 new mutations in 40 unrelated Spanish Niemann-Pick type C patients: genotype-phenotype correlations. *Clinical Genetics* **68**, 245–254 (2005).

37. Seddon, A. M., Curnow, P. & Booth, P. J. Membrane proteins, lipids and detergents: not just a soap opera. *Biochimica et Biophysica Acta (BBA) - Biomembranes* **1666**, 105–117 (2004).
38. Von Heijne, G. Membrane-protein topology. *Nature Reviews Molecular Cell Biology* **7**, 909–918 (2006).
39. Elofsson, A. & von Heijne, G. Membrane protein structure: Prediction versus reality. *Annual Review of Biochemistry* **76**, 125–140 (2007).
40. Cymer, F., von Heijne, G. & White, S. H. Mechanisms of integral membrane protein insertion and folding. *Journal of Molecular Biology* **427**, 999–1022 (2015).
41. Merklinger, E., Gofman, Y., Kedrov, A., Driessens, A., Ben-Tal, N., Shai, Y. & Rapaport, D. Membrane integration of a mitochondrial signal-anchored protein does not require additional proteinaceous factors. *Biochemical Journal* **442**, 381–389 (2012).
42. Ismail, N., Hedman, R., Lindén, M. & von Heijne, G. Charge-driven dynamics of nascent-chain movement through the SecYEG translocon. *Nature Structural and Molecular Biology* **22**, 145–149 (2015).
43. Hessa, T., Sharma, A., Mariappan, M., Eshleman, H. D., Gutierrez, E. & Hegde, R. S. Protein targeting and degradation are coupled for elimination of mislocalized proteins. *Nature* **475**, 394–399 (2011).
44. Wong, W. C., Maurer-Stroh, S. & Eisenhaber, F. Not all transmembrane helices are born equal: Towards the extension of the sequence homology concept to membrane proteins. *Biology Direct* **6**, 57 (2011).
45. Wong, W.-C., Maurer-Stroh, S., Schneider, G. & Eisenhaber, F. Transmembrane helix: simple or complex. *Nucleic Acids Research* **40**, W370–W375 (2012).
46. Wong, W. C., Maurer-Stroh, S. & Eisenhaber, F. More than 1,001 problems with protein domain databases: Transmembrane regions, signal peptides and the issue of sequence homology. *PLoS Computational Biology* **6** (ed Bourne, P. E.) 6 (2010).

47. Finn, R. D., Coggill, P., Eberhardt, R. Y., Eddy, S. R., Mistry, J., Mitchell, A. L., Potter, S. C., Punta, M., Qureshi, M., Sangrador-Vegas, A., Salazar, G. A., Tate, J. & Bateman, A. The Pfam protein families database: towards a more sustainable future. *Nucleic Acids Research* **44**, D279–D285 (2016).
48. Letunic, I., Doerks, T. & Bork, P. SMART 7: recent updates to the protein domain annotation resource. *Nucleic Acids Research* **40**, D302–D305 (2012).
49. Drew, D., Slotboom, D.-J., Friso, G., Reda, T., Genevaux, P., Rapp, M., Meindl-Beinker, N. M., Lambert, W., Lerch, M., Daley, D. O., Van Wijk, K.-J., Hirst, J., Kunji, E. & De Gier, J.-W. A scalable, GFP-based pipeline for membrane protein overexpression screening and purification. *Protein Science* **14**, 2011–2017 (2005).
50. Kawate, T. & Gouaux, E. Fluorescence-detection size-exclusion chromatography for precrystallization screening of integral membrane proteins. *Structure* **14**, 673–681 (2006).
51. Eshaghi, S., Hedrén, M., Nasser, M. I. A., Hammarberg, T., Thornell, A. & Nordlund, P. An efficient strategy for high-throughput expression screening of recombinant integral membrane proteins. *Protein Science* **14**, 676–683 (2005).
52. Cornvik, T., Dahlroth, S.-L., Magnusdottir, A., Herman, M. D., Knaust, R., Ekberg, M. & Nordlund, P. Colony filtration blot: a new screening method for soluble protein expression in *Escherichia coli*. *Nature Methods* **2**, 507–509 (2005).
53. Frauenfeld, J., Gumbart, J., van der Sluis, E. O., Funes, S., Gartmann, M., Beatrix, B., Mielke, T., Berninghausen, O., Becker, T., Schulten, K. & Beckmann, R. Cryo-EM structure of the ribosome–SecYE complex in the membrane environment. *Nature Structural & Molecular Biology* **18**, 614–621 (2011).
54. Rosenbusch, J., Lustig, A., Grabo, M., Zulauf, M. & Regenass, M. Approaches to determining membrane protein structures to high resolution: do selections of subpopulations occur? *Micron* **32**, 75–90 (2001).
55. Bayburt, T. H., Grinkova, Y. V. & Sligar, S. G. Self-assembly of discoidal phospholipid bilayer nanoparticles with membrane scaffold proteins. *Nano Letters* **2**, 853–856 (2002).

56. Duan, H., Civjan, N. R., Sligar, S. G. & Schuler, M. A. Co-incorporation of heterologously expressed Arabidopsis cytochrome P450 and P450 reductase into soluble nanoscale lipid bilayers. *Archives of Biochemistry and Biophysics* **424**, 141–153 (2004).
57. Schuler, M. A., Denisov, I. G. & Sligar, S. G. in *Methods in molecular biology* (Clifton, N.J.) 415–433 (2013).
58. Borch, J. & Hamann, T. The nanodisc: A novel tool for membrane protein studies. *Biological Chemistry* **390**, 805–814 (2009).
59. Vinothkumar, K. R. Membrane protein structures without crystals, by single particle electron cryomicroscopy. *Current Opinion in Structural Biology* **33**, 103–114 (2015).
60. Raunser, S. & Walz, T. Electron crystallography as a technique to study the structure on membrane proteins in a lipidic environment. *Annual Review of Biophysics* **38**, 89–105 (2009).
61. Vinothkumar, K. R. & Henderson, R. Structures of membrane proteins. *Quarterly Reviews of Biophysics* **43**, 65–158 (2010).
62. Murata, K. & Wolf, M. Cryo-electron microscopy for structural analysis of dynamic biological macromolecules. *Biochimica et Biophysica Acta (BBA) - General Subjects* **1862**, 324–334 (2018).
63. Grant, T. & Grigorieff, N. Measuring the optimal exposure for single particle cryo-EM using a 2.6 Å reconstruction of rotavirus VP6. *eLife* **4** (2015).
64. Bartesaghi, A., Merk, A., Banerjee, S., Matthies, D., Wu, X., Milne, J. L. S. & Subramaniam, S. 2.2 Å resolution cryo-EM structure of  $\beta$ -galactosidase in complex with a cell-permeant inhibitor. *Science (New York, N.Y.)* **348**, 1147–51 (2015).
65. Kühlbrandt, W. The resolution revolution. *Science* **343**, 1443 LP –1444 (2014).
66. Jones, D. T. Improving the accuracy of transmembrane protein topology prediction using evolutionary information. *Bioinformatics* **23**, 538–544 (2007).

67. Krogh, A., Larsson, B., von Heijne, G. & Sonnhammer, E. L. Predicting transmembrane protein topology with a hidden Markov model: Application to complete genomes. *Journal of Molecular Biology* **305**, 567–580 (2001).
68. Tusnády, G. E. & Simon, I. The HMMTOP transmembrane topology prediction server. *Bioinformatics* **17**, 849–850 (2001).
69. Viklund, H. & Elofsson, A. Best  $\alpha$ -helical transmembrane protein topology predictions are achieved using hidden Markov models and evolutionary information. *Protein Science* **13**, 1908–1917 (2004).
70. Viklund, H. & Elofsson, A. OCTOPUS: Improving topology prediction by two-track ANN-based preference scores and an extended topological grammar. *Bioinformatics* **24**, 1662–1668 (2008).
71. Käll, L., Krogh, A. & Sonnhammer, E. L. L. A combined transmembrane topology and signal peptide prediction method. *Journal of Molecular Biology* **338**, 1027–1036 (2004).
72. Bernsel, A., Viklund, H., Falk, J., Lindahl, E., von Heijne, G. & Elofsson, A. Prediction of membrane-protein topology from first principles. *Proceedings of the National Academy of Sciences* **105**, 7177–7181 (2008).
73. Kyte, J. & Doolittle, R. F. A simple method for displaying the hydropathic character of a protein. *Journal of Molecular Biology* **157**, 105–132 (1982).
74. Hessa, T., Meindl-Beinker, N. M., Bernsel, A., Kim, H., Sato, Y., Lerch-Bader, M., Nilsson, I., White, S. H. & von Heijne, G. Molecular code for transmembrane-helix recognition by the Sec61 translocon. *Nature* **450**, 1026–1030 (2007).
75. Bateman, A. *et al.* UniProt: A hub for protein information. *Nucleic Acids Research* **43**, D204–D212 (2015).
76. Petersen, T. N., Brunak, S., von Heijne, G. & Nielsen, H. SignalP 4.0: Discriminating signal peptides from transmembrane regions. *Nature Methods* **8**, 785–786 (2011).
77. Nugent, T. & Jones, D. T. Detecting pore-lining regions in transmembrane protein sequences. *BMC Bioinformatics* **13**, 1 (2012).

78. Guna, A. & Hegde, R. S. Transmembrane comain recognition during membrane protein biogenesis and quality control. *Current Biology* **28**, R498–R511 (2018).
79. Stansfeld, P. J., Goose, J. E., Caffrey, M., Carpenter, E. P., Parker, J. L., Newstead, S. & Sansom, M. S. MemProtMD: Automated insertion of membrane protein dstructures into rxplicit lipid membranes. English. *Structure* **23**, 1350–1361 (2015).
80. Coskun, Ü. & Simons, K. Cell membranes: The lipid perspective. *Structure* **19**, 1543–1548 (2011).
81. Park, J. H., Scheerer, P., Hofmann, K. P., Choe, H.-W. & Ernst, O. P. Crystal structure of the ligand-free G-protein-coupled receptor opsin. *Nature* **454**, 183–187 (2008).
82. Berman, H. M., Westbrook, J., Feng, Z., Gilliland, G., Bhat, T. N., Weissig, H., Shindyalov, I. N. & Bourne, P. E. The Protein Data Bank. *Nucleic Acids Research* **28**, 235–242 (2000).
83. Lomize, M. A., Pogozheva, I. D., Joo, H., Mosberg, H. I. & Lomize, A. L. OPM database and PPM web server: resources for positioning of proteins in membranes. *Nucleic Acids Research* **40**, D370–D376 (2012).
84. Kozma, D., Simon, I. & Tusnády, G. E. PDBTM: Protein Data Bank of transmembrane proteins after 8 years. *Nucleic Acids Research* **41**, D524–D529 (2012).
85. Tusnády, G. E., Dosztányi, Z. & Simon, I. TMDET: web server for detecting transmembrane regions of proteins by using their 3D coordinates. *Bioinformatics* **21**, 1276–1277 (2005).
86. Sharpe, H. J., Stevens, T. J. & Munro, S. A comprehensive comparison of transmembrane domains reveals organelle-specific properties. *Cell* **142**, 158–169 (2010).
87. White, S. H., Ladokhin, A. S., Jayasinghe, S. & Hristova, K. How membranes shape protein structure. *Journal of Biological Chemistry* **276**, 32395–32398 (2001).

88. Jensen, M. & Mouritsen, O. G. Lipids do influence protein function - The hydrophobic matching hypothesis revisited. *Biochimica et Biophysica Acta - Biomembranes* **1666**, 205–226 (2004).
89. Kauko, A., Hedin, L. E., Thebaud, E., Cristobal, S., Elofsson, A. & von Heijne, G. Repositioning of transmembrane  $\alpha$ -helices during membrane protein folding. *Journal of Molecular Biology* **397**, 190–201 (2010).
90. Kalvodova, L., Kahya, N., Schwille, P., Ehehalt, R., Verkade, P., Drechsel, D. & Simons, K. Lipids as modulators of proteolytic activity of BACE: Involvement of cholesterol, glycosphingolipids, and anionic phospholipids in vitro. *Journal of Biological Chemistry* **280**, 36815–36823 (2005).
91. Bondar, A. N., del Val, C. & White, S. H. Rhomboid protease dynamics and lipid interactions. *Structure* **17**, 395–405 (2009).
92. Van Meer, G., Voelker, D. R. & Feigenson, G. W. Membrane lipids: Where they are and how they behave. *Nature Reviews Molecular Cell Biology* **9**, 112–124 (2008).
93. Scott, K. A., Bond, P. J., Ivetic, A., Chetwynd, A. P., Khalid, S. & Sansom, M. S. Coarse-grained MD simulations of membrane protein-bilayer self-assembly. *Structure* **16**, 621–630 (2008).
94. Goetz, R. & Lipowsky, R. Computer simulations of bilayer membranes: Self-assembly and interfacial tension. *Journal of Chemical Physics* **108**, 7397–7409 (1998).
95. Helenius, A. & Simons, K. Solubilization of membranes by detergents. *Biochimica et Biophysica Acta (BBA) - Reviews on Biomembranes* **415**, 29–79 (1975).
96. Lichtenberg, D., Robson, R. J. & Dennis, E. A. Solubilization of phospholipids by detergents structural and kinetic aspects. *Biochimica et Biophysica Acta (BBA) - Reviews on Biomembranes* **737**, 285–304 (1983).
97. Op den Kamp, J. A. F. Lipid asymmetry in membranes. *Annual Review of Biochemistry* **48**, 47–71 (1979).

98. De Planque, M. R. R. & Killian, J. A. Protein-lipid interactions studied with designed transmembrane peptides: Role of hydrophobic matching and interfacial anchoring (Review). en. *Molecular Membrane Biology* **20**, 271–284 (2003).
99. Feiner, A.-S. & McEvoy, A. J. The Nernst equation. *Journal of Chemical Education* **71**, 493 (1994).
100. Qin, Y., Dittmer, P. J., Park, J. G., Jansen, K. B. & Palmer, A. E. Measuring steady-state and dynamic endoplasmic reticulum and Golgi Zn<sup>2+</sup> with genetically encoded sensors. *Proceedings of the National Academy of Sciences* **108**, 7351–7356 (2011).
101. Worley, J. F., McIntyre, M. S., Spencer, B., Mertz, R. J., Roe, M. W. & Dukes, I. D. Endoplasmic reticulum calcium store regulates membrane potential in mouse islet  $\beta$ -cells. *Journal of Biological Chemistry* **269**, 14359–14362 (1994).
102. Perry, S. W., Norman, J. P., Barbieri, J., Brown, E. B. & Gelbard, H. A. Mitochondrial membrane potential probes and the proton gradient: A practical usage guide. *BioTechniques* **50**, 98–115 (2011).
103. Schapiro, F. B. & Grinstein, S. Determinants of the pH of the Golgi complex. *Journal of Biological Chemistry* **275**, 21025–21032 (2000).
104. Llopis, J., McCaffery, J. M., Miyawaki, A., Farquhar, M. G. & Tsien, R. Y. Measurement of cytosolic, mitochondrial, and Golgi pH in single living cells with green fluorescent proteins. *Proceedings of the National Academy of Sciences* **95**, 6803–6808 (1998).
105. Hildebrand, P. W., Preissner, R. & Frömmel, C. Structural features of transmembrane helices. *FEBS Letters* **559**, 145–151 (2004).
106. Ulmschneider, M. B. & Sansom, M. S. Amino acid distributions in integral membrane protein structures. *Biochimica et Biophysica Acta - Biomembranes* **1512**, 1–14 (2001).
107. Bowie, J. U. Helix packing in membrane proteins. *Journal of Molecular Biology* **272**, 780–789 (1997).

108. Cuthbertson, J. M., Doyle, D. A. & Sansom, M. S. P. Transmembrane helix prediction: A comparative evaluation and analysis. *Protein Engineering, Design and Selection* **18**, 295–308 (2005).
109. Baeza-Delgado, C., Marti-Renom, M. A. & Mingarro, I. Structure-based statistical analysis of transmembrane helices. *European Biophysics Journal* **42**, 199–207 (2013).
110. Pogozheva, I. D., Tristram-Nagle, S., Mosberg, H. I. & Lomize, A. L. Structural adaptations of proteins to different biological membranes. *Biochimica et Biophysica Acta - Biomembranes* **1828**, 2592–2608 (2013).
111. Skasko, M., Wang, Y., Tian, Y., Tokarev, A., Munguia, J., Ruiz, A., Stephens, E. B., Opella, S. J. & Guatelli, O. HIV-1 Vpu protein antagonizes innate restriction factor BST-2 via lipid-embedded helix-helix interactions. *Journal of Biological Chemistry* **287**, 58–67 (2012).
112. Jayasinghe, S. MPtopo: A database of membrane protein topology. *Protein Science* **10**, 455–458 (2001).
113. Von Heijne, G. Control of topology and mode of assembly of a polytopic membrane protein by positively charged residues. en. *Nature* **341**, 456–458 (1989).
114. Andersson, H., Bakker, E. & von Heijne, G. Different positively charged amino acids have similar effects on the topology of a polytopic transmembrane protein in Escherichia coli. *Journal of Biological Chemistry* **267**, 1491–1495 (1992).
115. Rojo, E. E., Guiard, B, Neupert, W & Stuart, R. A. N-terminal tail export from the mitochondrial matrix. Adherence to the prokaryotic "positive-inside" rule of membrane protein topology. *The Journal of biological chemistry* **274**, 19617–22 (1999).
116. Hessa, T., Kim, H., Bihlmaier, K., Lundin, C., Boekel, J., Andersson, H., Nilsson, I. M., White, S. H. & von Heijne, G. Recognition of transmembrane helices by the endoplasmic reticulum translocon. *Nature* **433**, 377–381 (2005).
117. Granseth, E., von Heijne, G. & Elofsson, A. A study of the membrane-water interface region of membrane proteins. *Journal of Molecular Biology* **346**, 377–385 (2005).

118. Nilsson, J., Persson, B. & von Heijne, G. Comparative analysis of amino acid distributions in integral membrane proteins from 107 genomes. *Proteins: Structure, Function, and Bioinformatics* **60**, 606–616 (2005).
119. Braun, P. & von Heijne, G. The aromatic residues Trp and phe have different effects on the positioning of a transmembrane helix in the microsomal membrane. *Biochemistry* **38**, 9778–9782 (1999).
120. Situ, A. J., Kang, S. M., Frey, B. B., An, W., Kim, C. & Ulmer, T. S. Membrane anchoring of  $\alpha$ -helical proteins: Role of tryptophan. *Journal of Physical Chemistry B* **122**, 1185–1194 (2018).
121. Yau, W. M., Wimley, W. C., Gawrisch, K. & White, S. H. The preference of tryptophan for membrane interfaces. *Biochemistry* **37**, 14713–14718 (1998).
122. Chamberlain, A. K., Lee, Y., Kim, S. & Bowie, J. U. Snorkeling preferences foster an amino acid composition bias in transmembrane helices. *Journal of Molecular Biology* **339**, 471–479 (2004).
123. Strandberg, E. & Killian, J. A. Snorkeling of lysine side chains in transmembrane helices: How easy can it get? *FEBS Letters* **544**, 69–73 (2003).
124. Krishnakumar, S. S. & London, E. The control of transmembrane helix transverse position in membranes by hydrophilic residues. *Journal of Molecular Biology* **374**, 1251–1269 (2007).
125. Kandasamy, S. K. & Larson, R. G. Molecular dynamics simulations of model trans-membrane peptides in lipid bilayers: A systematic investigation of hydrophobic mismatch. *Biophysical Journal* **90**, 2326–2343 (2006).
126. Ulmschneider, M. B., Ulmschneider, J. P., Freites, J. A., von Heijne, G., Tobias, D. J. & White, S. H. Transmembrane helices containing a charged arginine are thermodynamically stable. *European Biophysics Journal* **46**, 627–637 (2017).
127. Davis, N. G. & Model, P. An artificial anchor domain: hydrophobicity suffices to stop transfer. *Cell* **41**, 607–614 (1985).
128. Junne, T., Kocik, L. & Spiess, M. The hydrophobic core of the Sec61 translocon defines the hydrophobicity threshold for membrane integration. *Molecular biology of the cell* **21**, 1662–70 (2010).

129. Simm, S., Einloft, J., Mirus, O. & Schleiff, E. 50 years of amino acid hydrophobicity scales: Revisiting the capacity for Peptide classification. *Biological research* **49**, 31 (2016).
130. Peters, C. & Elofsson, A. Why is the biological hydrophobicity scale more accurate than earlier experimental hydrophobicity scales? *Proteins: Structure, Function and Bioinformatics* **82**, 2190–2198 (2014).
131. Chothia, C. The nature of the accessible and buried surfaces in proteins. *Journal of Molecular Biology* **105**, 1–12 (1976).
132. Wolfenden, R. V., Cullis, P. M. & Southgate, C. C. Water, protein folding, and the genetic code. *Science (New York, N.Y.)* **206**, 575–7 (1979).
133. Cohn, E. J., McMeekin, T. L., Edsall, J. T. & Blanchard, M. H. Studies in the physical chemistry of amino acids, peptides and related substances. I. The apparent molal volume and the electrostriction of the solvent. *Journal of the American Chemical Society* **56**, 784–794 (1934).
134. Traube, J. Samml. them. u. them.-techn. *Vortr* **4**, 19–322 (1899).
135. Hine, J. & Mookerjee, P. K. Structural effects on rates and equilibria. XIX. Intrinsic hydrophilic character of organic compounds. Correlations in terms of structural contributions. *The Journal of Organic Chemistry* **40**, 292–298 (1975).
136. Cohn, E. J., Edsall, J. T., Kirkwood, J. G., Mueller, H., Oncley, J. L. & Scatchard, G. *Proteins, amino acids and peptides as ions and dipolar ions* **6**, 884 (1943).
137. Nozaki, Y. & Tanford, C. The Solubility of Amino in Aqueous Ethanol Acids and Two Glycine Dioxane Solutions Peptides. *The Journal of Biological Chemistry* **246**, 2211–2217 (1971).
138. Brambillasca, S., Yabal, M., Makarow, M. & Borgese, N. Unassisted translocation of large polypeptide domains across phospholipid bilayers. *Journal of Cell Biology* **175**, 767–777 (2006).
139. White, S. H. & Wimley, W. C. Membrane protein folding and stability: Physical principles. *Annual Review of Biophysics and Biomolecular Structure* **28**, 319–365 (1999).

140. Rose, G. D. & Wolfenden, R. Hydrogen bonding, hydrophobicity, packing, and protein folding. *Annu. Rev. Biophys. Biomol. Struct.* **22**, 381–415 (1993).
141. Janin, J. Surface and inside volumes in globular proteins [20]. *Nature* **277**, 491–492 (1979).
142. Wolfenden, R., Andersson, L., Cullis, P. M. & Southgate, C. C. Affinities of amino acid side chains for solvent water. *Biochemistry* **20**, 849–855 (1981).
143. Von Heijne, G. & Blomberg, C. Trans-membrane translocation of proteins: The direct transfer model. *European Journal of Biochemistry* **97**, 175–181 (1979).
144. Eisenberg, D., Schwarz, E., Komaromy, M. & Wall, R. Analysis of membrane and surface protein sequences with the hydrophobic moment plot. *Journal of Molecular Biology* **179**, 125–142 (1984).
145. Murzin, A. G., Brenner, S. E., Hubbard, T. & Chothia, C. SCOP: A structural classification of proteins database for the investigation of sequences and structures. *Journal of Molecular Biology* **247**, 536–540 (1995).
146. Wootton, J. C. & Federhen, S. [33] Analysis of compositionally biased regions in sequence databases. *Elsevier*, 554–571 (1996).
147. Pinho, A. J., Garcia, S. P., Pratas, D. & Ferreira, P. J. DNA sequences at a glance. *PLoS ONE* **8** (ed Gibas, C.) e79922 (2013).
148. Oliver, J. L., Bernaola-Galván, P., Guerrero-García, J. & Román-Roldán, R. Entropic profiles of DNA sequences through chaos-game-derived images. *Journal of Theoretical Biology* **160**, 457–470 (1993).
149. Troyanskaya, O. G., Arbell, O., Koren, Y., Landau, G. M. & Bolshoy, A. Sequence complexity profiles of prokaryotic genomic sequences: A fast algorithm for calculating linguistic complexity. *Bioinformatics* **18**, 679–688 (2002).
150. Wootton, J. C. Non-globular domains in protein sequences: Automated segmentation using complexity measures. *Computers and Chemistry* **18**, 269–285 (1994).
151. Shannon, C. E. A mathematical theory of communication. *Bell System Technical Journal* **27**, 379–423 (1948).

152. Lupas, A., Dyke, M. V. & Stock, J. Predicting coiled coils from protein sequences. *Science* **252**, 1162–1164 (1991).
153. Cao, T. B. & Saier, M. H. The general protein secretory pathway: phylogenetic analyses leading to evolutionary conclusions. *Biochimica et Biophysica Acta (BBA) - Biomembranes* **1609**, 115–125 (2003).
154. Drew, D., Fröderberg, L., Baars, L. & de Gier, J.-W. L. Assembly and over-expression of membrane proteins in Escherichia coli. *Biochimica et Biophysica Acta (BBA) - Biomembranes* **1610**, 3–10 (2003).
155. Dalbey, R. E., Kuhn, A., Zhu, L. & Kiefer, D. The membrane insertase YidC. *Biochimica et Biophysica Acta (BBA) - Molecular Cell Research* **1843**, 1489–1496 (2014).
156. Park, S. H., Das, B. B., Casagrande, F., Tian, Y., Nothnagel, H. J., Chu, M., Kiefer, H., Maier, K., De Angelis, A. A., Marassi, F. M. & Opella, S. J. Structure of the chemokine receptor CXCR1 in phospholipid bilayers. *Nature* **491**, 779–783 (2012).
157. Shao, S. & Hegde, R. S. Membrane protein insertion at the endoplasmic reticulum. *Annual Review of Cell and Developmental Biology* **27**, 25–56 (2011).
158. Kihara, A., Akiyama, Y. & Ito, K. FtsH is required for proteolytic elimination of uncomplexed forms of SecY, an essential protein translocase subunit. *Proceedings of the National Academy of Sciences of the United States of America* **92**, 4532–6 (1995).
159. Duong, F. & Wickner, W. Distinct catalytic roles of the SecYE, SecG and SecD-FyajC subunits of preprotein translocase holoenzyme. *The EMBO journal* **16**, 2756–68 (1997).
160. Koch, H. G. & Müller, M. Dissecting the translocase and integrase functions of the Escherichia coli SecYEG translocon. *The Journal of cell biology* **150**, 689–94 (2000).
161. Zimmer, J., Nam, Y. & Rapoport, T. A. Structure of a complex of the ATPase SecA and the protein-translocation channel. *Nature* **455**, 936–943 (2008).

162. Voorhees, R. M., Fernández, I. S., Scheres, S. H. W. & Hegde, R. S. Structure of the mammalian ribosome-Sec61 complex to 3.4 Å resolution. English. *Cell* **157**, 1632–1643 (2014).
163. Van den Berg, B., Clemons, W. M., Collinson, I., Modis, Y., Hartmann, E., Harrison, S. C. & Rapoport, T. A. X-ray structure of a protein-conducting channel. *Nature* **427**, 36–44 (2004).
164. Tam, P. C. K., Maillard, A. P., Chan, K. K. Y. & Duong, F. Investigating the SecY plug movement at the SecYEG translocation channel. *The EMBO journal* **24**, 3380–8 (2005).
165. Junne, T., Schwede, T., Goder, V. & Spiess, M. The plug domain of yeast Sec61p is important for efficient protein translocation, but is not essential for cell viability. *Molecular Biology of the Cell* **17** (ed Gilmore, R.) 4063–4068 (2006).
166. Park, E. & Rapoport, T. A. Preserving the membrane barrier for small molecules during bacterial protein translocation. *Nature* **473**, 239–242 (2011).
167. Martoglio, B., Hofmann, M. W., Brunner, J. & Dobberstein, B. The protein-conducting channel in the membrane of the endoplasmic reticulum is open laterally toward the lipid bilayer. *Cell* **81**, 207–214 (1995).
168. Gogala, M., Becker, T., Beatrix, B., Armache, J.-P., Barrio-Garcia, C., Berninghausen, O. & Beckmann, R. Structures of the Sec61 complex engaged in nascent peptide translocation or membrane insertion. *Nature* **506**, 107–110 (2014).
169. Walter, P & Blobel, G. Translocation of proteins across the endoplasmic reticulum III. Signal recognition protein (SRP) causes signal sequence-dependent and site-specific arrest of chain elongation that is released by microsomal membranes. *The Journal of cell biology* **91**, 557–61 (1981).
170. Rapoport, T. A. Protein translocation across the eukaryotic endoplasmic reticulum and bacterial plasma membranes. *Nature* **450**, 663–669 (2007).
171. Pool, M. R. Signal recognition particles in chloroplasts, bacteria, yeast and mammals. *Molecular Membrane Biology* **22**, 3–15 (2005).

172. Song, W., Raden, D., Mandon, E. C. & Gilmore, R. Role of Sec61alpha in the regulated transfer of the ribosome-nascent chain complex from the signal recognition particle to the translocation channel. *Cell* **100**, 333–43 (2000).
173. Fulga, T. A., Sinning, I., Dobberstein, B. & Pool, M. R. SRbeta coordinates signal sequence release from SRP with ribosome binding to the translocon. *The EMBO journal* **20**, 2338–47 (2001).
174. Pool, M. R., Stumm, J., Fulga, T. A., Sinning, I. & Dobberstein, B. Distinct modes of signal recognition particle interaction with the ribosome. *Science (New York, N.Y.)* **297**, 1345–8 (2002).
175. Shan, S. O. & Walter, P. Co-translational protein targeting by the signal recognition particle. *FEBS Letters* **579**, 921–926 (2005).
176. Petriman, N.-A., Jauß, B., Hufnagel, A., Franz, L., Sachelaru, I., Drepper, F., Warscheid, B. & Koch, H.-G. The interaction network of the YidC insertase with the SecYEG translocon, SRP and the SRP receptor FtsY. *Scientific Reports* **8**, 578 (2018).
177. Hizlan, D., Robson, A., Whitehouse, S., Gold, V. A., Vonck, J., Mills, D., Kühlbrandt, W. & Collinson, I. Structure of the SecY complex unlocked by a preprotein mimic. *Cell reports* **1**, 21–8 (2012).
178. Bischoff, L., Wickles, S., Berninghausen, O., van der Sluis, E. O. & Beckmann, R. Visualization of a polytopic membrane protein during SecY-mediated membrane insertion. *Nature Communications* **5**, 4103 (2014).
179. Egea, P. F. & Stroud, R. M. Lateral opening of a translocon upon entry of protein suggests the mechanism of insertion into membranes. *Proceedings of the National Academy of Sciences* **107**, 17182–17187 (2010).
180. Niesen, M., Muller-Lucks, A., Hedman, R., von Heijne, G. & Miller, T. F. Forces on nascent polypeptides during membrane insertion and translocation via the Sec translocon. *bioRxiv*, 310698 (2018).
181. Van Den Berg, B., Clemons, W. M., Collinson, I., Modis, Y., Hartmann, E., Harrison, S. C. & Rapoport, T. A. X-ray structure of a protein-conducting channel. *Nature* **427**, 36–44 (2004).

182. Emr, S. D., Hanley-Way, S. & Silhavy, T. J. Suppressor mutations that restore export of a protein with a defective signal sequence. *Cell* **23**, 79–88 (1981).
183. Veenendaal, A. K., van der Does, C. & Driesssen, A. J. The protein-conducting channel SecYEG. *Biochimica et Biophysica Acta (BBA) - Molecular Cell Research* **1694**, 81–95 (2004).
184. Li, W., Schulman, S., Boyd, D., Erlandson, K., Beckwith, J. & Rapoport, T. A. The plug domain of the SecY protein stabilizes the closed state of the translocation channel and maintains a membrane seal. *Molecular Cell* **26**, 511–521 (2007).
185. Junne, T., Schwede, T., Goder, V. & Spiess, M. Mutations in the Sec61p channel affecting signal sequence recognition and membrane protein topology. *Journal of Biological Chemistry* **282**, 33201–33209 (2007).
186. Saparov, S. M., Erlandson, K., Cannon, K., Schaletzky, J., Schulman, S., Rapoport, T. A. & Pohl, P. Determining the conductance of the SecY protein translocation channel for small molecules. *Molecular Cell* **26**, 501–509 (2007).
187. Samuelson, J. C., Chen, M., Jiang, F., Möller, I., Wiedmann, M., Kuhn, A., Phillips, G. J. & Dalbey, R. E. YidC mediates membrane protein insertion in bacteria. *Nature* **406**, 637–641 (2000).
188. Nagamori, S., Smirnova, I. N. & Kaback, H. R. Role of YidC in folding of polytopic membrane proteins. *The Journal of cell biology* **165**, 53–62 (2004).
189. Sommer, N., Junne, T., Kalies, K.-U., Spiess, M. & Hartmann, E. TRAP assists membrane protein topogenesis at the mammalian ER membrane. *Biochimica et Biophysica Acta (BBA) - Molecular Cell Research* **1833**, 3104–3111 (2013).
190. Voigt, S., Jungnickel, B., Hartmann, E. & Rapoport, T. A. Signal sequence-dependent function of the TRAM protein during early phases of protein transport across the endoplasmic reticulum membrane. *The Journal of cell biology* **134**, 25–35 (1996).
191. Conti, B. J., Devaraneni, P. K., Yang, Z., David, L. L. & Skach, W. R. Cotranslational stabilization of Sec62/63 within the ER Sec61 translocon is controlled by distinct substrate-driven translocation events. *Molecular cell* **58**, 269–83 (2015).

192. Meyer, H. A., Grau, H, Kraft, R, Kostka, S, Prehn, S, Kalies, K. U. & Hartmann, E. Mammalian Sec61 is associated with Sec62 and Sec63. *The Journal of biological chemistry* **275**, 14550–7 (2000).
193. Chirico, W. J., Waters, M. G. & Blobel, G. 70K heat shock related proteins stimulate protein translocation into microsomes. *Nature* **332**, 805–810 (1988).
194. Deshaies, R. J., Koch, B. D., Werner-Washburne, M., Craig, E. A. & Schekman, R. A subfamily of stress proteins facilitates translocation of secretory and mitochondrial precursor polypeptides. *Nature* **332**, 800–805 (1988).
195. Steel, G. J., Fullerton, D. M., Tyson, J. R. & Stirling, C. J. Coordinated activation of Hsp70 chaperones. *Science (New York, N.Y.)* **303**, 98–101 (2004).
196. Jadhav, B., McKenna, M., Johnson, N., High, S., Sinning, I. & Pool, M. R. Mammalian SRP receptor switches the Sec61 translocase from Sec62 to SRP-dependent translocation. *Nature Communications* **6**, 10133 (2015).
197. Von Heijne, G. Signal sequences: The limits of variation. *Journal of Molecular Biology* **184**, 99–105 (1985).
198. Von Heijne, G. The signal peptide. *J Membr Biol* **115**, 195–201 (1990).
199. Izard, J. W. & Kendall, D. A. Signal peptides: exquisitely designed transport promoters. *Molecular Microbiology* **13**, 765–773 (1994).
200. Giersch, L. M. Signal sequences. *Biochemistry* **28**, 923–930 (1989).
201. Choo, K., Tan, T. & Ranganathan, S. A comprehensive assessment of N-terminal signal peptides prediction methods. *BMC Bioinformatics* **10**, S2 (2009).
202. Liang, B. & Tamm, L. K. Structure of outer membrane protein G by solution NMR spectroscopy. *Proceedings of the National Academy of Sciences of the United States of America* **104**, 16140–5 (2007).
203. Posson, D. J., McCoy, J. G. & Nimigean, C. M. The voltage-dependent gate in MthK potassium channels is located at the selectivity filter. *Nature Structural & Molecular Biology* **20**, 159–166 (2013).

204. Palczewski, K., Kumashita, T., Hori, T., Behnke, C. A., Motoshima, H., Fox, B. A., Le Trong, I., Teller, D. C., Okada, T., Stenkamp, R. E., Yamamoto, M & Miyano, M. Crystal structure of rhodopsin: A G protein-coupled receptor. *Science (New York, N.Y.)* **289**, 739–45 (2000).
205. Wimley, W. C. The versatile  $\beta$ -barrel membrane protein. *Current Opinion in Structural Biology* **13**, 404–411 (2003).
206. McFadden, G. I. Chloroplast origin and integration. *Plant physiology* **125**, 50–3 (2001).
207. Gray, M. W., Burger, G & Lang, B. F. Mitochondrial evolution. *Science (New York, N.Y.)* **283**, 1476–81 (1999).
208. Fischer, K., Weber, A., Brink, S., Arbinger, B., Schünemann, D., Borchert, S., Heldt, H. W., Popp, B., Benz, R & Link, T. A. Porins from plants. Molecular cloning and functional characterization of two new members of the porin family. *The Journal of biological chemistry* **269**, 25754–60 (1994).
209. Zeth, K. & Thein, M. Porins in prokaryotes and eukaryotes: common themes and variations. *Biochemical Journal* **431**, 13–22 (2010).
210. Fairman, J. W., Noinaj, N. & Buchanan, S. K. The structural biology of  $\beta$ -barrel membrane proteins: a summary of recent reports. *Current Opinion in Structural Biology* **21**, 523–531 (2011).
211. Ulrich, T. & Rapaport, D. Biogenesis of beta-barrel proteins in evolutionary context. *International Journal of Medical Microbiology* **305**, 259–264 (2015).
212. Driessens, A. J. & Nouwen, N. Protein translocation across the bacterial cytoplasmic membrane. *Annual Review of Biochemistry* **77**, 643–667 (2008).
213. Papanikou, E., Karamanou, S. & Economou, A. Bacterial protein secretion through the translocase nanomachine. *Nature Reviews Microbiology* **5**, 839–851 (2007).
214. Bechtluft, P., Nouwen, N., Tans, S. J. & Driessens, A. J. M. SecB—A chaperone dedicated to protein translocation. *Mol. BioSyst.* **6**, 620–627 (2010).

215. Paetzel, M. Structure and mechanism of Escherichia coli type I signal peptidase. *Biochimica et Biophysica Acta (BBA) - Molecular Cell Research* **1843**, 1497–1508 (2014).
216. Lazar, S. W. & Kolter, R. SurA assists the folding of Escherichia coli outer membrane proteins. *Journal of bacteriology* **178**, 1770–3 (1996).
217. Volokhina, E. B., Grijpstra, J., Stork, M., Schilders, I., Tommassen, J. & Bos, M. P. Role of the periplasmic chaperones Skp, SurA, and DegQ in outer membrane protein biogenesis in Neisseria meningitidis. *Journal of bacteriology* **193**, 1612–21 (2011).
218. Wu, T., Malinvern, J., Ruiz, N., Kim, S., Silhavy, T. J. & Kahne, D. Identification of a multicomponent complex required for outer membrane biogenesis in escherichia coli. *Cell* **121**, 235–245 (2005).
219. Hagan, C. L., Kim, S. & Kahne, D. Reconstitution of outer membrane protein assembly from purified components. *Science* **328**, 890–892 (2010).
220. Noinaj, N., Kuszak, A. J., Balusek, C., Gumbart, J. C. & Buchanan, S. K. Lateral opening and exit pore formation are required for BamA function. *Structure (London, England : 1993)* **22**, 1055–62 (2014).
221. Müller, J. E., Papic, D., Ulrich, T., Grin, I., Schütz, M., Oberhettinger, P., Tommassen, J., Linke, D., Dimmer, K. S., Autenrieth, I. B. & Rapaport, D. Mitochondria can recognize and assemble fragments of a  $\beta$ -barrel structure. *Molecular Biology of the Cell* **22** (ed Glick, B.) 1638–1647 (2011).
222. Chacinska, A., Koehler, C. M., Milenkovic, D., Lithgow, T. & Pfanner, N. Importing mitochondrial proteins: machineries and mechanisms. *Cell* **138**, 628–44 (2009).
223. Wiedemann, N., Kozjak, V., Chacinska, A., Schönfisch, B., Rospert, S., Ryan, M. T., Pfanner, N. & Meisinger, C. Machinery for protein sorting and assembly in the mitochondrial outer membrane. *Nature* **424**, 565–571 (2003).
224. Paschen, S. A., Waizenegger, T., Stan, T., Preuss, M., Cyrklaff, M., Hell, K., Rapaport, D. & Neupert, W. Evolutionary conservation of biogenesis of  $\beta$ -barrel membrane proteins. *Nature* **426**, 862–866 (2003).

225. Gentle, I., Gabriel, K., Beech, P., Waller, R. & Lithgow, T. The Omp85 family of proteins is essential for outer membrane biogenesis in mitochondria and bacteria. *The Journal of cell biology* **164**, 19–24 (2004).
226. Tamm, L. K., Hong, H. & Liang, B. Folding and assembly of  $\beta$ -barrel membrane proteins. *Biochimica et Biophysica Acta (BBA) - Biomembranes* **1666**, 250–263 (2004).
227. Baker, J. A., Wong, W.-C., Eisenhaber, B., Warwicker, J. & Eisenhaber, F. Charged residues next to transmembrane regions revisited: “Positive-inside rule” is complemented by the “negative inside depletion/outside enrichment rule”. *BMC Biology* **15**, 66 (2017).
228. Moon, C. P., Zaccai, N. R., Fleming, P. J., Gessmann, D. & Fleming, K. G. Membrane protein thermodynamic stability may serve as the energy sink for sorting in the periplasm. *Proceedings of the National Academy of Sciences* **110**, 4285–4290 (2013).
229. MacCallum, J. L. & Tielemans, D. P. Hydrophobicity scales: A thermodynamic looking glass into lipid-protein interactions. *Trends in Biochemical Sciences* **36**, 653–662 (2011).
230. Von Heijne, G. The distribution of positively charged residues in bacterial inner membrane proteins correlates with the trans-membrane topology. *The EMBO Journal* **5**, 3021–3027 (1986).
231. Von Heijne, G. & Gavel, Y. Topogenic signals in integral membrane proteins. *European Journal of Biochemistry* **174**, 671–678 (1988).
232. Öjemalm, K., Botelho, S. C., Stüdle, C. & von Heijne, G. Quantitative analysis of SecYEG-mediated insertion of transmembrane  $\alpha$ -helices into the bacterial inner membrane. *Journal of Molecular Biology* **425**, 2813–2822 (2013).
233. Beuming, T. & Weinstein, H. A knowledge-based scale for the analysis and prediction of buried and exposed faces of transmembrane domain proteins. *Bioinformatics* **20**, 1822–1835 (2004).

234. Zhao, G. & London, E. An amino acid “transmembrane tendency” scale that approaches the theoretical limit to accuracy for prediction of transmembrane helices: Relationship to biological hydrophobicity. *Protein Science* **15**, 1987–2001 (2006).
235. Sonnhammer, E. L., von Heijne, G & Krogh, A. A hidden Markov model for predicting transmembrane helices in protein sequences. *Proceedings* **6**, 175–182 (1998).
236. Käll, L., Krogh, A. & Sonnhammer, E. L. L. Advantages of combined transmembrane topology and signal peptide prediction—the Phobius web server. *Nucleic Acids Research* **35** (2007).
237. Cserzö, M., Eisenhaber, F., Eisenhaber, B. & Simon, I. On filtering false positive transmembrane protein predictions. *Protein Engineering, Design and Selection* **15**, 745–752 (2002).
238. Cserzo, M., Eisenhaber, F., Eisenhaber, B. & Simon, I. TM or not TM: Transmembrane protein prediction with low false positive rate using DAS-TMfilter. *Bioinformatics* **20**, 136–137 (2004).
239. Käll, L. & Sonnhammer, E. L. Reliability of transmembrane predictions in whole-genome data. *FEBS Letters* **532**, 415–418 (2002).
240. Eisenhaber, B., Kuchibhatla, D., Sherman, W., Sirota, F. L., Berezovsky, I. N., Wong, W. C. & Eisenhaber, F. The recipe for protein sequence-based function prediction and its implementation in the ANNOTATOR software environment. *Methods in Molecular Biology* **1415**, 477–506 (2016).
241. Eisenhaber, F. A decade after the first full human genome sequencing: when will we understand our own genome? *Journal of Bioinformatics and Computational Biology* **10**, 1271001 (2012).
242. Sherman, W. A., Kuchibhatla, D. B., Limviphuvadh, V., Maurer-Stroh, S., Eisenhaber, B. & Eisenhaber, F. HPMV: Human protein mutation viewer — relating sequence mutations to protein sequence architecture and function changes. *Journal of Bioinformatics and Computational Biology* **13**, 1550028 (2015).

243. Sipos, L. & von Heijne, G. Predicting the topology of eukaryotic membrane proteins. *European Journal of Biochemistry* **213**, 1333–1340 (1993).
244. Gavel, Y., Steppuhn, J., Herrmann, R. & von Heijne, G. The 'positive-inside rule' applies to thylakoid membrane proteins. *FEBS Letters* **282**, 41–46 (1991).
245. Wallin, E. & von Heijne, G. Genome-wide analysis of integral membrane proteins from eubacterial, archaean, and eukaryotic organisms. *Protein Science* **7**, 1029–1038 (2008).
246. Beltzer, J. P., Fiedler, K., Fuhrer, C., Geffen, I., Handschin, C., Wessels, H. P. & Spiess, M. Charged residues are major determinants of the transmembrane orientation of a signal-anchor sequence. *Journal of Biological Chemistry* **266**, 973–978 (1991).
247. Kida, Y., Morimoto, F., Mihara, K. & Sakaguchi, M. Function of positive charges following signal-anchor sequences during translocation of the N-terminal domain. *Journal of Biological Chemistry* **281**, 1152–1158 (2006).
248. Nilsson, I. M. & von Heijne, G. Fine-tuning the topology of a polytopic membrane protein: Role of positively and negatively charged amino acids. *Cell* **62**, 1135–1141 (1990).
249. Bogdanov, M., Dowhan, W. & Vitrac, H. Lipids and topological rules governing membrane protein assembly. *Biochimica et Biophysica Acta - Molecular Cell Research* **1843**, 1475–1488 (2014).
250. Andersson, H. & von Heijne, G. Position-specific Asp-Lys pairing can affect signal sequence function and membrane protein topology. *Journal of Biological Chemistry* **268**, 21389–21393 (1993).
251. Kim, H., Paul, S., Jennity, J. & Inouye, M. Reversible topology of a bifunctional transmembrane protein depends upon the charge balance around its transmembrane domain. *Molecular Microbiology* **11**, 819–831 (1994).
252. Delgado-Partin, V. M. & Dalbey, R. E. The proton motive force, acting on acidic residues, promotes translocation of amino-terminal domains of membrane proteins when the hydrophobicity of the translocation signal is low. *Journal of Biological Chemistry* **273**, 9927–9934 (1998).

253. Ismail, N., Hedman, R., Schiller, N. & von Heijne, G. A biphasic pulling force acts on transmembrane helices during translocon-mediated membrane integration. *Nature Structural and Molecular Biology* **19**, 1018–1023 (2012).
254. Hartmann, E., Rapoport, T. A. & Lodish, H. F. Predicting the orientation of eukaryotic membrane-spanning proteins. *Proceedings of the National Academy of Sciences* **86**, 5786–5790 (1989).
255. Harley, C. A., Holt, J. A., Turner, R. & Tipper, D. J. Transmembrane protein insertion orientation in yeast depends on the charge difference across transmembrane segments, their total hydrophobicity, and its distribution. *Journal of Biological Chemistry* **273**, 24963–24971 (1998).
256. Sato, M., Hresko, R. & Mueckler, M. Testing the charge difference hypothesis for the assembly of a eucaryotic multispanning membrane protein. *Journal of Biological Chemistry* **273**, 25203–25208 (1998).
257. Dobson, L., Langó, T., Reményi, I. & Tusnády, G. E. Expediting topology data gathering for the TOPDB database. *Nucleic Acids Research* **43**, D283–D289 (2015).
258. Nakashima, H. & Nishikawa, K. The amino acid composition is different between the cytoplasmic and extracellular sides in membrane proteins. English. *FEBS Letters* **303**, 141–146 (1992).
259. Bahadur, R. R. Rates of convergence of estimates and test statistics. *The Annals of Mathematical Statistics* **38**, 303–324 (1967).
260. Bahadur, R. R. *Some limit theorems in statistics* (Society for Industrial and Applied Mathematics, 1971).
261. Sunyaev, S. R., Eisenhaber, F., Argos, P., Kuznetsov, E. N. & Tumanyan, V. G. Are knowledge-based potentials derived from protein structure sets discriminative with respect to amino acid types? *Proteins: Structure, Function and Genetics* **31**, 225–246 (1998).
262. Zachowski, A. Phospholipids in animal eukaryotic membranes: transverse asymmetry and movement. *Biochemical Journal* **294**, 1–14 (1993).

263. Yeung, T., Gilbert, G. E., Shi, J., Silvius, J., Kapus, A. & Grinstein, S. Membrane phosphatidylserine regulates surface charge and protein localization. *Science* **319**, 210–213 (2008).
264. Meindl-Beinker, N. M., Lundin, C., Nilsson, I., White, S. H. & von Heijne, G. Asn- and Asp-mediated interactions between transmembrane helices during translocon-mediated membrane protein assembly. *EMBO Reports* **7**, 1111–1116 (2006).
265. Oger, P. M. & Cario, A. Adaptation of the membrane in Archaea. *Biophysical Chemistry* **183**, 42–56 (2013).
266. Rutz, C., Rosenthal, W. & Schülein, R. A single negatively charged residue affects the orientation of a membrane protein in the inner membrane of Escherichia coli only when it is located adjacent to a transmembrane domain. *Journal of Biological Chemistry* **274**, 33757–33763 (1999).
267. Hedin, L. E., Öjemalm, K., Bernsel, A., Hennerdal, A., Illergård, K., Enquist, K., Kauko, A., Cristobal, S., von Heijne, G., Lerch-Bader, M., Nilsson, I. & Elofsson, A. Membrane insertion of marginally hydrophobic transmembrane helices depends on sequence context. *Journal of Molecular Biology* **396**, 221–229 (2010).
268. Öjemalm, K., Halling, K. K., Nilsson, I. & von Heijne, G. Orientational preferences of neighboring helices can drive ER insertion of a marginally hydrophobic transmembrane helix. *Molecular Cell* **45**, 529–540 (2012).
269. Devaux, P. F. Phospholipid flippases. *FEBS Letters* **234**, 8–12 (1988).
270. Devaux, P. F. & Morris, R. Transmembrane asymmetry and lateral domains in biological membranes. *Traffic* **5**, 241–246 (2004).
271. Bell, R. M., Ballas, L. M. & Coleman, R. A. Lipid topogenesis. *Journal of Lipid Research* **22**, 391–403 (1981).
272. Futerman, A. H. & Riezman, H. The ins and outs of sphingolipid synthesis. *Trends in Cell Biology* **15**, 312–318 (2005).

273. Tafesse, F. G., Huitema, K., Hermansson, M., Van Der Poel, S., Van Den Dikkenberg, J., Uphoff, A., Somerharju, P. & Holthuis, J. C. M. Both sphingomyelin synthases SMS1 and SMS2 are required for sphingomyelin homeostasis and growth in human HeLa cells. *Journal of Biological Chemistry* **282**, 17537–17547 (2007).
274. Di Paolo, G. & De Camilli, P. Phosphoinositides in cell regulation and membrane dynamics. *Nature* **443**, 651–657 (2006).
275. Killian, J. A. & von Heijne, G. How proteins adapt to a membrane-water interface. English. *Trends in Biochemical Sciences* **25**, 429–434 (2000).
276. Kuznetsov, V., Lee, H. K., Maurer-Stroh, S., Molnár, M. J., Pongor, S., Eisenhaber, B. & Eisenhaber, F. How bioinformatics influences health informatics: usage of biomolecular sequences, expression profiles and automated microscopic image analyses for clinical needs and public health. *Health Information Science and Systems* **1**, 2 (2013).
277. Huang, Y., Niu, B., Gao, Y., Fu, L. & Li, W. CD-HIT Suite: A web server for clustering and comparing biological sequences. *Bioinformatics* **26**, 680–682 (2010).
278. Suzek, B. E., Wang, Y., Huang, H., McGarvey, P. B. & Wu, C. H. UniRef clusters: A comprehensive and scalable alternative for improving sequence similarity searches. *Bioinformatics* **31**, 926–932 (2015).
279. White, S. H. & von Heijne, G. How translocons select transmembrane helices. en. *Annual Review of Biophysics* **37**, 23–42 (2008).
280. Van Der Walt, S., Colbert, S. C. & Varoquaux, G. The NumPy array: A structure for efficient numerical computation. *Computing in Science and Engineering* **13**, 22–30 (2011).
281. Osborne, A. R., Rapoport, T. A. & van den Berg, B. Protein translocation by the Sec61/Secy channel. *Annual Review of Cell and Developmental Biology* **21**, 529–550 (2005).

282. Hockenberry, D., Nuñez, G., Milliman, C., Schreiber, R. D. & Korsmeyer, S. J. Bcl-2 is an inner mitochondrial membrane protein that blocks programmed cell death. *Nature* **348**, 334–336 (1990).
283. Ungar, D. & Hughson, F. M. SNARE protein structure and function. *Annual Review of Cell and Developmental Biology* **19**, 493–517 (2003).
284. Kalbfleisch, T., Cambon, A. & Wattenberg, B. W. A bioinformatics approach to identifying tail-anchored proteins in the human genome. *Traffic* **8**, 1687–1694 (2007).
285. Allen, T. M. & Cullis, P. R. Liposomal drug delivery systems: From concept to clinical applications. *Advanced Drug Delivery Reviews* **65**, 36–48 (2013).
286. Nordlund, G., Brzezinski, P. & Von Ballmoos, C. SNARE-fusion mediated insertion of membrane proteins into native and artificial membranes. *Nature Communications* **5**, 4303 (2014).
287. Kutay, U., Hartmann, E. & Rapoport, T. A. A class of membrane proteins with a C-terminal anchor. *Trends in Cell Biology* **3**, 72–75 (1993).
288. Rabu, C., Wipf, P., Brodsky, J. L. & High, S. A precursor-specific role for Hsp40/Hsc70 during tail-anchored protein integration at the endoplasmic reticulum. *Journal of Biological Chemistry* **283**, 27504–27513 (2008).
289. Rabu, C., Schmid, V., Schwappach, B. & High, S. Biogenesis of tail-anchored proteins: the beginning for the end? *Journal of Cell Science* **122**, 3605–3612 (2009).
290. Johnson, N., Powis, K. & High, S. Post-translational translocation into the endoplasmic reticulum. *Biochimica et Biophysica Acta - Molecular Cell Research* **1833**, 2403–2409 (2013).
291. Abell, B. M., Pool, M. R., Schlenker, O., Sinning, I. & High, S. Signal recognition particle mediates post-translational targeting in eukaryotes. *EMBO Journal* **23**, 2755–2764 (2004).
292. Leznicki, P., Clancy, A., Schwappach, B. & High, S. Bat3 promotes the membrane integration of tail-anchored proteins. *Journal of Cell Science* **123**, 2170–2178 (2010).

293. Abell, B. M., Jung, M., Oliver, J. D., Knight, B. C., Tyedmers, J., Zimmermann, R. & High, S. Tail-anchored and signal-anchored proteins utilize overlapping pathways during membrane insertion. *Journal of Biological Chemistry* **278**, 5669–5678 (2003).
294. Steel, G. J., Brownsword, J. & Stirling, C. J. Tail-anchored protein insertion into yeast ER requires a novel posttranslational mechanism which is independent of the SEC machinery. *Biochemistry* **41**, 11914–11920 (2002).
295. Yabal, M., Brambillasca, S., Soffientini, P., Pedrazzini, E., Borgese, N. & Makarow, M. Translocation of the C terminus of a tail-anchored protein across the endoplasmic reticulum membrane in yeast mutants defective in signal peptide-driven translocation. *Journal of Biological Chemistry* **278**, 3489–3496 (2003).
296. Casson, J., McKenna, M., Haßdenteufel, S., Aviram, N., Zimmerman, R. & High, S. Multiple pathways facilitate the biogenesis of mammalian tail-anchored proteins. *Journal of Cell Science* **130**, 3851–3861 (2017).
297. Schuldiner, M., Metz, J., Schmid, V., Denic, V., Rakwalska, M., Schmitt, H. D., Schwappach, B. & Weissman, J. S. The GET complex mediates insertion of tail-anchored proteins into the ER membrane. *Cell* **134**, 634–645 (2008).
298. Wang, F., Brown, E. C., Mak, G., Zhuang, J. & Denic, V. A chaperone cascade sorts proteins for posttranslational membrane insertion into the endoplasmic reticulum. *Molecular Cell* **40**, 159–171 (2010).
299. Chang, Y. W., Chuang, Y. C., Ho, Y. C., Cheng, M. Y., Sun, Y. J., Hsiao, C. D. & Wang, C. Crystal structure of Get4-Get5 complex and its interactions with Sgt2, Get3, and Ydj1. *Journal of Biological Chemistry* **285**, 9962–9970 (2010).
300. Chang, Y. W., Lin, T. W., Li, Y. C., Huang, Y. S., Sun, Y. J. & Hsiao, C. D. Interaction surface and topology of Get3-Get4-Get5 protein complex, involved in targeting tail-anchored proteins to endoplasmic reticulum. *Journal of Biological Chemistry* **287**, 4783–4789 (2012).
301. Chartron, J. W., Suloway, C. J. M., Zaslaver, M. & Clemons, W. M. Structural characterization of the Get4/Get5 complex and its interaction with Get3. *Proceedings of the National Academy of Sciences* **107**, 12127–12132 (2010).

302. Chartron, J. W., VanderVelde, D. G., Rao, M. & Clemons, W. M. Get5 carboxyl-terminal domain is a novel dimerization motif that tethers an extended Get4/Get5 complex. *Journal of Biological Chemistry* **287**, 8310–8317 (2012).
303. Shao, S., Rodrigo-Brenni, M. C., Kivlen, M. H. & Hegde, R. S. Mechanistic basis for a molecular triage reaction. *Science* **355**, 298–302 (2017).
304. Mateja, A., Szlachcic, A., Downing, M. E., Dobosz, M., Mariappan, M., Hegde, R. S. & Keenan, R. J. The structural basis of tail-anchored membrane protein recognition by Get3. *Nature* **461**, 361–366 (2009).
305. Hu, J., Li, J., Qian, X., Denic, V. & Sha, B. The crystal structures of yeast Get3 suggest a mechanism for tail-anchored protein membrane insertion. *PLoS ONE* **4** (ed Mayer, C.) e8061 (2009).
306. Bozkurt, G., Stjepanovic, G., Vilardi, F., Amlacher, S., Wild, K., Bange, G., Favaloro, V., Rippe, K., Hurt, E., Dobberstein, B. & Sinning, I. Structural insights into tail-anchored protein binding and membrane insertion by Get3. *Proceedings of the National Academy of Sciences of the United States of America* **106**, 21131–6 (2009).
307. Suloway, C. J. M., Chartron, J. W., Zaslaver, M. & Clemons, W. M. Model for eukaryotic tail-anchored protein binding based on the structure of Get3. *Proceedings of the National Academy of Sciences of the United States of America* **106**, 14849–14854 (2009).
308. Yamagata, A., Mimura, H., Sato, Y., Yamashita, M., Yoshikawa, A. & Fukai, S. Structural insight into the membrane insertion of tail-anchored proteins by Get3. *Genes to Cells* **15**, 29–41 (2010).
309. Stefanovic, S. & Hegde, R. S. Identification of a targeting factor for posttranslational membrane protein insertion into the ER. *Cell* **128**, 1147–1159 (2007).
310. Favaloro, V., Spasic, M., Schwappach, B. & Dobberstein, B. Distinct targeting pathways for the membrane insertion of tail-anchored (TA) proteins. *Journal of Cell Science* **121**, 1832–1840 (2008).

311. Jonikas, M. C., Collins, S. R., Denic, V., Oh, E., Quan, E. M., Schmid, V., Weibezahl, J., Schwappach, B., Walter, P., Weissman, J. S. & Schuldiner, M. Comprehensive characterization of genes required for protein folding in the endoplasmic reticulum. *Science* **323**, 1693–1697 (2009).
312. Huh, W. K., Falvo, J. V., Gerke, L. C., Carroll, A. S., Howson, R. W., Weissman, J. S. & O’Shea, E. K. Global analysis of protein localization in budding yeast. *Nature* **425**, 686–691 (2003).
313. Zalisko, B. E., Chan, C., Denic, V., Rock, R. S. & Keenan, R. J. Tail-anchored protein insertion by a single Get1/2 heterodimer. *Cell Reports* **20**, 2287–2293 (2017).
314. Vitali, D. G., Sinzel, M., Bulthuis, E. P., Kolb, A., Zabel, S., Mehlhorn, D. G., Costa, B. F., Farkas, Á., Clancy, A., Schuldiner, M., Grefen, C., Schwappach, B., Borgese, N. & Rapaport, D. The GET pathway can increase the risk of mitochondrial outer membrane proteins to be mistargeted to the ER. *Journal of cell science* **131**, 734–764 (2018).
315. Mariappan, M., Mateja, A., Dobosz, M., Bove, E., Hegde, R. S. & Keenan, R. J. The mechanism of membrane-associated steps in tail-anchored protein insertion. *Nature* **477**, 61–69 (2011).
316. Stefer, S., Reitz, S., Wang, F., Wild, K., Pang, Y. Y., Schwarz, D., Bomke, J., Hein, C., Löhr, F., Bernhard, F., Denic, V., Dötsch, V. & Sinning, I. Structural basis for tail-anchored membrane protein biogenesis by the Get3-receptor complex. *Science* **333**, 758–762 (2011).
317. Rao, M., Okreglak, V., Chio, U. S., Cho, H., Walter, P. & Shan, S. O. Multiple selection filters ensure accurate tail-anchored membrane protein targeting. *eLife* **5** (2016).
318. Aviram, N., Ast, T., Costa, E. A., Arakel, E. C., Chuartzman, S. G., Jan, C. H., Haßdenteufel, S., Dudek, J., Jung, M., Schorr, S., Zimmermann, R., Schwappach, B., Weissman, J. S. & Schuldiner, M. The SND proteins constitute an alternative targeting route to the endoplasmic reticulum. *Nature* **540**, 134–138 (2016).

319. Haßdenteufel, S., Sicking, M., Schorr, S., Aviram, N., Fecher-Trost, C., Schuldiner, M., Jung, M., Zimmermann, R. & Lang, S. hSnd2 protein represents an alternative targeting factor to the endoplasmic reticulum in human cells. *FEBS Letters* **591**, 3211–3224 (2017).
320. Setoguchi, K., Otera, H. & Mihara, K. Cytosolic factor- and TOM-independent import of C-tail-anchored mitochondrial outer membrane proteins. *EMBO Journal* **25**, 5635–5647 (2006).
321. Kemper, C., Habib, S. J., Engl, G., Heckmeyer, P., Dimmer, K. S. & Rapaport, D. Integration of tail-anchored proteins into the mitochondrial outer membrane does not require any known import components. *Journal of Cell Science* **121**, 1990–1998 (2008).
322. Ngosuwan, J., Wang, N. M., Fung, K. L. & Chirico, W. J. Roles of cytosolic Hsp70 and Hsp40 molecular chaperones in post-translational translocation of presecretory proteins into the endoplasmic reticulum. *Journal of Biological Chemistry* **278**, 7034–7042 (2003).
323. Colombo, S. F., Longhi, R. & Borgese, N. The role of cytosolic proteins in the insertion of tail-anchored proteins into phospholipid bilayers. *Journal of Cell Science* **122**, 2383–2392 (2009).
324. Meineke, B., Engl, G., Kemper, C., Vasiljev-Neumeyer, A., Paulitschke, H. & Rapaport, D. The outer membrane form of the mitochondrial protein Mcr1 follows a TOM-independent membrane insertion pathway. *FEBS Letters* **582**, 855–860 (2008).
325. Ulmschneider, M. B., Ulmschneider, J. P., Schiller, N., Wallace, B. A., von Heijne, G. & White, S. H. Spontaneous transmembrane helix insertion thermodynamically mimics translocon-guided insertion. en. *Nature Communications* **5**, 4863 (2014).
326. Chen, Y., Pieuchot, L., Loh, R. A., Yang, J., Kari, T. M. A., Wong, J. Y. & Jedd, G. Hydrophobic handoff for direct delivery of peroxisome tail-anchored proteins. *Nature Communications* **5**, 5790 (2014).

327. Yagita, Y., Hiromasa, T. & Fujiki, Y. Tail-anchored PEX26 targets peroxisomes via a PEX19-dependent and TRC40-independent class I pathway. *Journal of Cell Biology* **200**, 651–666 (2013).
328. Costello, J. L., Castro, I. G., Camões, F., Schrader, T. A., McNeall, D., Yang, J., Giannopoulou, E.-A., Gomes, S., Pogenberg, V., Bonekamp, N. A., Ribeiro, D., Wilmanns, M., Jedd, G., Islinger, M. & Schrader, M. Predicting the targeting of tail-anchored proteins to subcellular compartments in mammalian cells. *Journal of Cell Science* **130**, 1675–1687 (2017).
329. Costa, E. A., Subramanian, K., Nunnari, J. & Weissman, J. S. Defining the physiological role of SRP in protein-targeting efficiency and specificity. *Science (New York, N.Y.)* **359**, 689–692 (2018).
330. Fueller, J., Egorov, M. V., Walther, K. A., Sabet, O., Mallah, J., Grabenbauer, M. & Kinkhabwala, A. Subcellular partitioning of protein tyrosine Phosphatase 1b to the endoplasmic reticulum and mitochondria Dependssensitively on the composition of its tail anchor. *PLoS ONE* **10** (ed Chen, Y.) e0139429 (2015).
331. Wu, S., Zhu, Z., Fu, L., Niu, B. & Li, W. WebMGA: A customizable web server for fast metagenomic sequence analysis. *BMC Genomics* **12**, 444 (2011).
332. Söding, J., Biegert, A. & Lupas, A. N. The HHpred interactive server for protein homology detection and structure prediction. *Nucleic Acids Research* **33**, W244–W248 (2005).
333. Eswar, N., Webb, B., Marti-Renom, M. A., Madhusudhan, M., Eramian, D., Shen, M.-y., Pieper, U. & Sali, A. Comparative protein structure modeling using MODELLER. *Current Protocols in Protein Science* **50**, 2.9.1–2.9.31 (2007).
334. Webb, B. & Sali, A. in *Current Protocols in Protein Science* 1, 2.9.1–2.9.37 (John Wiley & Sons, Inc., Hoboken, NJ, USA, 2016). arXiv: NIHMS150003.
335. Hofmann, K & Stoffel, W. 103. Konferenz der Gesellschaft für Biologische Chemie Studiengruppe Membranstruktur und -Transport Membranforum Frankfurt. *Biological Chemistry Hoppe-Seyler* **374**, 143–170 (1993).

336. Cao, B., Porollo, A., Adamczak, R., Jarrell, M. & Meller, J. Enhanced recognition of protein transmembrane domains with prediction-based structural profiles. *Bioinformatics* **22**, 303–309 (2006).
337. Montgomerie, S., Cruz, J. A., Shrivastava, S., Arndt, D., Berjanskii, M. & Wishart, D. S. PROTEUS2: a web server for comprehensive protein structure prediction and structure-based annotation. *Nucleic acids research* **36**, W202–W209 (2008).
338. Kurowski, M. A. & Bujnicki, J. M. GeneSilico protein structure prediction meta-server. *Nucleic Acids Research* **31**, 3305–3307 (2003).
339. Baker, N. A., Sept, D., Joseph, S., Holst, M. J. & McCammon, J. A. Electrostatics of nanosystems: Application to microtubules and the ribosome. *Proceedings of the National Academy of Sciences* **98**, 10037–10041 (2001).
340. Ashkenazy, H., Erez, E., Martz, E., Pupko, T. & Ben-Tal, N. ConSurf 2010: Calculating evolutionary conservation in sequence and structure of proteins and nucleic acids. *Nucleic Acids Research* **38**, W529–W533 (2010).
341. Ramsay, L., Macaulay, M., Degli Ivanissevich, S., MacLean, K., Cardle, L., Fuller, J., Edwards, K. J., Tuveson, S., Morgante, M., Massari, A., Maestri, E., Marmiroli, N., Sjakste, T., Ganal, M., Powell, W. & Waugh, R. A simple sequence repeat-based linkage map of Barley. *Genetics* **156**, 1997–2005 (2000).
342. Choi, J. Y., Wu, W. I. & Voelker, D. R. Phosphatidylserine decarboxylases as genetic and biochemical tools for studying phospholipid traffic. *Analytical Biochemistry* **347**, 165–175 (2005).
343. Gebert, N., Joshi, A. S., Kutik, S., Becker, T., McKenzie, M., Guan, X. L., Mooga, V. P., Stroud, D. A., Kulkarni, G., Wenk, M. R., Rehling, P., Meisinger, C., Ryan, M. T., Wiedemann, N., Greenberg, M. L. & Pfanner, N. Mitochondrial cardiolipin involved in outer-membrane protein biogenesis: Implications for Barth syndrome. *Current Biology* **19**, 2133–2139 (2009).
344. Borgese, N., Brambillasca, S. & Colombo, S. How tails guide tail-anchored proteins to their destinations. *Current Opinion in Cell Biology* **19**, 368–375 (2007).

345. Lan, L., Isenmann, S. & Wattenberg, B. W. Targeting and insertion of C-terminally anchored proteins to the mitochondrial outer membrane is specific and saturable but does not strictly require ATP or molecular chaperones. *The Biochemical journal* **349**, 611–621 (2000).
346. Saraogi, I. & Shan, S.-o. Molecular mechanism of co-translational protein targeting by the signal recognition particle. *Traffic* **12**, 535–542 (2011).
347. Raoult, D. & Forterre, P. Redefining viruses: lessons from Mimivirus. *Nature Reviews Microbiology* **6**, 315–319 (2008).
348. Lu, J. & Deutsch, C. Secondary structure formation of a transmembrane segment in Kv channels. *Biochemistry* **44**, 8230–8243 (2005).
349. Tu, L. W. & Deutsch, C. A folding zone in the ribosomal exit tunnel for Kv1.3 helix formation. *Journal of Molecular Biology* **396**, 1346–1360 (2010).
350. Tu, L., Khanna, P. & Deutsch, C. Transmembrane segments form tertiary hairpins in the folding vestibule of the ribosome. *Journal of Molecular Biology* **426**, 185–198 (2014).
351. Kudva, R., Pardo-Avila, F., Sandhu, H., Carroni, M., Bernstein, H. D. & von Heijne, G. The shape of the ribosome exit tunnel affects cotranslational protein folding. *bioRxiv*, 274191 (2018).
352. Ito, K., Chiba, S. & Pogliano, K. Divergent stalling sequences sense and control cellular physiology. *Biochemical and Biophysical Research Communications* **393**, 1–5 (2010).
353. Butkus, M. E., Prundeanu, L. B. & Oliver, D. B. Translocon "pulling" of nascent SecM controls the duration of its translational pause and secretion-responsive secA regulation. *Journal of Bacteriology* **185**, 6719–6722 (2003).
354. Yap, M. N. & Bernstein, H. D. The plasticity of a translation arrest motif yields insights into nascent polypeptide recognition inside the ribosome tunnel. *Molecular Cell* **34**, 201–211 (2009).
355. MacKinnon, A. L., Paavilainen, V. O., Sharma, A., Hegde, R. S. & Taunton, J. An allosteric Sec61 inhibitor traps nascent transmembrane helices at the lateral gate. *eLife* **2014** (2014).

356. Li, L., Park, E., Ling, J. J., Ingram, J., Ploegh, H. & Rapoport, T. A. Crystal structure of a substrate-engaged SecY protein-translocation channel. *Nature* **531**, 395–399 (2016).
357. Lu, J. & Deutsch, C. Electrostatics in the ribosomal tunnel modulate chain elongation rates. *Journal of Molecular Biology* **384**, 73–86 (2008).
358. Sadlish, H., Pitonzo, D., Johnson, A. E. & Skach, W. R. Sequential triage of transmembrane segments by Sec61 $\alpha$  during biogenesis of a native multispanning membrane protein. *Nature Structural and Molecular Biology* **12**, 870–878 (2005).
359. Cross, B. C. S. & High, S. Dissecting the physiological role of selective transmembrane-segment retention at the ER translocon. *Journal of Cell Science* **122**, 1768–1777 (2009).
360. Cymer, F. & von Heijne, G. Cotranslational folding of membrane proteins probed by arrest-peptide-mediated force measurements. *Proceedings of the National Academy of Sciences* **110**, 14640–14645 (2013).
361. Virkki, M. T., Peters, C., Nilsson, D., Sörensen, T., Cristobal, S., Wallner, B. & Elofsson, A. The positive inside rule is stronger when followed by a transmembrane helix. *Journal of Molecular Biology* **426**, 2982–2991 (2014).
362. Junne, T. & Spiess, M. Integration of transmembrane domains is regulated by their downstream sequences. *Journal of Cell Science* **130**, 372–381 (2017).
363. Ismail, N., Crawshaw, S., Cross, B., Haagsma, A. & High, S. Specific transmembrane segments are selectively delayed at the ER translocon during opsin biogenesis. *Biochemical Journal* **411**, 495–506 (2008).
364. Sato, Y., Sakaguchi, M., Goshima, S., Nakamura, T. & Uozumi, N. Integration of Shaker-type K<sup>+</sup> channel, KAT1, into the endoplasmic reticulum membrane: synergistic insertion of voltage-sensing segments, S3-S4, and independent insertion of pore-forming segments, S5-P-S6. *Proc Natl Acad Sci U S A* **99**, 60–5 (2002).
365. Sato, Y., Sakaguchi, M., Goshima, S., Nakamura, T. & Uozumi, N. Molecular dissection of the contribution of negatively and positively charged residues in

- S2, S3, and S4 to the final membrane topology of the voltage sensor in the K<sup>+</sup> channel, KAT1. *Journal of Biological Chemistry* **278**, 13227–13234 (2003).
366. Zhang, L., Sato, Y., Hessa, T., von Heijne, G., Lee, J.-K., Kodama, I., Sakaguchi, M. & Uozumi, N. Contribution of hydrophobic and electrostatic interactions to the membrane integration of the Shaker K<sup>+</sup> channel voltage sensor domain. *Proceedings of the National Academy of Sciences* **104**, 8263–8268 (2007).
367. Tu, L., Wang, J., Helm, A., Skach, W. & Deutsch, C. Transmembrane biogenesis of Kv1. 3. *Biochemistry* **39**, 824–836 (2000).
368. Mi, H., Huang, X., Muruganujan, A., Tang, H., Mills, C., Kang, D. & Thomas, P. D. PANTHER version 11: expanded annotation data from Gene Ontology and Reactome pathways, and data analysis tool enhancements. *Nucleic Acids Research* **45**, D183–D189 (2017).
369. Oliphant, T. E. *SciPy: Open source scientific tools for Python* 2007.
370. Remm, M & Sonnhammer, E. Classification of transmembrane protein families in the *Caenorhabditis elegans* genome and identification of human orthologs. *Genome Res.* **10**, 1679–1689 (2000).
371. O’Hayre, M., Vázquez-Prado, J., Kufareva, I., Stawiski, E. W., Handel, T. M., Seshagiri, S. & Gutkind, J. S. The emerging mutational landscape of G proteins and G-protein-coupled receptors in cancer. *Nature Reviews Cancer* **13**, 412–424 (2013).
372. Singh, A., Nunes, J. J. & Ateeq, B. Role and therapeutic potential of G-protein coupled receptors in breast cancer progression and metastases. *European Journal of Pharmacology* **763**, 178–183 (2015).
373. Bar-Shavit, R., Maoz, M., Kancharla, A., Nag, J. K., Agranovich, D., Grisaru-Granovsky, S. & Uziely, B. G protein-coupled receptors in cancer. *International Journal of Molecular Sciences* **17**, 1320 (2016).
374. Arakaki, A., Pan, W.-a. & Trejo, J. GPCRs in cancer: protease-activated receptors, endocytic adaptors and signaling. *International Journal of Molecular Sciences* **19**, 1886 (2018).

375. DeLano, W. L. The PyMOL molecular graphics system. *PyMOL. DeLano Scientific, San Carlos, CA, USA*, Version 1.2r3pre (2002).
376. Okada, T., Sugihara, M., Bondar, A.-N., Elstner, M., Entel, P. & Buss, V. The retinal conformation and its environment in rhodopsin in light of a new 2.2 Å crystal structure. *Journal of Molecular Biology* **342**, 571–583 (2004).
377. Murakami, M. & Kouyama, T. Crystal structure of squid rhodopsin. *Nature* **453**, 363–367 (2008).
378. Warne, T., Serrano-Vega, M. J., Baker, J. G., Moukhametzianov, R., Edwards, P. C., Henderson, R., Leslie, A. G. W., Tate, C. G. & Schertler, G. F. X. Structure of a  $\beta$ 1-adrenergic G-protein-coupled receptor. *Nature* **454**, 486–491 (2008).
379. Tan, Q., Zhu, Y., Li, J., Chen, Z., Han, G. W., Kufareva, I., Li, T., Ma, L., Fenalti, G., Li, J., Zhang, W., Xie, X., Yang, H., Jiang, H., Cherezov, V., Liu, H., Stevens, R. C., Zhao, Q. & Wu, B. Structure of the CCR5 chemokine receptor-HIV entry inhibitor maraviroc complex. *Science (New York, N.Y.)* **341**, 1387–90 (2013).
380. Burg, J. S., Ingram, J. R., Venkatakrishnan, A. J., Jude, K. M., Dukkipati, A., Feinberg, E. N., Angelini, A., Waghray, D., Dror, R. O., Ploegh, H. L. & Garcia, K. C. Structural biology. Structural basis for chemokine recognition and activation of a viral G protein-coupled receptor. *Science (New York, N.Y.)* **347**, 1113–7 (2015).
381. Thompson, A. A., Liu, W., Chun, E., Katritch, V., Wu, H., Vardy, E., Huang, X.-P., Trapella, C., Guerrini, R., Calo, G., Roth, B. L., Cherezov, V. & Stevens, R. C. Structure of the nociceptin/orphanin FQ receptor in complex with a peptide mimetic. *Nature* **485**, 395–399 (2012).
382. Kang, M. K. & Tullman-Ercek, D. Engineering expression and function of membrane proteins. *Methods* (2018).
383. Findlay, H. E. & Booth, P. J. The folding, stability and function of lactose permease differ in their dependence on bilayer lipid composition. *Scientific Reports* **7**, 13056 (2017).

384. Lu, P., Min, D., DiMaio, F., Wei, K. Y., Vahey, M. D., Boyken, S. E., Chen, Z., Fallas, J. A., Ueda, G., Sheffler, W., Mulligan, V. K., Xu, W., Bowie, J. U. & Baker, D. Accurate computational design of multipass transmembrane proteins. *Science* **359**, 1042–1046 (2018).